NONLINEAR DYNAMICS AND CHAOS OF A PIPE CONVEYING FLUID

by

CHRISTIAN SEMLER

Under the supervision of Professor M.P. Païdoussis.

A thesis submitted to
the Faculty of Graduate Studies and Research
in Partial Fulfilment of the Requirements for the Degree of
Master of Engineering

Department of Mechanical Engineering
McGill University
Montreal, Quebec, Canada

ABSTRACT

This thesis examines the planar dynamics of flexible pipes conveying fluid. The nonlinear equations of motion are derived for cantilevered pipes and for simply-supported pipes, using Hamilton's principle and the force balance method. The resulting equations are compared with previous derivations.

The linearized system is first studied, to get the critical parameters corresponding to the stability boundaries, i.e. the local bifurcations. Then, the nonlinear equations are investigated, both analytically and numerically. Centre manifold, normal form and bifurcation theories are used to obtain complete bifurcation sets which provide the qualitative dynamics of the system. It is shown that chaotic motions may arise under perturbation, or when the motions are constrained by motion-limiting restraints, through calculations of the Lyapunov exponents and the construction of phase portraits, bifurcation diagrams and power spectra. This modeling is in close agreement with experimental observations.

SOMMAIRE

Cette thèse traite de la dynamique plane d'un tube flexible parcouru par un fluide. Les équations non lineaires sont dérivées dans le cas d'un tube encastré-libre ou fixe aux deux extrémités, par le principe d'Hamilton et le principe de la quantité de mouvement, puis comparées à des équations derivées antérieurement. Le système linéaire est tout d'abord examine afin de trouver les différents paramètres critiques. Ensuite, les équations non linéaires sont étudiées analytiquement et numériquement. Les diverses théories utilisées (variétes centrales, formes normales et bifurcations) permettent d'obtenir la dynamique complète du système.

On a pu démontrer l'existence d'oscillations chaotiques pour le système perturbé ou soumis à des contraintes non linéaires en calculant les exposants de Lyapunov et en construisant des diagrammes de phase, de bifurcation et de puissance spectrale. La modélisation utilisée donne de bons résultats par rapport aux observations expérimentales.

ACKNOWLEDGMENTS

The author wishes to thank Professor M.P. Paidoussis for guidance, and for financial support through the Natural Sciences and Engineering Research Council of Canada and les Fonds pour la Formation de Chercheurs et l'Aide à la Recherche du Québec (FCAR).

Special thanks are due to Ms. France Duval, for constant support during the course of this work, and for typing a difficult manuscript.

Likewise, sincere thanks are forwarded to Ms. Laura Mitchell, Mr. Njuki Mureithi and to Ms. France Duval again, for proofreading the text.

Finally, the author acknowledges all the members of the flow induced vibration group for fruitful help and discussions, especially Mr. Njuki Mureithi and Dr. Guang-Xuan Li, for their many suggestions and their availability.

TABLE OF CONTENTS

NOMENCLATURE

a_1	Coefficient of the characteristic polynomial
A	Cross-sectional area
[A]	Linear matrix
[A']	Transformed matrix of [A]
[B]	Time dependent matrix
[B]	Matrix representing the flow on the stable and unstable manifold
C	Representation of $\cos(\omega_0 t+\phi)$
C_L, C_x	Axial contraction
d( )	Infinitesimal quantity
dV	Infinitesimal volume
ds, ds_0	Infinitesimal displacement in the tangential direction, in the deformed and undeformed body
dx,dy	Infinitesimal longitudinal, lateral displacement, in the Eulerian coordinates respectively
dX,dY	Infinitesimal longitudinal, lateral displacement, in the Lagrangian coordinates respectively
$d\gamma$, $d\mu$	Small deviation of γ and μ respectively
$d\mu_1$	Unfolding parameters
Df, [DP]	Jacobian matrix of f, P respectively
D/Dt	Material derivative
e	Axial elongation
E	Young modulus
E^*	Coefficient of viscosity
E^c	Centre eigenspace
E^s, E^u	Stable and unstable eigenspace ($*_{loc}$ means local)
f	N-dimensional vector field (f(x), f(x,t), $f_\mu(x)$ ...)
F_μ	Logistic or quadratic map
$()_F$	Relative to the fluid
g	N-dimensional vector field
g	Gravity acceleration
G	Gravitational energy
h	N-dimensional vector field

h	Coordinate transformation
H	Axial force
I	Moment of inertia
[I]	Identity matrix
k	Dimensional spring stiffness
K	Nondimensional spring stiffness
L	Length of the pipe
L	Lagrangian of the system
$L(\eta)$	Representation of the linear terms
m	Mass per unit length of the pipe
M	Mass per unit length of the fluid
M	Bending moment
[M]	Matrix with non-zero real part eigenvalues
N	Axial force
$N_1(\eta)$	Representation of nonlinear terms
$o(\epsilon)$	At least of order ϵ^2
$O(\epsilon)$	Order of ϵ
p, p_r	Generalized velocity
P, P'	Point in the undeformed and deformed pipe respectively
P	Fluid pressure force
P	Coordinate transformation
[P]	Modal matrix
$()_p$	Relative to the pipe
q, q_r	Generalized coordinates
q_r^0	Generalized coordinates of the fixed points
Q	Shearing stress
Q, Q'	Point in the undeformed and deformed pipe respectively
r	Amplitude of oscillatory motions
R	Radius of curvature
s	Coordinate in the tangential direction
S	Surface
S	Representation of $\sin(\omega_0 t+\phi)$
S_0, S_1	Cross-sectional area

t	Dimensional time
T	Kinetic energy
T	Tension in the fluid (Pressure force)
T_0	Externally applied tension
T_i	Test determinant in Routh's criteria
$u(\tau)$	N-dimensional vector field
u	Lagrangian longitudinal displacement
u_i	N-dimensional perturbation
U	Dimensional (before (2.44)) and nondimensional flow velocity
U_c	Critical flow velocity
U_{HB}	Hopf bifurcation flow belocity
U_0, U_1	X-dependent flow velocity
v	Lagrangian lateral displacement
v_i	N-dimensional perturbation
V	Potential energy
V	Volume
V	Velocity (of the fluid or the pipe)
V_i	Eigenvectors of [A]
W	Winding number
W	Work done by non-conservative forces
W^c	Centre manifold
W^s, W^u	Stable and unstable manifold
x	Longitudinal Eulerian coordinates
x	N-dimensional vector field
x_b	Location of the constraints
x_s	Location of the linear spring
X	Longitudinal Lagragian coordinates
y	Lateral Eulerian coordinates
y	N-dimensional vector field
Y	Lateral Lagragian coordinates
z	Coordinates
z	Buckled position of the pipe

i, j, k	Integer (subscript)
l, m, n	Integer (subscript)
[]	Matrix
{}	Vector
α	Coefficient proportinal to a friction factor
α	Internal dissipation coefficient
β	Mass ratio
γ	Nondimensional gravity
∂	Partial derivative
δ	Variational
δ	Dirac function
Δ	Variation of
ϵ	Strain
ϵ, ϵ'	Small parameter ($\epsilon<<1$)
η	Nondimensional longitudinal coordinate
η	Dissipation coefficient
θ	Tension in the tube
θ	Angle between the position of the pipe and the X-axis
κ	Curvature
λ	Complex eigenvalue of [A]
[Λ]	Diagonal matrix
μ	Variation of the flow velocity
μ	k-dimensional parameter
μ_1	Unfolding parameter
ν	Poisson ratio
ν	Velocity perturbation
ξ	Nondimensional longitudinal or tangential coordinate
ρ	Density
σ	Stress
σ	Lyapunov exponent
τ	Nondimensional time unit
ϕ	Frequency of oscillation
ϕ_r	Cantilever beam eigenfunction

ω	Frequency of the flow perturbation
ω_0	Natural frequency
$(\vec{i}, \vec{j}, \vec{k})$	Basic unit vectors
$(\vec{\tau}, \vec{n}, \vec{b})$	Frenet vectors
$\vec{r}$,	position vector
$\vec{V}_i$	eigenvector

CHAPTER I
INTRODUCTION

Over the last two decades, scientists and mathematicians have developed new tools in the field of dynamics, especially in the field of nonlinear dynamics. The study of relatively simple nonlinear oscillators (such as described by van der Pol's equation or Duffing's equation) and of simple sets of nonlinear equations has demonstrated that very complex, "rich" dynamical behaviour is possible (Guckenheimer and Holmes 1983); for these simple equations at least, the dynamics are now fairly well understood, and the implications of the complex behaviour observed have been elucidated. In the domain of fluid dynamics, nonlinearity is commonplace, and in many cases essential in the proper description of the phenomena involved; this domain, thus, provides a wide spectrum of problems in which these new dynamical tools can be applied.

Of particular interest, especially to engineers, is the domain of fluid-structure interaction, in which system behaviour is often complicated and difficult to understand (Paidoussis 1987). The model of a tube conveying fluid has become a paradigm in the study of fluid-structure interaction, as most of the so-called fluidelastic instabilities can be illustrated and studied both theoretically and experimentally with this system. Divergence and flutter were the most common types of instability in this physically simple system. However with the new tools of the nonlinear dynamics and the understanding of those simple oscillators, it is now possible to gain a more profound understanding of complex phenomena.

In the past, most of the theoretical studies were concerned with stability and were based on linearized analytical models. Bourrières (1939) was one of the first to study the dynamics of flexible pipes conveying fluid. The interest in vibration of pipelines served as the initial inspiration to many subsequent studies, such as those by

Housner (1952), Niordson (1953) and Benjamin (1961).

The particularly interesting problem of the dynamics of a cantilevered pipe conveying fluid was studied further by Gregory and Paidoussis (1966) and Paidoussis (1970), in the case of steady flow, and by Paidoussis and Issid (1974) for flow with a pulsating component; these references are representative of what has become an extensive body of literature. Excellent reviews and bibliographical surveys can be found in Paidoussis and Issid (1974) and Paidoussis (1987), especially for the study of the linearized equations. All these studies provided many results and explanations, especially with regard to the mechanism of instability. It is well known that the cantilevered pipe conveying fluid, a nonconservative system, loses stability by flutter - single degree of freedom flutter, known as a Hopf bifurcation. Physically, this instability occurs when the energy extracted by the pipe from the flow becomes more important than the energy lost by the pipe through the Coriolis force (a pipe-velocity-dependent force, effectively acting like damping).

For pipes fixed at both ends, the destabilizing centrifugal force, which acts as a compressive axial load, may overcome the restoring flexural force for sufficiently large flow velocity, and lead to divergence, another type of instability (Housner 1952). Divergence is, of course, the expected form of instability since the system, in this case, is conservative. Paidoussis and Issid (1974) proved that according to linear theory, coupled-mode flutter may follow divergence, at a higher flow velocity. However, nonlinear analyses by Holmes (1978) and Ch'ng (1978) showed that this was not possible; in other words, steady-state oscillatory motions are not possible.

Over the past 15 years, interest has grown in the nonlinear dynamical aspects of the problem of a pipe conveying fluid; this involves more interesting but also more complex analysis and will be the main subject of this study. Firstly,

a nonlinear analysis has the advantage of being able to predict the behaviour of the system beyond the critical values, while linear models predict exponential increase in amplitude after bifurcation. Experimental evidence (Dodds and Runyan 1965 and Paidoussis 1966) suggests that limit-cycle motion or a stable buckled state arise, so that the inclusion of nonlinear contributions is of particular interest, in order to improve agreement between theoretical prediction and experimental observation. Secondly, the nonlinear approach enables classification in a parameter space of the different possible types of qualitative behaviour of the system, by generating so-called bifurcation diagrams in the new terminology of dynamics. Finally, although Rousselet and Herrmann's work (1977, 1981), as well as some experimental work (Paidoussis, 1970), proved that the system was only weakly nonlinear, in some cases very interesting features were observed (Sethna and Shaw 1987, Bajaj 1987, Li and Paidoussis 1990).

For inextensible cantilevered pipes, a number of papers presenting a nonlinear analysis are of particular interest, and will be discussed briefly in what follows.

Bourrières (1939), more than fifty years ago, was the first to derive the nonlinear equations of the planar motion. He considered the force balance method and wrote down the full and exact nonlinear relationships, like the expression of the curvature for example. "Unfortunately", he then proceeded to simplify the system by linearization to obtain analytically some very interesting results, without undertaking any nonlinear analysis of the system. Although he could not find the critical flow velocity, he explained many characteristics of the system.

Subsequent research on the nonlinear dynamics of this system has been conducted by Rousselet and Herrmann (1977, 1981). They derived the equations in two different ways, the force balance and the energy methods, in order to

find a set of equations which could be considered exact. Although it was not stated explicitly, it is important to note the similarity of their equations with Bourrières' work, in the force balance method. It is only the unusual notation (introduction of an angle θ) that makes their work appear very different. Their derivation of Hamilton's principle for system of changing mass, however, is original, as they use a control volume approach in order to take into account the kinetic energy of the moving fluid. Unfortunately, one little mistake in the interconnection of certain terms led them to an equation that was partially wrong, but their general equation (before the interconnection) and the logic of their derivation is irreproachable. Moreover, because they took into account the friction force acting between the fluid and the deformed pipe and the resultant nonlinear pressure loss, they derived another equation for the fluid itself.

Another school, led essentially by Sethna, also tried to derive the general nonlinear equations by following a different approach. Lundgren, Sethna and Bajaj (1979) derived a set of integrodifferential equations which appears to be absolutely correct. No major approximation was made, except the assumption of zero gravity effects (which is perfectly valid for horizontal pipes and motions in a horizontal plane in any case), making the derivation complete. They kept, like Bourrières, the two equations in a general form without interconnecting them. These equations were also used by Bajaj et al. (1980), Edelstein et al. (1986) and by Steindl and Troger (1988). Lundgren et al. (1979) studied a pipe fitted with an inclined terminal nozzle, causing sinusoidal static deformation of the tube obtained through the nonlinear equations. Bajaj et al. (1980), like Rousselet and Herrmann, considered a parameter related to the pressure loss of the pipe. Using centre manifold theory and the method of averaging, they studied the nonlinear dynamics of a cantilevered pipe conveying fluid. After finding the critical

flow velocity, which was not an easy task, their major contribution was to reconstruct the periodic solution after the bifurcation. This was done by following the fundamental methods developed earlier by Chow and Mallet-Paret (1977) and also by Joseph and Sattinger (1972). It was also found that depending on the pressure loss in the pipe, either sub- or super-critical bifurcations may occur. Steindl and Troger (1988) extended their work by adding a rotationally symmetric elastic support in order to get even more complicated situations for loss of stability. Using centre manifold and normal form theories, they completed the bifurcation diagrams.

Other researchers have also studied the case of a pipe fixed at both ends. Thurman and Mote (1969) were mainly concerned with the oscillations of bands of moving materials, such as saw blades or conveyor belts, which are in the same general dynamical family as pipes supported at both ends. The centreline, in this case, is not considered inextensible anymore, so that the essential nonlinearity is associated with the axial tube elongation and the extension-induced tension in the tube, both of which are dependent on lateral deformation. All the other relationships (such as the moment/curvature for example) were assumed to be linear. Their major results, obtained by the Krylov-Bogoliubov method (Minorsky 1962) show the effects of the nonlinear terms on the fundamental period of oscillation.

Holmes (1977) was one of the first to use the tools of modern nonlinear dynamics in the study of a pipe conveying fluid with both ends supported. The only nonlinear term was associated with the deflection-induced tension in the pipe that he added to the linear equation derived by Paidoussis and Issid (1974). This is explained by the fact that his work took place at an early stage in the research of nonlinearities for such system. After discretization of the equation, Holmes was able to find many characteristics of the system, and he discussed the existence of local, as well as global

bifurcations. He also studied the panel flutter problem, which is qualitatively similar to that of a cantilevered pipe conveying fluid (loss of stability, via a Hopf bifurcation). Finally, Holmes (1978) proved that sustained flutter motion is impossible with the equations used for pipes with both ends supported, by studying the local and global stability of the equilibrium positions adopted after the first instability.

Namachchivaya and Tien (1989) are among the last to deal with nonlinear behaviour of supported pipes conveying pulsatile fluid. Their equations suffer from certain misunderstandings, especially of velocity-dependent terms. Indeed, their fluid velocity, their Hamilton's principle used in its linear form and their definition of the axial contraction are incompatible. Consequently, no nonlinear term proportional to velocity is present. Moreover, some nonlinear terms due to axial strain are missing. However, they found some interesting bifurcations near the subharmonic and the combination resonances, using a method of averaging.

The interconnections and relative interdependence of all these studies is not so obvious, so that it is difficult to reach a final statement in the equation of a pipe conveying fluid. The method, the notation and the progress in each derivation are, most of the time, completely different, even though similarities between some papers can be found. Furthermore, none of the "schools" compared their nonlinear equations to those of others. Consequently, one of the first tasks in this thesis will be to rederive the equations of motion (Chapter II) and compare them with previous derivations (Chapter III).

The study of chaos, usually associated with strong nonlinearities, has become more and more popular in recent dynamics research. This led Paidoussis and Moon (1988) and Paidoussis et al. (1989, 1990) to introduce some nonlinearities by motion-limiting constraints; similar considerations led Tang and Dowell (1988) to use a pipe

subjected to strong nonlinear forces due to two equi-spaced permanent magnets on either side near the lower tip of the pipe. In all those cases, experiments as well as theoretical results indicate that there exist regions of chaos beyond the Hopf bifurcation. Chaotic responses were found to occur after the instability of the limit cycle followed by a cascade of period-doubling bifurcations. This is one of the well-known routes to chaos developed by Feigenbaum (1983), but not the only one.

The perturbation of a homoclinic orbit leading to a "horse-shoe" scenario can also be encountered. Fundamentally, this has been explained by Smale (1963, 1967) and is treated in detail in Guckenheimer and Holmes (1983) and in Devaney (1987), and has been applied in our particular case by Li and Paidoussis (1990). In the simplest case, i.e. a four dimensional approximation, Li and Paidoussis found the conditions (known as the Double Degeneracy Conditions (DDC)) for chaos to occur. Steindl and Troger (1988) also give an example and some explanations about those conditions. Physically, such conditions occur when two types of instabilities arise simultaneously. This phenomenon was observed by Sugiyama et al. (1985). They added a linear spring at a point along the pipe and found multiple characteristics of stability in the transitional region. Indeed, during the transition between one instability and the other, the system can, in some cases, become subject to chaotic - or unpredictable - responses. Consequently, particular attention will be paid to such cases.

This study aims to clarify all these precepts, which will be summarized, discussed and used.

As the system is of an infinite number of degrees of freedom, a crucial choice has to be made at the very beginning of the study: to discretize the governing equations or not. The "well-known" linear equation of motion of a cantilevered pipe conveying fluid (Paidoussis and Issid 1974) is given by

(see Fig.1.1 and also Chapter II for the significance of the terms)

$$EIy'''' + [MU^2 - ((M+m)g - M\dot{U})(L-x)]y'' + 2MUy' + (M+m)gy' + (M+m)\ddot{y} = 0, \tag{1.1}$$

with $( )'$ being the derivative with respect to x , and $( )\cdot$ being the derivative with respect to time t.

Although the equation of motion is a homogeneous partial differential equation (PDE), it is still difficult to solve for exact solutions since the coefficient term explicilty depends on x. However, with a few assumptions (steady flow, dU/dt = 0, and neglecting gravity terms), the equation becomes much simpler:

$$EIy'''' + MU^2y'' + 2MUy' + (M+m)\ddot{y} = 0. \tag{1.2}$$

By transforming this into an eigenvalue problem, the stability conditions can be found quite easily. This has been done by Gregory and Paıdoussis (1966), and Rousselet and Herrmann (1977), for instance. Holmes and Marsden have been the only ones dealing with both a finite and an infinite dimensional analysis (Holmes 1977; Holmes and Marsden 1978), and their contribution is of major importance. For the panel flutter problem in the infinite dimensional analysis, they showed how a partial differential equation (PDE) could be recast as an ordinary differential equation (ODE) on a suitable function space, and introduced the centre manifold theory (Marsden and McCracken 1976; Carr 1981) in order to study the dynamics on a finite dimensional space without loss of qualitative information. Holmes' finite dimensional analysis consists of the Galerkin projection and a modal truncation, from which the PDEs are recast into a set of ODEs (Holmes 1977). For the panel flutter problem, a proof, demonstrating the fact that the flow defined by the Galerkin's approximation converges to the flow of the full nonlinear PDEs, is given. Unfortunately,

such a proof does not provide an approximation of the error when n is finite. This method is also used by Paidoussis (1970) - see Paidoussis and co-workers (1974, 1990).

In Chapter IV, the linearized equations for the case of a two-mode-model approximation are studied extensively. The critical parameters corresponding to the stability boundaries are found.

Depending on the eigenvalues of the linear matrix, three different types of instability may occur: divergence, flutter or concurrent divergence and flutter. In terms of dynamics, those points correspond to a pitchfork bifurcation (for systems with symmetry), a Hopf bifurcation and double degeneracy conditions (Langford 1983). The boundary conditions are investigated through Routh's criteria (Routh 1960), and the results found are checked through a direct eigenvalue analysis for certain representative parameters.

In Chapter V, the nonlinear equations are investigated both numerically and analytically. First, the existence and the stability of the new equilibrium positions are studied. Then, the qualitative dynamics of the system near all the degenerate points are examined using the bifurcation theory. For each degeneracy, the dimension of the system is reduced with use of the centre manifold theory, and the corresponding subsystem on the centre manifold is used to obtain the qualitative dynamical features. In order to simplify the equations on this subsystem, the normal form theory and the method of averaging are introduced.

The normal forms enable the detection and a simple explanation of complicated dynamics (such as the dynamics involving global bifurcations) and, hence, represent a powerful technique.

The existence of chaos near the doubly-degenerate fixed points is investigated, by adding a small perturbation on the flow velocity (pulsatile component) through the calculation of the Lyapunov exponents and the construction of

phase portraits, bifurcation diagrams and power spectra.

Finally, the dynamics of the cantilevered pipe constrained by motion-limiting restraints are examined. Chaotic regions are found to exist in the case of the autonomous system (no pulsatile flow velocity), and the route to chaos is shown to be via period-doubling bifurcations. With the inclusion of the inherent nonlinearities of the pipe in the equations of motion, the theoretical modeling gives very good agreement, qualitatively and quantitatively, with experimental observations.

This study aims to describe the fascinating behaviour of the cantilevered pipe conveying fluid by introducing and using all the new concepts of the nonlinear dynamics developed in the last few years. It also aims to discuss, clarify and prove the existence of complicated motions, such as chaotic oscillations, in this rather simple physical system.

CHAPTER II

EQUATIONS OF MOTION OF A PIPE CONVEYING FLUID

In this chapter, the general equations of a pipe conveying fluid and moving in a plane are derived. The classical theory of elasticity treats problems in which displacement and its derivatives are small. However, in the case treated here, the pipe may undergo large displacements, which will give rise to nonlinear terms. As was mentioned in the Introduction, and as will be discussed in the next chapter, a number of researchers have already tackled this problem. Nevertheless, the notation and the method used, as well as the extent to which the task was carried out, were rarely the same. Thus, it was decided to rederive the equations, in order to clarify some concepts and to obtain a set of equations which could be considered as complete as possible and error-free.

Before deriving the equations, some important concepts will first be introduced. Then, the equations will be derived using two different methods: the energy method, based on Hamilton's principle, and the force-balance method, generally considered to be simpler. Finally, the equation found will be transformed into its "standard" form by a perturbation method and into a set of ordinary differential equations (ODEs) by means of Galerkin method. In the derivation, the two cases, those of a cantilevered pipe and of a pipe fixed at both ends, have been separated completely.

2.1 ASSUMPTIONS

Here are the basic assumptions made for the pipe and the fluid.

- The fluid is incompressible.
- The velocity profile of the fluid is uniform (plug-flow approximation for a turbulent-flow

profile), but a small oscillatory component may be superimposed on the mean flow.

- The diameter of the pipe is small compared to its length, so that the pipe behaves like a Euler-Bernoulli beam.
- The motion is planar.
- The deflections of the pipe are large, but the strains are small.
- Rotatory inertia and shear deformation are neglected.
- In the case of a cantilevered pipe, the pipe centreline is inextensible.

2.2 INTRODUCTION OF SOME BASIC CONCEPTS

2.2.1 Notation

In elasticity, and more generally in continuum mechanics, in order to describe the position of material points, one usually has the choice between two sets of coordinate systems: one for the undeformed body and one for the deformed body. The deformation of a point is described by the relation of the coordinates of the same material point in the undeformed and deformed states (Eringen 1967). In the usual terminology, for a three-dimensional problem, X_k, representing the position of a material point P in its original state, stands for material or Lagrangian coordinates; x_k, representing the position of the same material point P in the deformed state, stands for the spatial or Eulerian coordinates. The motion can, therefore, be described either in terms of

$$x_k = x_k(X_1, X_2, X_3, t),$$

or in terms of

$$X_k = X_k(x_1, x_2, x_3, t),$$

t being the time[1].

The deformation gradients, deformation tensors, strain tensors and displacement vectors can then be expressed in either set of coordinates. In the infinitesimal deformation theory, the distinction between the Lagrangian and Eulerian strains disappears (Eringen 1967). However, the distinction absolutely must be made when nonlinear relationships are sought.

In elasticity, (x, y, z) are usually used to represent the location of a material point in an elastic deformable body, and (u, v, w) correspond to the displacements of the same material point. For a slender pipe with its initially undeformed state along the x-axis, y is then identical to the displacement v. The coordinate of a point always refers to the undeformed body which is represented by X. A point can also be represented by s, the curvilinear coordinate along the pipe. A schematic diagram for the physical system, as well as for the coordinates used, is given in Fig.2.1[2]. The pipe is assumed to be initially lying along the X-axis and oscillates in the (x,y) plane. Consequently, the following relationships will hold

$$\begin{aligned} x &= X + u, \\ y &= Y + v. \end{aligned} \qquad (2.1)$$

---

[1] It is noted that the same symbols in the equations appear in italics, while in the text, they appear in Roman script.

[2] The figures are numbered according to chapter; thus Fig.2.1 is the first figure associated with Chapter II. These are the main figures, and they are found together after the text in this thesis. Figures II(a),(b) etc. are small schematic figures inserted in the text.

2.2.2 Inextensibility condition

In the case of a clamped-free pipe, one may assume the pipe to be inextensible. This condition of inextensibility is very important and will thus be detailed here.

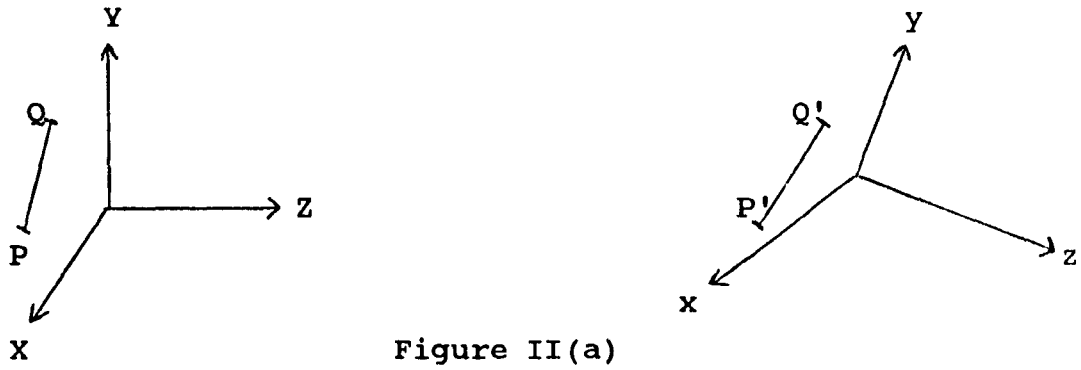

Figure II(a)

Let P and Q be two longitudinally-separated points on the pipe, as shown in Figure II(a); they are defined in the original (undeformed) coordinates (X, Y, Z). After transformation to the deformed-state coordinates, P → P' and Q → Q'. Let ds_0 be the distance between P and Q, and ds the distance between P'and Q'; thus,

$$P(X,\ Y,\ Z),\ Q(X+dX,\ Y+dY,\ Z+dZ),\ ds_0^2 = dX^2 + dY^2 + dZ^2,$$

$$P'(x,\ y,\ z),\ Q'(x+dx,\ y+dy,\ z+dz),\ ds^2 = dx^2 + dy^2 + dz^2. \tag{2.2}$$

For the sake of simplicity, for a two-dimensional problem (Z=0), one obtains

$$ds^2 - ds_0^2 = dx^2 + dy^2 - dX^2 - dY^2.$$

If X is the long axis of symmetry of the pipe, then Y = 0 (slender rod), and one can write

$$ds^2 - ds_0^2 = dx^2 + dy^2 - dX^2 - \left[\left(\frac{dx}{dX}\right)^2 + \left(\frac{dy}{dX}\right)^2 - 1\right] dX^2. \tag{2.3}$$

For an inextensible pipe, $ds^2 = ds_0^2$ by definition; hence,

$$(\frac{\partial x}{\partial X})^2 + (\frac{\partial y}{\partial X})^2 = 1. \qquad (2.4)$$

Also, in this case, dX is equivalent to ds, as they both represent an infinitesimal distance in the undeformed body. Hence,

$$dX = ds, \qquad (2.5)$$

and

$$(\frac{\partial x}{\partial s})^2 + (\frac{\partial y}{\partial s})^2 = 1. \qquad (2.6)$$

This relationship is illustrated in Figure II(b).

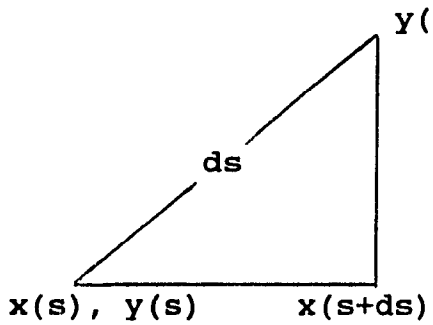

Figure II(b)

If the element was extensible, then after deformation, its deformed length would be longer or shorter than its original length ds, i.e. $(dx)^2 + (dy)^2 > \text{or} < (ds)^2$. The equality is valid only for the inextensible case, as

$$ds^2 = (x(s+ds)-x(s))^2 + (y(s+ds)-y(s))^2,$$

or

$$ds^2 = (\frac{\partial x}{\partial s} ds)^2 + (\frac{\partial y}{\partial s} ds)^2.$$

Introducing the displacements (u,v), as defined in (2.1), the following two important relationships are obtained:

$$(\frac{\partial x}{\partial s})^2 + (\frac{\partial y}{\partial s})^2 = 1, \quad (1+\frac{\partial u}{\partial s})^2 + (\frac{\partial v}{\partial s})^2 = 1. \qquad (2.7)$$

2.2.3 Expression for curvature

An exact expression for the curvature κ is useful in both the force balance and the energy method, and is thus presented here. Depending on the choice of the coordinate system, the expression for κ varies.

Mathematically speaking, κ is defined by

$$\vec{b} = \frac{\partial^2 \vec{r}}{\partial s^2} = \kappa \vec{n},$$

where $\vec{n}$ is the normal unit vector and $\vec{b}$ the binormal; hence,

$$\kappa = \left|\frac{\partial^2 \vec{r}}{\partial s^2}\right| = \sqrt{(\frac{\partial^2 x}{\partial s^2})^2 + (\frac{\partial^2 y}{\partial s^2})^2}. \qquad (2.8)$$

For more detail and more definitions, see Appendix 1. For a pipe the centreline of which is considered inextensible, the inextensibility condition leads to

$$\kappa = \frac{\frac{\partial^2 y}{\partial s^2}}{\sqrt{1-(\frac{\partial y}{\partial s})^2}}. \qquad (2.9)$$

Note that for a curve defined by y(x) rather than y(s) (Eulerian description), one has the familiar expression of curvature as follows

$$\kappa = \frac{\frac{\partial^2 y}{\partial x^2}}{(1+(\frac{\partial y}{\partial x})^2)^{\frac{3}{2}}}. \qquad (2.10)$$

Care must be taken as which expression for κ should be used, depending on the coordinate system in which the system dynamics is described.

2.3 EQUATIONS OF MOTION BASED ON THE ENERGY METHOD FOR A CANTILEVERED PIPE

2.3.1 Hamilton's principle

The energy method is based on Hamilton's principle, written usually as

$$\delta \int_{t_1}^{t_2} L \, dt + \int_{t_1}^{t_2} \delta W \, dt = 0, \tag{2.11}$$

where L is the Lagrangian of the system ($L = T_p + T_F - V_p - V_F$, T_p and V_p being the kinetic and potential energies associated with the pipe, and T_F and V_F the corresponding quantities for the enclosed fluid), and where δW is the virtual work due to forces not included in the Lagrangian.

However, this principle is only valid for closed systems, such as systems of particles and rigid bodies where there is no mass flux in or out of the system. Thus, an extended form of Hamilton's principle had to be developed. In the absence of dissipative forces ($\delta W = 0$), the statement of the appropriate form of Hamilton's principle is

$$\delta \int_{t_1}^{t_2} L \, dt = \int_{t_1}^{t_2} [MU(\frac{\partial \vec{R}}{\partial t} + U\vec{\tau}) . \delta \vec{R}] \, dt, \tag{2.12}$$

where $\vec{R}$ and $\vec{\tau}$ represent the position vector and the tangential unit vector at the free end of the pipe. This was done by Benjamin (1961) in the case of an Euler-Bernoulli beam conveying fluid. It was also rederived in a more general way by McIver (1973) who considered systems of changing mass.

The terms proportional to MU on the right-hand side of (2.12) are related to the energy accumulated or rejected by

the end of the tube. In other words, the right-hand side of (2.12) can be viewed as the virtual momentum transport across the open surface at the end of the pipe. As was elucidated by Benjamin (1961), this term is also directly related to the mechanism of instability; indeed, he proved that

$$\Delta W = - \int_0^{t_1} MU(\dot{\vec{R}}^2 + U\vec{\tau}.\dot{\vec{R}})\, dt$$

represents the energy gained by the pipe. If the pipe is fixed at both ends, then $\Delta W = 0$ (the system is conservative), but if one end is free to move, $\Delta W \neq 0$, the system becomes nonconservative (Paidoussis 1970). When U is small, it is clear that $\Delta W < 0$, which means that the system is stable (effect of the Coriolis force). However, for positive and sufficiently large U, ΔW might become positive, i.e. energy is extracted from the flow, and the system becomes unstable.

2.3.2 Order of magnitude considerations

Though the deflection of the pipe can be considered as large, an order of magnitude analysis may nevertheless be usefully undertaken. y or v corresponds to the lateral displacement which can still be expressed as "small" by writing

$$y = O(\epsilon). \qquad (2.14)$$

Looking for large deflection motions means that, in the equation, terms of higher order than the linear ones have to be kept. Consequently, and because of the symmetry of the system itself, the nonlinear equations will necessarily be of the third order, which means that terms of order $O(\epsilon^3)$ have to be present in the equations. However, the variational technique always requires one order higher than the one sought, so that all the expressions under the integrand have to be at least of the fourth order $O(\epsilon^4)$! Therefore, the different expressions, V and T for example, have to be exact

to $O(\epsilon^4)$ before any simplification can be undertaken. So, this method is a little more complicated than the force balance method, but it still remains powerful and will therefore be used.

2.3.3 Strain energy

It is very important to define an exact form of the strain energy in the case of large deflections, without simplifying terms of order $O(\epsilon^4)$. This problem was solved by Stoker (1968), with only one major (but not drastic) assumption: the strain is small even though the deflection can be large. He proved that in this case, "the deformation in the neighborhood of each point can be identified with a deformation to which the linear theory is applicable, providing a rational analytic basis for adopting Hooke's stress-strain relations". His analysis finally led to

$$V = \frac{E}{2}\int_0^L [A\epsilon^2 + I(1+\epsilon)^2\kappa^2]\, dX, \tag{2.15}$$

where X represents the Lagrangian coordinate, A the cross-sectional area, I the moment of inertia and ϵ the strain. In the case of a cantilevered pipe, assumed inextensible, $\epsilon = 0$, so that

$$V = \frac{EI}{2}\int_0^L \kappa^2\, dX = \frac{EI}{2}\int_0^L \kappa^2\, ds. \tag{2.16}$$

The expression of the curvature itself has been given in Section 2.2.

2.3.4 The gravitational energy

In general, the gravitational energy depends on the distribution of mass (Fung 1969), and is written as

$$G = \int \rho\phi(x)\ dV,$$

where ϕ is the gravitational potential per unit mass. In the important case of a uniform gravitational field, it becomes

$$G = \int \rho g x\ dV,$$

where g is the gravitational acceleration and x is a distance measured from a certain plane in a direction opposite to the gravitational field.

Consequently, with the notation used in this thesis,

$$G = -(m + M)\ g \int_0^L x\ ds; \tag{2.17}$$

or with the (u, v) notation, the gravitational energy is

$$G = -(m + M)\, g \int_0^L (X+u)\ dX. \tag{2.18}$$

2.3.5 Kinetic energy

The total kinetic energy of the system is the sum of the kinetic energy of the pipe, T_p, plus the kinetic energy of the fluid, T_F, defined by

$$T_P = \frac{m}{2}\int_0^L V_P^2\ ds, \tag{2.19}$$

and

$$T_F = \frac{M}{2}\int_0^L V_F^2\ ds. \tag{2.20}$$

As the position of the pipe is defined by

$$\vec{r} = x\vec{i}+y\vec{j} \quad or \quad \vec{r} = (X+u)\,\vec{i}+v\vec{j},$$

by definition, the velocity of the pipe is

$$\vec{V}_P = \frac{\partial \vec{r}}{\partial t} = \dot{x}\vec{i}+\dot{y}\vec{j} \quad or \quad \dot{u}\vec{i}+\dot{v}\vec{j}. \tag{2.21}$$

For a fluid element, the relative velocity with respect to the pipe has to be taken into account, i.e.

$$\vec{V}_F = \vec{V}_P + U\,\vec{\tau},$$

$\vec{\tau}$ being a unit vector, which may be expressed as

$$\vec{\tau} = \frac{x'\vec{i}+y'\vec{j}}{\sqrt{x'^2+y'^2}} \quad or \quad \frac{(1+u')\,\vec{i}+v'\vec{j}}{\sqrt{(1+u')^2+v'^2}},$$

in which (and henceforth) primes denote derivatives with respect to s. With the inextensibility condition, this simplifies to

$$\vec{\tau} = x'\vec{i}+y'\vec{j} = (1+u')\,\vec{i}+v'\vec{j}.$$

Consequently,

$$\begin{aligned}\vec{V}_F &= (\dot{x}\vec{i}+\dot{y}\vec{j}) + U\,(x'\vec{i}+y'\vec{j}) \\ &\quad - \left(\frac{\partial}{\partial t} + U\,\frac{\partial}{\partial s}\right)(x\vec{i}+y\vec{j}),\end{aligned} \tag{2.22}$$

or

$$\vec{V}_F = \frac{D\vec{r}}{Dt},$$

where D/Dt is the material derivative of the fluid element. By analogy, the accelerations of the pipe and of the fluid are, respectively,

$$\vec{a}_P = \frac{\partial^2 \vec{r}}{\partial t^2}, \quad \vec{a}_F = \frac{D^2\vec{r}}{Dt^2}. \tag{2.23}$$

Hence,

$$T_P = \frac{m}{2}\int_0^L (\dot{x}^2+\dot{y}^2)\ ds,$$

and

$$T_F = \frac{M}{2}\int_0^L [\,(\dot{x}+Ux')^2+(\dot{y}+Uy')^2\,]\ ds.$$

One important remark is that no term in U^2 appears in this expression after squaring the terms within it, as

$$U^2\ x'^2 + U^2\ y'^2 = U^2$$

because $x'^2 + y'^2 = 1$. This illustrates the importance of the right-hand side of (2.12) which provides the linear and nonlinear centrifugal force proportional to MU^2.

Finally, the total kinetic energy, T, may be written as

$$T = \frac{m}{2}\int_0^L (\dot{x}^2+\dot{y}^2)\ ds + \frac{M}{2}\int_0^L [\,(\dot{x}+Ux')^2+(\dot{y}+Uy')^2\,]\ ds. \qquad (2.24)$$

2.3.6 Derivation of the equations of motion

The usual variational techniques are used to find the different contributions in Hamilton's principle. Only the main steps will be described here.

i) Relationship between δx and δy

By applying the variational operator δ to the inextensibility condition, one obtains

$$x'\delta x' + y'\delta y' = 0,$$

$$\delta x' = -\frac{y'\delta y'}{\sqrt{1-y'^2}} = -y'\left(1+\frac{1}{2}y'^2\right)\delta y' + O(\epsilon^5);$$

hence,

$$\delta x = -\int_0^s \left[y'\delta y' + \frac{1}{2}y'^3\delta y'\right] ds. \qquad (2.25)$$

After integrating (2.25) by parts, one obtains

$$\delta x = -\left(y'+\frac{1}{2}y'^3\right)\delta y + \int_0^s \left(y''+\frac{3}{2}y'^2y''\right)\delta y\, ds + O(\epsilon^5). \qquad (2.26)$$

This relationship is very important in the derivation of the equations of motion, since terms in δx and δy are present due to the variational technique. Equation (2.26) proves that δx and δy are also related through the inextensibility condition, but under a different form.

One can also prove quite easily that (Appendix 2)

$$\int_0^L g(s)\left(\int_0^s f(s)\,\delta y\, ds\right) ds = \int_0^L \left(\int_s^L g(s)\, ds\right) f(s)\,\delta y\, ds. \qquad (2.27)$$

Equation (2.27) is also important, since terms of that form will arise from (2.26) in the process of relating δx to δy.

ii) Kinetic energy component

The variational operations on T leads to

$$\delta \int_{t_1}^{t_2} T\, dt = m\iint (\dot{x}\,\delta\dot{x} + \dot{y}\,\delta\dot{y})\, ds dt + M\iint \left[(\dot{x}+Ux')(\delta\dot{x} + U\,\delta x') + (\dot{y}+Uy')(\delta\dot{y} + U\,\delta y')\right] ds dt. \qquad (2.28)$$

However, $x'\delta x' + y'\delta y' = 0$; thus,

$$\begin{aligned}\delta\int_{t_1}^{t_2} T\,dt &= (m+M)\iint(\dot{x}\,\delta\dot{x} + \dot{y}\,\delta\dot{y})\,dsdt \\ &\quad + M\iint[Ux'\,\delta\dot{x} + U\dot{x}\,\delta x' + \\ &\qquad Uy'\,\delta\dot{y} + U\dot{y}\,\delta y']\,dsdt \\ &\quad - \begin{pmatrix} -\iint[(m+M)\ddot{x} + M\dot{U}x' + 2MUx']\,\delta x\,dsdt \\ -\iint[(m+M)\ddot{y} + M\dot{U}y' + 2MUy']\,\delta y\,dsdt \\ + MU\int[\dot{x}_L\delta x_L + \dot{y}_L\delta y_L]\,dt \end{pmatrix},\end{aligned} \tag{2.29}$$

where $x_L = x(L)$, $y_L = y(L)$ in the last term which arises from the operations of integrating by parts (Appendix 2). Also, the integral limlits, although not explicitly written, are understood to be from 0 to L for s, and from t_1 to t_2 for t.

iii) Potential energy component

In this case, two components have to be derived. Considering bending first, one can write

$$\delta\int_{t_1}^{t_2} V\,dt = \frac{EI}{2}\iint\delta(\kappa^2)\,dsdt;$$

however, from (2.9),

$$\kappa^2 = \frac{y''^2}{1 - y'^2} = y''^2\,(1 + y'^2) + O(\epsilon^5),$$

so that

$$\begin{aligned}\delta\int_{t_1}^{t_2} V\,dt &= \frac{EI}{2}\iint\delta(y''^2\,(1 + y'^2))\,dsdt \\ &\quad - EI\iint[(y'' + y''y'^2)'' - (y''^2y')']\,\delta y\,dsdt \\ &\quad - EI\iint[y'''' + 4y'y''y''' + y''^3 + y''''y'^2]\,\delta y\,dsdt\end{aligned} \tag{2.30}$$

Similarly, the gravity component yields (Appendix 2)

$$\delta \int_{t_1}^{t_2} G\,dt = -(m+M)\,g \iint \delta x\,ds dt - (m+M)\,g \iint \left[-\left(y' + \frac{1}{2}y'^3\right)\delta y + (L-s)\left(y'' + \frac{3}{2}y''y'^2\right)\delta y\right] ds dt. \tag{2.31}$$

iv) Right-hand side of Hamilton's principle

Applying the variational techniques to the right-hand side of Hamilton's principle leads to

$$\begin{aligned} rhs &= MU \int_{t_1}^{t_2} \left[\left(\dot{x}_L + Ux'_L\right)\delta x_L + \left(\dot{y}_L + Uy'_L\right)\delta y_L\right] dt \\ &= MU \int_{t_1}^{t_2} \left(\dot{x}_L \delta x_L + \dot{y}_L \delta y_L\right) dt \\ &\quad + MU^2 \int_{t_1}^{t_2} \left(x'_L \delta x_L + y'_L \delta y_L\right) dt \\ &= A + B. \end{aligned} \tag{2.32}$$

The first term, A, is the same as the one derived from the kinetic energy (2.29) and thus it can be cancelled. The second one, B, after use of the inextensibility condition (2.7) and condition (2.26) is equal to

$$B = MU^2 \iint \left[y'' + y'^2 y'' - y'' \int_s^L \left(y' y''\right) ds\right] \delta y\, ds dt \tag{2.33}$$

(see Appendix 2, (A2.4) for demonstration). The term B contributes to all the centrifugal force terms.

v) Final equation of motion of the pipe

After many tranformations and manipulations, the general equation of motion is found to be

$$(m+M)\ddot{y} + 2MU\dot{y}'(1+y'^2) + (m+M)\,gy'(1+\frac{1}{2}y'^2)$$
$$+ y''\left[\, MU^2(1+y'^2) + (M\dot{U} - (m+M)g)(L-s)(1+\frac{3}{2}y'^2)\,\right]$$
$$+ EI\left[\, y''''(1+y'^2) + 4\,y'y''y''' + y''^3\,\right]$$
$$-y''\left[\int_s^L\int_0^s (m+M)\,(\dot{y}'^2+y'\ddot{y}')\,dsds + \int_s^L (\frac{M\dot{U}}{2}y'^2+2MU\dot{y}'y'+MU^2y'y'')\,ds\right]$$
$$+y'\int_0^s (m+M)(\dot{y}'^2+y'\ddot{y}')\,ds = 0. \qquad (2.34)$$

This equation will be discussed in more detail in Section 2.5, after the equation of motions has been derived by the second method.

2.4 FORCE BALANCE METHOD IN VECTOR FORM FOR A CANTILEVERED PIPE

This derivation is based on Lundgren's et al. work (1979) which has been further derived into a single equation which is more appealing. It consists of equating the forces and moments acting on an element dX.

Consider an element of the pipe of length ds (Fig.2.1(b)) located at $\vec{r}$. Let $\vec{Q}$ and $\vec{M}$ represent the resultant force and bending moment on the left cross section, and $\vec{Q} + d\vec{Q}$ and $\vec{M} + d\vec{M}$ on the right cross section.

The force balance leads to

$$\frac{\partial \vec{Q}}{\partial s} + (m+M)\,g\vec{i} = m\,\frac{\partial^2 \vec{r}}{\partial t^2} + M\,\frac{D^2\vec{r}}{Dt^2}, \qquad (2.35)$$

and the moment balance to

$$\frac{\partial \vec{M}}{\partial s} + \vec{\tau} \times \vec{Q} = 0. \tag{2.36}$$

As the effect of rotary motion is neglected, and due to the Euler-Bernoulli hypothesis, one simply has

$$\vec{M} = EI\, \vec{\tau} \times \frac{\partial \vec{\tau}}{\partial s} = EI\, \vec{\tau} \times \vec{\kappa}. \tag{2.37}$$

Decomposing $\vec{Q}$ along the axial direction $\vec{\tau}$ and the normal direction $\vec{n}$ gives

$$\vec{Q} = (N - P)\vec{\tau} + \vec{\tau} \times \frac{\partial \vec{M}}{\partial s}, \tag{2.38}$$

where (N-P) is the axial force due to tension and fluid pressure. Combining (2.37) with (2.38) yields

$$\begin{aligned} \vec{Q} &= (N-P)\vec{\tau} + EI\, \vec{\tau} \times \frac{\partial}{\partial s}\left(\vec{\tau} \times \frac{\partial \vec{\tau}}{\partial s}\right) \\ &= (N-P)\vec{\tau} + EI\, \vec{\tau} \times \left(\vec{\tau} \times \frac{\partial^2 \vec{\tau}}{\partial s^2}\right) \\ &= (N-P)\vec{\tau} + EI \left[\left(\vec{\tau} . \frac{\partial^2 \vec{\tau}}{\partial s^2}\right)\vec{\tau} - \frac{\partial^2 \vec{\tau}}{\partial s^2}\right]. \end{aligned} \tag{2.39}$$

After some further manipulations involving the use of some properties of $\vec{\tau}$ and its derivatives (given in Appendix 1) and the projection along x and y, one obtains the following equations (corresponding to equations (2.17) and (2.18) in Lundgren's et al. paper):

$$(m+M)g - EI\frac{\partial^4 x}{\partial s^4} + \frac{\partial}{\partial s}\left[(N-P - EI\kappa^2)\frac{\partial x}{\partial s}\right] = m\frac{\partial^2 x}{\partial t^2} + M\frac{D^2 x}{Dt^2}$$

$$- EI\frac{\partial^4 y}{\partial s^4} + \frac{\partial}{\partial s}\left[(N-P - EI\kappa^2)\frac{\partial y}{\partial s}\right] = m\frac{\partial^2 y}{\partial t^2} + M\frac{D^2 y}{Dt^2}. \tag{2.40}$$

These two equations, of course, are coupled through the curvature κ, the axial force (N-P) and the inextensibility condition. The first equation is integrated from s to L, divided by $\partial x/\partial s$ to yield $(N-P-EI\kappa^2)$, and x is eliminated through the inextensibility condition. After many straightforward but tedious manipulations, one finally finds the same equation as that obtained by the energy method, i.e.

$$
\begin{aligned}
&(m+M)\,\ddot{y} + 2MU\dot{y}'(1+y'^2) + (m+M)\,gy'(1+\frac{1}{2}y'^2) \\
&+ y''\left[\, MU^2(1+y'^2) + (M\dot{U} - (m+M)\,g)\,(L-s)\,(1+\frac{3}{2}y'^2)\,\right] \\
&+ EI\left[\, y''''(1+y'^2) + 4\,y'y''y''' + y''^3\,\right] \\
&-y''\left[\int_s^L\int_0^s (m+M)\,(\dot{y}'^2+y'\ddot{y}')\,ds\,ds + \int_s^L (\frac{M\dot{U}}{2}y'^2+2MU\dot{y}'y'+MU^2y'y'')\,ds\right] \\
&+y'\int_0^s (m+M)\,(\dot{y}'^2+y'\ddot{y}')\,ds \;=\; 0.
\end{aligned}
\tag{2.41}
$$

Note that, in this derivation, the order needed was only $O(\epsilon^3)$ and terms of order $O(\epsilon^4)$ could be neglected.

2.5 PHYSICAL DISCUSSION OF THE EQUATION OF MOTION - NONDIMENSIONALIZED EQUATION

Before tackling the complete equation, its linear version is already of some interest

$$
\begin{aligned}
&EI\,y'''' + MU^2y'' + M\dot{U}(L-x)\,y'' + 2MU\dot{y}' \\
&- (m+M)\,g(L-x)\,y'' + (m+M)\,gy' + (m+M)\,\ddot{y} = 0.
\end{aligned}
\tag{2.42}
$$

First of all, this is the same equation as the one derived by Paidoussis and Issid (1974). One can find

- the inertia force = $(m + M)\ \partial^2 y/\partial t^2$,
- the Coriolis force = $2\ MU\ \partial^2 y/\partial x \partial t$,
- the centrifugal force = $MU^2\ \partial^2 y/\partial x^2$,
- forces due to gravity = $-(m + M)g\ [(L - x)\ y']'$,
- the flexural restoring force = $EI\ \partial^4 y/\partial x^4$,
- forces due to unsteady flow $\propto M\ dU/dt$.

Of course, dissipative terms have to be added to complete the equations. This is done by assuming that the internal dissipation of the pipe material is viscoelastic and of the Kelvin-Voigt type (Snowdon 1968). Moreover, this approximation is only applied on the linear restoring force, providing an additional term in the equation

$$E^* I \frac{\partial}{\partial t}\left(\frac{\partial^4 y}{\partial s^4}\right),$$

where E^* is the coefficient of viscosity, or the coefficient of internal dissipation. Other than for reasons of simplicity, and because, in any case, the Kelvin-Voigt dissipation is only an approximation, there is no justification for ignoring the effect of dissipation on the nonlinear flexural terms (see Appendix 3); nevertheless, for small dissipation, lumping all dissipative effects in a single term is justifiable. The damping associated with frictional forces due to surrounding air is neglected. Finally, a linear spring is also added, as explained in the Introduction. Acting only in the y-direction at a distance x_s, the spring, with a constant spring stiffness k, contributes to the equation by the term

$$k\ y\ \delta(x - x_s), \qquad (2.43)$$

where δ is the Dirac delta function, and where it is noted that k has units of force per unit length (note that δ has a unit of 1/displacement).

Introducing next the same nondimensional quantities as in the linear case,

$$\xi = \frac{x}{L},\ \eta = \frac{y}{L},\ \tau = \left(\frac{EI}{m+M}\right)^{\frac{1}{2}} \frac{t}{L^2},\ \alpha = \left(\frac{I}{E(m+M)}\right)^2 \frac{E^*}{L^2},$$
$$U = \left(\frac{M}{EI}\right)^{\frac{1}{2}} UL,\ \gamma = \frac{m+M}{EI} L^3 g,\ \beta = \frac{M}{m+M},\ K = \frac{kL^3}{EI}, \tag{2.44}$$

(2.34) may be rewritten in dimensionless form as follows:

$$\begin{aligned} &\alpha\,\dot{\eta}'''' + \eta'''' + \ddot{\eta} + 2U\sqrt{\beta}\,\dot{\eta}'(1+\eta'^2) + K\eta\,\delta(\xi-\xi_s) \\ &+ \eta''\left[U^2(1+\eta'^2) + (\dot{U}\sqrt{\beta}-\gamma)(1-\xi)\left(1+\frac{3}{2}\eta'^2\right)\right] \\ &+ \gamma\eta'\left(1+\frac{1}{2}\eta'^2\right) + \eta''''\eta'^2 + 4\eta'\eta''\eta''' + \eta''^3 \\ &- \eta''\left[\int_{\xi}^{1}\int_{0}^{\xi}(\dot{\eta}'^2+\eta'\ddot{\eta}')\,d\xi\,d\xi + \int_{\xi}^{1}\left(\frac{\dot{U}\sqrt{\beta}}{2}\eta'^2+2U\sqrt{\beta}\,\eta'\dot{\eta}'+U^2\eta'\eta''\right)d\xi\right] \\ &+ \eta'\int_{0}^{\xi}(\dot{\eta}'^2+\eta'\ddot{\eta}')\,d\xi\,d\xi = 0. \end{aligned} \tag{2.45}$$

Also of particular interest is the appearance in (2.45) of some nonlinear inertial terms that have to be replaced, as explained in the next section.

Physically, U in (2.45) is the nondimensional fluid velocity, γ represents the measure of relative gravity forces to the flexural one, β is the ratio of the fluid mass to the total mass per unit length, K represents the relative strength of the linear spring vis-à-vis the flexural restoring forces. For positive γ, the pipe is hanging, while for negative γ, the pipe is "standing" with the free end above the fixed one.

2.6 TRANSFORMATION OF THE NONLINEAR INERTIAL TERMS

In dynamical theory, it is convenient to write the equations into a standard, first-order form, namely

$$\dot{x} = f(x,t),\ x \in \mathbb{R}^n,\ t \in \mathbb{R}, \tag{2.46}$$

where f is a nonlinear function of x and t. Therefore, no nonlinear inertial terms may be present. A perturbation procedure is applied here, to replace the nonlinear inertial terms in (2.45) with the first order terms.

As it was introduced in Section 2.3.2., ϵ represents a small parameter. Equation (2.38) can thus be written as

$$L(\eta) + [N_1(\eta) + N_2(\eta)] = O(\epsilon^4), \tag{2.47}$$

in which L(η) represents the linear terms (order O(ϵ)) and N_i the nonlinear terms (of order O(ϵ^3));

$$L(\eta) = \dot{\eta} + 2U\sqrt{\beta}\dot{\eta}' + \eta''[U^2 + (\dot{U}\sqrt{\beta} - \gamma)(1-\xi)] + \gamma\eta' + \eta'''',$$

$$N_1(\eta) = 2U\sqrt{\beta}\dot{\eta}'\eta'^2 + \eta''\left[U^2 + \frac{3}{2}(\dot{U}\sqrt{\beta} - \gamma)(1-\xi)\right]\eta'^2 + \frac{\gamma\eta'^3}{2} + \eta''''\eta'^2 + 4\eta'\eta''\eta''' + \eta''^3,$$

$$N_2(\eta) = \eta'\int_0^{\xi}(\dot{\eta}'^2 + \eta'\ddot{\eta}')\,d\xi - \eta''\left[\int_{\xi}^{1}\int_0^{\xi}(\dot{\eta}'^2 + \eta'\ddot{\eta}')\,d\xi\,d\xi + \int_{\xi}^{1}\left(\frac{\dot{U}\sqrt{\beta}}{2}\eta'^2 + 2U\sqrt{\beta}\eta'\dot{\eta}' + U^2\eta'\eta''\right)d\xi\right] \tag{2.48}$$

(for simplicity, α and K are not taken into account here). By By properly rescaling the variable η, equation (2.47) can also be represented by

$$L(\eta) + \epsilon'[N_1(\eta) + N_2(\eta)] = 0, \tag{2.49}$$

where ϵ' represents a small parameter.

The term of major interest is

$$M(\ddot{\eta}) \; - \; \int_0^{\xi} \eta' \ddot{\eta}' d\xi ;$$

it appears within the two integrals in $N_2(\eta)$. The idea is to write an equivalent of that term to order ϵ' as in a usual perturbation technique. If the study were limited to first order (in ϵ') analysis, as all nonlinear terms are cubic, one would have

$$\eta \; - \; \eta_0 + O(\epsilon'),$$

$$L[\eta_0] \; - \; 0,$$

by collecting zero-order coefficients of ϵ'. L being linear, $L(\eta_0')$ is clearly defined, so that

$$\int_0^{\xi} \eta_0' \, L(\eta_0') \; d\xi \; - \; 0,$$

$$\int_0^{\xi} \eta' \, L(\eta') \; d\xi \; - \; O(\epsilon'). \tag{2.50}$$

Consequently, after the substitution of $L(\eta)$ in (2.49) and some rearrangements, one obtains the desired term

$$\int_0^{\xi} \eta' \ddot{\eta}' d\xi = - \int_0^{\xi} [2U\sqrt{\beta}\,\eta'\dot{\eta}'' + \eta'\eta'''(U^2 + (\dot{U}\sqrt{\beta} - \gamma)(1-\xi)) + \eta'\eta''(2\gamma - \dot{U}\sqrt{\beta}) + \eta'\eta''''' \,] \, d\xi + O(\epsilon'). \tag{2.51}$$

Integration of (2.51) from ξ to 1 yields the other nonlinear inertial term. Finally, after some long but straightforward manipulations, one obtains

$$\ddot{\eta} + 2U\sqrt{\beta}\,\dot{\eta}' + \eta''(U^2 + (\dot{U}\sqrt{\beta} - \gamma)(1-\xi)) + \gamma\eta' + \eta'''' + \epsilon' N(\eta) = 0, \tag{2.52}$$

where

$$N(\eta) = 2U\sqrt{\beta}\,\dot{\eta}'\eta'^{2} + \eta''\left[U^{2} + \frac{3}{2}(\dot{U}\sqrt{\beta}-\gamma)(1-\xi)\right]\eta'^{2}$$
$$+ \frac{1}{2}(\dot{U}\sqrt{\beta}-\gamma)\eta'^{3} + 3\eta'\eta''\eta''' + \eta''^{3}$$
$$+ \eta'\int_{0}^{\xi}\{\dot{\eta}'^{2}-2U\sqrt{\beta}\,\eta'\dot{\eta}''-\eta'\eta'''[U^{2}+(\dot{U}\sqrt{\beta}-\gamma)(1-\xi)]+\eta''\eta''''\}\,d\xi\,d\xi$$
$$- \eta''\int_{\xi}^{1}\int_{0}^{\xi}\{\dot{\eta}'^{2}-2U\sqrt{\beta}\,\eta'\dot{\eta}''-\eta'\eta'''[U^{2}+(\dot{U}\sqrt{\beta}-\gamma)(1-\xi)]+\eta''\eta''''\}\,d\xi\,d\xi$$
$$- \eta''\int_{\xi}^{1}\{(\dot{U}\sqrt{\beta}-\gamma)\eta'^{2} + 2U\sqrt{\beta}\,\eta'\dot{\eta}' + U^{2}\eta'\eta'' + \eta''\eta'''\}\,d\xi. \qquad (2.53)$$

2.7 CASE OF A PIPE FIXED AT BOTH ENDS

In this case, only the derivation by the energy method will be presented. Moreover, in order to simplify the derivation, the (u,v) notation will be used. As the inextensibility condition cannot be applied anymore, two equations will be derived, one in the x-direction and one in the y-direction. dX and ds are not identically equal anymore, but are still related through the condition

$$\frac{dX}{ds} = \frac{1}{1+\epsilon}. \qquad (2.54)$$

2.7.1 Strain energy

The strain energy will be used as defined in Section 2.4.3,

$$V = \frac{E}{2}\int_{0}^{L}[A\epsilon^{2} + I(1+\epsilon)^{2}\kappa^{2}]\,dX. \qquad (2.55)$$

Let θ be the angle between the position of the pipe and the X-axis to simplify this expression. θ is thus defined by

$$\begin{aligned} \sin\theta &= \frac{v'}{1+\epsilon(x)} \\ \cos\theta &= \frac{1+u'}{1+\epsilon(x)} \\ 1+\epsilon &= \sqrt{(1+u')^2+v'^2}, \end{aligned} \tag{2.56}$$

and the curvature κ becomes

$$\kappa = \frac{\partial\theta}{\partial s}. \tag{2.57}$$

Using the X-coordinate leads to

$$\kappa = \frac{\partial\theta}{\partial X}\frac{\partial X}{\partial s} = \frac{1}{1+\epsilon}\frac{\partial\theta}{\partial X},$$

which simplifies the expression (2.55) to

$$V = \frac{E}{2}\int_0^L [A\epsilon^2 + I(\frac{\partial\theta}{\partial X})^2]\, dX. \tag{2.58}$$

$\partial\theta/\partial X$ is found <u>exactly</u> by differentiation of $\tan\theta$,

$$\begin{aligned} \tan\theta &= \frac{v'}{1+u'} \\ \frac{\theta'}{\cos^2\theta} &= \frac{v''(1+u') - v'u''}{(1+u')^2} \\ \theta' = \frac{\partial\theta}{\partial X} &= \frac{v''(1+u') - v'u''}{(1+u')^2+v'^2}. \end{aligned}$$

In order to get an exact expression for the potential, one has to find an exact expression of θ' up to 4th order without making any prior simplification. Thus, recalling that u is of second order $O(\epsilon^2)$ and v of first order $O(\epsilon)$,

$$\theta' = v'' - v''u' - v''v'^2 - v'u'' + O(\epsilon^5)$$
$$\theta'^2 = v''^2 - 2v''^2u' - 2v''^2v'^2 - 2v'v''u'' + O(\epsilon^5) . \qquad (2.59)$$

Moreover, in the axial direction, an external tension might be applied, leading to

$$V = \frac{EA}{2}\int_0^L \left(\frac{T_0}{EA} + \epsilon\right)^2 dX + \frac{EI}{2}\int_0^L \left(\frac{\partial\theta}{\partial X}\right)^2 dX. \qquad (2.60)$$

2.7.2 Gravitational energy

The expression is the same as in Section 2.3.4., i.e.

$$G = -(m + M)\, g \int_0^L (X + u)\, dX. \qquad (2.61)$$

2.7.3 Right-hand side of Hamilton's principle

This is simply zero, since $\vec{r}$ (vector position at the end) does not vary in this case: $\delta\vec{r}_L = 0$.

2.7.4 Kinetic energy

As the right-hand side in the statement of Hamilton's principle is equal to 0 for a pipe fixed at both ends, it is clear that the contribution of the fluid forces is not the same as in the case of the cantilevered pipe. Hence, the derivation of the kinetic energy is very important. Although the inextensibility condition is not true anymore, one basic assumption still holds, the incompressibility of the fluid.

When a bar is loaded with tension, the axial elongation is accompanied by a lateral contraction, i.e. the width of the bar becomes smaller as its length increases. Within the elastic range, the Poisson ratio ν is constant (Timoshenko and Gere 1961),

$$\nu = \frac{\text{lateral strain}}{\text{axial strain}}.$$

For a cube of length 1, after loading, one has

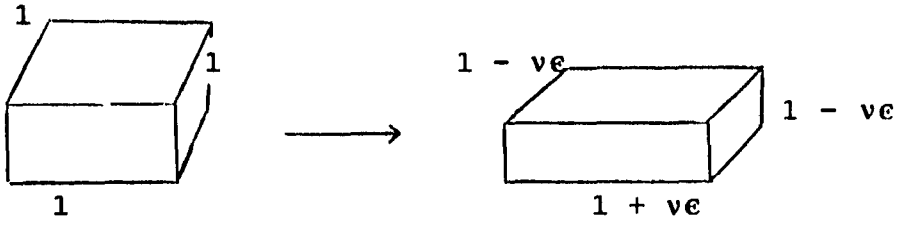

Figure II(c)

The change of volume is

$$\Delta V = V_2 - V_1$$

$$\Delta V = (1 + \epsilon)(1 - \nu\epsilon)^2 - 1$$
$$= \epsilon(1-2\nu) + O(\epsilon^2).$$

But actually for rubber-like material, $\nu = 0.5$; here, this will be simplified by taking $\nu = 0.5$. Thus, $\Delta V = 0$.

In the case of a beam, this conservation of volume leads, for any initial volume of length dx, to

$$dx.S_0 = dx\,(1 + \epsilon)\,S_1.$$

The rate of mass being constant, as ρ itself is constant, one also obtains

$$U_0 S_0 = U_1 S_1,$$

$$U_1(X) = U_0 \frac{S_0}{S_1} = U_0(1 + \epsilon). \qquad (2.62)$$

This shows that the velocity of the fluid with respect to the pipe is not constant. Hence, the absolute velocity is

$$\vec{V}_F = \vec{V}_P + U(X)\vec{\tau}$$

$$= (\dot{x}\vec{i} + \dot{y}\vec{j}) + U(1+\epsilon)\left(\frac{x'}{1+\epsilon}\vec{i} + \frac{y'}{1+\epsilon}\vec{j}\right)$$

as by definition $\epsilon = (x'^2 + y'^2)^{1/2} - 1$. Consequently,

$$\vec{V}_F = \left(\frac{\partial}{\partial t} + U\frac{\partial}{\partial X}\right)\vec{r}. \qquad (2.63)$$

The relationship (2.22) derived in Section 2.3.5 is still valid. The only difference is that the inextensibility condition is not valid, so that U^2 terms in this case appear from the kinetic energy and not from the right-hand side of (2.12). Hence,

$$T_P = \frac{m}{2}\int_0^L (\dot{u}^2+\dot{v}^2)\, dX, \qquad (2.64a)$$

$$T_F = \frac{M}{2}\int_0^L [(\dot{u} + U(1+u'))^2 + (\dot{v} + Uv')^2]\, dX. \qquad (2.64b)$$

2.7.5 Derivation of the equation of motion

Variational techniques are applied again, with two independant variants, δu and δv. After many integrations by parts, one finally obtains

$$(m+M)\ddot{u} + M\dot{U} + 2MU\dot{u}' + MU^2u'' + M\dot{U}u'$$
$$-E\bar{I}(v''''v'+v''v''') + (T_0-EA)v'v'' - EA\,u'' \qquad (2.65a)$$
$$-(m+M)\,g = 0,$$

$$
\begin{aligned}
&(m + M)\,\ddot{v} + M\dot{U}v' + 2MU\dot{v}' + MU^2v'' - T_0v'' \\
&+ EIv'''' - EI[3u'''v''+4u''v''' \\
&\qquad +2u'v''''+v'u''''+2v'^2v''''+8v'v''v'''+2v''^3] \\
&+ (T_0-EA)\,(u''v'+u'v''+\frac{3}{2}v'^2v'') \;=\; 0,
\end{aligned}
\tag{2.65b}
$$

where one now has two independent equations, instead of one.

2.8 ANALYSIS OF THE EQUATION - TRANSFORMATION OF THE PDEs INTO A SET OF ODEs

2.8.1 Discussion

Once the equations of motion have been derived, the next task is to choose a general approach to solve them. There are actually two different philosophies of analysis for doing so. The first one known as the Galerkin method consists of discretizing the equations to obtain a set of ODEs. The deflection of the pipe is expressed as the superposition of the infinite set of normal modes of a cantilever beam. This is admissible, as those functions satisfy the prerequisite conditions:

- same boundary conditions;
- linear independence.

Moreover, as outlined by Bisplinghoff et al. (1957), the system is very similar in its characteristics to a simple cantilever beam, since the mode shapes do not depend on physical properties, such as EI or ρ. Of course, this approach is useful only if the motion of the tube can be approximated adequately by a small number of these modes.

Gregory and Païdoussis (1966) proved that this was the case for small values of β ($\beta < 0.3$), but that for higher β, the third and higher cantilever modes begin to play an important role. Sugiyama et al. (1985) noted that "an increase of material damping suppresses the contribution of

higher modes and hence allows the lower mode approximation". In light of modern dynamics, this approach is valid, as the main purpose is to find qualitatively the characteristics of the system. This was justified by many authors, such as Païdoussis and Moon (1988) or Holmes (1977, 1978). According to Holmes (1977), "the two mode approximation exhibits the qualitative behaviour of 4, 6 or higher mode models, and of the full infinite dimensional system". He showed that the flows defined by the Galerkin approximation, in the panel problem, converge to the flow of the full nonlinear partial differential equation of the panel. The work done by Païdoussis et al. (1990) highlighted however some quantitative difference with the experiments. The main problem lies in the difficulty of estimating the error due to truncation. Some methods tend to improve the rate of convergence of the conventional mode superposition method (Léger and Wilson 1988), but cannot be applied here, as this finite element method is based on discretized equations.

The second method consists of keeping the original equation and trying to solve it. This was done by Gregory and Païdoussis (1966) with gravity neglected, but even in this case, the conditions of stability were difficult to find. For the nonlinear case, only Sethna's school (see Lundgren et al. 1979, Bajaj et al. 1980) and more recently Steindl and Troger (1988) provide other methods.

In conclusion, the discretization procedure is simpler in practice, but may introduce some quantitative errors in the results. Nevertheless, it provides a powerful qualitative tool, especially for small values of β, as in the case considered here.

2.8.2 Discretization procedure

The infinite dimensional model is discretized by Galerkin method, with the cantilever beam eigenfunctions $\phi_r(\xi)$ being used as a suitable set of base functions and $q_r(\tau)$ being

the corresponding generalized coordinates; thus,

$$\eta(\xi,\tau) = \sum \Phi_r(\xi)\, q_r(\tau). \tag{2.66}$$

Substituting the above expression into (2.53), multiplying by $\phi_i(\xi)$ and integrating from 0 to 1 leads to

$$0 = \ddot{q}_i + c_{ij}\dot{q}_j + k_{ij}q_j + \epsilon(\alpha_{ijkl}\, q_j q_k q_l + \beta_{ijkl}\, q_j q_k \dot{q}_l + \gamma_{ijkl}\, q_j \dot{q}_k \dot{q}_l), \tag{2.67}$$

where c_{ij}, k_{ij}, a_{ij}, b_{ij}, d_{ij}, α_{ijkl}, β_{ijkl} and γ_{ijkl} are coefficients computed from the integrals of the eigenfunctions $\phi_i(\xi)$, analytically (Paidoussis and Issid 1974) or numerically (Appendix 4).

Moreover, assuming that the fluid flow can have small sinusoidal fluctuations,

$$U \to U(1 + \epsilon\nu \sin \omega t), \tag{2.68}$$

certain terms should be added to (2.67), namely

$$+ \epsilon(2\sqrt{\beta} \sin\omega t\, a_{ij}\dot{q}_j + 2U\nu \sin\omega t\, b_{ij} q_j + \sqrt{\beta}\nu\omega \cos\omega t\, d_{ij} q_j).$$

In order to use the available tools of dynamics theory, the above second order equation is transformed into a set of first order ordinary differential equations. Introducing the generalized coordinates $p_i = \dot{q}_i$, (2.67) may be written in the matrix form

$$\begin{Bmatrix}\dot{q}\\ \dot{p}\end{Bmatrix} = \begin{bmatrix}0 & I\\ -K & -C\end{bmatrix}\begin{Bmatrix}q\\ p\end{Bmatrix} + \epsilon\{f(q,p)\} + \epsilon\nu\{g(q,p,t)\}, \tag{2.69}$$

i.e.

$$\dot{y} = [A]\, y + \epsilon f(y) + \epsilon\nu\, g(y,t), \tag{2.70}$$

where f is a 3rd order polynomial function ($O(\epsilon^3)$) (cubic nonlinear terms), g is a function of [a], [b] and [d], and [A] is a 2N x 2N matrix, $[A(U,G,\beta,K,\xi_s)]$. The computation of [A] can be found in Appendix 5 for a two-mode approximation (N = 2). Its remarkable simplicity should not go unnoticed.

CHAPTER III

COMPARISON WITH PREVIOUS DERIVATIONS

In this chapter, the nonlinear equations of motion obtained by different authors are described and compared in detail. Moreover, in order to get a more "comparable" set of equations, a standardization of the notation is undertaken.

3.1 CASE OF A CANTILEVERED PIPE

3.1.1 Bourrières' work

Bourrières' work is very original, all the more so since it was written in 1939. He studied the case of planar motion of two strings, one of them moving with respect to the other. The pipe and the fluid represented by the strings are assumed to be inextensible, and the string representing the fluid is supposed to be infinitely flexible. Using the force balance method, Bourrières obtained the equations relative to the tube and the fluid. The relationship between the shearing force Q and the bending moment M, and the condition of inextensibility provides the nonlinear terms. A set of seven equations with nine parameters is found, the phenomenon being dependent on two variables: the nonlinear coordinate s and the time t. After some algebraic manipulations, Bourrières eliminated the fluid friction force and found the following five equations:

$$\begin{cases} ((\theta+T)x')' - (Qy')' - (m+M)\ddot{x} - 2MU\dot{x}' - MU^2x'' = 0, \\ ((\theta+T)y')' + (Qx')' - (m+M)\ddot{y} - 2MU\dot{y}' - MU^2y'' = 0, \\ x'^2 + y'^2 = 1, \\ Q = -M', \\ M = EI\,(x'y'' - y'x'') = \dfrac{EI}{R}, \end{cases} \tag{3.1}$$

where R is the radius of curvature, and θ and T the tension in the tube and in the fluid, respectively. The approach given by Bourrières was very original and would have led him eventually to expressions similar to the ones derived in Chapter II. Unfortunately, Bourrières considered only the linear case for his study. Consequently, without approximation, the only difference lies in the dU/dt term, which is not surprising, since Bourrières had not taken into account any effect of unsteadiness in the flow. The expression for Q and M is correct, as well as the expression of the curvature. That makes Bourrières' work irreproachable. The next task is to combine all the five equations (3.1) into one equation, using all the relationships, and to compare this last one with (2.41). This will not be repeated here since it has already been done by Rousselet and Herrmann.

3.1.2 Rousselet and Herrmann's work

Rousselet and Herrmann (1977) derived the equations of motion in two different ways: the force balance method and the energy method. They obtained a final set of equations, fairly close to the one found in Chapter II, with some minor differences.

Their first method follows the work done by Bourrières, and thus, it is not surprising to find equations which are very similar to his. Two differences simply arise from the following:

- the addition of gravity forces;
- the assumption that unsteady flow velocity effects may be present.

The notation used by Rousselet and Herrmann is completely different, as they wanted to study articulated pipes. In that case, the introduction of θ, the angle of inclination of the pipe in the (x, y) plane, was more appropriate.

The application of Newton's law led them to

$$\begin{aligned}
&\frac{\partial}{\partial s}\left((N-P)\cos\theta\right) - \frac{\partial}{\partial s}\left(Q\sin\theta\right) + (m+M)g \\
&\quad = (m+M)\frac{\partial^2 x}{\partial t^2} + M\dot{U}\cos\theta - \frac{MU^2}{R}\sin\theta - 2MU\frac{d\theta}{dt}\sin\theta, \\
&\frac{\partial}{\partial s}\left((N-P)\sin\theta\right) + \frac{\partial}{\partial s}\left(Q\cos\theta\right) \\
&\quad = (m+M)\frac{\partial^2 y}{\partial t^2} + 2MU\frac{d\theta}{dt}\cos\theta + \frac{MU^2}{R}\cos\theta + M\dot{U}\sin\theta;
\end{aligned} \tag{3.2}$$

however, sin θ and cos θ are related to x and y by

$$\sin\theta = \frac{\partial y}{\partial s},$$

$$\cos\theta = \frac{\partial x}{\partial s}.$$

Using the inextensibility condition and the definition of the curvature κ, it is easy to prove that

$$\begin{aligned}
\frac{1}{R}\frac{\partial x}{\partial s} &= \frac{\partial^2 y}{\partial s^2}, \\
-\frac{1}{R}\frac{\partial y}{\partial s} &= \frac{\partial^2 x}{\partial s^2}.
\end{aligned} \tag{3.3}$$

Rewriting again (3.2) and (3.3), one obtains

$$\begin{aligned}
&\frac{\partial}{\partial s}\left((N-P)\frac{\partial x}{\partial s}\right) - \frac{\partial}{\partial s}\left(Q\frac{\partial y}{\partial s}\right) + (m+M)g \\
&\quad = (m+M)\frac{\partial^2 x}{\partial t^2} + 2MU\frac{\partial^2 x}{\partial s\partial t} + MU^2\frac{\partial^2 x}{\partial s^2} + M\dot{U}\frac{\partial x}{\partial s}, \\
&\frac{\partial}{\partial s}\left((N-P)\frac{\partial y}{\partial s}\right) + \frac{\partial}{\partial s}\left(Q\frac{\partial x}{\partial s}\right) \\
&\quad = (m+M)\frac{\partial^2 y}{\partial t^2} + 2MU\frac{\partial^2 y}{\partial s\partial t} + MU^2\frac{\partial^2 y}{\partial s^2} + M\dot{U}\frac{\partial y}{\partial s}.
\end{aligned} \tag{3.4}$$

In this form, the similarity with Bourrières' equations is self-evident. Note that κ and the condition of inextensibility have already been used implicitly. At this stage, Rousselet and Herrmann have manipulated the whole set of equations to arrive at a final one. This will be discussed after the presentation of their energy method.

One should emphasize the originality of the variational technique used by the authors. Indeed, they derived a "Hamilton's principle in the case of a cantilevered pipe conveying fluid", different from Benjamin's. They started from d'Alembert's generalized principle applied to a single particle, and then, introduced a control volume (an infinitesimal volume) containing a certain number of particles. The fluid particles were allowed to enter or leave the control volume with a known motion (U in practice). Substituting the resulting particle acceleration to the governing equation of motion led them to another expression of Hamilton's principle for systems of changing mass. The description of the derivation can be found in Rousselet's thesis (1975). Finally, a unique equation, identical to the one obtained through the force balance method, was found.

With the different relationships defined in Rousselet's thesis, it was possible to convert that equation into standard notation. After some manipulations, the nondimensional equation found is

$$\ddot{\eta} + 2U\sqrt{\beta}\dot{\eta}'(1+\dot{\eta}'^2) + \eta''\left[U^2(1+\eta'^2) - \gamma(1-\xi)\left(1+\frac{3}{2}\eta'^2\right) + \dot{U}\sqrt{\beta}(1-\xi)\right]$$

$$+ \gamma\eta'\left(1+\frac{1}{2}\eta'^2\right) + \eta''''(1+\eta'^2) + 4\eta'\eta''\eta''' + \eta''^3 + \eta'\int_0^{\xi}(\ddot{\eta}'^2+\eta'\ddot{\eta}')\,d\xi$$

$$- \eta''\left[\int_{\xi}^{1}\int_0^{\xi}(\dot{\eta}'^2+\eta'\ddot{\eta}')\,d\xi\,d\xi + \int_{\xi}^{1}(2U\sqrt{\beta}\eta'\dot{\eta}'+U^2\eta'\eta'')\,d\xi\right] = 0. \qquad (3.5)$$

Thus, two differences can be pointed out in the nonlinear terms of the unsteady velocity. These differences come from an error in the following relationship used by Rousselet and Herrmann,

$$\int_0^L F(x)\left(\int_0^x (\tan\theta)'\right)\delta w dx dx - \int_0^L \left(\int_x^L F(x)\,dx\right)(\tan\theta)'\delta w dx. \quad (3.6)$$

This relationship is correct, but if F is of order 0, then $\tan\theta$ must be taken to the third order, which was not done. As explained in Section 2.3.2, this relationship (derived in 2.3.6) had to be rigorous up to order $O(\epsilon^4)$. Except for these two differences (which might be negligible), (2.41) and (3.5) given by Rousselet and Herrmann are the same. This gives confidence in the correctness of the equation derived in this thesis, since the derivations are based on two different starting points and on two different methods.

Rousselet and Herman also considered the effects on the fluid of the friction or of a pressure drop, and derived a flow equation. The two partial differential equations are coupled through the nonlinear terms.

3.1.3 Sethna's work

Lundgren, Sethna and Bajaj (1979) derived equations of motion by the force balance method. The assumptions made are the same as in the other work; but from a mathematical point of view, they tried to be as rigorous as possible. The force balance method in Section 2.4 follows the same procedure, so that all their equations were checked very carefully and appeared to be exact. They used:

- the condition of inextensibility;
- the exact expression for curvature.

All the nonlinearities are related to the $(N\text{-}P\text{-}EI\kappa^2)$: κ is nonlinear, but also N-P (axial force and pressure drop) through a nonlinear integral.

They stopped their derivation at an early stage, without taking advantage of the inextensibility condition. In their subsequent paper (Bajaj et al. 1980), some nonlinear terms are apparently missing, especially nonlinear velocity-dependent terms. Under the form of an integrodifferential set of equations and neglecting, for the moment, the unsteady flow velocity, one may read (Equation 5 in their paper)

$$\begin{cases} \left(\frac{\partial x}{\partial s}\right)^2+\left(\frac{\partial y}{\partial s}\right)^2 = 1 \\ EIy'''' + 2MU\dot{y}' + MU^2y'' + (m+M)\ddot{y} = NL, \end{cases} \tag{3.7}$$

where

$$NL = -\frac{3}{2}EI\frac{\partial}{\partial s}\left(y'\left(x''^2+y''^2\right)\right) - (m+M)\frac{\partial}{\partial s}\left(y'\int_s^L (x'\ddot{x}+y'\ddot{y})\,ds\right).$$

At first glance these equations seem wrong (as no nonlinear velocity-dependent terms are present); however, they are absolutely right. They have been obtained by the force balance method in which the evaluation of the nonlinear terms related to (N-P) has been carried out by projection onto the $\vec{j}$th and $\vec{\tau}$th direction, and not the $\vec{i}$th and $\vec{j}$th direction (Fig.2.1). The U and U^2 terms are actually hidden in the nonlinear inertial term. Indeed, eliminating x through the condition of inextensibility leads to

$$\begin{aligned} &(m+M)\ddot{y}(1-y'^2) + 2MU\dot{y}' + MU^2y'' \\ &+ EI\left(y'''' + 3y'y''y''' + \frac{3}{2}y''^3\right) \\ &+ y'\int_0^s (m+M)\left(\dot{y}'^2+y'\ddot{y}'\right)ds \\ &- y''\left(\int_s^L\int_0^s (m+M)\left(\dot{y}'^2+y'\ddot{y}'\right)dsds - \int_s^L (m+M)\ddot{y}y'ds\right) = 0. \end{aligned} \tag{3.8}$$

In order to show that this equation can be brought to a familiar form, one considers the linear equation and uses a perturbation technique, as in Section 2.6.
From

$$(m+M)\ \ddot{y} + 2MU\dot{y}' + MU^2y'' + EIy'''' = 0,$$

one has, after multiplication by y' and integration from s to L,

$$\int_s^L (m+M)\ \ddot{y}y'ds = -\int_s^L [2MU\dot{y}'y' + MU^2y''y']\ ds - EI\int_s^L y''''y'ds$$
$$= -\int_s^L [2MU\dot{y}'y' + MU^2y''y']\ ds + EIy'''y' - \frac{1}{2}EIy''^2. \tag{3.9}$$

Multiplying $(1+y'^2)$ throughout (3.8), keeping cubic nonlinear terms and replacing nonlinear inertial terms, leads after manipulations to

$$\begin{aligned}
&(m+M)\ddot{y} + 2MU\dot{y}'(1+y'^2) + MU^2y''(1+y'^2) \\
&+ EI\left(y''''(1+y'^2) + 3y'y''y''' + \frac{3}{2}y''^3\right) \\
&- y''\left(\int_s^L\int_0^s (m+M)\ (\dot{y}'^2+y'\ddot{y}')\ dsds\right. \\
&\left. + \int_s^L [2MU\dot{y}' + MU^2y''y']\,ds - EIy'''y' + \frac{1}{2}EIy''^2\right) \\
&+ y'\int_0^s (m+M)\ (\dot{y}'^2+y'\ddot{y}')\ ds = 0.
\end{aligned} \tag{3.10}$$

This equation is obviously identical to (2.41) after the addition of the unsteady and gravitation terms.

In conclusion, their derivation is irreproachable. No linear terms are missing, except the gravity terms that have been neglected. However, the different steps from one equation to another were not very clear; hence, verification was not easy. They used some implicit relationships of the curvature (given in Appendix 1) and a perturbation procedure that was not explained either.

Finally, like Rousselet and Herrmann, they also found an equation for the flow velocity, by considering a force balance method on a fluid element,

$$M\alpha\,(U_0^2-U^2) \;-\; M\int_0^L (\ddot{x}x' + \ddot{y}y')\,ds \;-\; M\dot{U}L \;=\; 0\,, \qquad (3.11)$$

where U_0 is the constant flow velocity when the tube is not in motion, α represents the resistance to the fluid motion (proportional to a friction factor) and $M\alpha U_0^2$ represents the constant pressure force at the fixed end s = 0 of the tube.

3.2 CASE OF A PIPE FIXED AT BOTH ENDS

In this section, three papers are discussed, as they are representative of all the derivations. Again, a standardization of the notation is undertaken. Many differences have been found, most of them due to the assumptions made, but some of them also due to erroneous derivation.

3.2.1 Thurman and Mote's work

As pointed out in the Introduction, Thurman and Mote (1969) were mainly concerned with the oscillations of bands of moving materials. They considered an axially-moving strip, simply supported at its ends, and tried to show how the axial

motion could significantly reduce the applicability of the linear analysis. The centreline being extensible, nonlinearities are associated with the axial tube elongation and the extension-induced tension in the tube. Therefore, the strain and the tension have the general form

$$\begin{aligned} \epsilon &= \frac{T_0}{EA} + \sqrt{(1+u')^2+v'^2}-1, \\ T &= T_0 + EA(\sqrt{(1+u')^2+v'^2}-1). \end{aligned} \tag{3.12}$$

Since they considered a linear moment curvature relationship and a linear approximation for the velocities, the equations of motion they obtained are

$$EI\, v'''' - (T_0 - MU^2)\, v'' + 2MU\dot{v}' + (m+M)\,\ddot{v} = (EA-T_0)\left(\frac{3}{2}v'^2v'' + u'v'' + u''v'\right)$$

$$M\ddot{u} - EA\, u'' = (EA - T_0)\, v'v''. \tag{3.13}$$

These are actually a simplified set of (2.65). The differences come from the assumptions made:

- no gravity forces,
- steady flow velocity,
- linear moment-curvature relationship,
- simple approximation of the fluid velocity.

Consequently, on the basis of the assumptions made, the equations derived are correct, which should be underlined as they were derived more than twenty years ago!

3.2.2 Holmes' work

Holmes was one of the first to use the new tools of modern dynamics, and thus, he was not concerned with the derivation of the equations. He only considered the nonlinear term associated with the deflection-induced tension in the pipe. From the linear equations obtained by Païdoussis and Issid (1974), he added the effect of the axial extension. To

a first order approximation, he considered the axial force induced by lateral motions equal to

$$H = \sigma A = (Ee + \eta \dot{e})\, A,$$

with

$$e = -\frac{1}{2}\int_0^L (y')^2\, ds,$$

and with the assumption of Kelvin-Voigt viscoelasticity. Thus, the axial force H is added to the linear equation, where

$$H = -\frac{EA}{2L}\int_0^L (y'^2)\, ds - \frac{\eta A}{L}\int_0^L (y'\dot{y}')\, ds. \qquad (3.14)$$

The addition of this extra deflection-dependent axial force leads to one equation with two cubic, nonlinear terms. Consequently, the only essential nonlinearity is related to the extensibility. This is explained by the fact that his work took place at an early stage in the research in the field of nonlinearities. As a mathematician, he was more interested in studying an existing equation rather than deriving it. Of particular interest is the manifestation of nonlinear viscous damping. However, the assumption of Kelvin-Voigt viscoelasticity for the pipe is already an approximation (Snowdon 1968).

3.2.3 Namachchivaya and Tien's work

This study is one of the most recent ones and is thus, of particular interest. The equation of motion is derived from the energy principle, and the methodology follows the one proposed by Paidoussis and Issid (1974), who were looking for a linear equation.

A linear moment-curvature relationship is assumed, and gravity is neglected.

For the axial strain, first order nonlinearities are considered, leading to

$$V = \frac{EA}{2} \int_0^L \left(\frac{T_0}{EA} + u' + \frac{1}{2} v'^2\right)^2 dx. \qquad (3.15)$$

This is not justified, as explained in Section 2.3.2. Indeed, to find 3rd order nonlinearities, the strain energy has to be exact to the 4th order, which is not the case here. Moreover, with the above definition and the application of the variational techniques, expressions in the u and v directions should appear (equation in δu and δv), which are missing.

Concerning the expression of the kinetic energy and Hamilton's principle, the following comments may be outlined.

a) Hamilton's principle is used in its linear form

$$\delta \int_{t_1}^{t_2} L \, dt = \int_{t_1}^{t_2} \left[-MU^2 \, \delta C_L + MU(\dot{v}_L + U v'_I) \delta v_L\right] dt \, , \qquad (3.16)$$

with the definition of the axial contraction

$$c_x = \frac{1}{2} \int_0^x v'^2 \, d\xi .$$

There is no justification for doing so in a nonlinear analysis.

b) With the above definitions, $C_L \neq 0$, so that the right-hand side of (3.16) does not vanish, which is in contradiction with the derivation made.

c) As in the potential energy case, the kinetic energy must be exact to 4th order. Namachchivaya and Tien took the following expression

$$T_F = \frac{M}{2}\int_0^L [(\dot{v} + Uv')^2 + [U(1 - \frac{1}{2}v'^2) - \dot{C}_x]^2]\,dx. \quad (3.17)$$

This hybrid expression is incorrect (the factor U is missing in front of C_x); even if correct, it would only be valid for a linear analysis of the cantilevered pipe (Housner 1952, McIver 1973 and Section 2.7.4). Finally, the equation obtained is

$$(m+M)\,\ddot{v}+2MU\dot{v}'+[MU^2-T_0+M\dot{U}(L-x)]\,v''+EIv''''-EA[(u'+\frac{1}{2}v'^2)\,v']' = 0.$$

By defining an average axial strain

$$\epsilon_0(t) = \frac{1}{L}\int_0^L (u'+\frac{1}{2}v'^2)\,dx = \frac{1}{2L}\int_0^L v'^2 dx,$$

this equation, in the end, is the same as the one derived by Holmes (1977). Consequently, some terms involving EA are missing, as well as nonlinear terms associated with the fluid velocity. Many mistakes were found in the derivation itself.

CHAPTER IV
LINEAR ANALYSIS

Systems of physical interest have parameters which appear in the defining system of equations; for example, in the present study, such parameters are the flow velocity U, the mass ratio β and the spring stiffness K. In dynamics, this is described by the following equation

$$\dot{x} = f_{\mu}(x); \quad x \in \mathbb{R}^n, \quad \mu \in \mathbb{R}^k, \tag{4.1}$$

where μ represents a k-dimensional parameter (Iooss and Joseph 1981). Bifurcations are said to occur when the system exhibits more than one, and usually qualitatively different, states as the system parameter μ goes through a critical value. A bifurcation set consists of the loci in μ-space which correspond to systems for which structural stability breaks down in specific ways. Bifurcation diagrams are the loci in the (x,μ) product space of parts of the invariant set of (4.1). Local bifurcations occur when some eigenvalue of the linearized system at a fixed point crosses the imaginary axis. It is therefore interesting to study the behaviour of the linearized system as a function of the system parameters. Consequently, the matrix [A] found in Chapter II (equation 2.70) is studied in great detail. Of course, when only two modes are considered, [A] is a 4 x 4 matrix.

Some classical bifurcations are sought by analyzing the eigenvalues of the matrix [A]:

- the Hopf bifurcation: [A] has a pair of purely imaginary eigenvalues;
- the Saddle-Node bifurcation: [A] has a zero eigenvalue;
- a Doubly-Degenerate bifurcation: [A] has both of them.

For a low dimensional problem, two different methods may be applied: Routh's criteria and a direct eigenvalue analysis.

4.1 ROUTH'S CRITERIA

4.1.1 Presentation of the method

Routh (1960) proved that if the characteristic equation can be written as

$$a_n \lambda^n + a_{n-1} \lambda^{n-1} + \ldots + a_0 = 0, \tag{4.2}$$

then, a necessary and sufficient condition for stability is that, provided a_n is positive, all the test determinants T_1 to T_n should be positive, where

$$T_1 = |a_{n-1}|$$

$$T_2 = \begin{vmatrix} a_{n-1} & a_n \\ a_{n-3} & a_{n-2} \end{vmatrix}$$

$$T_3 = \begin{vmatrix} a_{n-1} & a_n & 0 \\ a_{n-3} & a_{n-2} & a_{n-1} \\ a_{n-5} & a_{n-4} & a_{n-3} \end{vmatrix} \quad \ldots \tag{4.3}$$

If (4.2) is a quartic, these conditions become:

- static stability boundary: $\lambda = 0$
  i.e.: $a_0 < 0 \Rightarrow$ statically unstable
  $a_0 > 0 \Rightarrow$ statically stable;
- dynamic stability boundary: $T_3 = 0$
  and $a_1/a_3 > 0$ where
  $T_3 = a_1 a_2 a_3 - a_0 a_3^2 - a_4 a_1^2$;
- double degeneracy condition: $a_0 = 0$
  and $T_3 = 0$ which leads to
  $a_0 = 0$ and $a_1 = a_2 a_3$,
  since a_4 can be taken equal to 1.

All the coefficients a_0 to a_4 were computed analytically as functions of the main parameters U, γ, β, K and ξ_s using MACSYMA (Rand 1984) and are presented in Appendix 5.

4.1.2 Results[1]

All the conditions $a_0 = 0$, $T_3 = 0$ and $a_1 = a_2\, a_3$ are computed, solved numerically and then plotted in the parameter space.

i) Case without a spring

The boundary conditions are represented in the (β,U) space and in the (γ, U) space, with γ and β as control parameters, respectively.

For static instability (curve $a_0 = 0$ in Fig.4.1(a) independent of β), the correspondence with previous results is excellent (Fig.4.1(b) taken from Paidoussis (1970)), since the instability always occurs in the same mode and the influence of higher modes is not very important.

For dynamic instability (Figs.4.1-4.2(a,b), the correspondence is good, quantitatively and qualitatively, only when β is small ($\beta < 0.2$). For larger values of β, the influence of higher modes is considerable, which explains the differences found. Notice also the qualitative difference for very small values of β. Paidoussis in 1969, wrote "for still lower values of γ ($\gamma < -55.9$), both the first and second mode frequencies, for $U = 0$, lie on the imaginary axis. With increasing flow, the system does not regain stability." This is not what was found with Routh's criteria, which shows the existence of a minimum value of $U_{critical}$ not equal to zero.

In fact, the results presented in Fig.4.1(a) and Fig.4.2(a) are incomplete, since only the condition $T_3 = 0$ was

---

[1] It should be mentioned here that all the parameters are varied, except the damping coefficient $\alpha = 0.005$.

taken into account. Since a_3 is always positive (Appendix 5), the investigation of the coefficient a_1 (Fig.4.3) leads to the conclusion that Routh's criteria provide results only on the right side of the curve $a_1 = 0$. This demonstrates the limitations of the method: coupled-mode flutter cannot be predicted by Routh's criteria. Therefore, information concerning the dynamics may sometimes be lost.

Fig.4.4(a) shows that double degeneracy conditions are possible, since the two curves, $a_0 = 0$ and $a_1 = a_2\, a_3$ cross for some (β, γ) pair. These conditions are discussed in detail in the next section.

ii) Case with a spring

This case is general as it does include the previous when K = 0. It should be mentioned that the location of the spring is kept constant here, $\xi_s = 0.8$, for clarity. When this value was modified, only a qualitative change in the figures was observed.

Again, divergence is represented by the curve $a_0 = 0$. This condition is a second order equation in γ (for fixed U), leading consequently to either zero, one or two value(s) of γ a as solution (Appendix 5). The shapes of the solution curves can be divided into two classes, represented by the case K = 0 and the case K = 100 (Fig.4.5). For low values of K, divergence occurs only for negative γ, while it becomes possible for positive ones for large values of K. Hence, for a constant positive γ (hanging pipe), buckling occurs only if the stiffness is greater than a critical value K_{cr}. However, this critical value can be modified by changing the location of the spring: the bigger ξ_s, the smaller K_{cr}.

For flutter, Fig.4.6(a,b,c) illustrates the influence of the different parameters. The projection of the condition $T_3 = 0$ in various planes illuminates the influence of the parameters on the dynamic stability boundaries. For example, for a constant γ, the critical flow velocity

increases with β. One should note the qualitative similarity in each figure when a control parameter is changed. Again, only small values of β ($\beta < 0.3$) have been considered to satisfy the condition of the two-mode-model assumption. It should also be emphasized that the results agree very well with those given by Sugiyama et al. (1985), for the same number of degrees of freedom. Moreover, this two-mode approximation has an error of 1% for divergence and 10% for flutter, at $\beta = 0.25$, in comparison with an infinite dimensional model (Sugiyama et al. 1985). Thus, in an investigation of the qualitative behaviour of the pipe, this linear analysis is sufficient to provide a complete set of parameters (U, γ, β, K) to study all types of bifurcation. Indeed, this thesis is more concerned with the post-bifurcation behaviour than with the actual critical parameters where instability occurs, as will be seen in Chapter V.

The double degeneracy conditions were also studied extensively (Fig.4.7). As explained previously, these conditions are met when $a_0 = 0$ and $a_1 = a_2\ a_3$, written as

$$\begin{cases} f_1(U,\gamma,\beta,K) = 0, \\ f_2(U,\gamma,\beta,K) = 0. \end{cases}$$

From a numerical point of view, three of the four parameters are kept constant, and the fourth one is varied until the two conditions are satisfied. Of course, the two conditions are not always satisfied. Again, two different types of solution are found.

When $K < 40$, $U_{cr} = f(\gamma, \beta)$ is a "closed loop", i.e. a curve which retraces its path (no hysteresis). Fig.4.7(a) represent a projection of those closed loops in the (γ, U) plane, for different values of K, when β is varied as a control parameter ($0 < \beta < 0.3$). These closed loops are explained by the fact that the curve $a_0 = 0$ is independent of β while the curve $a_1 = a_2\ a_3$ is not univalent (or one-to-one)

as a function of β, in the (β, U) or (β, γ) plane (see Fig.4.4(b)). For small values of K, the range for γ to achieve a double degeneracy condition is rather small. Moreover, γ is negative in this range. This is not surprising, since the static instability is only due to the effect of gravity, when the stiffness of the spring is small.

When $K > 40$, all the curves have the same qualitative shape. Thus, only the results for $K = 100$ are presented. The range for γ is much larger, and the relevant fact is that double degeneracy can occur for positive values of γ (achievable more easily experimentally). Fig.4.7(c,d,e) represents different projections in the parameter space of the same conditions. They are, however, useful as they complete one another.

4.1.3 Conclusion

An extensive study of the linear equations was undertaken, bringing out the influence of each parameter on the critical conditions. It is important to mention that all the degeneracy conditions may be satisfied with various sets of parameters, which is remarkable. Hence, it will be easy to adjust the theoretical values to some experimental ones to get all the possible instabilities. Therefore, in the theoretical study, only a few sets of parameters are considered, without loss of generality, since only quantitative differences may be observed, if these parameters are modified.

4.2 DIRECT EIGENVALUE ANALYSIS

Since the analysis of Routh's criteria can only provide the boundaries of the instabilities, and in order to check the results previously obtained, a direct eigenvalue analysis was undertaken. Indeed, from Figs.4.1 - 4.6, it is difficult to tell what kind of instability occurs.

Two specific examples from the previous results were chosen; a complete study of the influence of all parameters would not yield a better insight into the problem, since most cases are qualitatively equivalent. Hence, the following cases were chosen:

- a case without a spring: $K = 0$ and $\beta = 0.001$;
- a case with a spring: $K = 100$ at $\xi_s = 0.8$ and $\beta = 0.18$.

The "poverty" of the results obtained by Routh's criteria for these two cases is shown in Fig.4.8(a,b). Only the boundaries can be represented, and it is not obvious how the system behaves within or outside them.

In the four-dimensional space $(q_1, q_2, \dot{q}_1, \dot{q}_2)$, as well as in the infinite one, the origin (0) is always a fixed (or equilibrium) point. To investigate its stability, the linearized form of the equation is solved for its eigenvalues λ_i, $i = 1, \ldots, 4$.

For a particular system, the four eigenvalues are plotted in the form of an Argand diagram (the imaginary part of the eigenvalue versus the real part), with the dimensionless flow velocity U as a parameter.

4.2.1 Case without a spring

All the results are summarized in Fig.4.9, for different values of γ. Each value of γ has been chosen to represent a different qualitative phenomenon.

i) $\gamma > -8$ ($\gamma = 0$ in Fig.4.9(a))

For low dimensionless flow velocity U, the four eigenvalues are in two complex conjugate pairs, $\lambda_2 = \lambda^*_1$ and $\lambda^*_4 = \lambda_3$ with negative real parts[2]; the origin is stable[3].

---

[2] The "*" denotes the complex conjugate of the eigenvalue.

[3] The negative real part at U = 0 comes from the effect of the viscoelastic dissipation. It may be recalled that $\alpha = 0.005$.

For U = 4.42, the real part of the first pair, Re ($\lambda_{1,2}$), becomes zero, while Im ($\lambda_{1,2}$) $\neq$ 0. This situation corresponds to the well-known Hopf bifurcation, $U = U_H$, represented physically by flutter-type, or in the nonlinear domain by limit-cycle motions.

The real parts of the other two eigenvalues λ_3, λ_4 remain negative with increasing U, and, hence, play no role in the stability of the system. This case corresponds qualitatively to system parameters used previously by Paidoussis et al. (1989) and confirms their results.

ii) $-31.4 < \gamma < -8$ ($\gamma = -20$ in Fig.4.9(b))

For zero nondimensional flow velocity, the situation is completely different from that in Fig.4.9(a). The first "pair" (λ_1, λ_2) is wholly real with λ_1 positive, while the other pair still remains a complex conjugate with negative real parts. Thus, the origin is statically unstable at U = 0, since no oscillatory component is associated with an eigenvalue with positive real part (Im (λ_1) = 0 and Re (λ_1) > 0). Physically, this corresponds to a case of divergence: the pipe is buckled under its own weight, and buckling occurs in the first mode.

When U is increased, the system regains stability ($\lambda_1 = 0$ at U = 2.9). As will be proved later (Chapter V), this corresponds to a subcritical pitchfork bifurcation.

Finally, at U = 3.55, the same case as in i) is encountered: the origin becomes unstable again (but dynamically, not statically) through a Hopf bifurcation. Note that the other two eigenvalues still play no role in determining stability (negative real part); both instabilities occur in the first mode.

iii) $48.43 < \gamma < -31.4$ ($\gamma = -40$ in Fig.4.9(c))

Again, at zero flow velocity, the origin is unstable; but this time, the system does not regain stability.

At U = 2.65, the second real eigenvalue λ_2 also becomes positive. Physically, no change can be observed, since no oscillatory component is involved yet. However, for a slightly higher flow velocity, U = 2.68, λ_1 and λ_2 coalesce to become eventually complex conjugate again, but with positive real parts. At this point flutter-type motion may arise[4].

iv) $-31.4 < \gamma < -57.5$ ($\gamma = -55$ in Fig.4.9(d))

From a physical point of view, this corresponds to the same case as iii). However, flutter-type motions now arise due to the coupling between the first and the second mode, at U = 1.8.

Notice that the mode coalescence at U = 1.67 is not physically significant, since the eigenvalues have negative real parts.

v) $\gamma < -57.5$ ($\gamma = -60$ in Fig.4.9(e))

At zero flow velocity, two eigenvalues are positive; while the other two are negative. The instability is static; since all four eigenvalues are real, the system is buckled either in the first or the second mode. Coupled-mode flutter arises at U = 1.5, as in the previous case.

4.2.2 Case with a spring

The procedure followed is the same as in the previous section, U and γ being the parameters varied.

i) $\gamma > 80$ ($\gamma = 100$ in Fig.4.10(a))

This corresponds again to the "traditional" Hopf bifurcation, since the system loses stability because a pair of complex conjugate eigenvalues crosses the imaginary axis

---

[4] This flutter is also called coupled-mode flutter, even though it comes from the coalescence of two associated eigenvalues. A distinction should, however, be made.

with a non-zero frequency, at U = 13. For high values of γ, the spring only adds some stiffness to the pipe but is unable to cause any static instability.

ii) $\underline{4.96 < \gamma < 71.94}$ (γ = 60 in Fig.4.10(b))

It is important to note that different types of instability may occur. For low dimensionless flow velocity U, the origin is obviously stable. For higher flow velocities, one conjugate pair of eigenvalues becomes wholly real (U = 8.55) until one of them eventually becomes positive (U = 11.47). This point corresponds to the static instability or divergence. For still higher U (U = 12.48), the system loses stability through a Hopf bifurcation, as the other pair crosses the imaginary axis. Finally, at U = 15.07, the first eigenvalue crosses the imaginary axis again, but from the right to the left, meaning that the system again regains "static" stability. This value, in practice, has no real physical meaning, since the system has lost dynamic instability prior to this. However, the boundaries found from the previous analysis (Routh's criteria) are now clearly explained.

The two extreme cases, γ = 4.96 and γ = 71.94 are qualitatively different: in the first case, a double zero eigenvalue occurs (Fig.4.10(c)); in the second, double degeneracy conditions (one zero eigenvalue plus one pair of complex conjugate eigenvalues with zero real part) occur (Fig.4.10(c,d)).

iii) $\underline{71.94 < \gamma < 80}$ (γ = 75 in Fig.4.10(e))

This case corresponds to a hybrid form of a) and b): a Hopf bifurcation occurs first (U = 12.63); followed by static instability (U = 12.96), and by a restabilization at U = 14.69. Again, from a physical point of view, only the flutter-type motions can be observed.

iv) $\gamma < 4.96$ ($\gamma = -40$ in Fig.4.10(f))

From Fig.4.10(f), it is obvious that no dynamic instability occurs. The system loses stability through a pitchfork bifurcation at U = 3.439, and, with increasing flow velocity, a second static instability occurs. No restabilization is found; from a physical point of view, two different static equilibria may be observed. Consequently, for $\gamma < 4.96$, the top curve $a_0 = 0$ in Fig.4.8(b) no longer represents a restabilization, but rather a second static instability.

v) Remarks

With this direct eigenvalue analysis, it is now possible to distinguish more precisely the different regions of stability. Indeed, for the a_0 curves, static restabilization or instability in the second mode may occur, depending on the value of γ; it is important to note that Routh's criteria are unable to distinguish between these two physically distinct phenomena. Hence, the complete stability map obtained from the linearized equations can be drawn (Fig.4.11(a,b)).

Finally, it should be recalled that the study of the linearized system near the origin has limitations. Theoretically, it is not possible to study the behaviour of the system after bifurcation. Thus, the study of the linearized system is only valid for the first instability. Concerning the restabilization (and other bifurcations), this also strictly applies to systems that are linearly unstable at U = 0, as U is increased. When static instability occurs, a new analysis can be undertaken near the new fixed point which behaves, from a topological point of view, like the origin. This will be done in the next chapter, since the inclusion of the nonlinear terms is necessary to find the position of the new "origin."

CHAPTER V
NONLINEAR ANALYSIS

Whereas the linear approximation of the system can only predict the instabilities of the origin, the nonlinear analysis may provide a deeper and more interesting insight into the problem.

One usually starts the study of a nonlinear system $dx/dt = f(x)$ by finding the zeros of f, i.e.

$$f(x) = 0. \tag{5.1}$$

These zeros, x_0, are referred to as fixed points, equilibria or stationary solutions. Linearization at these points can characterize the behaviour of solutions near x_0. This is done by studying the linear system

$$\frac{d\xi}{dt} = Df(x_0)\xi, \qquad \xi \in \mathbf{R}^n, \tag{5.2}$$

where $Df = [\partial f_i/\partial x_j]$ is the Jacobian matrix of the first partial derivatives of the function f at the fixed point x_0, and $\xi = x - x_0$, $|\xi| << 1$.

Actually, the study of the linearized system defined by (5.2) can only provide qualitative responses of the nonlinear system in some cases, namely when $Df(x_0)$ has no zero or no purely imaginary eigenvalues (Hartman-Grobman theorem). When $Df(x_0)$ has no eigenvalues with a zero real part, x_0 is called a hyperbolic or nondegenerate fixed point. Hence, from a practical point of view, the interesting problem is to find the degenerate fixed points. This was done partially in Chapter IV, since the origin 0 is a "natural" fixed point; the stability of the origin was investigated through the eigenvalues of the linearized matrix [A].

Consequently, the next task is to find the other zeros of the nonlinear system and to investigate their stability.

However, nonlinear systems possess limit-sets other than fixed points which are the simplest type of limit-sets. For planar flows, for example, all possible "non-wandering sets" fall into three classes:

- fixed points;
- closed orbits;
- the union of fixed points and the trajectories connecting them.

The third class will be discussed in detail in Section 5.3. The second one, the closed or periodic orbits, appears very frequently, especially after a Hopf bifurcation. However, as Holmes (1977) underlined, this is not the only way; the Hopf bifurcation only describes the behaviour near the origin 0, the newly unstable fixed point. In a general nonlinear case, where globally-attracting nonlinear terms exist (as in the present study), other attracting limit-sets may exist. By definition, "flutter exists when the state of the system falls into the basin of attraction of a limit cycle or of a recurrent motion. As $t \to \infty$, the state tends to [either] one of periodic, almost periodic, or "strange" non-periodic oscillations of limited amplitude" (Holmes 1977). The present study will prove that flutter with the above definition exists in the system, and will explain why, numerically and analytically.

Then, a deep analysis of the system near some bifurcation points, with the new tools of nonlinear dynamics, will allow a more precise clarification of these points. The use of the centre manifold and normal form theories gives complete bifurcation sets in the (γ, U) plane. The investigation of doubly-degenerate fixed points is of particular interest, and leads to the notion of chaos which occurs only in some very particular cases.

In the last section, in order to increase the possibilities for chaos to occur, other nonlinearities are introduced into the system; specifically, the effects of

motion-limit constraints, modelled by a cubic spring, are studied, and a comparison with previous studies is undertaken.

5.1 STABILITY OF THE FIXED POINTS

In this section, efforts to find all the fixed points of (2.70) and investigate their stability will be undertaken. The approach is similar to that used in Chapter IV, but the fixed points other than 0 have to be determined first.

5.1.1 Methodology

Recalling that the equations of motion are

$$\begin{cases} \dot{q}_i = p_i, \\ \dot{p}_i = -k_{ij}q_j - c_{ij}p_j - \alpha_{ijkl}q_jq_kq_l \\ \qquad - \beta_{ijkl}q_jq_kp_l - \gamma_{ijkl}q_jp_kp_l, \end{cases}$$

the fixed points are given by

$$\begin{cases} \dot{q}_i = 0, \\ \dot{p}_i = 0, \end{cases}$$

that is to say

$$k_{ij}q_j + \alpha_{ijkl}q_jq_kq_l = 0. \tag{5.3}$$

For a two-mode model, i = 2, two nonlinear equations with two unknowns q_1 and q_2 are solved. Since the coefficients α_{ijkl} are computed numerically, it is impossible to find analytic solutions to the problem. Once (q^0_1, q^0_2) are found, the stability of that new fixed point is investigated through a perturbation

$$\begin{cases} q_i = q_i^0 + u_i, \\ p_i = v_i, \end{cases}$$

which leads, to a first order approximation, to

$$\begin{cases} \dot{u}_i = v_i, \\ \dot{v}_i = -k_{ij}u_j - c_{ij}v_j - \alpha_{ijkl}(u_j q_k^0 q_l^0 + q_j^0 u_k q_l^0 + q_j^0 q_k^0 u_l) \\ \qquad\qquad - \beta_{ijkl} q_j^0 q_k^0 v_l \\ \qquad\qquad = 0, \end{cases}$$

i.e.

$$\begin{cases} \dot{u}_i = v_i, \\ \dot{v}_i = -k_{ij}u_j - c_{ij}v_j - (\alpha_{ijkl} + \alpha_{ikjl} + \alpha_{iljk}) q_k^0 q_l^0 u_j \\ \qquad\qquad - \beta_{ijkl} q_j^0 q_k^0 v_l. \end{cases} \tag{5.4a}$$

The system (5.4) can be transformed into a matrix form

$$\begin{Bmatrix} \dot{u}_i \\ \dot{v}_i \end{Bmatrix} = [A^0] \begin{Bmatrix} u_i \\ v_i \end{Bmatrix}, \tag{5.4b}$$

$[A^0]$ being a function of k_{ij}, c_{ij}, α_{ijkl} and β_{ijkl}, and having a dimension of 4 for a 2-mode model.

Depending on the parameters, different qualitative and quantitative behaviours may be found. As in the linear analysis near the origin, K, ξ_s and β are kept constant, K = 100, ξ_s = 0.8 and β = 0.13. Depending on the values of γ and U, none, two or four fixed points may exist in addition to the zero fixed point (see Section 4.2.2 and Fig.4.11(b)). Hence, an Argand diagram for the new fixed points is not relevant, and another notation (Holmes 1977) is used to present the results found. The fixed point 0 corresponds to the pipe lying along the x-axis (initial position) and is represented by {0}. Due to the symmetry of the problem, the first new pair of fixed points can be represented by {±1}, and the second pair by {±2}. The stability of each point depends on the four eigenvalues of the matrix $[A^0]$ defined by (5.4). The four eigenvalues are represented by a quartet $\lambda = (\pm,\pm,\pm,\pm)$, where "+" stands for an eigenvalue with a

positive real part, and "-" for an eigenvalue with a negative real part. For example, a stable fixed point is represented by λ = (-,-,-,-), and if it undergoes a Hopf bifurcation, it becomes λ = (+,+,-,-). Similarly, a saddle-node bifurcation is characterized by λ = (0,±,±,±) and a doubly-degenerate fixed point by λ = (0,0,0,±).

5.1.2 Results : some cases are discussed separately.

i) γ = 76 (Fig.5.1(a))

The origin {0} = (-,-,-,-) is stable for small flow velocities. It undergoes a Hopf bifurcation (+,+,-,-) at U = 12.65 and a pitchfork bifurcation at U = 13.10, where {±1} = {+,+,-,-}, an unstable fixed point, appears (see also Section 5.2). {0} and {±1} coalesce at U = 14.72, the velocity at which a saddle-node bifurcation occurs, {0} = {±1} = (+,+,0,-). Physically, this means that there exists one unstable static equilibrium position in the velocity range 12.65 < U < 13.1, and three unstable static eiquilibria positions when 13.1 < U <14.72; flutter type motion is predominant for U >12.65.

ii) γ = 60 (Fig.5.1(b))

The stable origin {0} becomes unstable through a pitchfork bifurcation (+,-,-,-) at U = 11.47. Two stable static equilibria appear, {±1} = (-,-,-,-), until U = 12.43 where subcritical Hopf bifurcations occur (+,+,-,-). Again, limit-cycle motion may be present, since no stable equilibrium exists. At U = 12.48, it is the origin {0} that undergoes a Hopf bifurcation. The three fixed points {0} and {±1} coalesce at U = 15.07 (λ = (+,+,0,-)). A numerical investigation confirms the results found: limit-cycle oscillations were found before the first Hopf bifurcation at U = 12.43, due to the subcritical bifurcation of {±1}. The orbit is attracted either by one of the stable fixed points or by the attracting periodic limit-set.

iii) $\gamma = 20$ (Fig.5.1(c))

Again, the origin {0} is stable for small flow velocities, and undergoes a pitchfork bifurcation (+,-,-,-) at U = 8.45. The unstable origin {0} undergoes another bifurcation at U = 13.23, a Hopf bifurcation. Thus, it becomes unstable from a dynamic point of view (λ = (+,+,+,-)). At U = 13.81, the two static equilibria also become unstable through a subcritical Hopf bifurcation (+,+,-,-). For still higher flow velocities (U = 14.85), a static bifurcation occurs at the origin {0} which restabilizes in one mode (+,+,-,-) (but {0} is still unstable); a second unstable pair of equilibria {±2} exists, (+,+,+,-) which is also unstable. Hence, five unstable fixed points coexist in the system. Finally, the two pairs {±1} and {±2} coalesce at U = 15.4 through a saddle-node bifurcation (+,+,0,-), and disappear for higher flow velocities.

From a physical point of view, one may observe limit-cycle motions for U > 13.81, and both static equilibrium and limit-cycle oscillations in the velocity range 13.23 < U < 13.81. Qualitatively, this was also found by Holmes (1977) in the panel flutter problem.

iv) $\gamma = -60$ (Fig.5.1(d))

This case corresponds to a "standing" pipe, and the origin {0} is a saddle for small velocity (+,-,-,-), and two stable equilibria {±1} = (-,-,-,-) exist. At U = 12.71, the origin undergoes another static bifurcation (+,+,-,-), and the second pair {±2} of equilibria appears (+,-,-,-), until U = 16 where the two pairs coalesce. Physically, one should only see one equilibrium. Some flutter-type motions have, however, been observed numerically (see next section).

5.1.3 Physical implications

The results found in the previous section are very interesting. For certain flow velocity, different steady-

states may exist in the system: stable equilibria, unstable equilibria and periodic limit-sets coexist. To better understand the previous bifurcation diagrams, it is helpful to examine the phase flow portraits for some special parameters (see Appendix 10 for construction).

For $\gamma = -60$ and $U = 7.5$, $\{0\}$ is a saddle-point and two stable equilibria exist. Fig.5.1(e) illustrates the stable and unstable manifolds of the origin $\{0\}$; all solutions tend to one of the stable equilibria. The pipe is unstable from a static point of view, i.e. it is buckled.

For $\gamma = -60$ and $U = 13.1$ the dynamics are more complicated: five equilibria exist (Fig.5.1(f)). The origin $\{0\}$ is a saddle, as well as the second pair $\{\pm 2\}$ (not all the stable and unstable manifolds have been computed for clarity). The first pair $\{\pm 1\}$ is "weakly" attracting. Flows with initial conditions close to the equilibrium are attracted by one of the fixed point $\{\pm 1\}$. However, other attracting sets also exist: one may observe either oscillations around one of the equilibria or global oscillations around the five equilibria. Those oscillations do not come from local bifurcations; as in the case of the pendulum, they represent an energy state for which the oscillations do not die out. For Duffing's equation for example, solutions lie on level curves of the Hamiltonian energy H of the system. These solutions are closed orbits representing a global stability state (Guckenheimer and Holmes 1983).

The case $\gamma = -80$ and $U = 8.76$ in Fig.5.1(g) depicts the boundary between two states: for $U < 8.76$, no closed orbit can be found, even with very large initial conditions. The limit-set tracks flows with big initial conditions, but it is not "suficiently attracting". The flow is finally attracted by one of the stable equilibria. Numerically, this process of finding the critical velocity U can be repeated for different values of γ. The stability map of Fig.4.11(b) can be then completed (Fig.5.1(h)).

5.2 STANDARD FORMS, CENTRE MANIFOLD, NORMAL FORMS

The main purpose of this section is to describe qualitatively the dynamics of the system. The idea is to reduce the dimension of the system at the degenerate fixed points, so as to be able to study it in a clearer, simpler way.

The asymptotic behaviour of the solution near a hyperbolic or nondegenerate fixed point is determined by linearization. Hence, in this case, there exist local stable and unstable manifolds W^s_{loc}, W^u_{loc}, of the same dimensions n_s, n_u as those of the eigenspaces E^s, E^u of the linearized system, and tangent to E^s, E^u at the fixed point (Guckenheimer and Holmes 1983). The behaviour of the system on those stable or unstable manifolds is completely defined.

In the case of a degenerate fixed point (i.e. with at least one eigenvalue with zero real part), a third component, the centre manifold W^c_{loc}, tangent to the centre eigenspace E^c, has to be taken into account. The stability properties of the dynamical system along the stable and unstable manifolds are known, so that one can restrict the study of the dynamics near the degenerate point to the study of the flow on the centre manifold. This is the main idea of centre manifold theory (Carr 1981). For example, if the fixed point contains a single zero eigenvalue, the dimension of the centre space is one, and if the degenerate fixed point has a pair of purely imaginary eigenvalues, the dimension of the centre space becomes two.

The centre manifold theory is important, especially in the case of high or infinite dimensional problems, since one thereby extracts an essential model on a low dimensional space that captures the local (bifurcational) behaviour. Consequently, after putting the system in its standard form, one determines the centre manifold and the subsystem on this manifold. Combined with bifurcation theory, i.e. when the

system has variable parameters, the method is particularly powerful. Indeed, for low-dimensional problems, a complete classification of most of the "famous" bifurcations was undertaken twenty years ago (Takens 1973, 1974) and can be applied directly in this thesis. The resulting "simplified" subsystems are called normal forms.

5.2.1 Standard forms

In this section, the standard forms are formulated. Depending on the degree of degeneracy of the fixed point, different situations may arise.

Recalling first (4.1),

$$\dot{x} = f_\mu(x), \quad x \in \mathbb{R}^n, \quad \mu \in \mathbb{R}^k, \tag{5.5}$$

one wants to find a value μ_0 for which the flow of (5.5) is not structurally stable, and draw the qualitative aspects of the flow for small changes of μ. The classification of the bifurcations mentioned in the previous section is based on the theory of transversality in differential topology.

Many possibilities can be listed, depending on the Jacobian derivatives $D_x f_\mu$ evaluated at the bifurcation point (x_0, μ_0). Thus, for a simple zero eigenvalue,

$$[D_x f_\mu] = \begin{bmatrix} 0 & 0 \\ 0 & [M] \end{bmatrix}; \tag{5.6}$$

for a simple pure imaginary pair,

$$[D_x f_\mu] = \begin{bmatrix} \begin{bmatrix} 0 & -\omega \\ \omega & 0 \end{bmatrix} & 0 \\ 0 & [M] \end{bmatrix}; \tag{5.7}$$

for a double zero, nondiagonalizable,

$$[D_x f_\mu] = \begin{bmatrix} \begin{bmatrix} 0 & 1 \\ 0 & 0 \end{bmatrix} & 0 \\ 0 & [M] \end{bmatrix}; \tag{5.8}$$

and for a simple zero plus a pure imaginary pair,

$$[D_x f_\mu] = \begin{bmatrix} \begin{bmatrix} 0 & -\omega & 0 \\ \omega & 0 & 0 \\ 0 & 0 & 0 \end{bmatrix} & 0 \\ 0 & [M] \end{bmatrix}. \tag{5.9}$$

In each case [M] is a matrix of appropriate dimension, with all nonzero real-part eigenvalues.

Consequently, starting from the original equation

$$\dot{y} = [A]y + \epsilon f(y) + \epsilon v[B(t)]y, \tag{5.10}$$

evaluated at the critical values, the system may be brought into one of the standard forms cited above. Before giving this standard form for the three different (degenerate) situations, let us recall some properties of matrices.

If [A] is a real 4 x 4 matrix (the case of an N x N matrix is identical), it can be put either into a diagonal form or into its Jordan form,

$$[A'] = [\Lambda] = [\lambda_i], \tag{5.11}$$

or

$$[A'] = \begin{bmatrix} \lambda_1 & 1 & 0 & 0 \\ 0 & \lambda_2 & 1 & 0 \\ 0 & 0 & \lambda_3 & 1 \\ 0 & 0 & 0 & \lambda_4 \end{bmatrix}. \tag{5.12}$$

If the four eigenvalues are real, the transformed matrix is still real, which is the most simple case. However, assuming that the eigenvalues of [A] are (in general) complex conjugates

$$\lambda_k = \sigma_k + i\omega_k,$$

none of the above forms ((5.11) and (5.12)) is satisfactory since the transformed matrix [A'] becomes complex. In this latter case, let V_k be the eigenvectors associated with the eigenvalues λ_k. By definition,

$$[A]\{V_k\} = \lambda_k\{V_k\} = (\sigma_k + i\omega_k)\{V_k\}. \tag{5.13}$$

These eigenvectors can also be written generally as

$$V_k = V_k^R + iV_k^I \tag{5.14}$$

with V_k^R standing for the real part of $\{V_k\}$ and V_k^I for the imaginary part. Hence, from (5.13),

$$[A]\{V_k^R + iV_k^I\} = (\sigma_k + i\omega_k)\{V_k^R + iV_k^I\},$$

i.e.

$$\begin{cases} [A]\{V_k^R\} = \sigma_k\{V_k^R\} - \omega_k\{V_k^I\} \\ [A]\{V_k^I\} = \omega_k\{V_k^R\} + \sigma_k\{V_k^I\}. \end{cases} \tag{5.15}$$

Constructing the modal matrix [P] consisting of the real (V_k^R) and imaginary (V_k^I) parts of the eigenvectors, the transformed matrix [A'] becomes

$$[A'] = \begin{bmatrix} \sigma_1 & -\omega_1 & 0 & 0 \\ \omega_1 & \sigma_1 & 0 & 0 \\ 0 & 0 & \sigma_2 & -\omega_2 \\ 0 & 0 & \omega_2 & \sigma_2 \end{bmatrix}. \tag{5.16}$$

The matrix [A'] in this new basis is real again, which is desired. Letting $\sigma_1 = 0$, for example, leads immediately to the form (5.7).

In the case of a zero eigenvalue, by taking the modal matrix $[P] = [V_1, V_2, \mathrm{Re}(V_3), \mathrm{Im}(V_3)]$, the matrix [A'] becomes

$$[A'] = \begin{bmatrix} 0 & 0 & 0 & 0 \\ 0 & \sigma_1 & 0 & 0 \\ 0 & 0 & \sigma_2 & -\omega_2 \\ 0 & 0 & \omega_2 & \sigma_2 \end{bmatrix},$$

($\sigma_1 < 0$). The other cases can be constructed similarly, except for the double zero eigenvalue when one has to find the Jordan form (Appendix 6).

Finally, after constructing the modal matrix [P] and letting y = [P]x, the system can be brought into the standard form,

$$\dot{x} = [A']x + \epsilon[P^{-1}]f([P]x) + \epsilon v[P^{-1}][B][P]x, \qquad (5.17)$$

with [A'] taking one of the forms (5.6)-(5.9), depending on the degeneracy of the fixed point.

5.2.2 Centre manifold

Starting from the standard form (5.17), the centre manifold can be computed. In general, this can be a complicated task. However, it is easier to be found with an order analysis. This was suggested by Sethna and Shaw (1987) and proved by Li and Paidoussis (1990). Consequently, only a brief outline following Li and Paidoussis' work is given here. Equation (5.17) can be rewritten as

$$\begin{aligned} \dot{x} &= [A]x + \epsilon\, f(x,y) + \epsilon v(B_{11}x + B_{12}y), \quad x \in \mathbb{R}^n \\ \dot{y} &= [B]y + \epsilon\, g(x,y) + \epsilon v(B_{21}x + B_{22}y), \quad x \in \mathbb{R}^m, \end{aligned} \qquad (5.18)$$

where [A] contains either zero or purely imaginary eigenvalues, [B] contains eigenvalues with non-zero real parts, the B_{ij} being time-dependent functions and both f and g being homogeneous cubic nonlinear polynomials.

Considering ϵ as a variable (with $d\epsilon/dt = 0$), the centre manifold can be written as

$$y = h(x,\epsilon), \tag{5.19}$$

with the boundary conditions

$$h(0,0) = 0, \quad \frac{\partial h}{\partial x}(0,0) = 0, \quad \frac{\partial h}{\partial \epsilon}(0,0) = 0. \tag{5.20}$$

After various differentiations, substitutions and an order analysis, the flow on the centre manifold is found to be

$$\dot{x} = [A]x + \epsilon\, f(x,0) + \epsilon v B_{11} x + O(\epsilon^2). \tag{5.21}$$

It is noted that equation (5.21) can be obtained by neglecting the stable (or unstable) component in (5.18). Practically, those operations are straightforward.

Consequently, the analysis is now restricted to the centre manifold, which is of dimension 1, 2 or 3 depending on the eigenvalues of the fixed point.

5.2.3 Normal forms

After using centre manifold theory, which enables the reduction of the dimension of the problem to its minimum value, the subsystem defined on the centre manifold itself can still be very complicated. The idea of normal form theory is to reduce, to the simplest form, the vector field $f_\mu(x)$ which defines the flow on the centre manifold,

$$\dot{x} = f_\mu(x); \tag{5.22}$$

Note that (5.22) is similar to (5.5), but does not represent the same problem, the flow here being restricted to the centre manifold. In the vocabulary of dynamics, "as simple as possible" means in some sense "irreducible" (Guckenheimer and Holmes 1983). The idea of normal forms begins with finding a near-identity coordinate transformation P

$$x = y + P(y), \tag{5.23}$$

where P is a polynomial. Therefore, (5.22) becomes

$$\dot{y} = (I + DP(y))^{-1} \; f_{\mu}(y + P(y)). \tag{5.24}$$

In terms of power series, one tries to find a sequence of coordinate transformations P, which removes terms of increasing degree from the Taylor series of (5.24) at the fixed point 0. Hence, all inessential terms are removed up to some degree from the Taylor series (Guckenheimer and Holmes 1983). For the simplest cases, a general normal form has already been derived.

Here, as many methods as possible are used in the different examples, that is to say:

- the standard normal form in the case of one zero eigenvalue;
- the method of averaging yielding the normal form in the case of a pair of purely imaginary eigenvalues;
- the computation (in detail) of the normal form in the case of a double zero eigenvalue,;
- the use of available normal forms in the doubly-degenerate case.

i) Zero eigenvalue bifurcation

As proved in the linear analysis, zero eigenvalue occurs for a standing pipe (represented by negative gravity $\gamma < 0$). For $\gamma = -25$ for example, the critical flow velocity for a simple zero eigenvalue is 3.05.

Processing the centre manifold theory allows the reduction of the dimension of the full system, in the neighbourhood of $U_c = 3.05$, to a one-dimensional subsystem. The calculations are performed using the computer algebra system MACSYMA, accomplishing the following steps:

- computation of the linear matrix [A], as a function of the control parameter $\mu = U - U_c$;
- calculation of the eigenvalues of [A] at the critical velocity;
- construction of the modal matrix [P], evaluated at the critical parameters (see Appendix 7 for proof);
- computation of the nonlinear terms;
- computation of the standard form;
- evaluation of the flow on the centre manifold through (5.21).

For the system parameters considered ($U_c = 3.05$, $\gamma = -25$, $\beta = 0.2$, $K = 0$), the procedure yields

$$\dot{x} = (-4.44\mu - 10.85x^2)x. \qquad (5.25)$$

From (5.25), it is clear that the bifurcation occuring at the critical parameter is a subcritical pitchfork bifurcation.

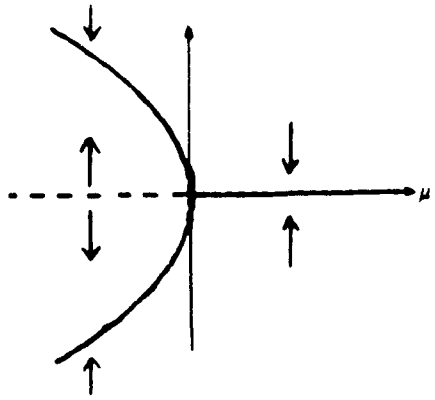

Figure V(a)

When $\mu < 0$ ($U < U_c$), the origin is unstable, and solutions diverge (depending on the initial conditions) to one of the stable equilibria.

When $\mu > 0$ ($U > U_c$), the origin becomes stable, and the two symmetric equilibrium positions disappear; the system regains stability. This was also found through the numerical integration of the equations (Fig.5.2(a,b)).

These results of course are familiar, since the system (and the equations) has some symmetry properties (the differential equation (5.5) is symmetric or equivariant with respect to the transformation $x \to -x$ ($f_\mu(-x) = -f_\mu(x)$)); in this case, some transversality conditions cannot be satisfied, and hence, neither saddle-node nor transcritical bifurcations can occur; in terms of normal forms, the bifurcations are represented by

$$dx/dt = \mu - x^2 \qquad \text{(saddle-node)},$$
$$dx/dt = \mu x - x^2 \qquad \text{(transcritical)},$$
$$dx/dt = \mu x - x^3 \qquad \text{(pitchfork)}.$$

(See Guckenheimer and Holmes 1983, pp. 145-150 for more details.)

Moreover, the equilibrium positions can be evaluated very easily from (5.25). Letting $dx/dt = 0$ yields

$$x_{eq} = \pm \sqrt{\frac{-4.44\mu}{10.85}} = \pm 0.64\sqrt{-\mu}. \qquad (5.26)$$

Using the modal matrix [P], one can reconstruct the stationary solution

$$\begin{cases} q_{1eq} = x_{eq}, \\ q_{2eq} = -0.192x_{eq}, \end{cases} \qquad (5.27)$$

and through the Galerkin transformation, obtain the deflection of any point on the beam.

The results found (Fig.5.2(c)) are in qualitative and quantitative agreement for small values of μ ($-.1 \leq \mu < 0$) for the set of parameters chosen. Moreover, the parabolic shape is obtained. Note that, in the numerical integration of the equations, the system regains stability at velocity U,

larger than the one predicted by the linear theory. Of course, this prediction is not possible with the centre manifold theory. Finally, it should be recalled that many (simpler) methods can be used to find static solutions.

ii) The Hopf bifurcation

The Hopf bifurcation may be the most important bifurcation from an engineer's point of view, since it corresponds to dynamic instability causing flutter-type motions. Therefore, it has been studied extensively, physically and mathematically, by many authors (Marsden and McCracken 1976). In this case, $D_x f_\mu$ takes the form (5.7), and the normal form is given by

$$\begin{aligned} \dot{r} &= (d\mu + ar^2)r, \\ \dot{\phi} &= (\omega_0 + c\mu + br^2), \end{aligned} \tag{5.28}$$

in which μ is directly related to the change of the parameters (the flow velocity in this case), and a, b, c and d are coefficients to be computed from normal form theory. For example, if the flow on the centre manifold is defined by

$$\begin{cases} \dot{x}_1 = -\omega_0 x_2 + \epsilon f_1(x_1, x_2), \\ \dot{x}_2 = \omega_0 x_1 + \epsilon f_2(x_1, x_2), \end{cases} \tag{5.29}$$

a is simply obtained by

$$a = \frac{1}{8}\,(f_{1,12} + 3f_{1,30} + 3f_{2,03} + f_{2,21}), \tag{5.30}$$

where (Li and Paidoussis 1990)

$$f_i = f_{i,30}x_1^3 + f_{i,21}x_1^2x_2 + f_{i,12}x_1x_2^2 + f_{i,03}x_2^3,$$

or

$$f_i = f_{i,jk}\, x_1^j x_2^k, \quad i = 1,2, \quad j + k = 3.$$

In the case of an autonomous system, the normal form and the averaging method yield the same results. The second one is used here.

Starting from (5.22), one seeks solutions of the form

$$\begin{cases} x_1 = r\cos(\omega_o \tau + \phi) = rC, \\ x_2 = r\sin(\omega_o \tau + \phi) = rS, \end{cases} \tag{5.31}$$

where C stands for $\cos(\omega_0 t + \phi)$ and S for $\sin(\omega_0 t + \phi)$. Hence, from the left-hand side of (5.22),

$$\begin{cases} \dot{x}_1 = \dot{r}C - r(\omega_0 \tau + \dot{\phi})S, \\ \dot{x}_2 = \dot{r}S + r(\omega_0 \tau + \dot{\phi})C, \end{cases}$$

and from the right-hand side

$$\begin{cases} \dot{x}_1 = -r\omega_0 S + \epsilon\, f_1(rC,\ rS), \\ \dot{x}_2 = r\omega_0 C + \epsilon\, f_2(rC,\ rS). \end{cases}$$

Equating the two sets of expressions leads to

$$\begin{cases} \dot{r}C - r\dot{\phi}S = \epsilon\, f_1(rC,\ rS), \\ \dot{r}S + r\dot{\phi}C = \epsilon\, f_2(rC,\ rS), \end{cases}$$

which can be simplified into

$$\begin{cases} \dot{r} = \epsilon\,(f_1 C + f_2 S), \\ r\dot{\phi} = \epsilon\,(f_2 C - f_1 S). \end{cases} \tag{5.32}$$

The problem is now in standard form and meets the assumptions of the theorems for averaging (Sanders and Verhulst 1985). Hence,

$$\begin{cases} (\dot{r})_{av} = \dfrac{\omega}{2\pi} \displaystyle\int_0^{\frac{2\pi}{\omega}} (f_1 C + f_2 S)\, d\tau, \\ (r\dot{\phi})_{av} = \dfrac{\omega}{2\pi} \displaystyle\int_0^{\frac{2\pi}{\omega}} (f_2 C - f_1 S)\, d\tau, \end{cases} \tag{5.33}$$

in which integrals r and $\dot{\phi}$ are assumed to be constant. The advantage of the averaging method is that it is based on several basic comparison theorems which compare solutions of (5.22) and the averaged equations (5.33) (Chow and Mallet-Paret 1977). For solutions valid for time of $O(\epsilon^{-1})$, any solutions of (5.33) can be shown to be close to those of (5.22) for sufficiently small ϵ.

The algebra involved in carrying out these calculations can become tedious; however, it is easily handled on a computer with a symbolic manipulation program, such as MACSYMA. This was done with the same parameter values as those used by Li and Paidoussis (1990) for comparison with the normal form theory and their calculations of unfolding parameters. With $\gamma = 25$, $\beta = 0.2$ and a critical flow velocity $U_c = 7.093$, one obtains

$$\begin{cases} \dot{r} = 2.77\mu r - 89.663 r^3, \\ \dot{\phi} = 16.16 - 0.903\mu + 106.529 r^2. \end{cases} \tag{5.34}$$

The nonlinear coefficient a equals $-89.663 < 0$. This shows that the corresponding Hopf bifurcation is supercritical.

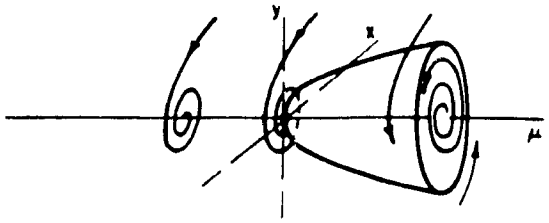

Figure V(b)

Moreover, under this normal form, the radius of the limit cycle (in the new coordinates !) can be obtained, by letting dr/dt = 0, or

$$r_{1c} = \pm \sqrt{\frac{2.77}{-a}\mu}\,. \tag{5.35}$$

From a physical point of view, for $\mu < 0$ ($U < U_c$), the origin is stable (no limit cycle), and it becomes unstable for $\mu > 0$. These results are familiar (Fig.5.3(a,b)). Of more interest is the use of these results in the original coordinates. Letting

$$\begin{cases} r = r_{1c} = 0.176\sqrt{\mu}\,, \\ \dot{\phi} = \dot{\phi}_{1c} = 16.16 + 1.802\mu, \end{cases} \tag{5.36}$$

one can easily reconstruct the original equation on the centre manifold: from $\{y\} = [P]\{x\}$, and by approximating $\{x\}$ as

$$\{x\} = \begin{Bmatrix} r_{1c}\cos(\dot{\phi}_{1c}\tau) \\ r_{1c}\sin(\dot{\phi}_{1c}\tau) \\ 0 \\ 0 \end{Bmatrix},$$

one obtains

$$\{y\} = \begin{Bmatrix} y_1 \\ y_2 \\ y_3 \\ y_4 \end{Bmatrix} = \begin{Bmatrix} r_{1c}\cos(\dot{\phi}_{1c}\tau) \\ -0.3421 r_{1c}\sin(\dot{\phi}_{1c}\tau) \\ -16.16\ r_{1c}\sin(\dot{\phi}_{1c}\tau) \\ -5.53\ r_{1c}\cos(\dot{\phi}_{1c}\tau) \end{Bmatrix}.$$

As expected, $y_3 = dy_1/dt$ and $y_4 = dy_2/dt$. The displacements and velocities at the end of the pipe are computed through the Galerkin approximation

$$\begin{cases} x(1,\tau) = y_1(\tau)\ \phi_1(1) + y_2(\tau)\ \phi_2(1), \\ \dot{x}(1,\tau) = y_3(\tau)\ \phi_1(1) + y_4(\tau)\ \phi_2(1). \end{cases} \qquad (5.37)$$

The results are compared with those obtained by numerical integration (Fig.5.3(c,d)). The phase plot gives very good results for $\mu = 0.3$, as well as the time trace (not shown). Considering the fact that μ is "not very small" (as required in the theory), the approximations of the flow on the centre manifold are excellent. The bifurcation diagram in Fig.5.3( ) also confirms all these results. Again, the bifurcation type is clearly defined, and agreement for a large range of μ is obtained.

Consequently, not only the qualitative aspect of the bifurcation has been found, but also the quantitative behaviour after the bifurcation. This is very interesting: the type of bifurcation has been clarified, the post-bifurcation behaviour has been predicted, and complicated equations have been transformed into a much simpler system.

iii) Double zero eigenvalue problem

From the linear analysis, it was found that in the case of the elastically-supported pipe (by the linear spring), a double zero eigenvalue can occur. The strategy used in this section follows the one described in the case of the zero

eigenvalue, but presents some practical differences. Indeed, the transformation into a standard form is not so easy in this case, since a double zero eigenvalue occurs with only one independent eigenvector (for computation of the Jordan form, see Appendix 6). After evaluating the flow on the centre manifold and neglecting the other components, the subsystem obtained is

$$\dot{x} = \begin{bmatrix} 0 & 1 \\ 0 & 0 \end{bmatrix} x + \epsilon \begin{bmatrix} 0 & 0 \\ \mu_1 & \mu_2 \end{bmatrix} x + \epsilon f(x). \tag{5.38}$$

In dynamics vocabulary, μ_1 and μ_2 are called unfolding parameters, and represent the deviation of the real parameters from their critical value. These parameters are necessary to capture all the possible behavioural characteristics of the system. In the case of a double zero eigenvalue, two parameters are necessary to unfold the dynamics of the problem (codimension two bifurcation).

One follows the strategy of normal forms, in which all the non-essential nonlinear terms of f are eliminated ("non-essential" meaning that they do not affect the qualitative dynamics). This was discussed in the previous section and developed by Li and Paidoussis (1990). First, one introduces the coordinate transformation,

$$x = y + \epsilon P(y).$$

Differentiating with respect to time yields

$$\dot{x} = \dot{y}\,[I + \epsilon DP(y)],$$

where DP is the Jacobian matrix of [P]. After substituting into (5.22) and simplifying, one obtains

$$\begin{aligned} \dot{y} &= L(y) + \epsilon(DL.P(y) - DP.L(y) + f(y)) + O(\epsilon^2) \\ &= L(y) + \epsilon g(y), \end{aligned} \tag{5.39}$$

with

$$DL = \begin{bmatrix} 0 & 1 \\ 0 & 0 \end{bmatrix},$$

and

$$g(y) = DL.P(y) - DP.L(y) + f(y). \qquad (5.40)$$

In the case of the double zero eigenvalues with certain symmetry properties, the normal form is shown to be

$$g(y) = \begin{cases} 0 \\ a_3 y_1^3 + b_3 y_1^2 y_2 \end{cases} \qquad (5.41)$$

(Takens 1974; Guckenheimer and Holmes 1983). The problem now becomes the following: knowing L(y), f(y) and g(y), what is the polynomial P which satisfies (5.40)? Recalling that f, g and P are "third" order polynomials, they can be written as

$$f_i(y) = f_{i,k,3-k}\ y_1^k\ y_2^{3-k},$$
$$g_i(y) = g_{i,k,3-k}\ y_1^k\ y_2^{3-k},$$
$$p_i(y) = p_{i,k,3-k}\ y_1^k\ y_2^{3-k},$$

with i = 1,2 and k = 0 to 3.

Equating the different coefficients leads to the eight equations given in Appendix 8. Finally, one obtains

$$\begin{cases} a_3 = f_{2,30} \\ b_3 = f_{2.21} + 3f_{1.30}. \end{cases} \qquad (5.42)$$

For the parameters β = 0.18, K = 100 and ξ_s = 0.8 chosen in the linear analysis (see Fig.4.10(c)), the critical values for U and γ are

$$U_{cr} = 14.61,$$
$$\gamma_{cr} = 4.96,$$

which corresponds to a hanging pipe.

After computation of the normal forms, one finds

$$\begin{cases} a_3 = 20023 > 0 \\ b_3 = 4213.6 > 0 \end{cases}$$

Substituting in (5.41) and rescaling y_1 and y_2 by $y_1/(b_3)^{1/2}$ and $y_2/(b_3)^{1/2}$ respectively, the following equations are obtained:

$$\begin{cases} \dot{y}_1 = y_2 \\ \dot{y}_2 = \mu_1 y_1 + \mu_2 y_2 + 4.752\, y_1^3 + y_1^2 y_2 . \end{cases} \tag{5.43}$$

The two unfolding parameters are related to the deviations of U and γ, μ and $d\gamma$ respectively, through

$$\begin{aligned} \mu_1 &= 74.70\mu - 1.44 d\gamma , \\ \mu_2 &= 5.13\mu . \end{aligned} \tag{5.44}$$

Of importance are the respective signs of a_3 and b_3. This situation has been studied in detail in Guckenheimer and Holmes (1983, pp.337-376), and the corresponding bifurcation set, with associated phase portraits, is shown in Fig.5.4(a). The analysis of the normal form (5.43), hence, brings out the emergence of global bifurcations involving the coalescence of closed orbits, as well as saddle connections. For $d\gamma = 0$ and $\mu > 0$, one obtains $\mu_1 > 0$, $\mu_2 > 0$ which corresponds to limit-cycle motion. For $\mu < 0$, the solutions converge to one fixed point. In this case again, an essential two-dimensional model has been used to describe the behaviour of the system around the critical point, illuminating the onset of flutter and divergence, as well as the interaction between them. Numerical integration of the equations in the neighbourhood of (0) (U = 14.61, γ = 4.96), has indeed demonstrated the appearance of limit-cycle motion (Fig.5.4(b,c)), which gives some confidence in the normal form found. However, in the special case studied, it should be recalled that among the four eigenvalues, one of them is strictly positive, making the

fixed point (0) unstable (existence of an unstable manifold).

Finally, it should be mentioned that, in the case of the panel flutter problem, Holmes and Marsden (1978) argue that forced oscillations could become chaotic. This will be discussed in Section 5.3.

iv) Doubly-degenerate case

The case of a doubly-degenerate situation was investigated recently by Li and Paidoussis (1990), and a complete bifurcation analysis near the doubly-degenerate fixed point was undertaken by Sethna and Shaw (1987). Hence, not all the details are presented here. After proceeding as in i), the autonomous system is brought to the form

$$\dot{x} = L(x) + \epsilon f(x), \quad x \in \mathbb{R}^3, \tag{5.45}$$

where

$$DL = \begin{bmatrix} \epsilon\mu_1 & -(\omega_0 + \epsilon\mu_3) & 0 \\ \omega_0 + \epsilon\mu_3 & \epsilon\mu_1 & 0 \\ 0 & 0 & \epsilon\mu_2 \end{bmatrix}, \tag{5.46}$$

and where f is a third order polynomial in x. Using normal form theory (and following the strategy described in iii) and in Li and Paidoussis), and transforming the result into polar coordinates leads to the subsystem

$$\begin{cases} \dot{r} = \epsilon(\mu_1 r - (a_{11}r^2 + a_{12}z^2))r + O(\epsilon^2) \\ \dot{z} = \epsilon(\mu_2 z + (a_{21}r^2 + a_{22}z^2))z + O(\epsilon^2) \\ \dot{\phi} = \omega_0 + O(\epsilon), \end{cases} \tag{5.47}$$

where a_{11}, a_{12}, a_{21}, a_{22} are given by

$$\begin{cases} a_{11} = (f_{2,210} + 3f_{2,030} + 3f_{1,300} + f_{1,120})/8 \\ a_{12} = (f_{2,012} + f_{1,102})/2 \\ a_{21} = (f_{3,201} + f_{3,021})/2 \\ a_{21} = f_{3,003}. \end{cases} \tag{5.48}$$

In physical terms, r represents the amplitude of oscillatory motions of the pipe, z represents the buckled positions of the pipe and $d\phi/dt$ the frequency of oscillations. It is interesting to note that the first two equations of (5.47) and the third one are decoupled, providing immediately

$$\phi = \omega_0 t + \theta_0 + O(\epsilon)$$

A rescaling procedure can transform the first two equations in their usual form (Guckenheimer and Holmes (1983), pp. 396-411),

$$\begin{aligned} \dot{r} &= r(\mu_1 + r^2 + bz^2), \\ \dot{z} &= z(\mu_2 + cr^2 + dz^2), \quad d = \pm 1. \end{aligned} \tag{5.49}$$

This system has been studied by Takens (1974) who found nine topologically-distinct equivalent classes. Results obtained from three different sets of parameters are presented now for comparison; the case studied by Li and Paidoussis (1990) (Case 1) has also been considered (note, however, that the notation is not the same):

Case 1:	U = 2.245	γ = -46.001	β = 0.2	K = 0,
Case 2:	U = 12.598	γ = 71.941	β = 0.18	K = 100,
Case 3:	U = 15.111	γ = 46.88	β = 0.25	K = 100.

The location of the linear spring is constant, $\xi_s = 0.8$. In all three cases, $d - bc \neq 0$. Two tables are presented below, showing the coefficients found and the corresponding equivalent class defined in Guckenheimer and Holmes (1983), p. 399).

Table 5.1 Normal form coefficients

	d	c	b
Case 1	-1	-1.518	3.954
Case 2	-1	-0.070	-24.31
Case 3	-1	-3.390	1.656

Table 5.2 Respective signs and equivalent class

	d	c	b	d-bc	Class
Case 1	-1	-	+	+	VIa
Case 2	-1	-	-	-	VIII
Case 3	-1	-	+	+	VIa

Starting from (5.49), the classification of the different unfoldings can be undertaken. For example, one can easily show that pitchfork bifurcations occur from 0 on the lines $\mu_1 = 0$ and $\mu_2 = 0$, and also that pitchfork bifurcations occur from $((-\mu_1)^{1/2}, 0)$ on the line $\mu_2 = c\mu_1$, and from $(0, (-\mu_2/d)^{1/2}$ on the line $\mu_2 = d\mu_1/b$ (See Appendix 9). The behaviour of the system remains simple, as long as Hopf bifurcations do not occur from the newly fixed point. This is the case when $d - bc < 0$. Hence, in case 2, no Hopf bifurcation can occur, while it is possible in cases 1 and 3.

The bifurcation sets, and the associated phase portraits can be constructed for the different unfoldings; it is evident that in case 2 (Fig.5.5(a)), no global bifurcations are involved, while in the other two cases, a heteroclinic loop (or saddle loop) emerges (Fig.5.5(b)).

5.3 IN SEARCH OF CHAOS

In the previous section, the use of the modern tools of nonlinear dynamics has shown how complicated equations can be recast into simple ones, and how these simple equations can, in turn, generate very interesting bifurcation sets. Of course, by studying lower dimensional subsystems, the discussion of all the possible motions may not be complete. However, the comparison of the equations on the subsystem with those of some well-known oscillators (such as the oscillator described by Duffing's equation) may provide guidance as to where chaotic motions may exist. For the moment, for a dynamical system like the cantilevered pipe conveying fluid, only a few different "routes to chaos" have been recorded and have been studied extensively in the last decade.

One of them is associated with the class of dynamical systems which possess homoclinic or heteroclinic orbits when unperturbed. In two-dimensional systems, this idea was developed by Melnikov (1963) and other researchers through Silnikov's example in three-dimensional space (Wiggins 1988).

Heteroclinic orbits are defined as trajectories connecting distinct non-hyperbolic fixed points; homoclinic orbits as trajectories connecting a saddle point to itself. They are not indicative of any complicated motions in themselves, rather of a boundary (or separatrix) between two qualitatively-distinct motions. In continuum mechanics, they often arise as structures separating two distinct phases of continua. More specifically, they may arise in the phase space of the Euler-Lagrange equations associated with minimizing some type of energy function of a system (Wiggins 1988). Practically speaking, when perturbed, these homoclinic or heteroclinic orbits are, however, often associated with chaotic motions. Indeed, the intersection of manifolds usually causes an infinite number of intersections among the stable

and unstable manifolds, yielding either homoclinic or heteroclinic intersections. These lead to the well-known tangles that can be described by Smale's horseshoes (Smale 1963,1967).

Another route to chaos, developed by Feigenbaum (1983), is associated with period-doubling. It is usually illustrated by the one-dimensional map

$$F_\mu(x) = \mu x\,(1 - x), \tag{5.50}$$

where μ is a parameter to be varied. This map is called the quadratic, or logistic map. For some value of μ ($\mu > 4$), the behaviour of F_μ^2 on a restrained interval is very similar to that of F_μ on its original domain [0, 1]. A new fixed point is expected in this interval; it becomes a period-two point for F_μ. Eventually, this "fixed point" will itself period-double, just as the first fixed point did for F_μ, producing period-four points. Continuing this procedure, one expects to see F_μ undergo a series of period-doublings, as μ increases. Mathematically, one can define a renormalization operator. This renormalization method, in fact, describes a universal behaviour which represents this famous route to chaos.

Another frequently occuring route to chaos is called intermittency. This concept has been developed by Pomeau and Manneville (1980) and is discussed in detail in Bergé et al. (1984). Suppose that the dynamical variables are observed as functions of time. Intermittency occurs as follows. For a certain control-parameter value, the observed variables undergo periodic oscillations that are regular and stable. If that control parameter is slightly modified, these regular periodic oscillations are interrupted by "bursts". Further modification will cause more frequent bursts, and the duration of the regular oscillations decreases. Hence, intervals of regular behaviour, present for varying periods of time, are separated by chaotic portions. Again, the logistic map can be used to illustrate transitions to chaos by intermittency.

A further route to chaos, exhibiting universal

behaviour, may also be obtained through quasiperiodicity and mode-locking. These topics, discussed by Jensen et al. (1984) and Bak (1986), are illustrated by circle maps of the form

$$\theta_{n+1} = f(\theta) = \theta_n + \Omega + g(\theta_n), \qquad (5.51)$$

where

$$g(\theta_n) = g(\theta_{n+1}).$$

A "winding number" characterizes the behaviour of (5.51) under iteration. It is defined by

$$W = \lim_{n \to \infty} (f^n(\theta) - \theta)/n.$$

It represents the average increase in the angle θ per iteration. For a mode-locked state, W is a rational number; for quasiperiodic states, it becomes irrational, and for chaotic state, the winding number is not defined. For more details, see Jensen et al. (1984).

Finally, it may be important to mention that chaos is always associated with strange attractors, i.e. attracting sets with a fractal dimension (Mandelbrot 1983; Grassberger and Procaccia 1983; Moon 1987). There are no methods to provide necessary and sufficient conditions for a strange attractor to exist. Hence, many researchers, beginning to study nonlinear systems, overlook some crucial points, such as those outlined in the previous section. The presence of horseshoes, for example, highlights the possibility of chaos, i.e. it yields existence conditions but not the attractivity of the strange attractor.

Moreover, the existence of a strange attractor, or of any other stable steady state, in fact, does not preclude the existence of other steady states. This will be illustrated through various examples in this section.

5.3.1 Numerical investigations near the degenerate points

The study of the normal forms for different sets of parameters has allowed the classification of degenerate fixed points through very rich bifurcation sets. It has proved that under certain conditions, homoclinic and heteroclinic bifurcations may occur, also demonstrating that global bifurcations can be detected by means of local analysis.

Li and Paidoussis (1990) found regions for chaos to exist, in the vicinity of the doubly-degenerate point, by perturbing these heteroclinic orbits. The perturbations were associated with the variation of the flow velocity assumed to be equal to

$$U = U_0 + \varepsilon\nu \sin\omega t.$$

However, double degeneracy was only possible for negative γ, which corresponds physically to a standing pipe. In order to achieve this double degeneracy for positive γ, a linear spring was added here. Although doubly-degenerate fixed points exist for sufficiently large stiffness K, the normal forms found have proved that heteroclinic bifurcations did not always exist.

Hence here, case 3, U = 15.1, γ = 43.8, K = 100, ξ_s = 0.8 and β = 0.25 is considered. All the conditions to get chaotic motions are satisfied, and chaotic motions are found to exist. This is illustrated by a bifurcation diagram, the corresponding phase portraits, some theoretical FFT power spectra and the calculation of the Lyapunov exponents. For more details on the construction of the actual figures, see Appendix 10.

Through the variation of the perturbation ν, different characteristics of the system may be observed:

- oscillations around one of the fixed points (ν = 0.5, Fig.5.6(a));
- quasiperiodic oscillations around the whole system, since the attracting limit cycles of

the two fixed points are involved ($\nu = 2$, Fig.5.6(b));

- periodic oscillations around the two fixed points (notice that the origin is still unstable) ($\nu = 5$, Fig.5.7(c));
- periodic oscillations involving period-doubling (observed in both the phase portrait and the power spectrum) ($\nu = 8$, Fig.5.6(d));
- chaotic oscillations ($\nu = 11$, Fig.5.6(e)).

All results are summarized in two bifurcation diagrams. Fig.5.6(f1) represents the maximum displacement of the tip (free end) as a function of the perturbation ν. Periodic regions are clearly defined. However, in order to distinguish between quasiperiodic and chaotic oscillations, the calculation of the Lyapunov exponents is necessary (Fig.5.6(f2)).

The sign of the Lyapunov exponent provides the qualitative dynamics of the system: $\sigma > 0$ for chaotic motions, $\sigma = 0$ for periodic motions, and $\sigma < 0$ for a stable fixed point. However, for periodically-forced dynamical systems, the n-dimensional ordinary differential equation (ODE),

$$\dot{x} = f(x,t), \quad x \in \mathbf{R}^n,$$

can always be recast in an (n + 1)-dimensional ODE,

$$\dot{x} = f(x,\theta),$$
$$\dot{\theta} = 1; \quad (x,\theta) \in \mathbf{R}^n \times \mathbf{R}.$$

The exponent corresponding to the time variable is always zero. Hence, since this zero exponent is always missing in the computation, for the non-autonomous system, the case $\sigma < 0$ also corresponds to periodic motions (oscillating at the externally-applied frequency). When $\sigma = 0$, both the forcing frequency and the system response frequency are present.

Qualitatively, the results obtained agree very well with the ones given by Li and Païdoussis (1990).

Finally, it should be mentioned that the forcing frequency is very important. It was chosen close to the natural frequency of the system ($\omega_0 = 12.79$) to "achieve" resonance. For lower values of ω, only periodic oscillations are observed (Fig.5.6(g)). Hence, further studies should also investigate the effect of the forcing frequency as done in previous analysis (Tousi and Bajaj 1985, Bajaj 1987, Tang and Dowell 1988, Namachchivaya and Tien 1989). From a quantitative point of view, the value of the perturbation ν can no longer be considered as small, which was one of the assumptions made. One justification is that the study of the normal form (5.47) only provides guidance as to where chaos may exist; it is usually difficult to prove that the strange attractor will indeed be the attracting set.

Moreover, it is still unclear how the saddle connections behave in high-dimensional spaces. The study of this problem is beyond the scope of the present thesis and is left to future investigation. Perhaps other "universal" characteristics of strange attractors and chaotic oscillations will appear in this rather simple case of a pipe conveying fluid!

5.3.2 Investigation of the constrained cantilevered pipe

Nonlinear vibrations of a constrained pipe conveying fluid have been studied extensively over the past few years. Païdoussis and Moon (1988) and Païdoussis et al. (1989, 1990) have demonstrated that chaotic oscillations exist, both theoretically and experimentally. They proved that beyond the Hopf bifurcation, regions of period-doubling occur and lead to chaos. The first theoretical studies were based on the simplest analytical model (two-degrees-of-freedom or four-dimensional model) in which the only nonlinear effects are due to the motion-limiting constraints. In a refined model (N = 4

or 5), Paidoussis et al. (1990) compared qualitative and quantitative results with experimental ones. Again, they showed that beyond the Hopf bifurcation, as the flow velocity is increased, a pitchfork bifurcation is followed by a cascade of period-doubling bifurcations leading to chaos.

Here, the "simplest" model is used (i.e. N = 2), but the nonlinearities of the pipe are taken into account.

Fig.(5.7) represents schematically the experimental system and a corresponding idealization of the motion constraints by a cubic spring. In Fig.5.7(b,c), the force-displacement curves of the real (experimental) constraints and of the idealized (cubic spring) ones are shown. Hence, to approximate accurately the real constraints, high values of K (nondimensional spring stiffness) are necessary. Paidoussis et al. (1989) took a value of K = 100 to overcome some numerical problems (with higher values, the numerical scheme was diverging), and obtained sometimes unrealistic quantitative results, especially for the displacement of the pipe which was found, in some cases, to be greater than the length of the pipe itself! Their conclusion was that the two-degrees-of-freedom model was insufficient to physically represent the real system. In comparison with the experimental characteristics, the nondimensional stiffness chosen here is $K = 10^5$, and the two-degrees-of-freedom approximation is considered. Hence, the nondimensional forces due to impact are

$$F = K\,\delta(\xi - \xi_b)^3 = 10^5\,\delta(\xi - \xi_b)^3,$$

where δ represents the Dirac delta function and ξ_b the location of the impact. Note that a change of the stiffness K ($K = 10^5$ or $K = 10^6$) only modifies the gap between the pipe and the constraints.

In order to compare all the theoretical results with the experimental ones, some parameter values were taken from Paidoussis and Moon (1988), $\gamma = 26.75$, $\beta = 0.213$ (see Fig.6 of

that paper). For a sufficiently high value of ξ_b ($\xi_b = 0.75$), a pitchfork bifurcation, followed by a series of period-doubling bifurcations, arises, leading to chaotic motions. The variable parameter chosen is the dimensionless flow velocity U. At U = 7.35, a Hopf bifurcation occurs, leading to periodic oscillations (Fig.5.8(a)). A new periodic orbit is created through a pitchfork bifurcation at U = 9.22. This last bifurcation breaks the "symmetry" of the system, as shown in Fig.5.8(b). Mathematically, this comes from the crossing of a Floquet multiplier associated with the periodic trajectory, with the unit circle at +1 (Tousi and Bajaj 1985, Païdoussis et al. 1989). Physically, the system oscillates around a newly generated steady-state. Finally, the period-doubling bifurcation is clearly visible at U = 10.2 (Fig.5.8(c)) and at U = 10.295 (Fig.5.8(d)). At U > 10.35, the motion becomes narrow-band chaotic, and wide-band chaotic at U > 10.38 (Fig.5.8(g,h)). From a physical point of view, the mechanism leading to chaos is related to the interaction of limit-cycle motion and potential wells associated with divergence of the pipe at the constraints.

All these characteristics can be observed either in the phase-plane portraits or in the corresponding power spectra (chaotic oscillations being associated with a wide frequency band). Notice however that the main frequency is still present at U = 10.4.

Again, all the results are summarized in two bifurcation diagrams where the maximum tip displacement and the Lyapunov exponents are plotted as functions of the flow velocity U (Fig.9(a,b)). For the autonomous system, $\sigma < 0$ represents stable equilibria, $\sigma = 0$ corresponds to periodic oscillations and $\sigma > 0$ proves the existence of chaotic motions.

It is observed that, after the region of chaos, the system "regains stability," which corresponds exactly to experimental investigations: for higher flow velocities,

beyond the chaotic regions, the system becomes unstable by divergence. This clearly appears in the bifurcation diagrams as well as in Fig.5.10. The oscillations are periodic for U = 10.82 and are damped for even higher flow velocities. An investigation of the existence of fixed points (similarly to Section 5.1) indicates that a subcritical saddle-node bifurcation occurs at U = 9.85; two fixed points exist beyond that value of U; one of them stable, and the other one unstable (Iooss and Joseph 1981). The computation of their respective eigenvalues leads to the conclusion that the stable fixed point becomes "more and more" stable when U increases, until finally it becomes the strongest limit set in the system. By setting initial conditions close to the stable equilibrium, the detection of the fixed points is possible, even in chaotic regions (Fig.5.10(c)). Hence, different attractors coexist. This illustrates the last remark of the introduction of the section.

All the previous results prove that "the simplest" analytical model (N = 2) can be used to study the autonomous "infinite" dimensional model with good accuracy, when the nonlinearities of the pipe are taken into account. Of course, the thresholds of the Hopf and period-doubling bifurcations are lower than in reality, since they essentially depend on linear analysis. However, not only were the qualitative features found numerically, but also very good agreement with experimental observations can be achieved with the nonlinear model. Numerically, using the nonlinear model, the qualitative features of a constrained cantilevered pipe conveying fluid were in close agreement with the experimental observations.

CHAPTER VI
CONCLUSION

6.1 RECAPITULATION OF THE FUNDAMENTAL WORK UNDERTAKEN

In this thesis, the nonlinear dynamics of a tube conveying fluid have been examined theoretically by means of a two-degree-of-freedom (four-dimensional) analytical model.

Two distinct methods, one based on Hamilton's principle and the other on the Newtonian approach, were used to derive the equations of motion. Hamilton's principle was used in its general form, applied to the tube fluid system, which is an "open" system since fluid is flowing in and out of it. In Hamilton's principle (associated to an energy or a variational principle), terms of up to fourth order had to be considered in order to find an exact third order nonlinear differential equation. Therefore, particular attention was paid to the formulation of the kinetic and potential energies. At that order of magnitude, many concepts had to be justified and clarified: the set of coordinates to be used (the stress tensors and displacement vectors do not have the same expressions in the Euler and Lagrange coordinates), the inextensibility condition for the cantilevered pipe and its implications, an exact expression of the potential energy and the fluid velocity, and so on. Hence, all the energy terms used in Hamilton's principle had to be derived very carefully. In the case of the pipe fixed at both ends, some "controversial" concepts were also clarified.

For the Newtonian approach, a force balance method in vector form was considered. The inextensibility condition and the expression of the curvature (and some of its characteristics) were used, but terms of fourth order $O(\epsilon^4)$ could be neglected.

It was found that the two methods yielded identical results. The energy method was more tedious than the force balance method, mostly because of the aforementioned fourth order terms that had to be retained in the equations. However, the derivation of the equations of motion of a system with two different methods has its usefulness, from both scientific and utilitarian points of view, since it gives confidence in the results obtained.

The final equations were discussed from a physical point of view, put in a standard form (using an approximate method to transform the nonlinear inertial terms), and discretized with the Galerkin method. Expressing the deflection of the pipe as the superposition of the normal modes of a cantilever beam, the partial differential equations were recast into a set of ordinary differential equations. The nonlinear coefficients defined from integrals of the eigenfunctions of the beam and their derivatives were computed numerically.

Then, the nonlinear equations of motion obtained by different authors were described, discussed and compared. For this purpose, some careful derivations were necessary to get a comparable set of equations. For the cantilevered pipe, the equations were divided into three classes. Appearing under a different format, it was proved that those three sets of equations were (almost) identical. For the pipe fixed at both ends, however, none of the nonlinear equations derived previouslywere found to be complete and exact. Some approximate equations were nevertheless found by different authors.

The linear system was then studied in order to find the critical parameters corresponding to the following stability boundaries: divergence, flutter and concurrent divergence and flutter. Two different methods were applied: Routh's criteria, and a direct eigenvalue analysis. Hence, not only were the stability boundaries found, but also the

types of instability within those boundaries were identified.

The instabilities were studied further using the nonlinear equations. Both the existence and stability of all the fixed points were investigated by computing the eigenvalues, and the results obtained verified by numerically integrating the governing equations. Some physical consequences were discussed.

Using the centre manifold theory, the number of dimensions of the system at the degenerate fixed point was reduced, to obtain a simplified subsystem. In the case of a zero eigenvalue, a pitchfork bifurcation (divergence), was found to occur. Using the method of averaging, supercritical Hopf bifurcations were obtained, and the approximation of the simplified subsystem on the centre manifold was compared with the actual flow computed numerically. Very good agreement was found between them.

Near some fixed points of higher degeneracy (codimension-two bifurcation), the qualitative dynamics were also examined. Using normal form theory, the behaviour of the system in the neighbourhood of those highly degenerate fixed points was described clearly, and its evolution while varying the parameters was discussed in detail.

This local bifurcation analysis revealed the existence of homoclinic and heteroclinic orbits. The non-autonomous system was studied near the doubly-degenerate point. Depending on the perturbation of the flow velocity, periodic, quasi-periodic and chaotic oscillations were proved to exist. This was confirmed by constructing time-trace plots, phase portraits, bifurcation diagrams and power spectra, and by calculating the corresponding Lyapunov exponents.

Finally, the case of a cantilevered pipe, constrained by motion-limiting restraints, was investigated. The analytical model of the impact forces is close to the experimental one, but the pipe itself was still approximated

by a two-degree-of-freedom model. With increasing flow velocity, beyond the Hopf bifurcation, regions of chaotic oscillations were found.

As in previous studies, the mechanism leading to chaos was to be related to the interaction of limit-cycle motion and potential wells associated with divergence of the pipe at the constraints, and the route chaos was via period-doubling bifurcations. Again, phase orbits, bifurcation diagrams, power spectra were constructed, and Lyapunov exponents calculated. With this "refined" model, the theoretical displacements of the pipe were very close to experimental observation. In particular, as the flow velocity was increased, the chaotic oscillations disappeared and the system finally became only statically unstable.

6.2 SUGGESTIONS FOR FURTHER INVESTIGATION

There are many possible directions in which the work presented in this thesis could be extended.

The order of discretization of the equation and the approximation of this infinite dimensional system could be reviewed. The study could start from the partial differential equations, say by using the Lyapunov-Schmidt approach, or the number of degrees of freedom of the discretized system could be increased. In both cases, qualitative and quantitative comparisons with the model developed here might be interesting.

Refinements could also be made to the modeling of the fluid. Thus, the fluid forces could be formulated by means of ideal flow theory, rather than by considering the fluid as an infinitely flexible rod (plug flow). Moreover, even in the case of the plug flow theory, nonlinearities of the flow components could be considered.

A complete and detailed experimental study, in parallel with the theory developed in this thesis may be of

great interest.

Concerning bifurcation theory, the use of some new software like the AUTO packages (Doedel 1986) would allow systematic construction of the bifurcation diagrams, and the verification of the results found here.

In terms of nonlinear dynamics, it is still unclear what the implications of saddle-node connections within high dimensional spaces are. A deeper investigation in that direction would perhaps be useful to explain the onset of chaos near the doubly-degenerate fixed points.

Finally, in the case of the non-autonomous system, attention should be paid to the influence of the forcing frequency. Chaotic oscillations associated with quasi-periodicity and mode-locking might be present in the system. The study of the parametric and combination resonances from a nonlinear point of view might lead to the uncovering of even richer dynamics.

REFERENCES

Bajaj, A.K., Sethna, P.R., and Lundgren, T.S., 1980, "Hopf bifurcation phenomena in tubes carrying a fluid", SIAM Journal of Applied Mathematics, Vol. 39, pp. 213-230.

Bajaj, A.K., 1987, "Nonlinear dynamics of tubes carrying a pulsatile flow", Dynamics and Stability of Systems, Vol. 2, No. 1, pp. 19-41.

Bak, P., 1986, "The Devil's staircase", Physics Today, Vol. 39, December, pp. 38-45.

Benjamin, T.B., 1961, "Dynamics of a system of articulated pipes conveying fluid. I. Theory; II. Experiments", Proceedings of the Royal Society (London), Series A, Vol. 261, pp. 457-486 and 487-499.

Bergé, P., Pomeau, Y., and Vidal, C., 1984, Order within Chaos. New York: John Wiley.

Bisplinghoff, R.L., Ashley, H. and Halfman, R.L., 1957, Aeroelasticity. Reading: Addison-Wesley.

Bourrières, F.-J., 1939, "Sur un phénomène d'oscillation auto-entretenue en mécanique des fluides réels", Publications Scientifiques et Techniques du Ministère de l'Air, Numéro 147.

Carr, J., 1981, Applications of Center Manifold Theory. New York: Springer.

Ch'ng, E., 1977, A Theoretical Analysis of Nonlinear Effects on the Flutter and Divergence of a Tube Conveying Fluid. AMS Report No. 1343, Department of Aerospace and Mechanical Sciences. Princeton, New Jersey: Princeton University.

Chow, S.N., and Mallet-Paret, J., 1977, "Integral averaging and bifurcation", Journal of Differential Equations, Vol. 26, pp. 112-159.

Devaney, R.L., 1986, An Introduction to Chaotic Dynamical Systems. Menlo Park, California: Benjamin/Cummings.

Doedel, E., 1986, AUTO: Software for Continuation and Bifurcation Problems in Ordinary Differential Equations, Preprint.

Dodds, H.L.Jr., and Runyan, H.L., 1965, "Effect of high velocity fluid flow on the bending vibrations and static divergence of a simply supported plate", NASA Technical Note D-2870.

Edelstein, W.S., Chen, S.S. and Jendrzejczyk, J.A., 1986, "A finite element computation of the flow-induced oscillations in a cantilevered tube", Journal of Sound and Vibration, Vol. 107(1), pp. 121-129.

Eringen, A.C., 1967, Mechanics of Continua. New York: Wiley.

Feigenbaum, M.J., 1983, "Universal behaviour in nonlinear systems", pp.101-138, in Nonlinear Dynamics and Turbulence, G. Barenblatt, G. Iooss, and D.D. Joseph (eds.). Boston: Pitman.

Fung, Y.C., 1969, A first course in continuum mechanics. Englewood Cliffs, New Jersey: Prentice-Hall.

Grassberger, P. and Procaccia, I., 1983, "Characterization of strange attractors", Physical Review Letters, Vol. 50, pp. 189-208.

Gregory, R.W., and Paidoussis, M.P., 1966, "Unstable oscillation of tubular cantilevers conveying fluid. I. Theory; II. Experiments", Proceedings of the Royal Society (London), Series A, Vol.293, pp. 512-527 and 528-542.

Guckenheimer, J., and Holmes, P.J., 1983, Nonlinear Oscillations, Dynamical Systems and Bifurcations of Vector Fields. New York: Springer.

Holmes, P.J., 1977, "Bifurcations to divergence and flutter in flow-induced oscillations: a finite-dimensional analysis", Journal of Sound and Vibration, Vol. 53, pp. 471-503.

Holmes, P.J., 1978, "Pipes supported at both ends cannot flutter", Journal of Applied Mechanics, Vol. 45, pp. 669-622.

Holmes, P.J., and Marsden, J.E., 1978, "Bifurcations to divergence and flutter in flow-induced oscillations: an infinite-dimensional analysis", Automatica, Vol. 14(4), pp. 367-384.

Housner, G.W., 1952, "Bending vibrations of a pipe line containing flowing fluid", Journal of Applied Mechanics, Vol. 19, pp. 205-208.

Iooss, G., and Joseph, D.D., 1981, Elementary Stability and Bifurcation Theory. New York: Springer.

Jensen, M. H., Bak, P., and Bohr, T., 1984, "Transition to chaos by interaction of resonances in dissipative systems. I. Circle maps". Physical Review, Vol. 30 A, pp. 1960-1969.

Joseph, D.D., and Sattinger, D.H., 1972, "Bifurcating time periodic solutions and their stability", Archive for Rational Mechanics and Analysis, Vol. 45, pp. 79-109.

Langford, W.F., 1983, "A review of interactions of Hopf and steady-state bifurcations", pp.215-237 in Nonlinear dynamics and Turbulence, G. Barenblatt, G. Iooss, and D.D. Joseph (eds.). Boston: Pitman.

Léger, P., and Wilson, E.L., 1988, "Modal summation methods for structural dynamics computations", Earthquake Engineering and Structural Dynamics, Vol. 16, pp. 23-27.

Li, G.X., and Paidoussis, M.P., 1990, "Stability, double degeneracy and chaos in cantilevered pipes conveying fluid". Submitted to Physica D.

Lundgren, T.S., Sethna, P.R., and Bajaj, A.K., 1979, "Stability boundaries for flow-induced motions of tubes with an inclined terminal nozzle", Journal of Sound and Vibration, Vol. 64, pp.553-571.

Mandelbrot, B., 1983, The Fractal Geometry of Nature. San Francisco: W.H. Freeman.

Marsden, J.E., and McCracken, M., 1976, The Hopf Bifurcation and Its Applications. New York: Springer.

McIver, D.B., 1973, "Hamilton's principle for systems of changing mass", Journal of Engineering Mathematics, Vol. 7, pp. 249-261.

Melnikov, V.K., 1963, "On the stability of the centre for time periodic perturbations", Transactions of the Moscow Mathematical Society, Vol. 12, pp. 1-57.

Minorsky, N., 1962, Nonlinear Oscillations. New York: Van Nostrand.

Moon, F.C., 1987, Chaotic Vibrations: An Introduction for Applied Scientists and Engineers. New York: John Wiley.

Namachchivaya, N.S., and Tien, W.M., 1989, "Bifurcation behavior of nonlinear pipes conveying pulsating flow", Journal of Fluids and Structures, Vol. 3, pp. 609-629.

Niordson, F.I., 1953, "Vibrations of a cylindrical tube containing flowing fluid", Kungliga Tekniska Högskolans Handlingar, No. 73.

Paidoussis, M.P., 1966, "Dynamics of flexible slender cylinders in axial flow - I. Theory", Journal of Fluid Mechanics, Vol. 26, pp. 717-736.

Paidoussis, M.P., 1970, "Dynamics of tubular cantilevers conveying fluid", Journal of Mechanical Engineering Science, Vol. 12, pp. 85-103.

Paidoussis, M.P., 1987, "Flow-induced instabilities of cylindrical structures", Applied Mechanics Reviews, Vol. 40, pp. 163-175.

Paidoussis M.P., Cusumano, J.P., and Copeland, G.S., 1988, "Low-dimensional chaos in a flexible tube conveying fluid", (submitted for publication to Journal of Applied Mechanics in July 1989).

Paidoussis, M.P., and Issid, N.T., 1974, "Dynamic stability of pipes conveying fluid", Journal of Sound and Vibration, Vol. 33, pp. 267-294.

Paidoussis, M.P., Li, G.X., and Moon, F.C., 1989, "Chaotic oscillations of the autonomous system of a constrained pipe conveying fluid", Journal of Sound and Vibration, Vol. 135,

pp. 1-19.

Païdoussis, M.P., Li, G.X., and Rand, R.H., 1989, "Chaotic motions of a constrained pipe conveying fluid: comparison between simulation, analysis and experiment", accepted for publication in Journal of Applied Mechanics in November 1990.

Païdoussis, M.P., and Moon, F.C., 1988, "Nonlinear and chaotic fluidelastic vibrations of a flexible pipe conveying fluid", Journal of Fluids and Structures, Vol. 2, pp. 567-591.

Pomeau, Y., and Manneville, P., 1980, "Intermittent Transition to Turbulence in Dissipative Dynamical Systems", Communications in Mathematical Physics, Vol. 74, pp. 189-197.

Rand, R.H., 1984, Computer Algebra in Applied Mathematics: An Introduction to MACSYMA. Boston: Pitman.

Rousselet, J., 1975, Dynamic behavior of pipes conveying fluid near critical velocities. (Ph.D. Dissertation, Stanford University.)

Rousselet, J., and Herrmann, G., 1977, "Flutter of articulated pipes at finite amplitude", Journal of Applied Mechanics, Vol. 44, pp. 154-158.

Rousselet, J., and Herrmann, G., 1981, "Dynamic behavior of continuous cantilevered pipes conveying fluid near critical velocities", Journal of Applied Mechanics, Vol. 48, pp.945-947.

Routh, E.J., 1960, Dynamics of System of Rigid Bodies. Part II. Articles, pp. 290-301. New York: Dover.

Sanders, J.A., and Verhulst, F., 1985, Averaging Methods in Nonlinear Dynamical Systems. New York: Springer.

Sethna, P.R., and Shaw, S.W., 1987, "On codimension-three bifurcations in the motion of articulated tubes conveying a fluid", Physica D, Vol. 24, pp. 305-327.

Smale, S., 1963, "Diffeomorphisms with many periodic points". In Differential and Combinatorial Topology, S.S. Cairns (ed.), pp. 63-80. Princeton: Princeton University Press.

Smale, S., 1967, "Differentiable dynamical systems", Bulletin of the American Mathematical Society, Vol. 73, pp. 747-817.

Snowdon, J.C., 1968, Vibration and Shock in Damped Mechanical Systems. New York: John Wiley.

Steindl, A., and Troger, H., 1988, "Flow induced bifurcations to 3-dimensional motion of tubes with elastic support", pp. 128-138 in Trends in Applications of Mathematics to Mechanics, J.F. Besserling and W. Eckhaus (eds.). Berlin: Springer.

Stoker, J.J., 1968, Nonlinear elasticity. New York: Gordon and Breach.

Sugiyama, Y. Tanaka, Y., Kishi, T., and Kawagoe, H., 1985, "Effect of a spring support on the stability of pipes conveying fluid", Journal of Sound and Vibration, Vol. 100, pp. 257-270.

Takens, F., 1974, "Singularities of Vector Fields", Publications Mathématiques (Institut des Hautes Etudes Scientifiques), vol. 43, pp. 47-100.

Tang, D.M., and Dowell, E.H., 1988, "Chaotic oscillations of a cantileverd pipe conveying fluid", Journal of Fluids and Structures, Vol. 2, pp. 263-283.

Thompson, J.M.T., and Stewart, H.B., 1986, Nonlinear Dynamics and Chaos. Chichester: John Wiley.

Thurman, A.L., and Mote, C.D. Jr., 1969, "Non-linear oscillation of a cylinder containing flowing fluid", Journal of Engineering for Industry, Transactions of the American Society of Mechanical Engineers, Vol. 91, pp. 1147-1155.

Timoshenko, S.P., and Gere, J.M., 1961, Theory of Elastic Stability. New York: McGraw-Hill.

Tousi, S., and Bajaj, A.K., 1985, "Period-doubling bifurcations and modulated motions in forced mechanical systems", Journal of Applied Mechanics, Vol.57, pp.446-452.

Wiggins, S., 1988, Global Bifurcations and Chaos: Analytical Methods. New York: Springer.

APPENDIX 1

Interesting properties of the curvature κ and the unit vector τ

Let the location of a material point be given by

$$\vec{r} = x\vec{i} + y\vec{j} + z\vec{k}, \tag{A1.1}$$

where $\vec{i}$, $\vec{j}$, $\vec{k}$ are fixed orthogonal unit vectors.

As it was proved for an inextensible pipe, the arc length s can be used as the material variable. Hence,

$$\vec{\tau} = \frac{\partial \vec{r}}{\partial s} = \frac{\partial x}{\partial s}\,\vec{i} + \frac{\partial y}{\partial s}\,\vec{j} + \frac{\partial z}{\partial s}\,\vec{k}, \tag{A1.2}$$

and the normal and the binormal vectors, $\vec{n}$ and $\vec{b}$, are given by

$$\frac{\partial \vec{\tau}}{\partial s} = \kappa\vec{n}, \quad \vec{b} = \vec{\tau}\times\vec{n}, \tag{A1.3}$$

where κ is the curvature of the centreline.

By definition, one has

$$\vec{\tau}.\frac{\partial \vec{\tau}}{\partial s} = 0, \quad \vec{\tau}.\vec{b} = 0. \tag{A1.4}$$

$\vec{\tau}$ being a unit vector, for a two-dimensional problem,

$$|\vec{\tau}| = \left(\frac{\partial x}{\partial s}\right)^2 + \left(\frac{\partial y}{\partial s}\right)^2 = 1, \tag{A1.5}$$

($\vec{\tau}$, $\vec{n}$, $\vec{b}$) representing orthogonal vectors.

Using (A1.3) through (A1.5) and Frenet-Serret formulas yields

$$\frac{\partial \vec{\tau}}{\partial s}.\frac{\partial^2 \vec{\tau}}{\partial s^2} = \vec{b}.\frac{\partial \vec{b}}{\partial s} = \frac{1}{2}\,\frac{\partial}{\partial s}(\kappa^2), \tag{A1.6}$$

$$\vec{\tau} \cdot \frac{\partial^2 \vec{\tau}}{\partial s^2} = -\kappa^2, \qquad \text{(A1.7)}$$

$$\vec{\tau} \cdot \frac{\partial^3 \vec{\tau}}{\partial s^3} = -\frac{3}{2} \frac{\partial}{\partial s}(\kappa^2). \qquad \text{(A1.8)}$$

APPENDIX 2

Derivation of the equations of motion by the energy method: additional proofs

Equation 2.27

$$\alpha = \int_{t_1}^{t_2} \int_{0}^{L} g(s) \left(\int_{0}^{s} f(s)\ \delta y\ ds \right) dsdt.$$

Integrating by parts leads to

$$\alpha = \int_{t_1}^{t_2} \left[\left(\int_{0}^{s} g(s)\ ds \right) \left(\int_{0}^{s} f(s)\ \delta y\ ds \right) \right]_{0}^{L} dt -$$

$$\int_{t_1}^{t_2} \int_{0}^{L} f(s)\ \delta y \left(\int_{0}^{s} g(s)\ ds \right) dsdt$$

$$- \int_{t_1}^{t_2} \left(\int_{0}^{L} g(s)\ ds \right) \left(\int_{0}^{L} f(s)\ \delta y\ ds \right) dt -$$

$$\int_{t_1}^{t_2} \int_{0}^{L} \left(\int_{0}^{s} g(s)\ ds \right) f(s)\ \delta y\ dsdt$$

$$- \int_{t_1}^{t_2} \int_{0}^{L} \left(\int_{0}^{L} g(s)\, ds \right) f(s)\ \delta y\ dsdt -$$

$$\int_{t_1}^{t_2} \int_{0}^{L} \left(\int_{0}^{s} g(s)\ ds \right) f(s)\ \delta y\ dsdt$$

$$- \int_{t_1}^{t_2} \int_{0}^{L} \left(\int_{0}^{L} g(s)\ ds - \int_{0}^{s} g(s)\ ds \right) f(s)\ \delta y\ dsdt,$$

$$\alpha = \int_{t_1}^{t_2} \int_0^L \left(\int_s^L g(s)\, ds \right) f(s)\ \delta y\ ds dt. \qquad \text{(A2.1)}$$

Equation 2.29

From (2.28), one obtains

$$\begin{aligned}
\delta \int_{t_1}^{t_2} T\, dt = & \; m \iint (\dot{x}\delta\dot{x} + \dot{y}\delta\dot{y})\ ds dt \\
& + M \iint [\,(\dot{x} + Ux')\ \delta\dot{x} + (\dot{y} + Uy')\ \delta\dot{y} \\
& \qquad + \dot{x}U\,\delta x' + \dot{y}U\,\delta y']\ ds dt \\
= & - \iint [\,(m+M)\ddot{x} + M\dot{U}x' + MUx']\ \delta x\ ds dt \\
& - \iint [\,(m+M)\ddot{y} + M\dot{U}y' + MUy']\ \delta y\ ds dt \\
& + M \int [U\dot{x}\ \delta x\,|_0^L - \int_0^L (U\dot{x}'\ \delta x)\ ds]\, dt \qquad \text{(A2.2)} \\
& + M \int [U\dot{y}\ \delta y\,|_0^L - \int_0^L (U\dot{y}'\ \delta y)\ ds]\, dt \\
= & - \iint [\,(m+M)\ddot{x} + M\dot{U}x' + 2MUx']\ \delta x\ ds dt \\
& - \iint [\,(m+M)\ddot{y} + M\dot{U}y' + 2MUy']\ \delta y\ ds dt \\
& + MU \int [\dot{x}_L\ \delta x_L + \dot{y}_L\ \delta y_L]\ dt.
\end{aligned}$$

Equation 2.31

$$\delta \int G\, dt = (m + M)\, g \iint \delta x\ ds dt.$$

From (2.25) one obtains

$$\delta \int G\,dt = (m + M)g \iint \left[-\left(y' + \frac{1}{2}y'^3\right)\delta y + \int_0^s y''\left(1 + \frac{3}{2}y'^2\right)\delta y\,ds\right] ds dt.$$

Using the relationship (2.27) yields

$$\begin{aligned}\delta \int G\,dt &= (m + M)g \iint \left[-\left(y' + \frac{1}{2}y'^3\right)\delta y + \left(\int_s^L ds\right) y''\left(1 + \frac{3}{2}y'^2\right)\delta y\,ds\right] ds dt \\ &= (m + M)g \iint \left[-\left(y' + \frac{1}{2}y'^3\right) + (L - s)\,y''\left(1 + \frac{3}{2}y'^2\right)\right]\delta y\,ds dt.\end{aligned} \tag{A2.3}$$

Equation 2.33

From (2.7) and (2.26), one has

$$x_L = \sqrt{1 - y_L'^2},$$

$$\delta x_L = -\left(y_L' + \frac{1}{2}y_L'^3\right)\delta y_L + \int_0^L \left(y'' + \frac{3}{2}y'^2y''\right)\delta y\,ds.$$

δx_L being exact to fourth order $O(\epsilon^5)$,

$$x_L'\delta x_L = \left(1 - \frac{1}{2}y_L'^2\right)\delta x_L + O(\epsilon^5).$$

Thus

$$x_L'\,\delta x_L = -y_L'\,\delta y_L + \int_0^L \left(y'' + \frac{3}{2}y'^2y''\right)\delta y\,ds - \frac{1}{2}y_L'^2 \int_0^L y''\,\delta y\,ds,$$

and

$$B = \iint \left[\left(y'' + \frac{3}{2} y'^2 y'' \right) \delta y - \frac{1}{2} y_L'^2 \, y'' \, \delta y \right] \, ds dt \, .$$

By integrating by parts, it is easily proved that

$$y_L'^2 = y'^2 + \int_s^L (y' y'') \, ds.$$

Therefore

$$B = \iint \left[y''(1 + y'^2) - y'' \int_s^L y' y'' \, ds \right] \delta y \, ds dt. \qquad \text{(A2.4)}$$

APPENDIX 3

Internal dissipation

The potential energy defined by (2.15) has been derived by Stoker (1968) by assuming an usual Hooke's stress strain relation

$$\sigma = Ee. \tag{A3.1}$$

The assumption of a Kelvin-Voigt viscoelastic stress-strain relationship yields

$$\sigma = Ee + E^* \left(\frac{\partial e}{\partial t}\right), \tag{A3.2}$$

where E^* is the coefficient of internal dissipation. Following Stoker's approach (1968) and with (A3.2), the element of strain energy becomes

$$dV = \frac{Eb}{2} e^2 \, dxdz + \frac{E^* b}{2} e\left(\frac{\partial e}{\partial t}\right) dxdz. \tag{A3.3}$$

With the condition of inextensibility ($\epsilon = 0$), the strain energy becomes

$$\begin{aligned} V = {} & \frac{Eb}{2} \int_{-h}^{h} \int_{0}^{L} (\kappa z)^2 \, dxdz + \frac{E^* b}{2} \int_{-h}^{h} \int_{0}^{L} \kappa z \, \frac{\partial}{\partial t} (\kappa z) \, dxdz \\ & - \frac{EI}{2} \int_{0}^{L} \kappa^2 \, dx + \frac{E^* I}{2} \int_{0}^{L} \kappa \, \frac{\partial \kappa}{\partial t} \, dx, \end{aligned} \tag{A3.4}$$

with 2h being the thickness of the pipe, and with the usual definition of the moment of inertial I.
Thus,

$$V = \frac{EI}{2}\int_0^L \kappa^2 dx + \frac{E^* I}{2}\frac{\partial}{\partial t}\int_0^L \frac{1}{2}(\kappa^2)\, dx - (\frac{EI}{2} + \frac{E^{**} I}{2}\frac{\partial}{\partial t})\int_0^L \kappa^2\, dx. \tag{A3.5}$$

Consequently, in (2.30) derivatives with respect to time should be taken into account.

APPENDIX 4

Linear and nonlinear coefficients of (2.58), analytical and numerical investigations

The following constants are needed in the coefficients of equation (2.58).

$$a_{ij} = \int_0^1 \phi_i \phi'_j \, d\xi, \quad b_{ij} = \int_0^1 \phi_i \phi''_j \, d\xi, \quad d_{ij} = \int_0^1 \phi_i \phi''_j (1 - \xi) \, d\xi,$$

$$c_{ij} = \alpha \lambda_i^4 \delta_{ij} + 2\sqrt{\beta} U a_{ij}, \; k_{ij} = \lambda_i^4 \delta_{ij} + U^2 b_{ij} + \gamma (a_{ij} - d_{ij}),$$

$$\alpha_{ijkl} = U^2 a_{ijkl} + \gamma b_{ijkl} + c_{ijkl}, \; \beta_{ijkl} = 2U\sqrt{\beta} \, d_{ijkl}, \quad \text{(A4.1)}$$

$$\gamma_{ijkl} = \int_0^1 \phi_i \phi'_j \left\{ \int_0^1 \phi'_k \phi'_l \, d\xi \right\} d\xi - \int_0^1 \phi_i \phi''_j \left\{ \int_\xi^1 \int_0^\xi \phi'_k \phi'_l \, d\xi d\xi \right\} d\xi,$$

where ϕ_i' and ϕ_i'' denote the first and second derivatives with respect to ξ, respectively, λ_i are the beam eigenvalues, and δ_{ij} is the Kronecker delta function. The other 4th order tensors are defined as follows

$$a_{ijkl} = \int_0^1 \phi_i \phi''_j \phi'_k \phi'_l d\xi - \int_0^1 \phi_i \phi'_j \left\{ \int_0^\xi \phi'_k \phi'''_l d\xi \right\} d\xi$$

$$+ \int_0^1 \phi_i \phi''_j \left\{ \int_\xi^1 \int_0^\xi \phi'_k \phi'''_l d\xi \, d\xi \right\} d\xi - \int_0^\xi \phi_i \phi''_j \left\{ \int_0^\xi \phi'_k \phi''_l d\xi \right\} d\xi,$$

$$b_{ijkl} = -\frac{3}{2}\int_0^1 \phi_i\phi''_j\phi'_k\phi'_l(1-\xi)\,d\xi - \frac{1}{2}\int_0^1 \phi_i\phi'_j\phi'_k\phi'_l\,d\xi$$
$$+\int_0^1 \phi_i\phi'_j\left\{\int_0^\xi \phi'_k\phi'''_l(1-\xi)\,d\xi\right\}d\xi$$
$$-\int_0^1 \phi_i\phi''_j\left\{\int_\xi^1\int_0^\xi \phi'_k\phi'''_l(1-\xi)\,d\xi\,d\xi\right\}d\xi$$
$$+\int_0^1 \phi_i\phi''_j\left\{\int_\xi^1 \phi'_k\phi'_l\,d\xi\right\}d\xi,$$

$$c_{ijkl} = 3\int_0^1 \phi_i\phi'_j\phi''_k\phi'''_l\,d\xi + \int_0^1 \phi_i\phi''_j\phi''_k\phi''_l\,d\xi$$
$$-\int_0^1 \phi_i\phi''_j\left\{\int_\xi^1\int_0^\xi \phi''_k\phi''''_l\,d\xi\,d\xi\right\}d\xi$$
$$+\int_0^1 \phi_i\phi'_j\left\{\int_0^\xi \phi''_k\phi''''_l\,d\xi\right\}d\xi - \int_0^1 \phi_i\phi''_j\left\{\int_\xi^1 \phi''_k\phi'''_l\,d\xi\right\}d\xi,$$

$$d_{ijkl} = \int_0^1 \phi_i\phi'_j\phi'_k\phi'_l\,d\xi - \int_0^1 \phi_i\phi'_j\left\{\int_0^\xi \phi'_k\phi''_l\,d\xi\right\}d\xi$$
$$+\int_0^1 \phi_i\phi''_j\left\{\int_\xi^1\int_0^\xi \phi'_k\phi''_l\,d\xi\,d\xi\right\}d\xi - \int_0^1 \phi_i\phi''_j\left\{\int_\xi^1 \phi'_k\phi'_l\,d\xi\right\}d\xi.$$

All the second order coefficients a_{ij}, etc., can be integrated analytically (Paidoussis and Issid 1974), but the fourth order ones, a_{ijkl}, etc., have to be computed numerically. Numerical results, for N = 2, are given below.

ijkl	a_{ijkl}	b_{ijkl}	c_{ijkl}
1111	19.04300	-15.47582	-16.38627
1112	75.16431	-66.13101	1273.4900
1121	5.159856	-6.87628E-001	312.24010
1122	550.0317	-391.3416	-12049.75
1211	-76.2256	29.970540	-57.86457
1212	10.58940	-7.747796	-957.4738
1221	130.0725	-19.9508	223.60980
1222	-365.766	189.0040	8597.1480
2111	-6.221161	4.7676860	-57.86487
2112	85.266840	-13.06411	-1396.075
2121	10.589240	-25.27128	662.21970
2122	-377.9241	185.38710	8597.0570
2211	28.328190	-45.49551	-138.4738
2212	40.006210	-291.7209	6096.2080
2221	52.167130	53.324680	598.09860
2222	3566.6040	-2243.0460	-56848.40

ijkl	d_{ijkl}	γ_{ijkl}
1111	5.4004670	4.5967860
1112	8.7476610	-3.595960
1121	-37.88905	-3.595960
1122	46.627310	25.174220
1211	-2.579286	-3.595965
1212	-1.395648	6.1173500
1221	28.626770	6.1173500
1222	-42.84314	-22.19125
2111	-2.579337	-3.595973
2112	-1.395711	6.1173620
2121	28.626890	6.1173620
2122	-42.84148	-22.19130
2211	28.70733	25.174110
2212	47.09172	-22.19126
2221	-200.643	-22.19126
2222	262.7219	144.72510

APPENDIX 5

Algebraic computation of the matrix [A] and of the Routh's criteria

This is an output file generated by MACSYMA. The matrix [A] and the coefficients of the characteristic polynomial are computed as a function of U, γ, β and K. The viscous damping α and the location of the spring ξ_s are kept constant. The number of mode is equal to 2.

```
RATPRINT:FALSE$
FLOAT2BF:TRUE$
NMODE : 2$

/* ALFA IS THE DAMPING COEFFICIENT */
/* XS IS THE POSITION OF THE LINEAR SPRING */

ALFA : 0.005$
XS: 0.8$

/* EIGENVALUES */

LAM[1]:1.875104$
LAM[2]:4.694091$

/* CALCUL PHI(I) */
/* ************ */

FOR I:1 THRU NMODE DO(
 SIG[I]:(SINH(LAM[I])-SIN(LAM[I]))/(COSH(LAM[I])+COS(LAM[I])),
 W : LAM[I]*XB,
 PHI[I] : COSH(W)-COS(W)-SIG[I]*(SINH(W)-SIN(W)))$
```

```
/* CALCUL Cij, Bij, Eij */
/* ******************** */

FOR I:1 THRU NMODE DO ( FOR J:1 THRU NMODE DO(
  IF I=J THEN (
    BB[I,J] : 2.0,
    CC[I,J] : LAM[I]*SIG[I]*(2.0-LAM[I]*SIG[I]),
    EE[I,J] : 2.0-0.5*CC[I,J] )
         ELSE (
    TAU : (LAM[I]/LAM[J])**2,
    UN : (-1)**(I+J),
    BB[I,J] : 4.0/(TAU+UN),
    CC[I,J] : 4.0*(LAM[J]*SIG[J]-LAM[I]*SIG[I])/(UN-TAU),
    EE[I,J] : (4.0*(LAM[J]*SIG[J]-LAM[I]*SIG[I]+2.0)*UN-
     2.0*(1.0+TAU**2)*BB[I,J])/(1.0-TAU**2)-CC[I,J])))$



/* KRONECKER'S SYMBOL */

FOR I:1 THRU NMODE DO ( FOR J:1 THRU NMODE DO(
  IF I=J THEN (DELTA[I,J]:1.)
         ELSE (DELTA[I,J]:0.)))$

/* COMPUTATION OF A_ij */
/* ****************** */

/* STIFFNESS MATRIX = KK and DAMPING MATRIX  = DA */

FOR I:1 THRU NMODE DO ( FOR J:1 THRU NMODE DO(
KK[I,J]:-(U**2*CC[I,J]+GAM*EE[I,J]+LAM[I]**4*DELTA[I,J]+
K*PHI[I]*PHI[J]),
DA[I,J]:-(2.*U*SQRT(BETA)*BB[I,J]+ALFA*LAM[I]**4*DELTA[I,J])
))$
```

```
A31 : KK[1,1]$
A32 : KK[1,2]$
A33 : DA[1,1]$
A34 : DA[1,2]$
A41 : KK[2,1]$
A42 : KK[2,2]$
A43 : DA[2,1]$
A44 : DA[2,2]$

/* DEFINITION OF THE MATRIX A */


A : MATRIX([0,0,1,0],[0,0,0,1],
[A31,A32,A33,A34],[A41,A42,A43,A44]) ;
```

$$\text{Col 1} = \begin{bmatrix} 0 \\ 0 \\ 2 \\ -0.85824\,U - 2.10527\,K - 1.57088\,GAM - 12.36236 \\ 2 \\ -1.87385\,U + 0.20322\,K + 0.42232\,GAM \end{bmatrix}$$

$$\text{Col 2} = \begin{bmatrix} 0 \\ 0 \\ 2 \\ 11.74323\,U + 0.20322\,K + 0.42232\,GAM \\ 2 \\ 13.29427\,U - 0.01962\,K - 8.64714\,GAM - 485.51831 \end{bmatrix}$$

```
        [                1                ]
        [                                 ]
        [                0                ]
Col 3 = [                                 ]
        [ - 4.0 SQRT(BETA) U - 0.06181    ]
        [                                 ]
        [    - 1.51892 SQRT(BETA) U       ]


        [                0                ]
        [                                 ]
        [                1                ]
Col 4 = [                                 ]
        [     9.51892 SQRT(BETA) U        ]
        [                                 ]
        [ - 4.0 SQRT(BETA) U - 2.42759    ]

/* COMPUTE CHARACTERISTIC POLYNOMIAL OF [A] */
/* **************************************** */

P : DETERMINANT(A-L*IDENT(4))$
P : EXPAND(P)$

/* ********************************************************** */
/* RESULTS */
/* ********************************************************** */
(C25) A0 : COEFF(P,L,0);
/* ********************************************************** */
          4                2                    2               2
10.59538 U  - 29.9768 K U  - 17.63035 GAM U  + 252.34479  U
               2                                                 2
- 1.49012E-8 K  + 18.06371 GAM K + 1022.3887 K + 13.4052 GAM

+ 869.58862 GAM + 6002.15039
```

```
/* ********************************************************** */
(C26) A1 : COEFF(P,L,1);
/* ********************************************************** */
                        3              2
- 14.0700 SQRT(BETA) U  + 1.26172 U  + 6.87377 SQRT(BETA) K U

+ 37.4935 SQRT(BETA) GAM U + 1991.522 SQRT(BETA) U + 5.1119 K

+ 4.34794 GAM + 60.02148
/* ********************************************************** */
(C27) A2 : COEFF(P,L,2);
/* ********************************************************** */
                       2              2
(D27) 30.45851 BETA U  - 12.43603 U  + 9.95761 SQRT(BETA) U

           + 2.12488 K + 10.21801 GAM + 498.03064

/* ********************************************************** */
(C28) A3 : COEFF(P,L,3);
/* ********************************************************** */
(D28)                      8.0 SQRT(BETA) U + 2.4894
/*  ***********************************************************
*                                                              /
```

APPENDIX 6

Jordan form in the case of a double zero eigenvalue

In the case of a double zero eigenvalue, the linear part has to be put into the standard form

$$[Df] = \begin{bmatrix} \begin{bmatrix} 0 & 1 \\ 0 & 0 \end{bmatrix} & 0 \\ 0 & [M] \end{bmatrix}. \qquad \text{(A6.1)}$$

In the case of a 2 x 2 matrix, taking the eigenvector as one of the vectors forming the new base leads automatically to the suggested form. In the case of a 4 x 4 matrix, however, this is not true anymore. Assuming for example that the eigenvalues λ_3 and λ_4 of [M] are real (and not equal to zero), the modal matrix is taken equal to

$$[P] = \left[\begin{pmatrix} \\ \vec{V}_1 \\ \\ \end{pmatrix} \begin{pmatrix} \alpha \\ \beta \\ \gamma \\ \delta \end{pmatrix} \begin{pmatrix} \\ \vec{V}_3 \\ \\ \end{pmatrix} \begin{pmatrix} \\ \vec{V}_4 \\ \\ \end{pmatrix} \right], \qquad \text{(A6.2)}$$

where $\vec{V}_1$ is the eigenvector associated with the zero eigenvalue, and $\vec{V}_3$ and $\vec{V}_4$ are the eigenvectors associated with λ_3 and λ_4 respectively. The quartet (α, β, γ, δ) are the four unknowns of the problem. Since

$$[P]^{-1}.[A].[P] = [Df],$$

one obtains

$$[A].[P] - [P].[Df] = 0. \qquad \text{(A6.3)}$$

(for the case chosen, [M] is diagonal). Substituting [A], [P] and [Df] in the above equations yields the four unknowns α, β, γ and δ and the corresponding modal matrix [P].

Appendix 7

Computation of the modal matrix at the critical parameters

Considering μ as a small parameter, it is not necessary to compute a modal matrix different from the one obtained at the critical parameter: here one assumes that all the parameters are fixed except the flow velocity U, and that the matrix [A], at the critical velocity U_{cr}, contains a pair of purely imaginary eigenvalues. Hence the corresponding eigenvectors $\vec{X}_1$ and $\vec{X}_2$ are complex conjugate. In (5.2.1), proof was given that if $U = U_{cr}$ and

$$[P]_{cr} = [Re\ (\vec{X}_{1,cr}), Im\ (\vec{X}_{1,cr})],$$

then

$$[P]^{-1}_{cr} . [A] . [P]_{cr} = \begin{pmatrix} 0 & -\omega \\ \omega & 0 \end{pmatrix}.$$

If $U = U_{cr} + \epsilon\mu$ and $[P] = [Re(X_1), Im(X_1)]$, then

$$[P]^{-1}\ [A(\epsilon\mu)]\ [P] = \begin{pmatrix} \epsilon\mu_1 & -(\omega + \epsilon\mu_2) \\ (\omega + \epsilon\mu_2) & \epsilon\mu_1 \end{pmatrix},$$

where $\epsilon\mu_1$ and $\epsilon\mu_2$ are small parameters function of $\epsilon\mu$ (in dynamics, they are called "unfolding" parameters).

To order ϵ, [P] can be taken equal to

$$[P] = [P]_{cr} + \epsilon\ [P'].$$

Starting from the original equation, at $\mu \neq 0$,

$$\dot{x} = [A]x + f(x), \qquad \text{(A7.1)}$$

and transforming the system with the modal matrix [P] yields

$$\dot{y} = \begin{pmatrix} \epsilon\mu_1 & -(\omega + \epsilon\mu_2) \\ \omega + \epsilon\mu_2 & \epsilon\mu_1 \end{pmatrix} y + [P]^{-1} f([P]y) .$$

Using now (A7.1) and keeping approximation of order ϵ leads to

$$\dot{y} = \begin{pmatrix} \epsilon\mu_1 & -(\omega+\epsilon\mu_2) \\ \omega+\epsilon\mu_2 & \epsilon\mu_1 \end{pmatrix} y + [P_{cr}]^{-1} f([P_{cr}]y) + O(\epsilon^2) . \quad \text{(A7.2)}$$

Hence the modal matrix can still be computed at the critical parameters.

Appendix 8

Normal form in the case of a double zero eigenvalue

In the case of a double zero eigenvalue, the standard form corresponds to the Jordan form. Hence, the linear operator is equal to

$$L = \begin{pmatrix} 0 & 1 \\ 0 & 0 \end{pmatrix}, \tag{A8.1}$$

The nonlinear function f has the form

$$f(y) = f_{i,(k,3-k)}\, y_1^k\, y_2^{3-k}, \quad i = 1,2, \quad k = 0,3, \tag{A8.2}$$

and the transformation polynomial h can be defined by

$$h(y) = h_{i,(k,3-k)}\, y_1^k\, y_2^{3-k}, \quad i = 1,2, \quad k = 0,3. \tag{A8.3}$$

The computation of g(y) = L. h(y) - Dh. L(y) + f(y), with the use of (A8.1) to (A8.3), yields the following eight equations

$$\begin{aligned}
& h_{2,03} - h_{1,12} + f_{1,03} = g_{1,03}, \\
& h_{2,12} - 2h_{1,21} + f_{1,12} = g_{1,12}, \\
& h_{2,21} - 3h_{1,30} + f_{1,21} = g_{1,21}, \\
& h_{2,30} + f_{1,30} = g_{1,30}, \\
& -h_{2,12} + f_{2,03} = g_{2,03}, \\
& -2h_{2,21} + f_{2,12} = g_{2,12}, \\
& -3h_{2,30} + f_{2,21} = g_{2,21}, \\
& f_{2,30} = g_{2,30}.
\end{aligned} \tag{A8.4}$$

The normal form g usually used (Guckenheimer and Holmes 1983, p.371) is

$$\begin{aligned} g_{1,03} &= g_{1,12} = g_{1,21} = g_{1,30} = 0, \\ g_{2,03} &= g_{2,12} = 0, \\ g_{2,21} &= b_3, \\ g_{2,30} &= a_3. \end{aligned} \tag{A8.5}$$

Equating the two sets of equations yields

$$\begin{aligned} a_3 &= f_{2,30}, \\ b_3 &= f_{2,21} + 3f_{1,30}. \end{aligned} \tag{A8.6}$$

Appendix 9

Construction of the unfolding for the case VIII

The subsystem may be written as

$$\begin{aligned} \dot{r} &= r(\mu_1 + r^2 + bz^2), \\ \dot{z} &= z(\mu_2 + cr^2 + dz^2), \quad d = -1, \quad \alpha = d - bc < 0. \end{aligned} \tag{A9.1}$$

i) Determination of the fixed points

$$\begin{aligned} r[\mu_1 + r^2 + bz^2] &= 0, \\ z[\mu_2 + cr^2 - z^2] &= 0. \end{aligned} \tag{A9.2}$$

The origin (r, z) = (0, 0) is always an equilibrium point. Depending on μ_1 and μ_2, three other equilibria may exist

$$\begin{aligned} &(r,z) = (0,\sqrt{\mu_2}), \quad \mu_2 > 0, \\ &(r,z) = (\sqrt{-\mu_1},0), \quad \mu_1 < 0, \\ &(r,z) = \left(\sqrt{\frac{b\mu_2 + \mu_1}{\alpha}},\sqrt{\frac{c\mu_1 - \mu_2}{\alpha}}\right), \\ &\qquad \frac{b\mu_2 + \mu_1}{\alpha}, \quad \frac{c\mu_1 - \mu_2}{\alpha} > 0. \end{aligned} \tag{A9.3}$$

ii) Stability analysis

The characteristics of the flow are determined by the eigenvalues of the matrix [A] of the linearized system at the equilibrium points denoted by (r_0, z_0). [A] can be determined from the original subsystem (A9.1),

$$[A] = \begin{pmatrix} \mu_1 + 3r^2 + bz^2 & 2brz \\ 2crz & \mu_2 + cr^2 - 3z^2 \end{pmatrix}. \tag{A9.4}$$

Hence, for (0, 0),

$$[A] = \begin{pmatrix} \mu_1 & 0 \\ 0 & \mu_2 \end{pmatrix}, \tag{A9.5}$$

a pitchfork bifurcation occurs if $\mu_1 = 0$ or $\mu_2 = 0$.

For $(0, \sqrt{\mu_2})$, $\mu_2 > 0$,

$$[A] = \begin{pmatrix} \mu_1 + b\mu_2 & 0 \\ 0 & -2\mu_2 \end{pmatrix}, \tag{A9.6}$$

a new pitchfork bifurcation occurs if $\mu_1 + \mu_2 = 0$.

For $(\sqrt{-\mu_1}, 0)$, $\mu_1 < 0$

$$[A] = \begin{pmatrix} -2\mu_1 & 0 \\ 0 & \mu_2 - c\mu_1 \end{pmatrix}, \tag{A9.7}$$

another pitchfork bifurcation occurs if $\mu_2 - c\mu_1 = 0$.

In the three cases, the stability of all the fixed points is determined very easily.

Finally, for the last fixed point (with $\alpha < 0$),

$$[A] = \begin{pmatrix} \dfrac{2\mu_1 + 2b\mu_2}{\alpha} & \dfrac{2b}{\alpha}\sqrt{(b\mu_2+\mu_1)(c\mu_1-\mu_2)} \\ \dfrac{2c}{\alpha}\sqrt{(b\mu_2+\mu_1)(c\mu_1-\mu_2)} & \dfrac{2\mu_2 - 2c\mu_1}{\alpha} \end{pmatrix} \tag{A8.8}$$

Since $\alpha < 0$, no bifurcation can occur for this fixed point. Hence, without loss of information, one can set $\mu_1 = 0$, and the eigenvalues of [A] can be found. It appears that one eigenvalue is always positive and the other one negative, the fixed point is a saddle; the complete bifurcation set can be drawn easily (Figure 5.5(a)).

APPENDIX 10

Computation of phase portraits, bifurcation diagrams and Lyapunov exponents

In all the computations, a fourth-order Runge-Kutta scheme has been used. Starting from (2.70), a four-dimensional vector space, the generalized coordinates (q_1, q_2, $\dot{q}_1$, $\dot{q}_2$), are computed numerically. In all cases, the nondimensional time step used is $\Delta t = 0.005$. Then, using the cantilever beam eigenfunctions $\phi_r(\xi)$, the displacements and velocities of the extremity of the pipe can be obtained,

$$\begin{cases} \eta(1,\tau) = \phi_1(1)\, q_1(\tau) + \phi_2(1)\, q_2(\tau), \\ \dot{\eta}(1,\tau) = \phi_1(1)\, q_3(\tau) + \phi_2(1)\, q_4(\tau). \end{cases}$$

Hence, the time trace is just a representation of the tip displacement as a function of time τ. The phase portrait represents the velocity function of the displacement of the end.

To construct bifurcation diagram, the maximum displacement of the end of the pipe is represented as a function of the parameter varying (U or ν in practice). The transient terms are first discarded (20 time units). Then the displacement of the pipe is recorded each time the sign of the velocity changes.

To construct the power spectra, an existing subroutine within the generic plotting package Genplot is used. The FFT transform is implemented only for even powers of 2 number of points (8, 16, 32, 64...). The Y variable is first set to the absolute value of the complex transform, normalized by the square root of the number of data points, then transformed into a dB scale. The X variable represents the nondimensional frequency. In all the calculations, the number of points used is 4096.

Concerning the calculation of the Lyapunov exponents, some additional explanation may be useful. A complete discussion can be found in Guckenheimer and Holmes (1983) for mathematical definitions, and in Moon (1987) for practical calculations.

Consider the system

$$\dot{y} = f(y), \tag{A10.1}$$

with a solution $\phi(\tau)$ corresponding to a set of initial conditions $\phi(\tau_0) = \phi_0$. To determine if this solution is stable or not, one considers another solution $\phi_1(\tau)$ corresponding to different initial conditions. Then, it is possible to define the variational vector function $u(\tau) = \phi_1(\tau) - \phi(\tau)$, such that $\|u\| << 1$. Hence, the differential equation for u may easily be obtained,

$$\dot{u} = Df(\phi)\,u, \tag{A10.2}$$

where $Df(\phi)$ is the Jacobian matrix function for the vector field f(y) along the trajectory $\phi(\tau)$. If $\phi_1(\tau)$ approaches $\phi(\tau)$, then $u(\tau)$ will tend to zero while if it diverges away from it, then $u(\tau)$ will tend to grow. This is expressed by

$$\| u(\tau) \| \sim e^{\sigma\tau}. \tag{A10.3}$$

Of course, this exponential behaviour is only valid on a small time interval. Hence, in the computations, the vector function $u(\tau)$ is renormalized. The so-called Lyapunov exponents are defined by

$$\sigma = \lim_{\tau\to\infty} \frac{1}{\tau} \ln(\|u(\tau)\|/\|u(0)\|), \tag{A10.4}$$

and two trajectories may be considered to converge or diverge exponentially on the average. In an n-dimensional space, there exist n Lyapunov exponents, the largest dominating the dynamics of the system. Hence, the solution $u(\tau)$ will converge to the direction of most rapid growth, which is associated with the largest exponent.

To calculate this largest Lyapunov exponent, the fourth order system is replaced by an eighth order system. The first four equations compute a given trajectory $\phi(\tau)$ and the last four compute the variational vector function $u(\tau)$ defined by (A10.2) along the trajectory $\phi(\tau)$. A fourth order Runge-Kutta scheme is used again. In the calculation presented, the time step $\Delta t = 0.005$. Calculations were carried out with 100 nondimensional time units, beyond the first 20 to discard the transcient terms, and the renormalization was carried out every 0.1 time units ($= 20 \times \Delta t$).

FIGURES

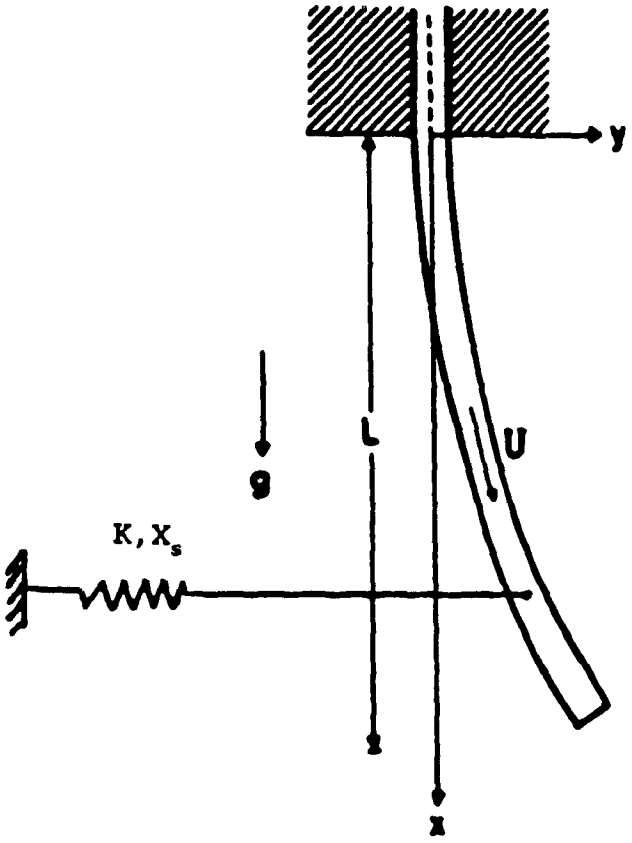

Fig.1.1 Schematic of the system.

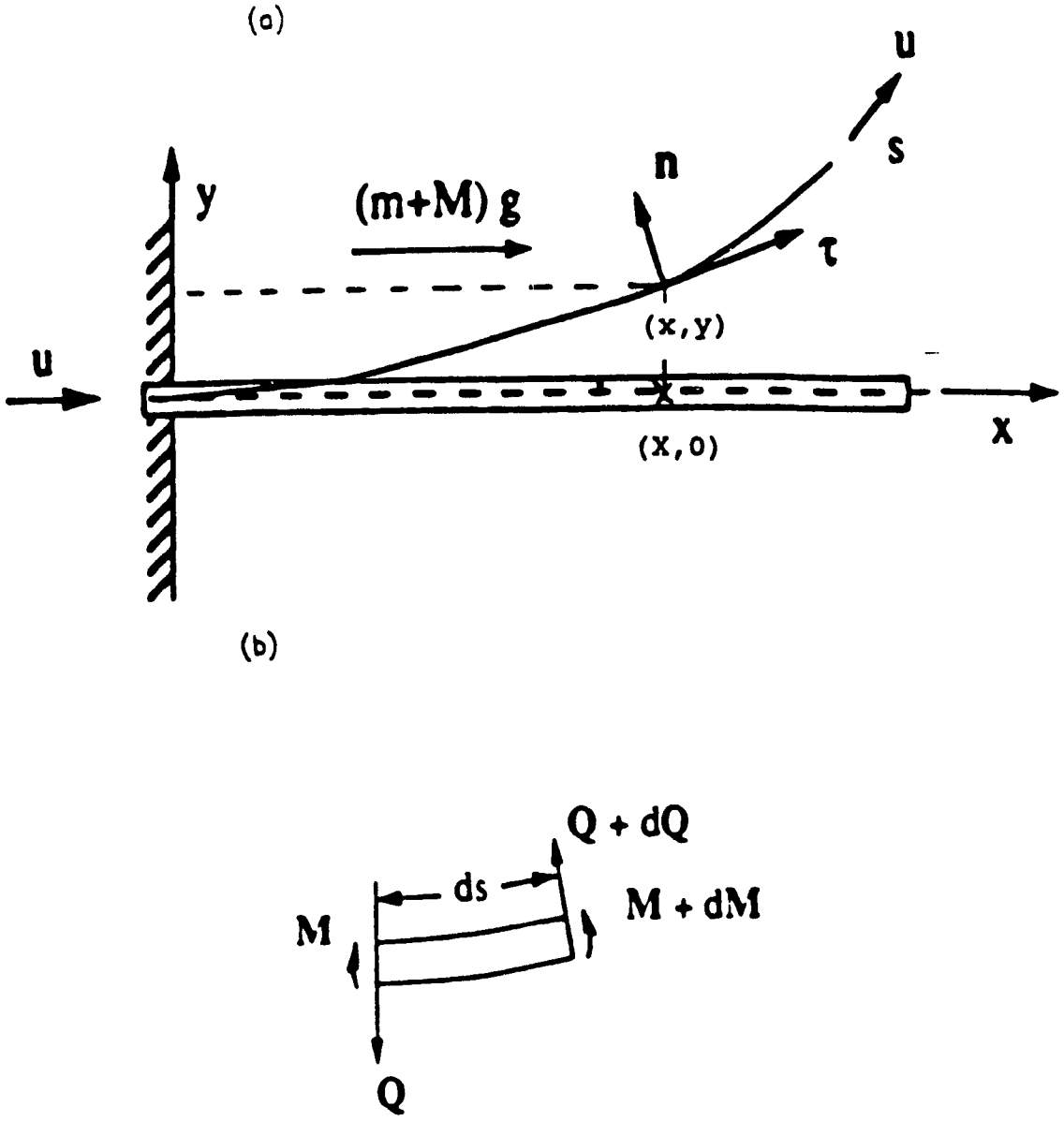

Fig.2.1 (a) Schematic of the system and notation, (b) free-body diagram of an element.

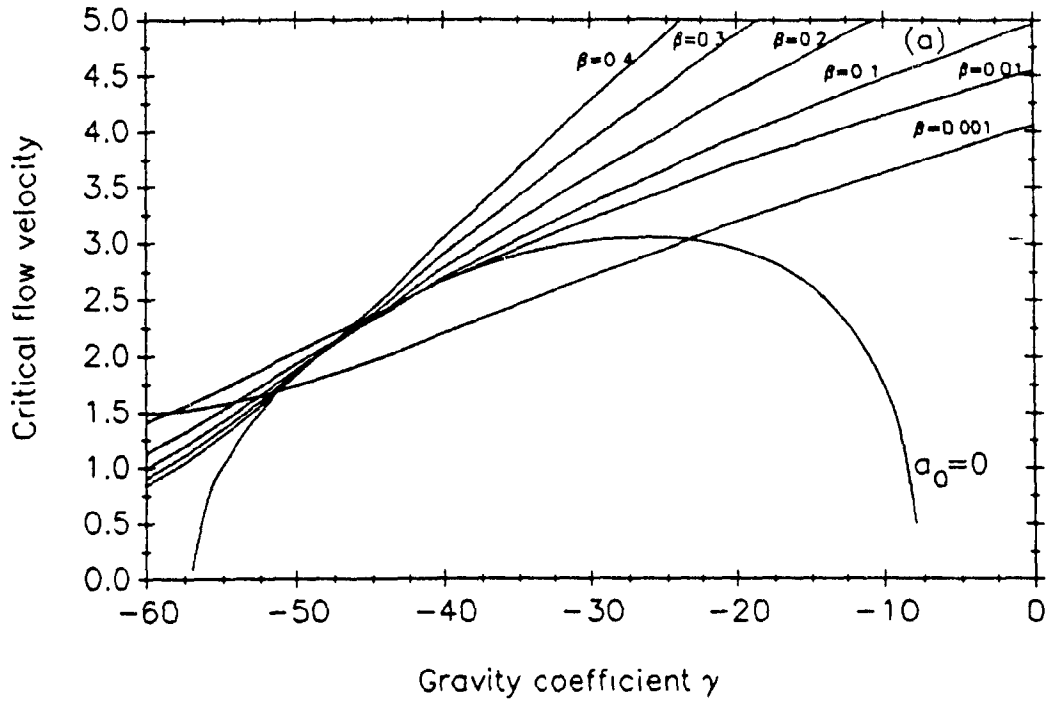

Fig.4.1 (a) Static (a_0 = 0) and dynamic (T_3 = 0) stability boundaries for different β in the (γ, U) plane. K = 0.

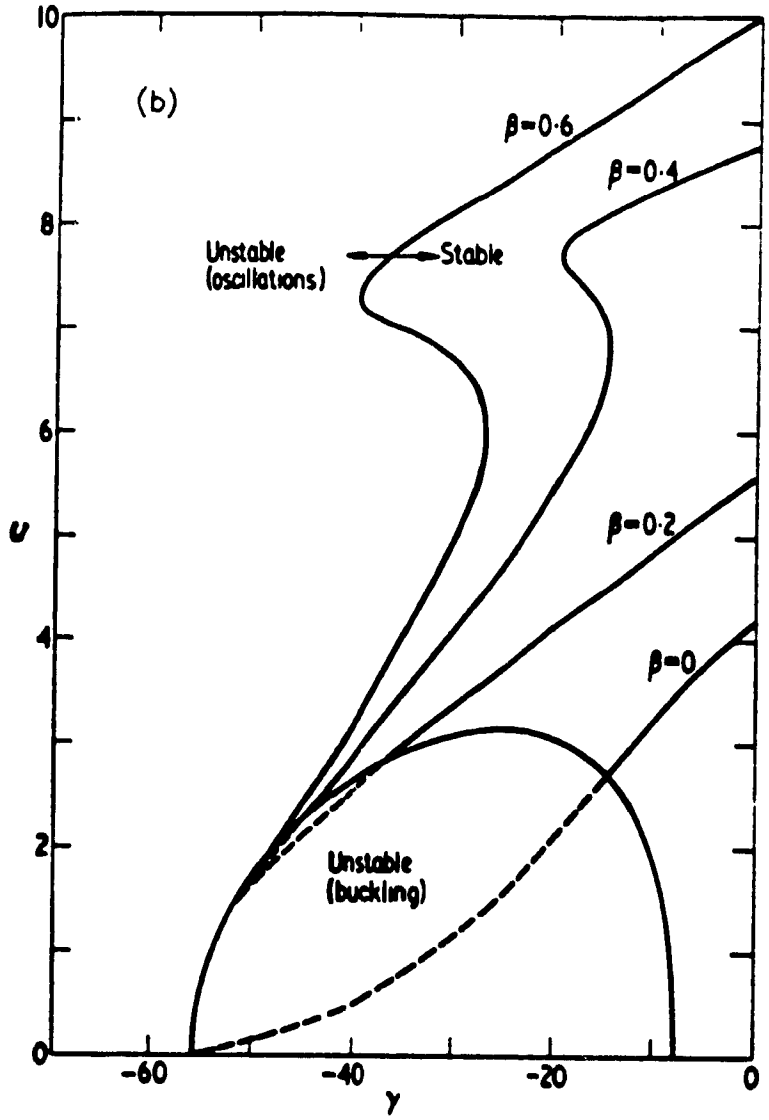

Fig.4.1 (b) Stability boundaries with a higher mode approximation (taken from Paidoussis 1969),in the (γ, U) plane. No spring (K=0).

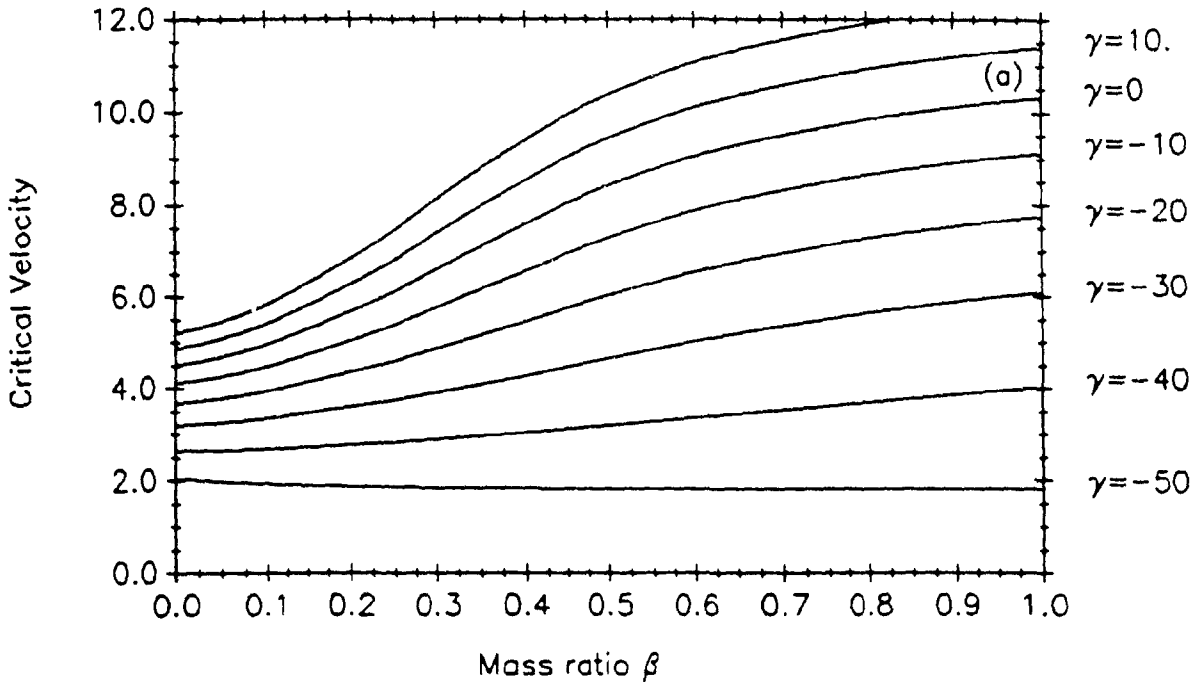

Fig.4.2 (a) Dynamic stability boundaries ($T_3 = 0$) for different γ in the (β, U) plane. K = 0.

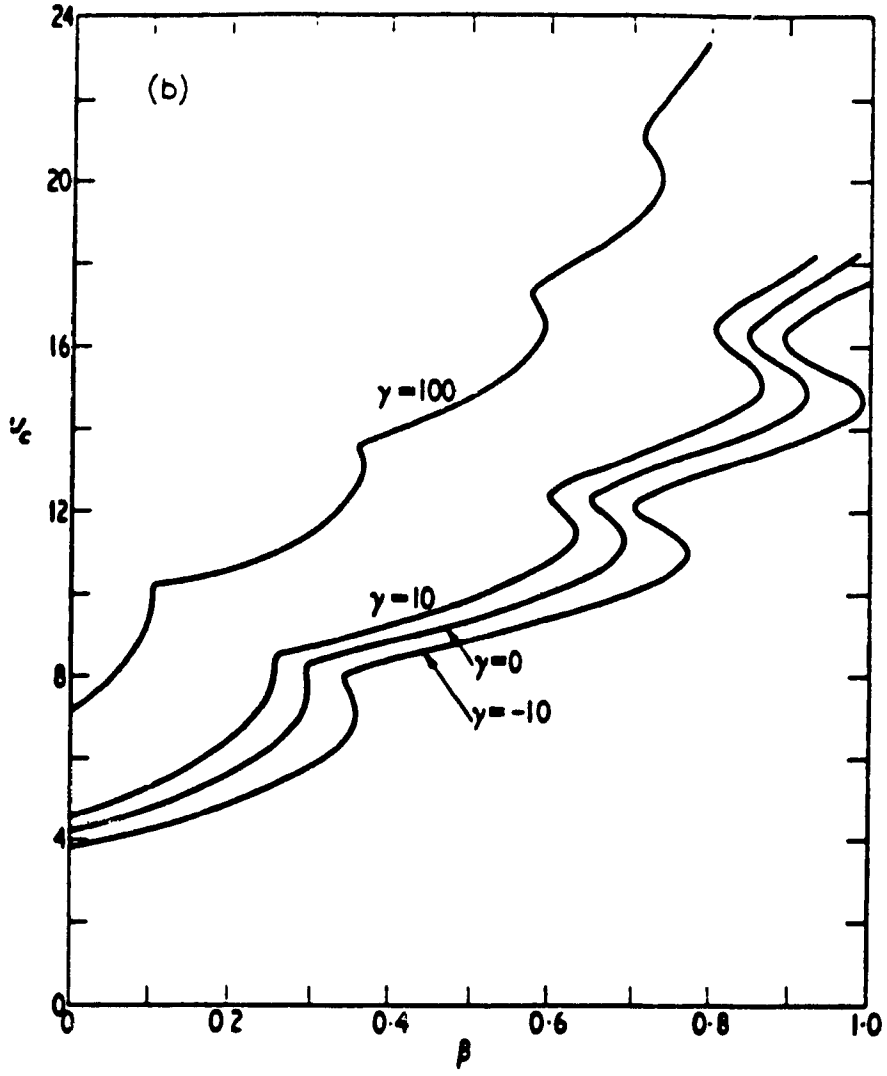

Fig.4.2 (b) Dynamic stability boundaries with a higher mode approximation (taken from Païdoussis 1969), in the (β, U) plane. K = 0.

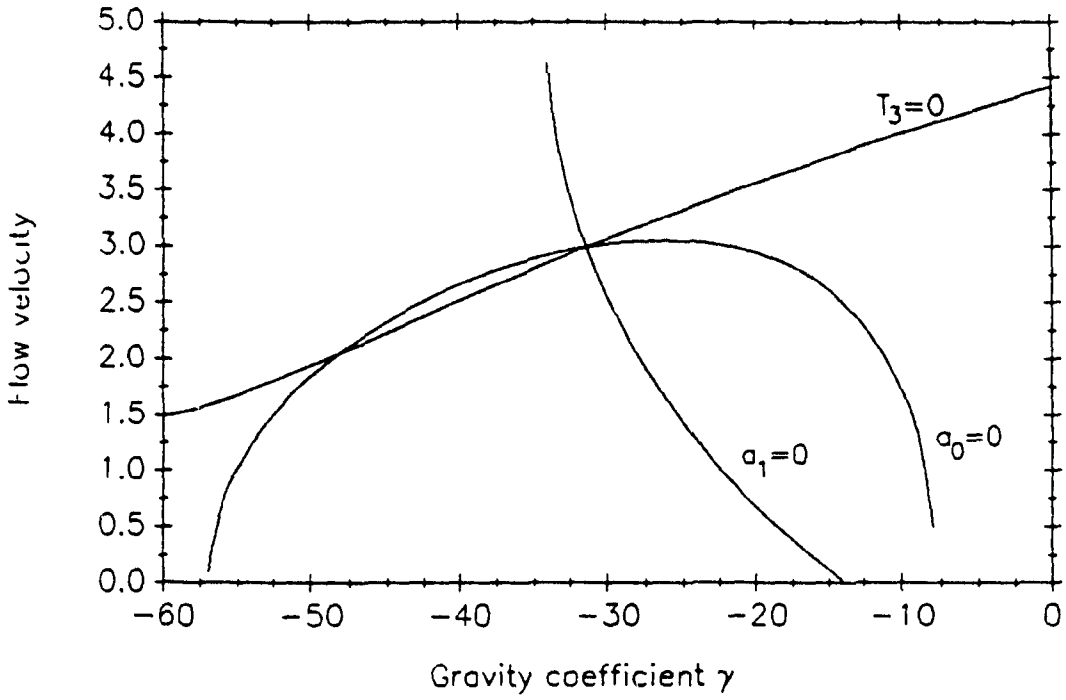

Fig.4.3 Conditions $a_0 = 0$, $a_1 = 0$ and $T_3 = 0$ in the (γ, U) plane. $\beta = 0.001$, $K = 0$.

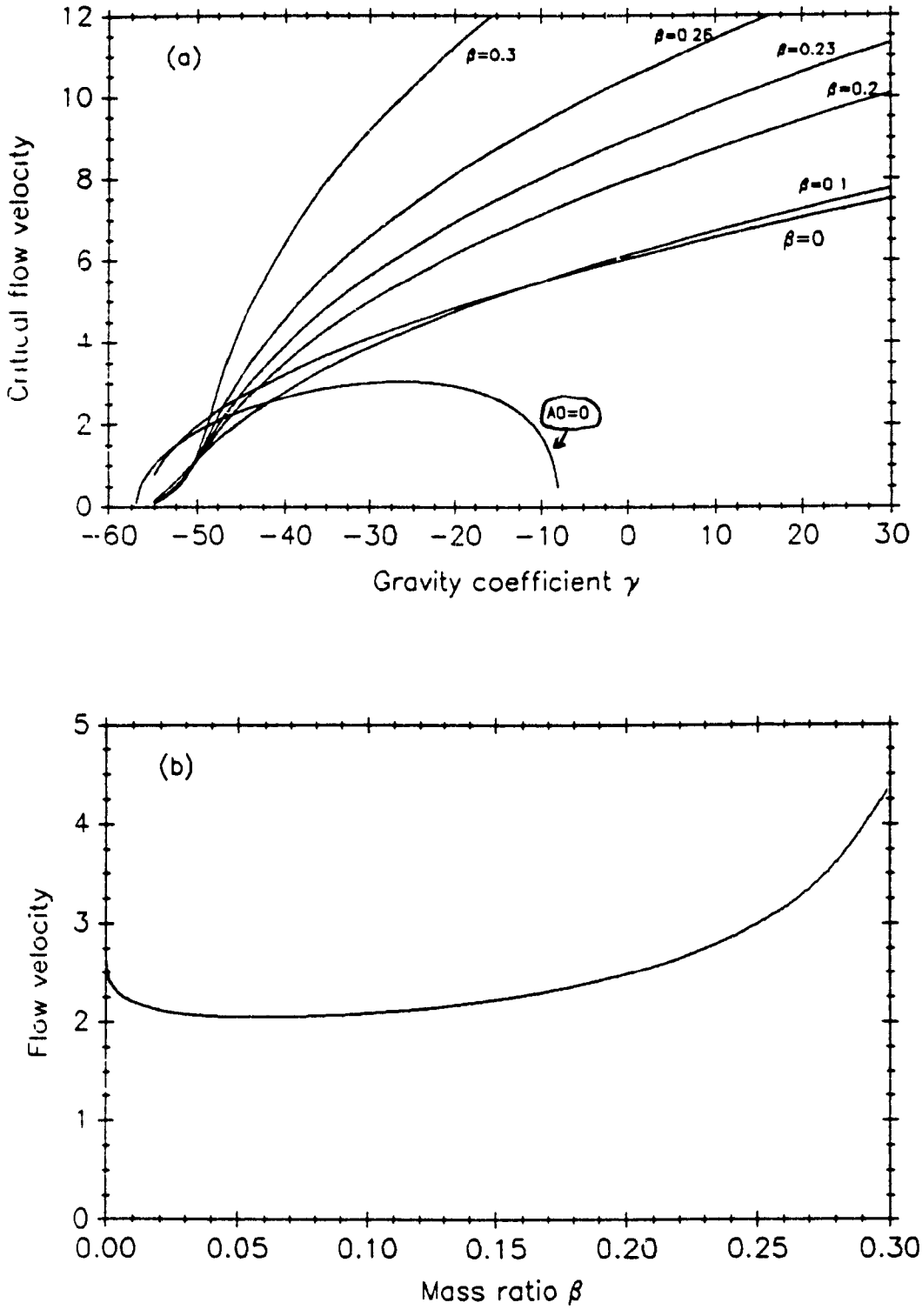

Fig.4.4 (a) Condition $a_0 = 0$ and $a_1 = a_2\ a_3$ for various values of β, (b) the non-univalent curve $a_1 = a_2\ a_3$ for $\gamma = -45$.

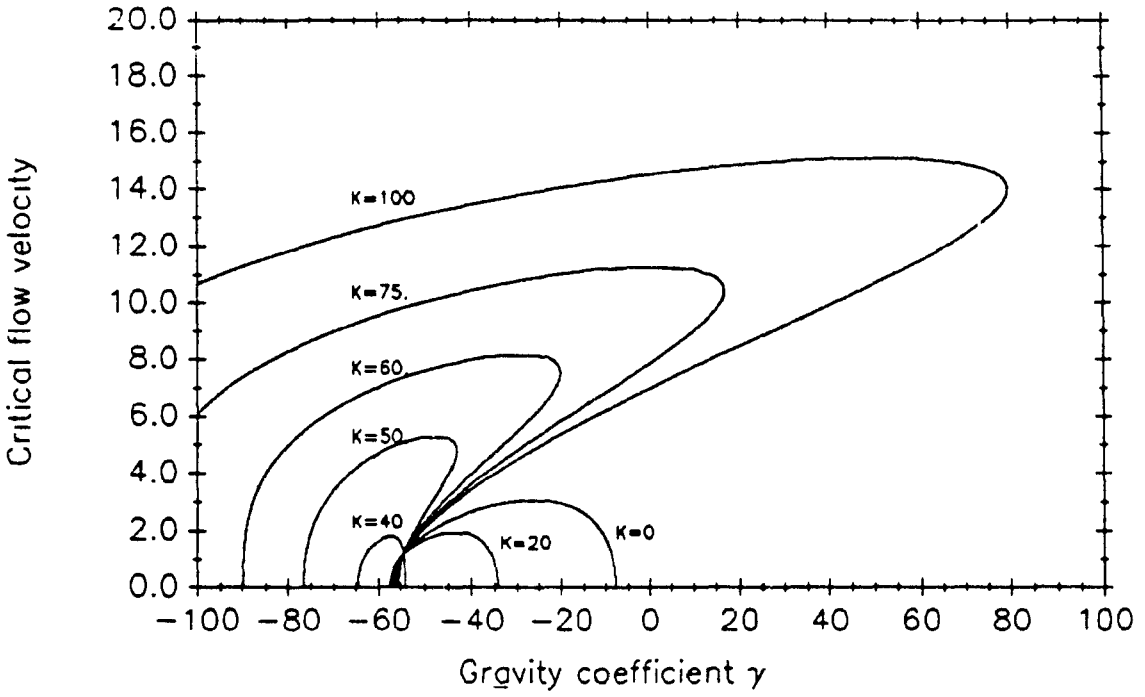

Fig.4.5 Static stability boundaries for different values of K (a_0 = 0). The location of the spring is constant ξ_s = 0.8.

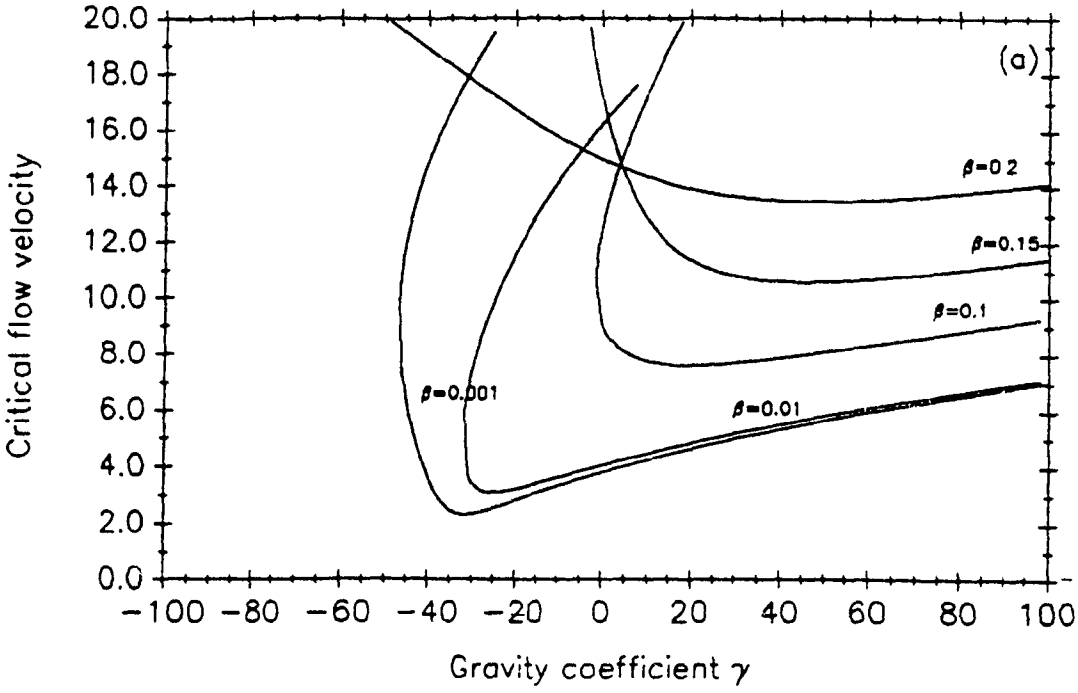

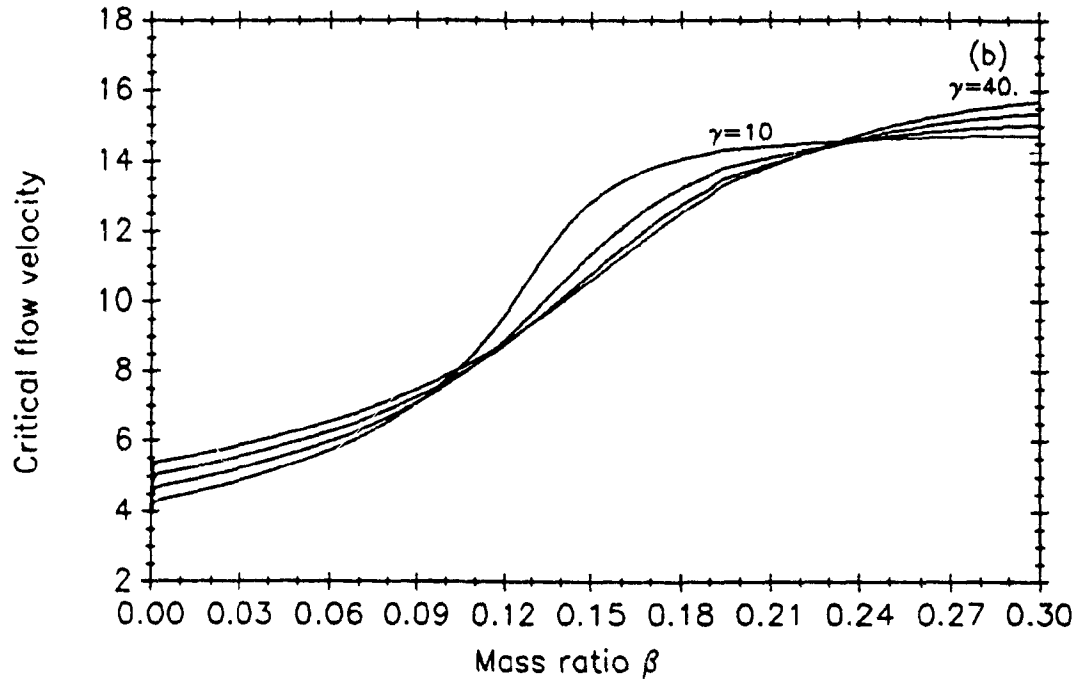

Fig.4.6 Dynamic stability boundaries ($T_3 = 0$), (a) in the (γ, U) plane, (b) in the (β, U) plane. K = 100, $\xi_s = 0.8$.

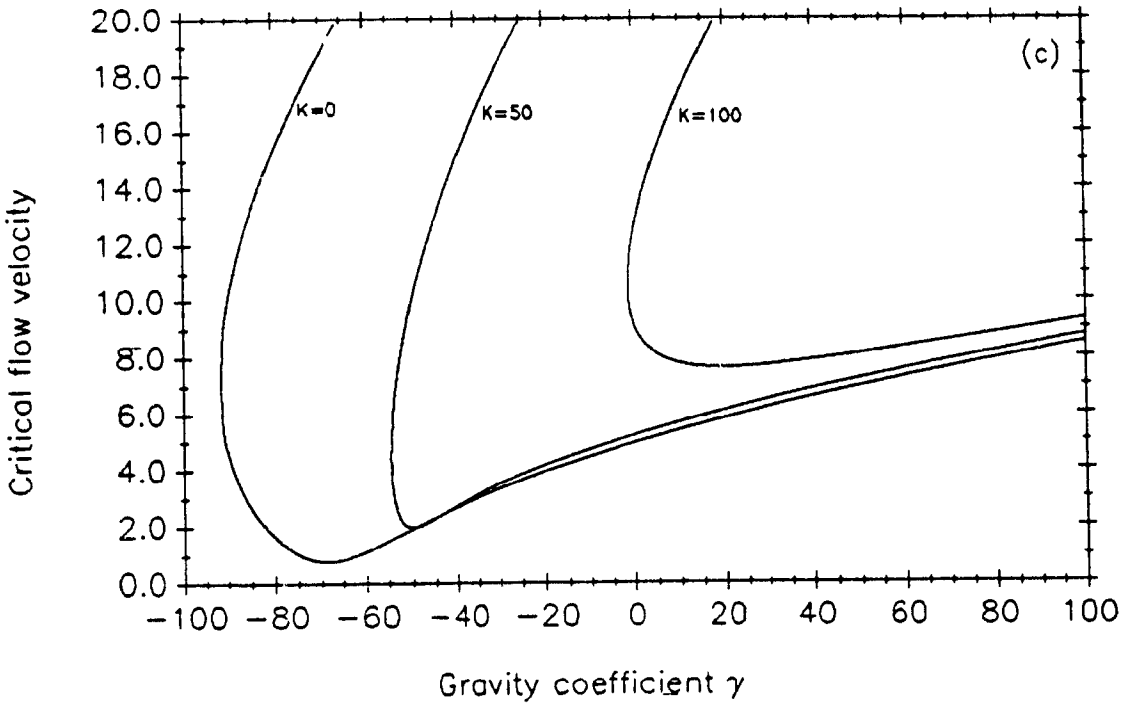

Fig.4.6 (c) Effect of the spring stiffness K on the dynamic stability boundaries. $\xi_s = 0.8$, $\beta = 0.1$.

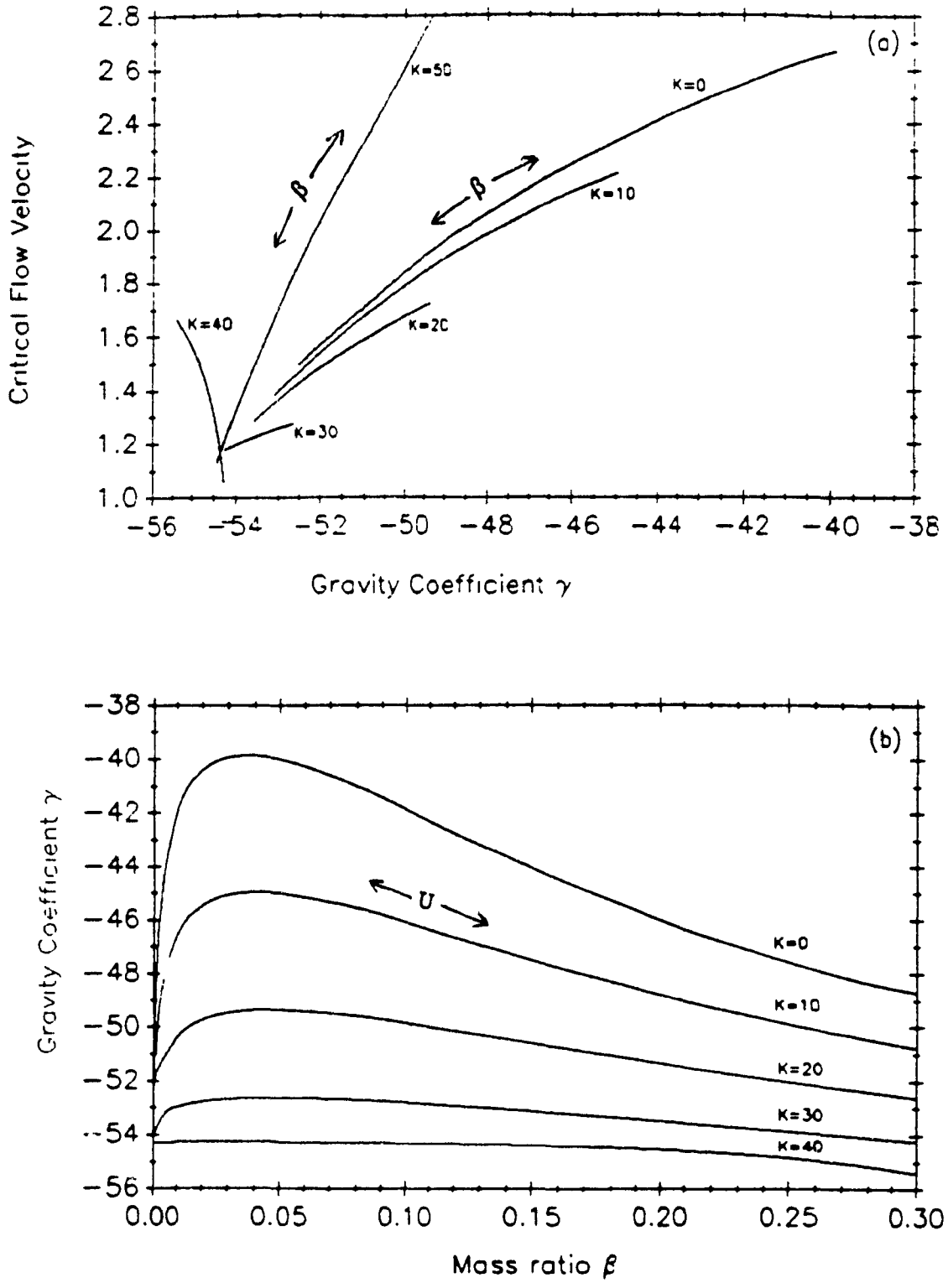

Fig.4.7 Double degeneracy conditions, (a) in the (γ, U) plane for different K (β is the control parameter varying), (b) in the (β, U) plane (U varying). ξ = 0.8.

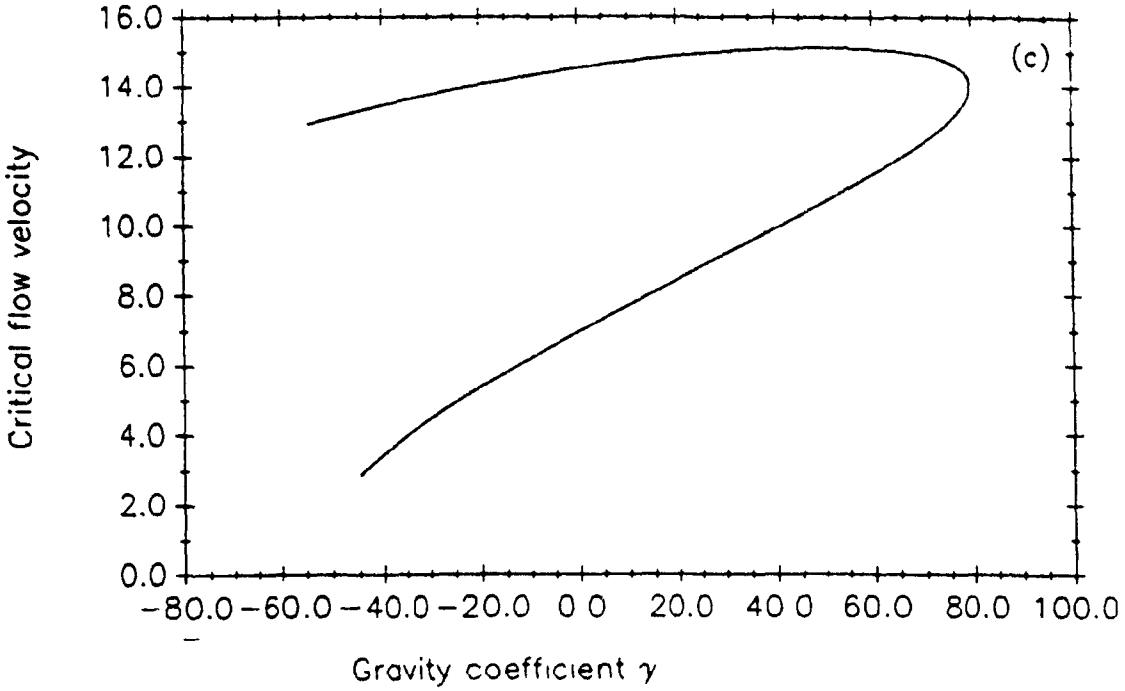

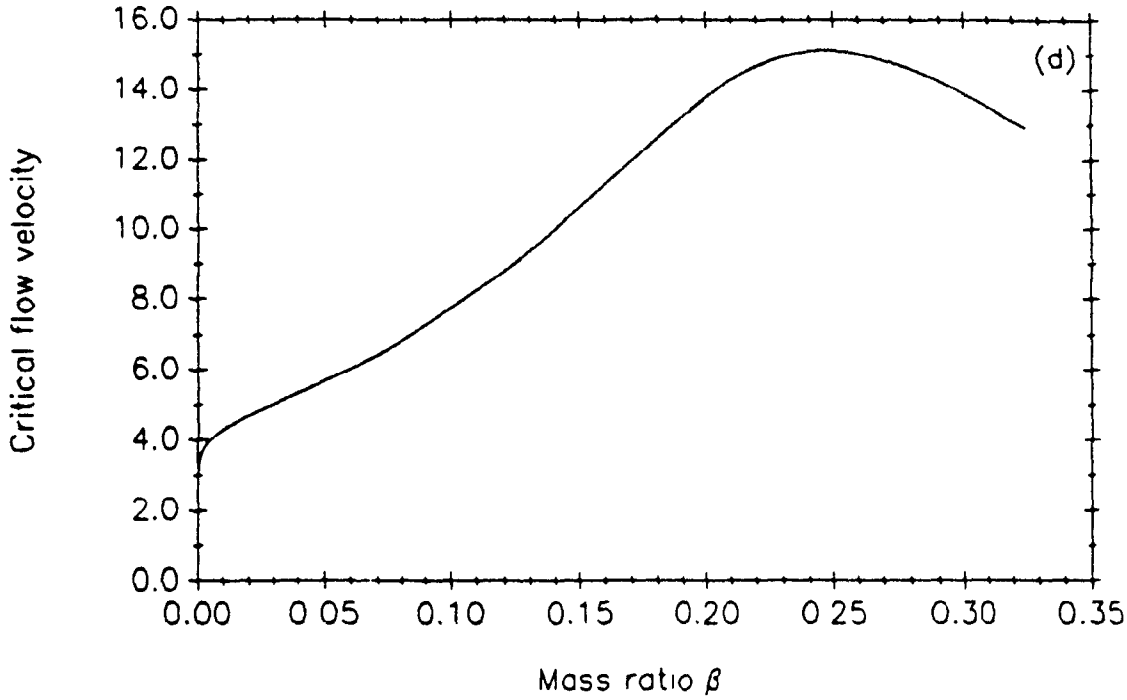

Fig.4.7 Double degeneracy conditions, (c) in the (γ, U) plane, (d) in the (β, U) plane. K = 100, ξ_s = 0.8.

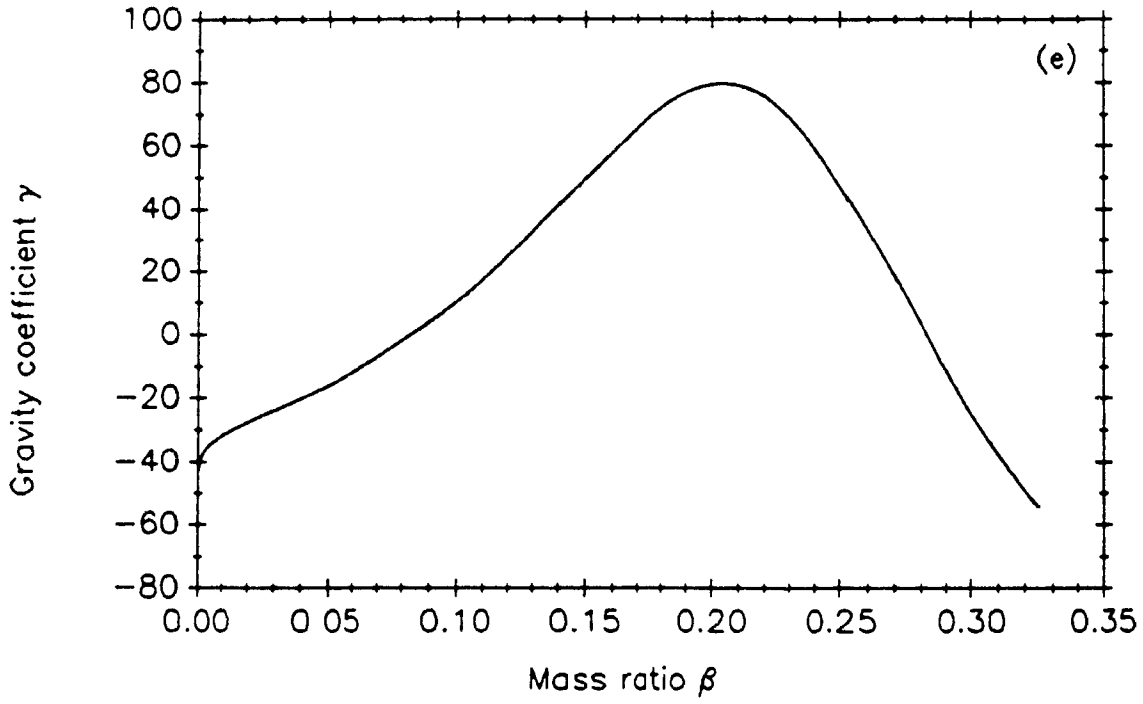

Fig.4.7 (e) Double degeneracy conditions in the (β, γ) plane. K = 100, ξ_s = 0.8.

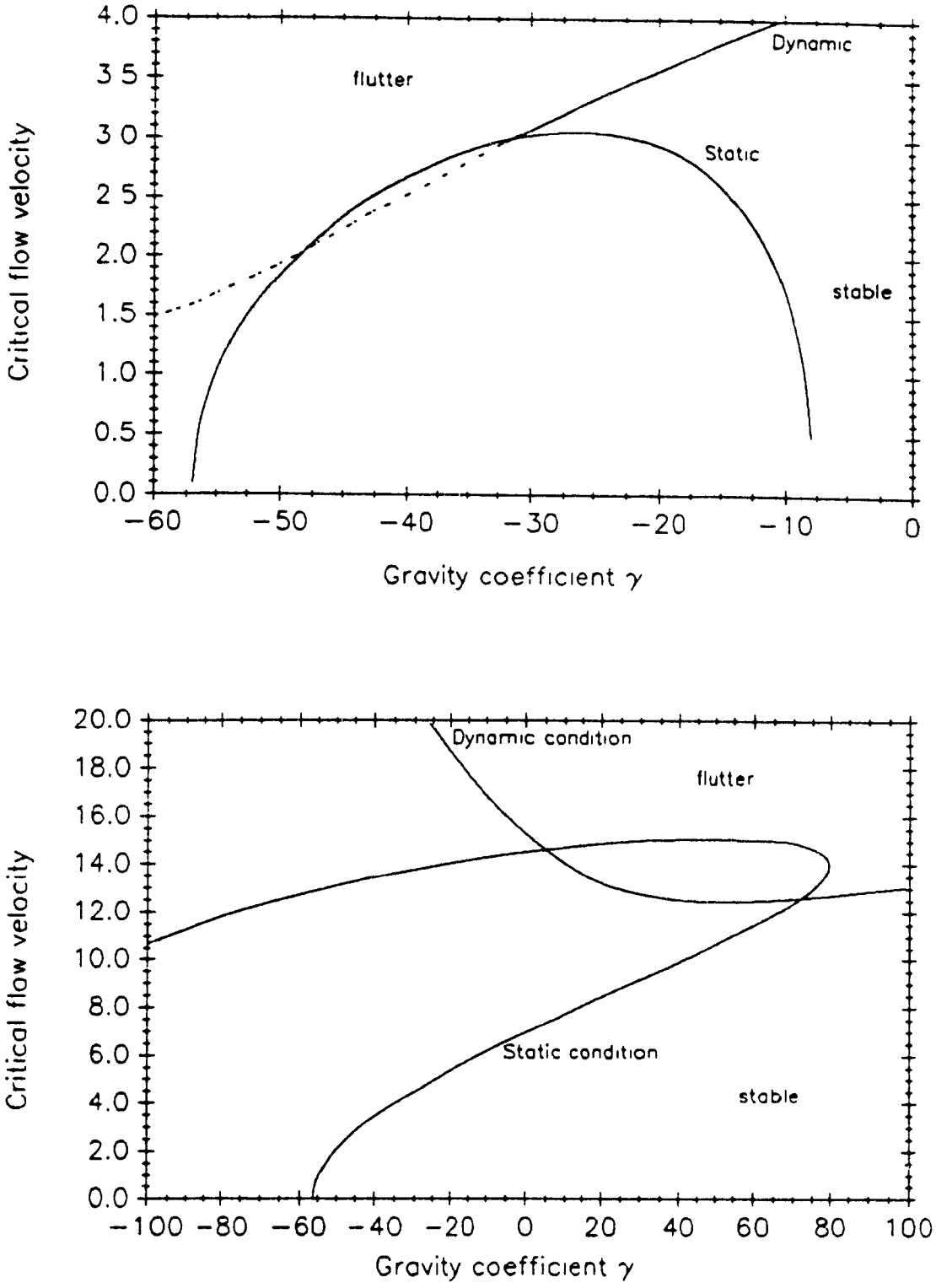

Fig.4.8 Summary of the results obtained by Routh's criteria (a) K = 0, β = 0.001, (b) K = 100, ξ_s = 0.8 and β = 0.18.

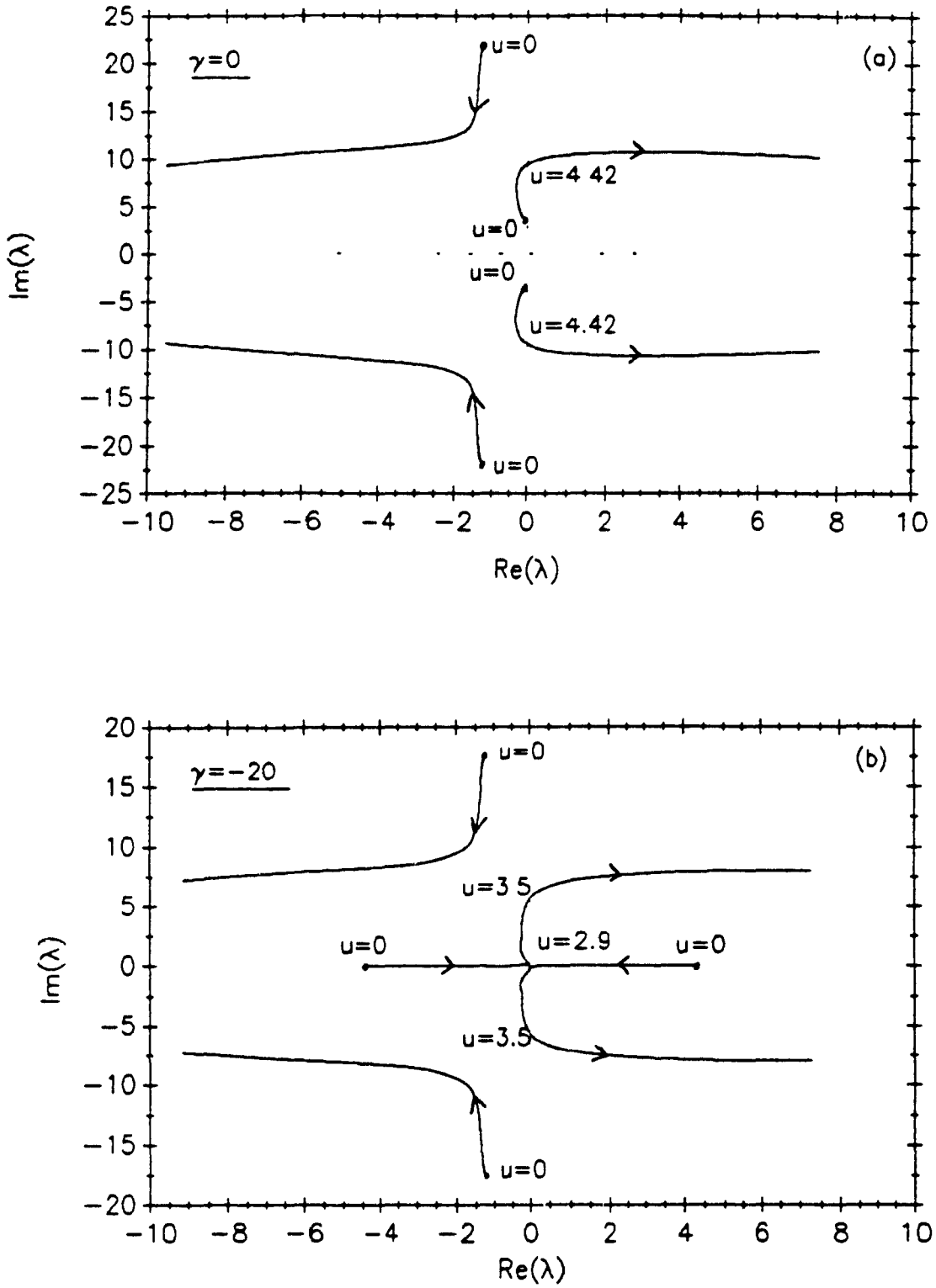

Fig.4.9 Eigenvalues of the linearized system: an Argand diagram, K = 0, β = 0.001, (a) γ = 0, (b) γ = -20.

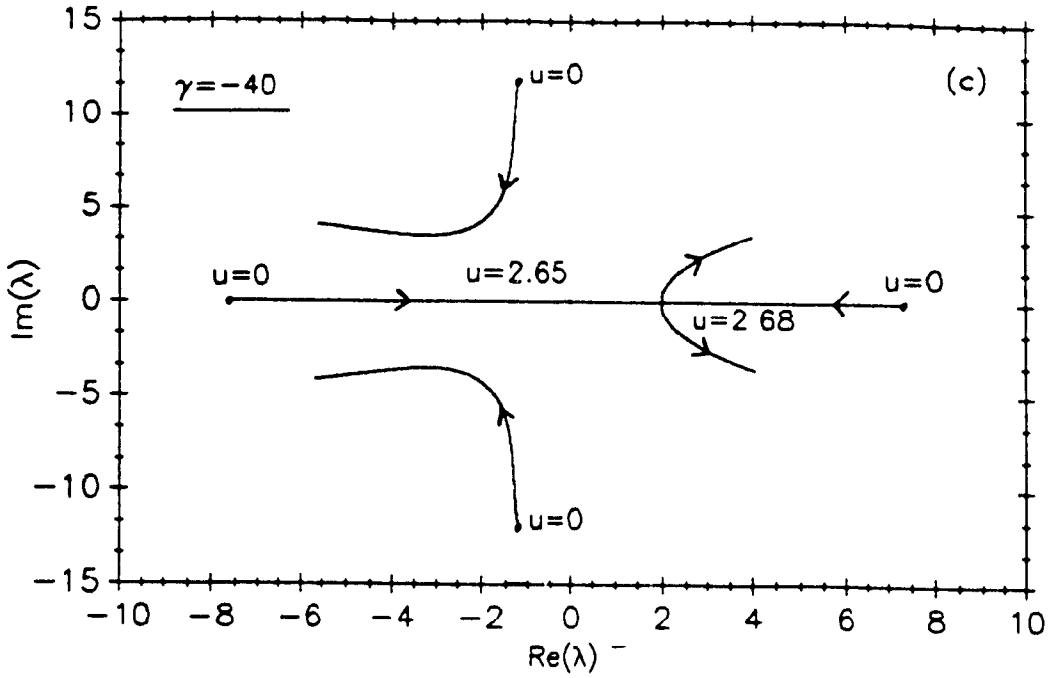

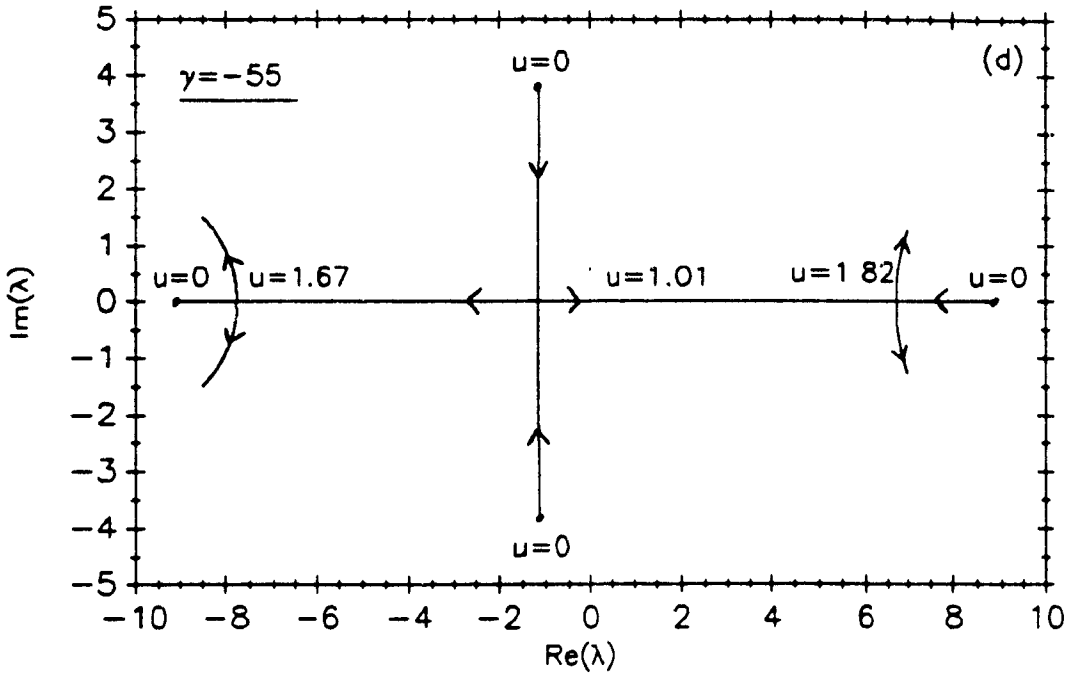

Fig.4.9 Argand diagram, K = 0, β = 0.001, (c) γ = -40, (d) γ = -55.

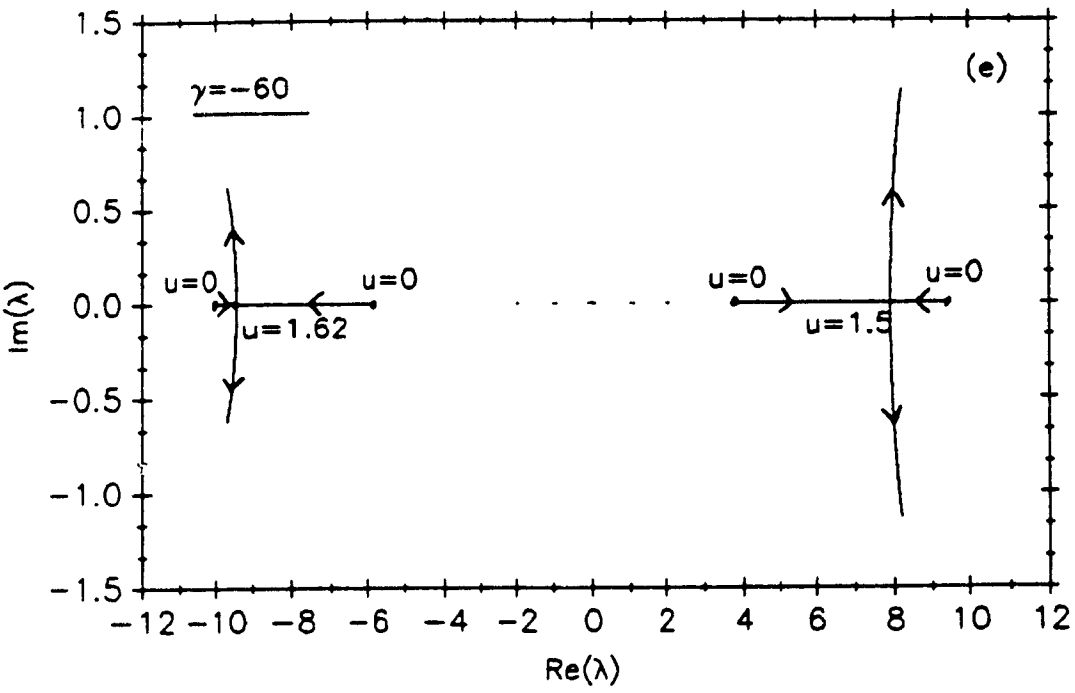

Fig.4.9 (e) Argand diagram, K = 0, β = 0.001, γ = -60.

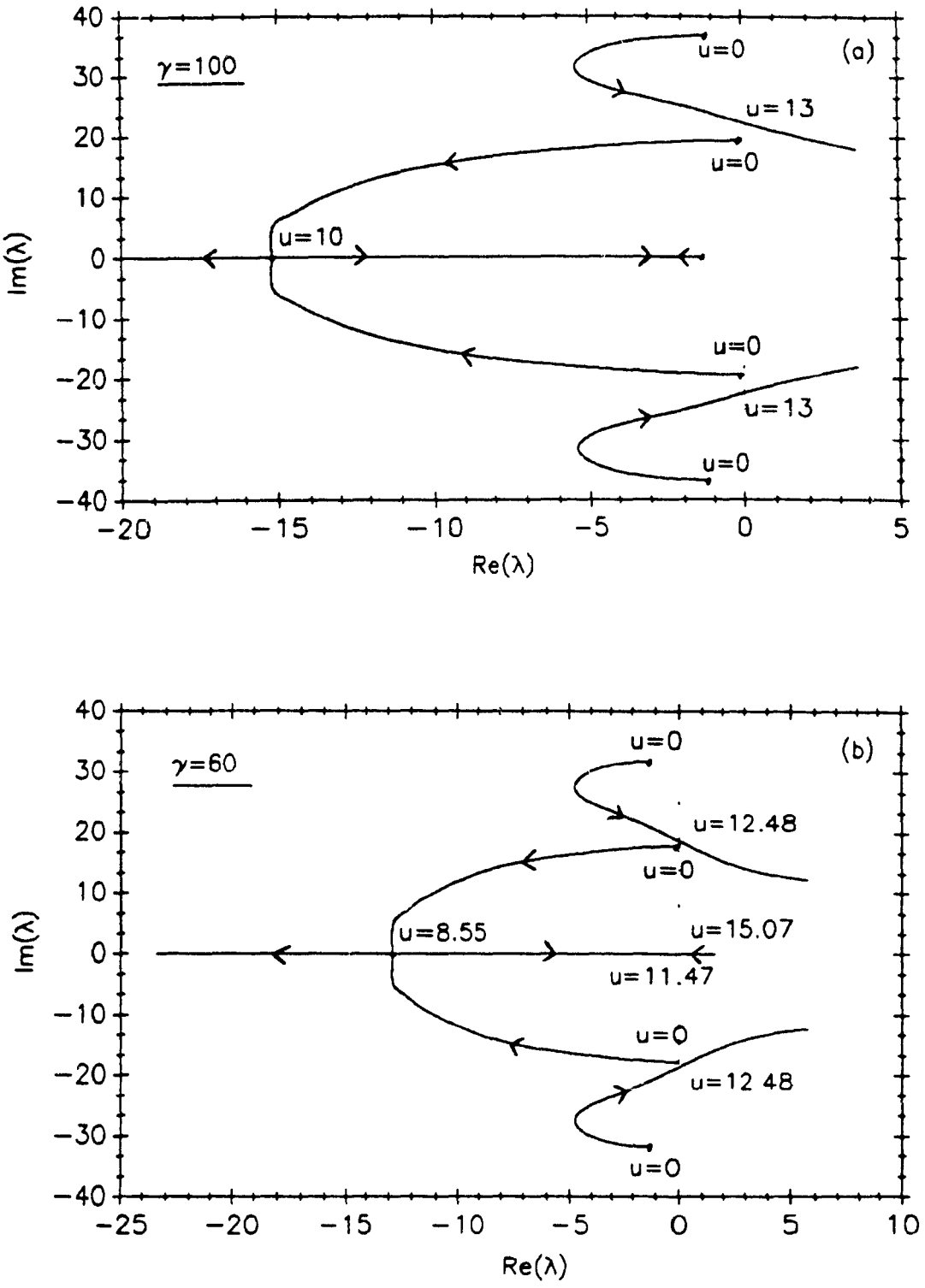

Fig.4.10 Argand diagram, case with a spring, K = 100, ξ_s = 0.8, β = 0.18, (a) γ = 100, (b) γ = 60.

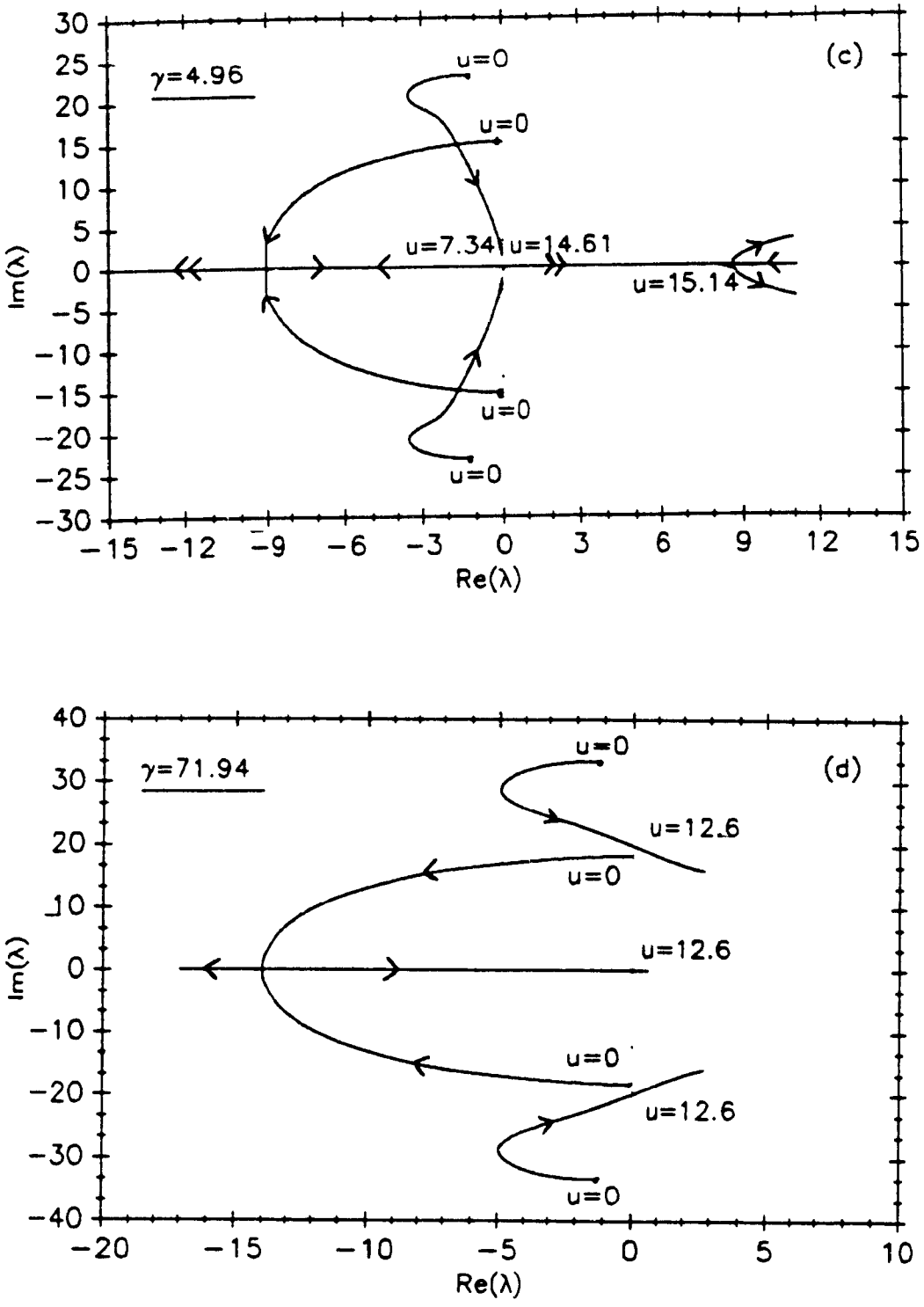

Fig.4.10 Argand diagram, K = 100, ξ_s = 0.8, β = 0.18, (c) γ = 4.96, (d) γ = 71.94.

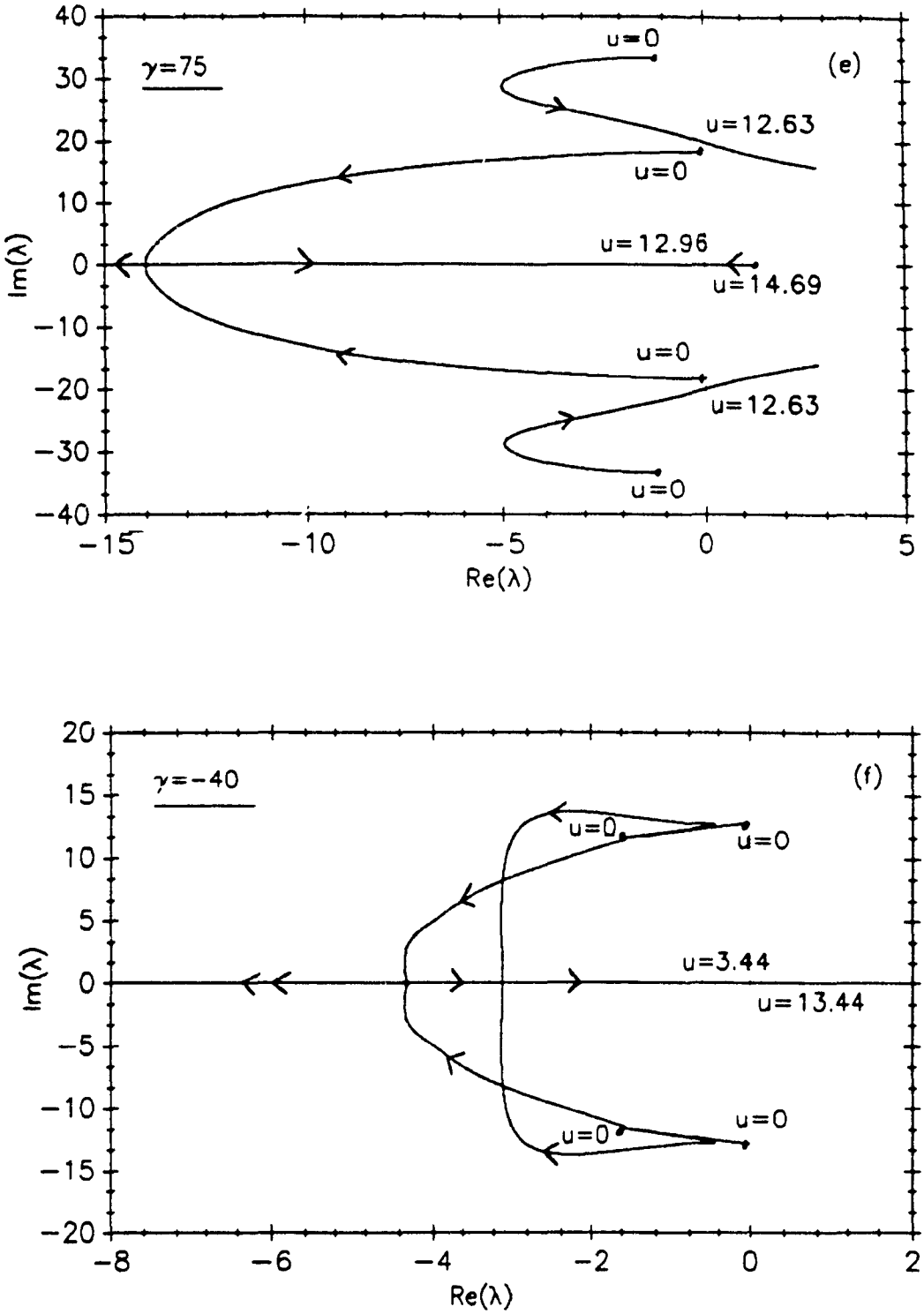

Fig.4.10 Argand diagram, K = 100, ξ_s = 0.8, β = 0.18, (e) γ = 75, (f) γ = -40.

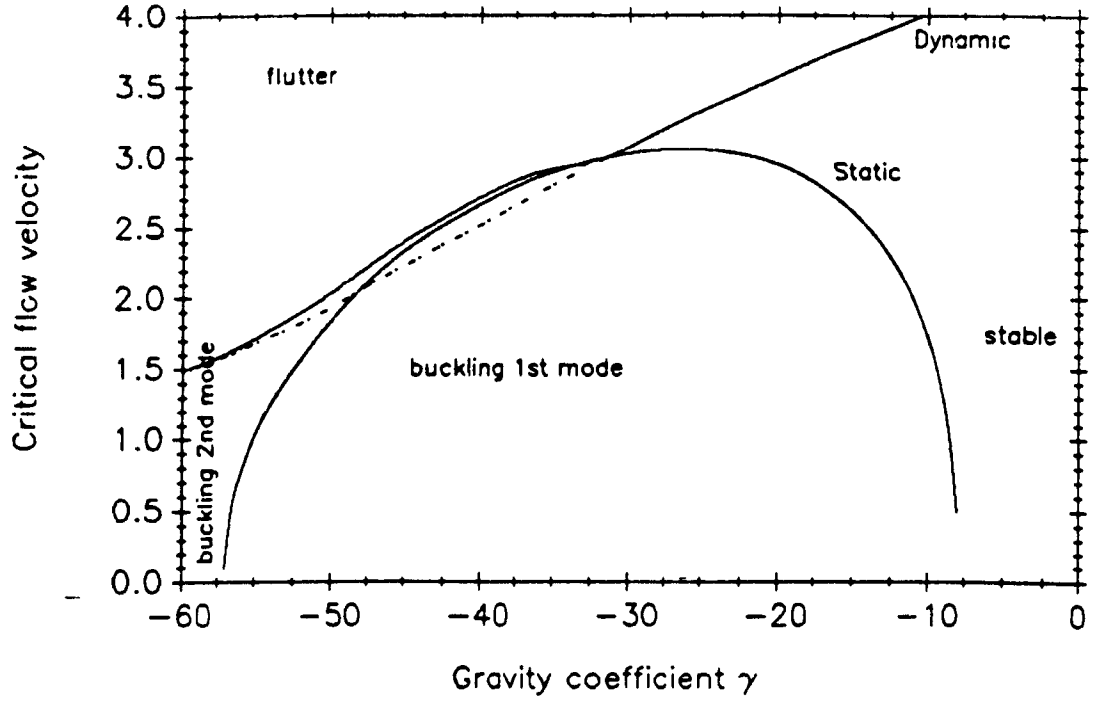

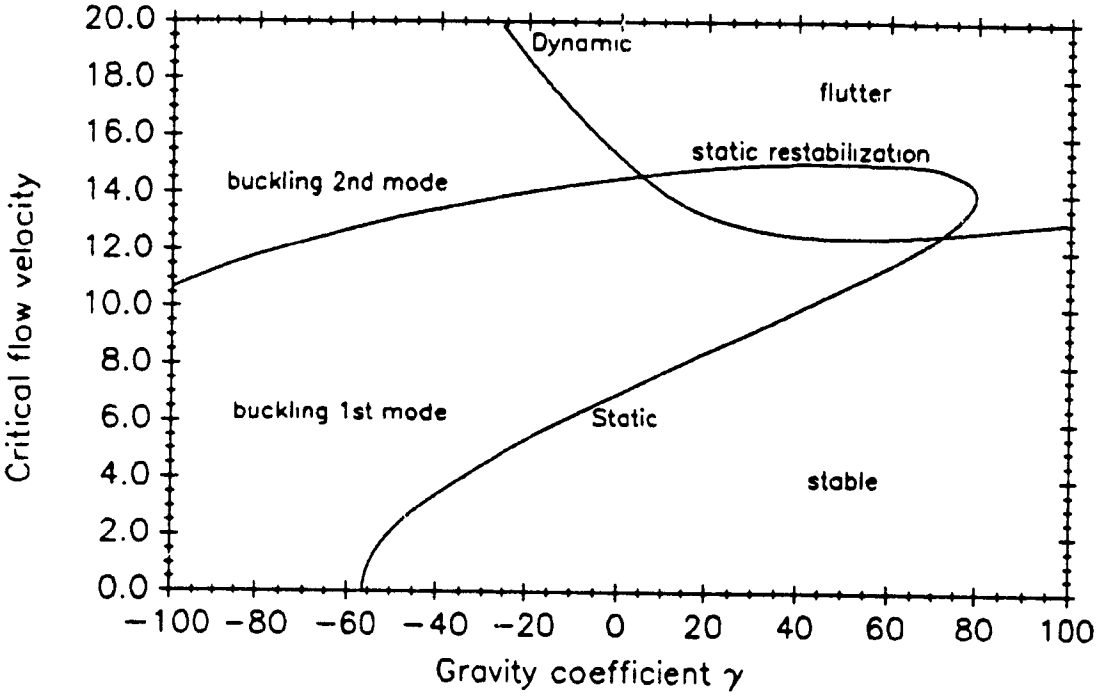

Fig.4.11 Stability map obtained from the linearized equations, (a) $K = 0$, $\beta = 0.001$, (b) $K = 100$, $\xi_s = 0.8$, $\beta = 0.18$.

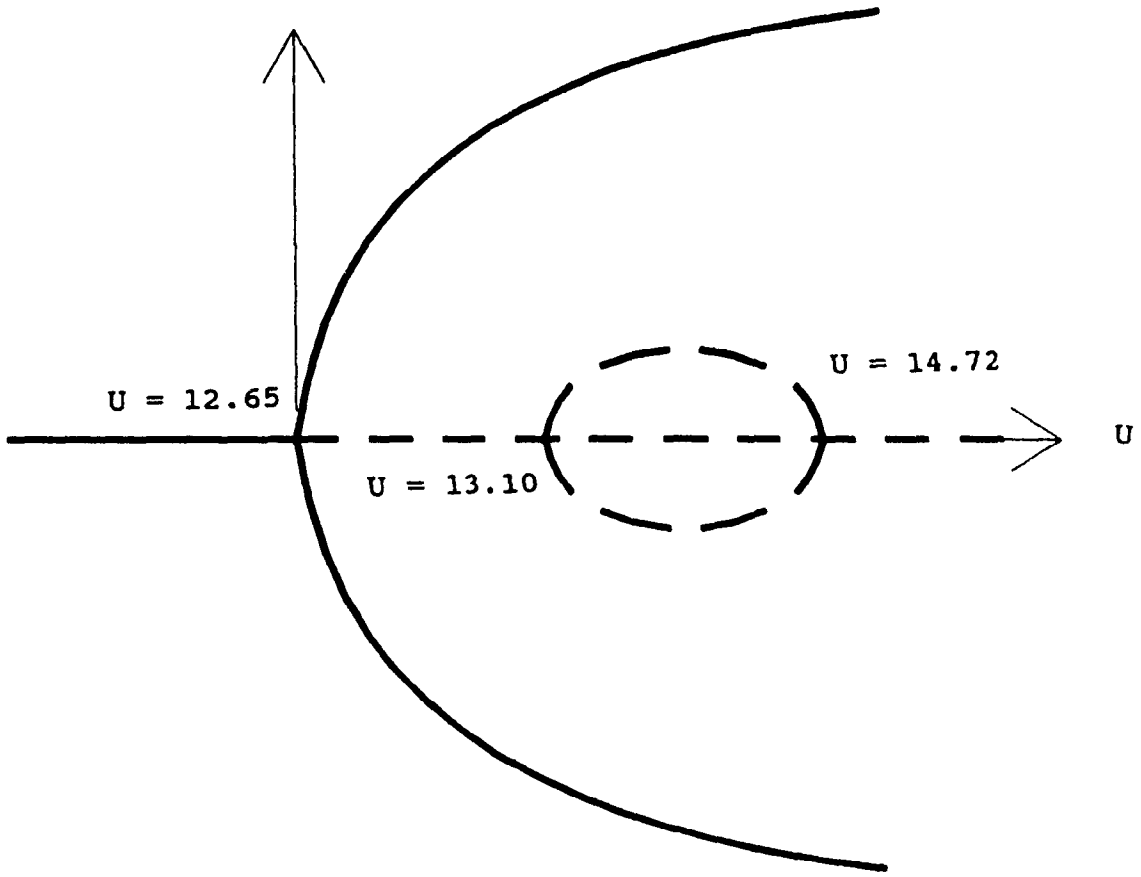

Fig.5.1(a) Bifurcation diagram: maximum displacement of the end of the pipe versus flow velocity. $K = 100$, $\xi_s = 0.8$, $\beta = 0.18$, $\gamma = 76$, $\alpha = 0.005$.

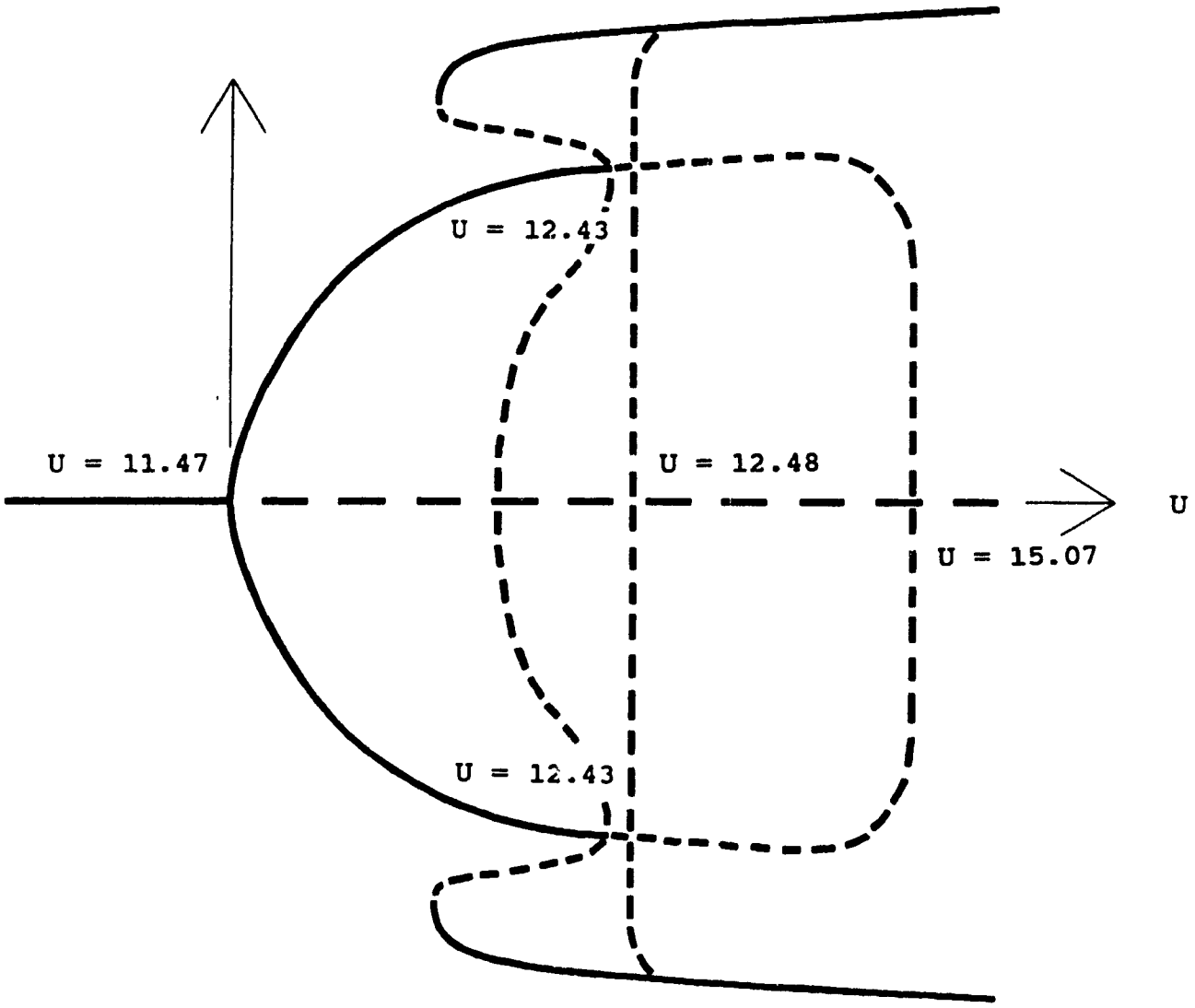

Fig.5.1(b) Bifurcation diagram: maximum displacement of the end of the pipe versus flow velocity. $K = 100$, $\xi_s = 0.8$, $\beta = 0.18$, $\gamma = 60$, $\alpha = 0.005$.

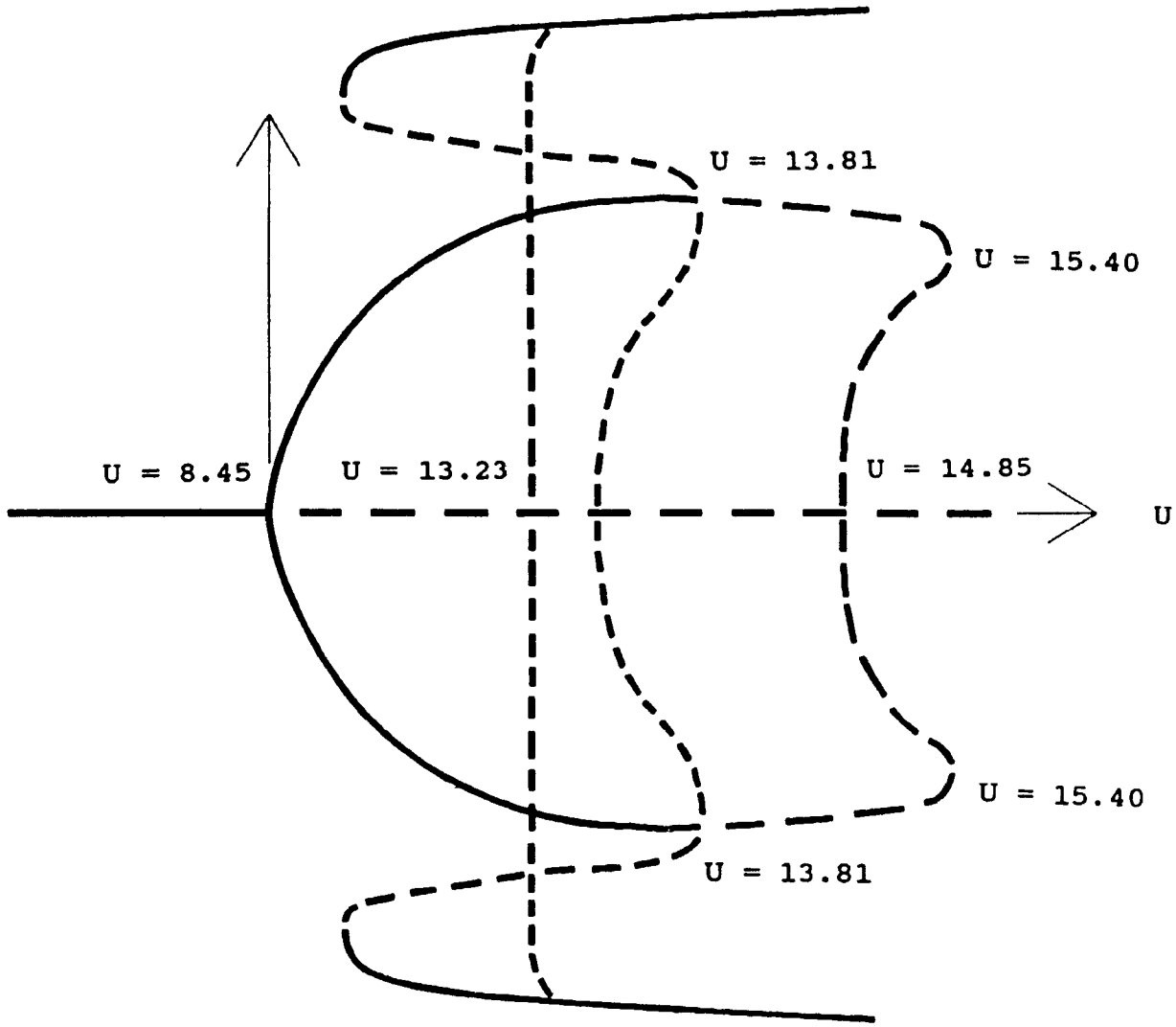

Fig.5.1(c) Bifurcation diagram: maximum displacement of the end of the pipe versus flow velocity. $K = 100$, $\xi_s = 0.8$, $\beta = 0.18$, $\gamma = 20$, $\alpha = 0.005$.

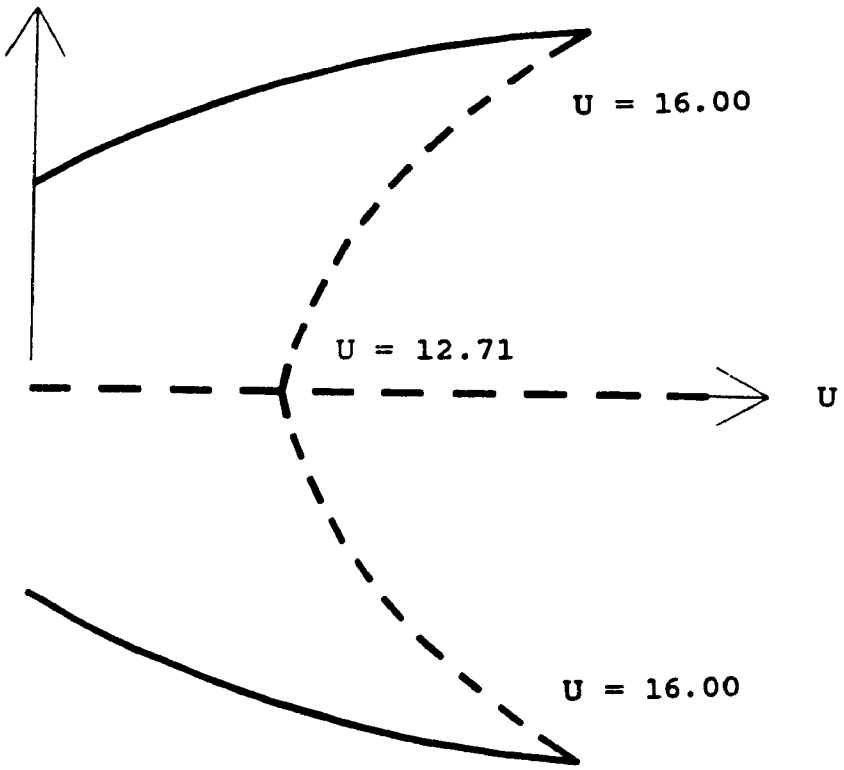

Fig.5.1(d) Bifurcation diagram: maximum displacement of the end of the pipe versus flow velocity. $K = 100$, $\xi_s = 0.8$, $\beta = 0.18$, $\gamma = -60$, $\alpha = 0.005$.

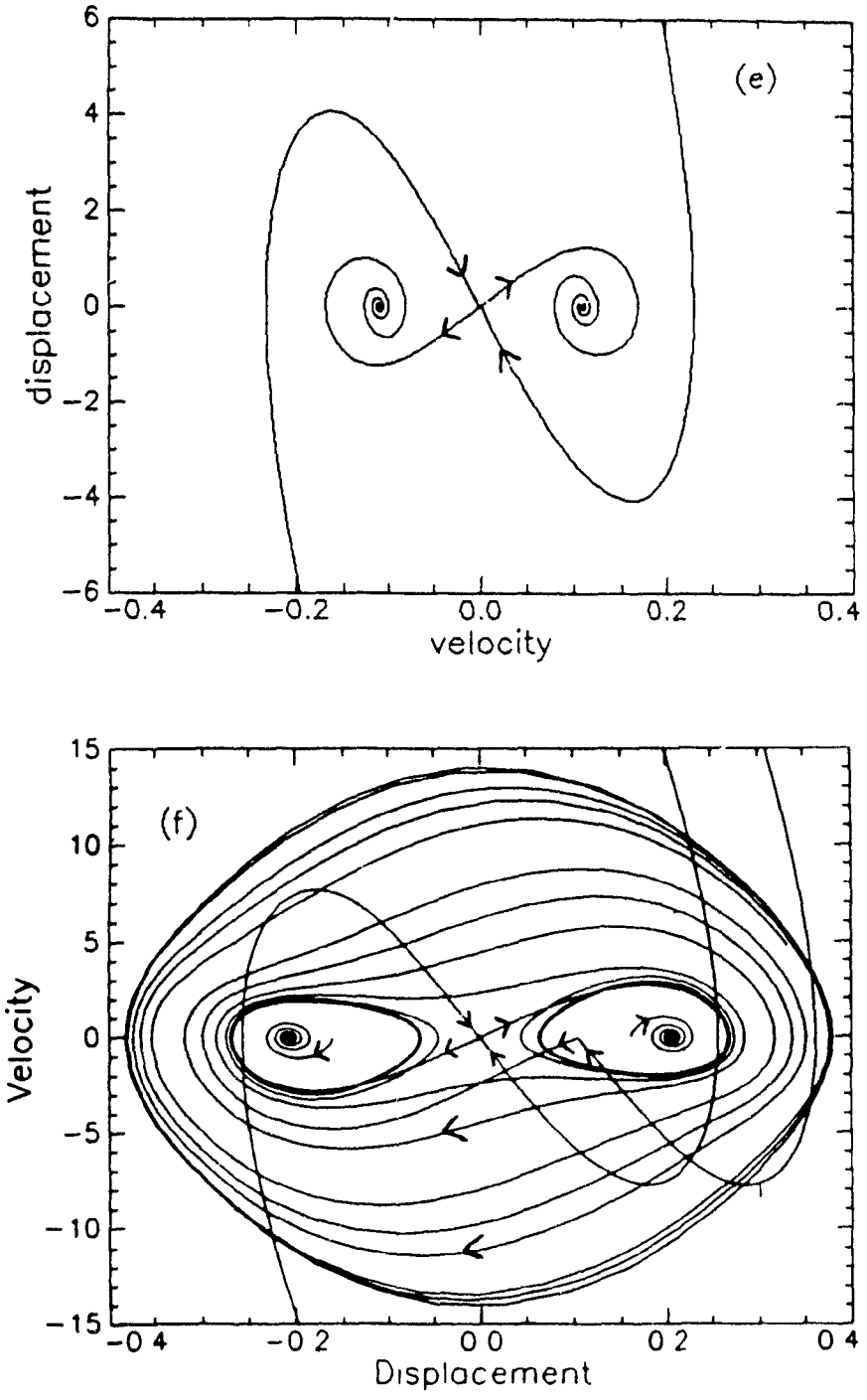

Fig.5.1. Phase portraits representing (e) the saddle {0} and the two stable equilibria {±1} at U = 7.5, (f) three saddles, {0} and {±2}, two stable equilibria {±1} and oscillatory motions at U = 13.1. γ = -60, K = 100, ξ_s = 0.8, β = 0.18, α = 0.005 (for clarity, not all the manifolds are represented).

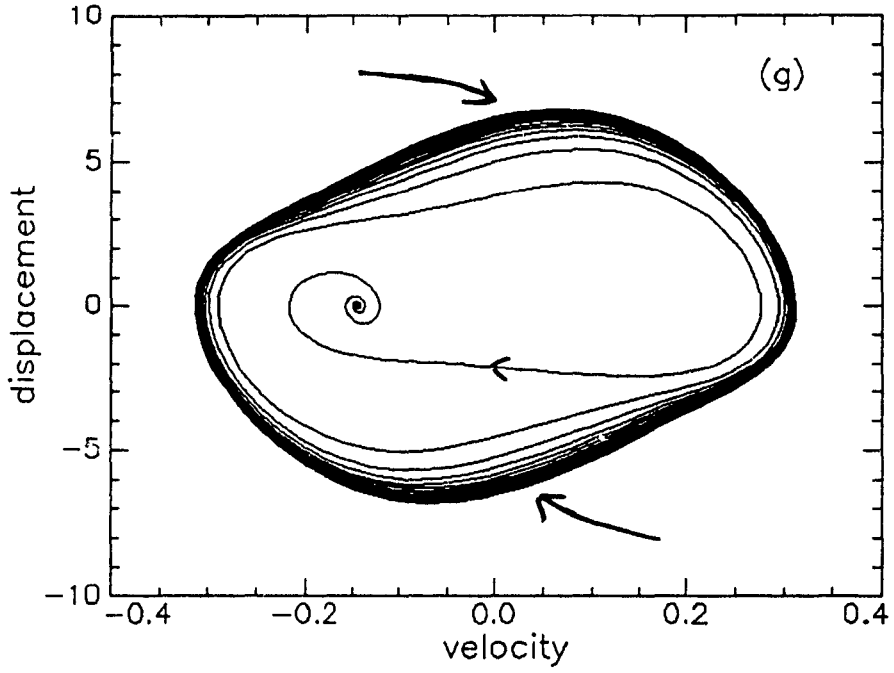

Fig.5.1(g) Phase portrait representing the onset of oscillatory motions at U = 8.76, γ = -80, K = 100, ξ_s = 0.8, β = 0.18.

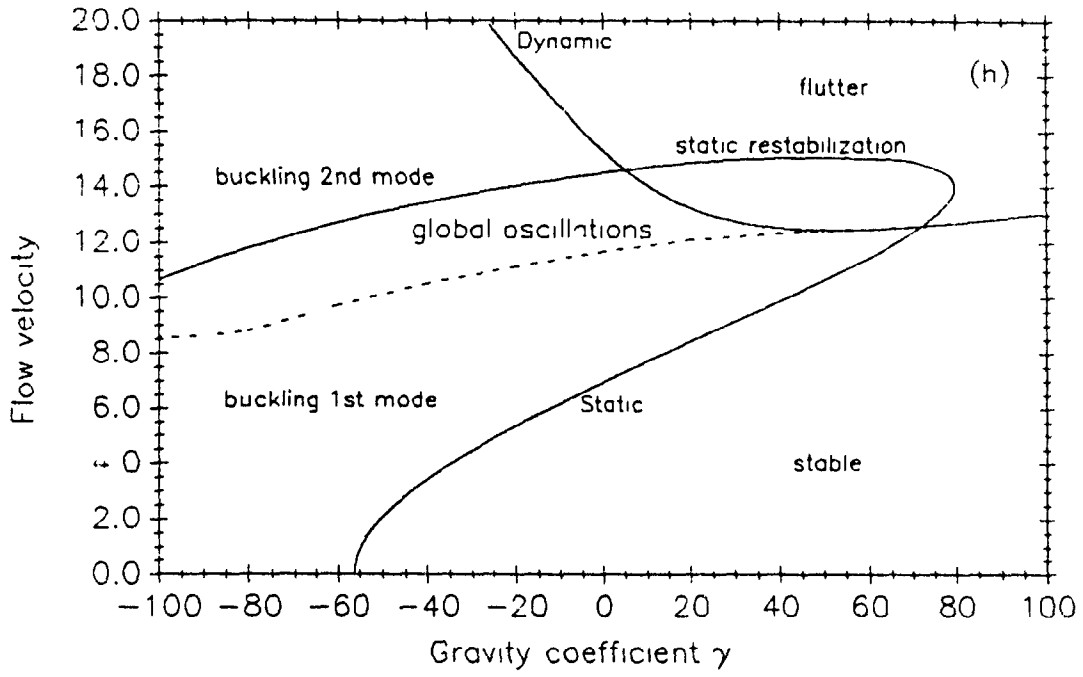

Fig.5.1(h) Completed stability map. K = 100, ξ_s = 0.8, β = 0.18, α = 0.005 (see Fig.4.11).

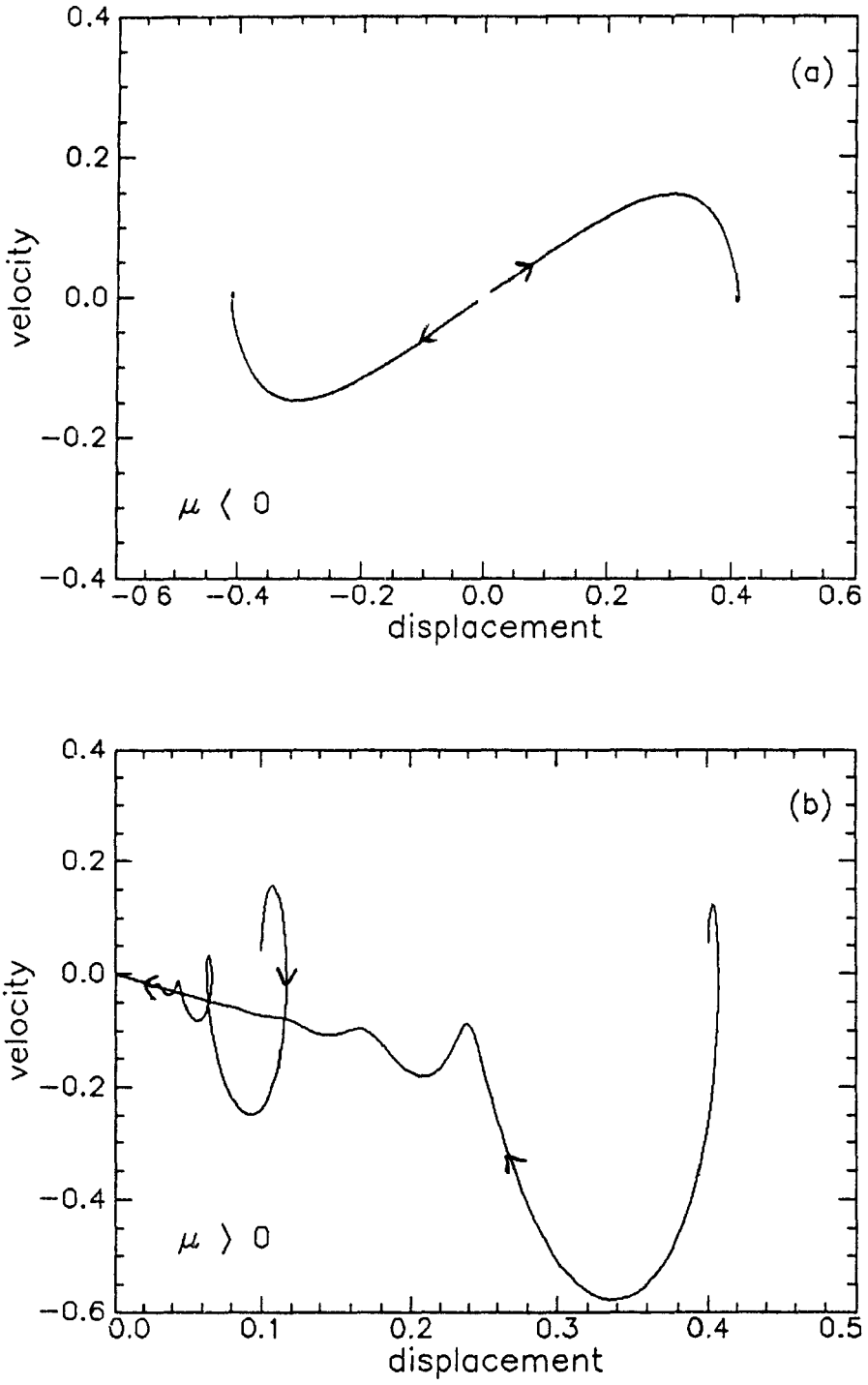

Fig.5.2 Phase diagrams showing the transition of stability of the origin through a pichfork bifurcation. U_{cr} = 3.05, γ = -25, β = 0.2, K = 0, α = 0.005. (a) U = 2.99, (b) U = 7.3.

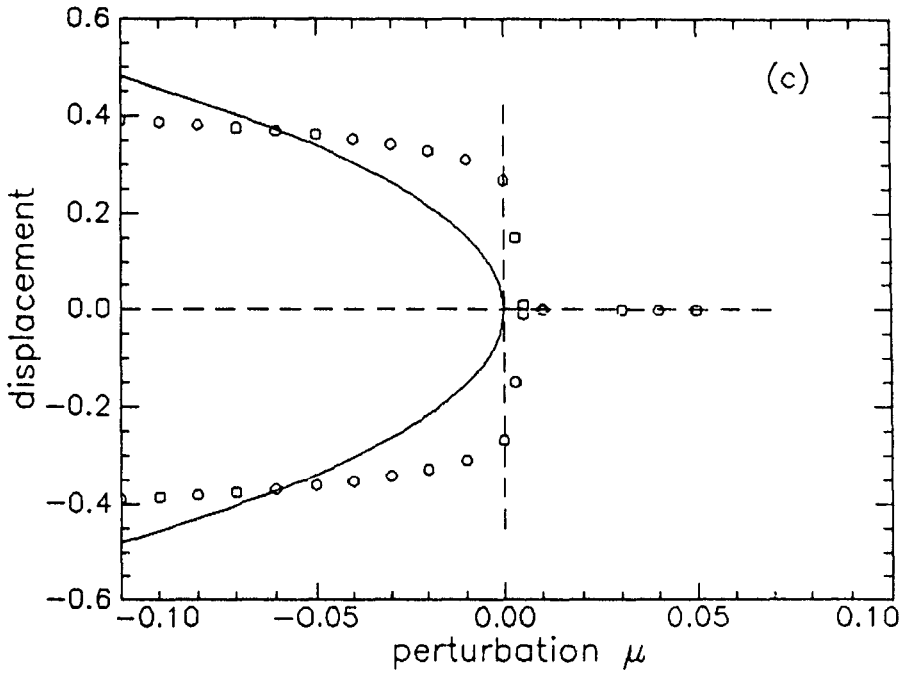

Fig.5.2 (c) Bifurcation diagram for the same parameters as (a) and (b), —— centre manifold approximation, o-o-o numerical integration.

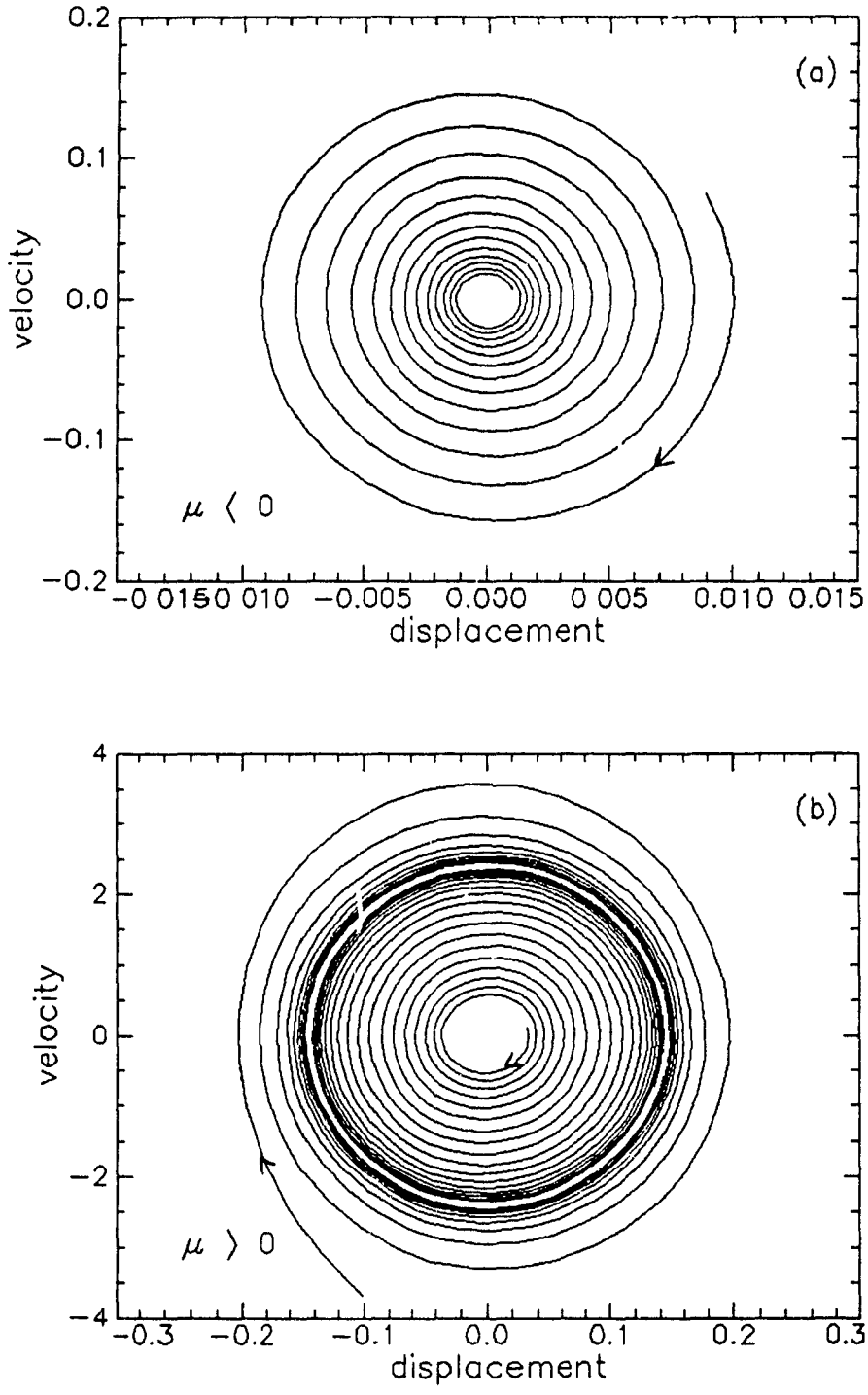

Fig.5.3 Phase diagrams illustrating the transition of instability of the origin through a Hopf bifurcation. U_{cr} = 7.09, γ = 25, β = 0.2, K = 0, α = 0.005, (a) U = 7.0, (b) U = 7.3.

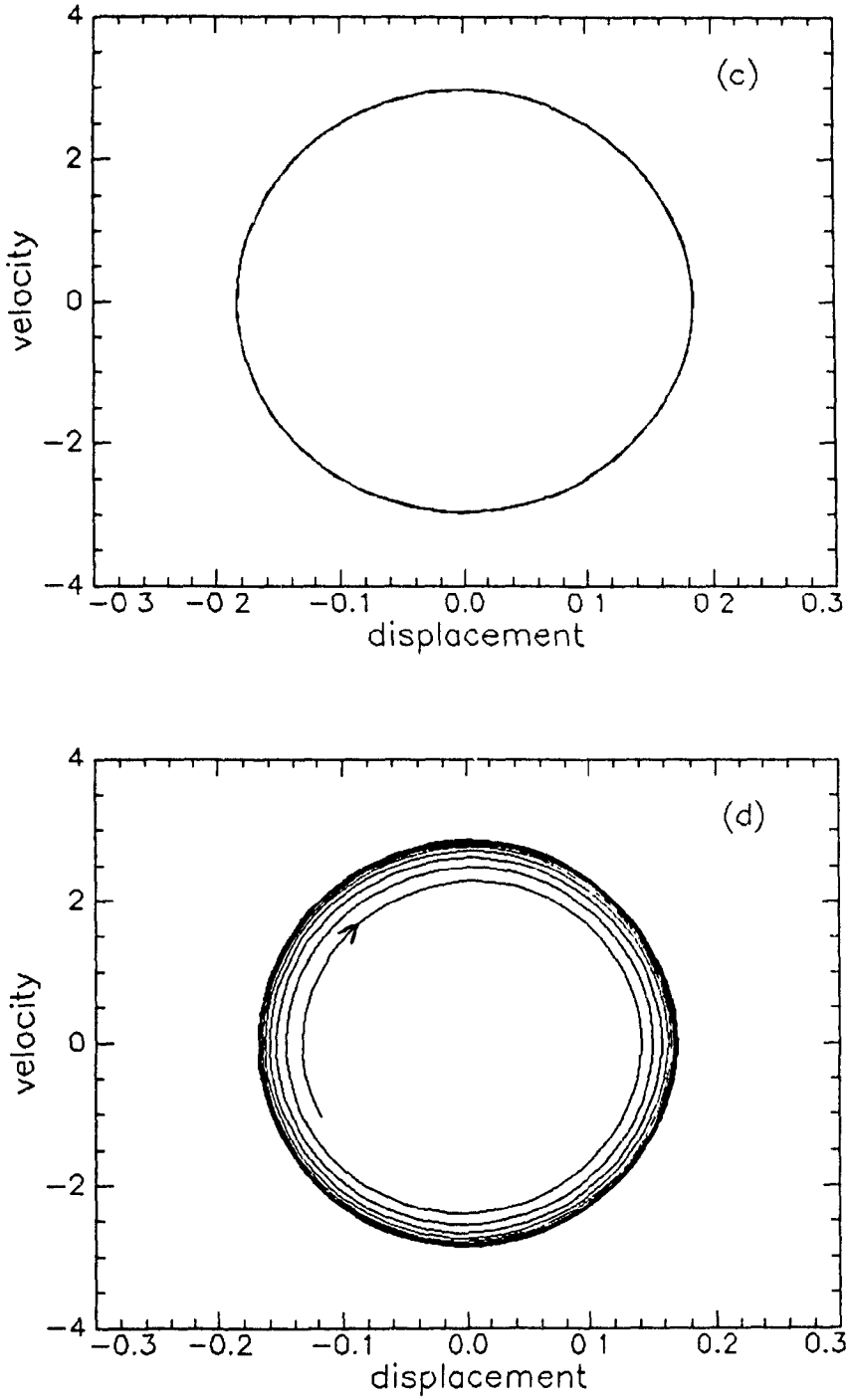

Fig.5.3 Phase diagrams beyond the Hopf bifurcation (μ = 0.3) (c) centre manifold approximation, (d) numerical integration. U_c = 7.09, γ = 25, β = 0.2, K = 0, α = 0.005.

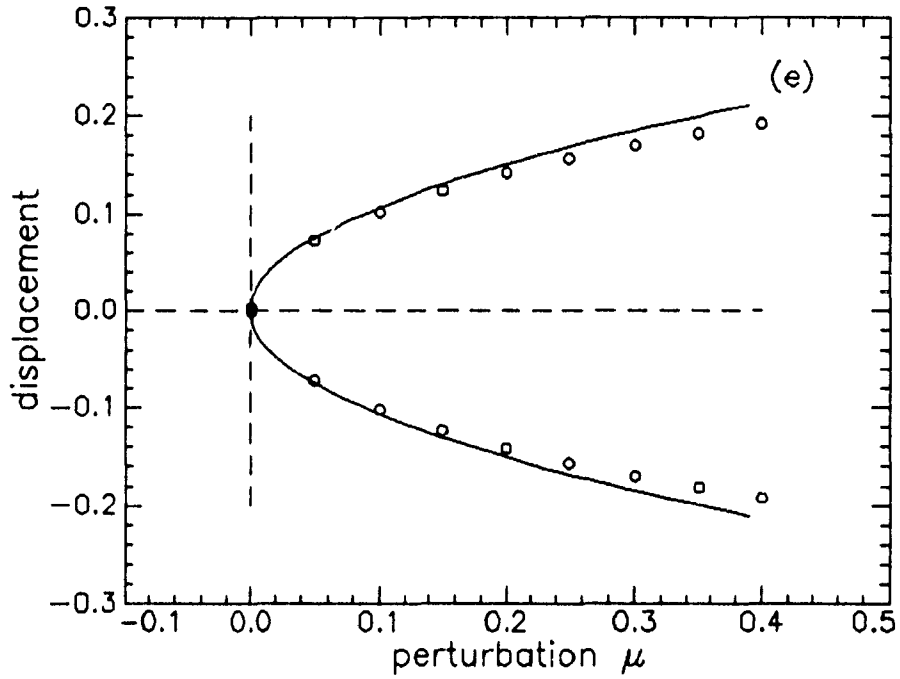

Fig.5.3 (e) Bifurcation diagram for the same parameters as (a) and (b), —— centre manifold approximation, o-o-o numerical integration.

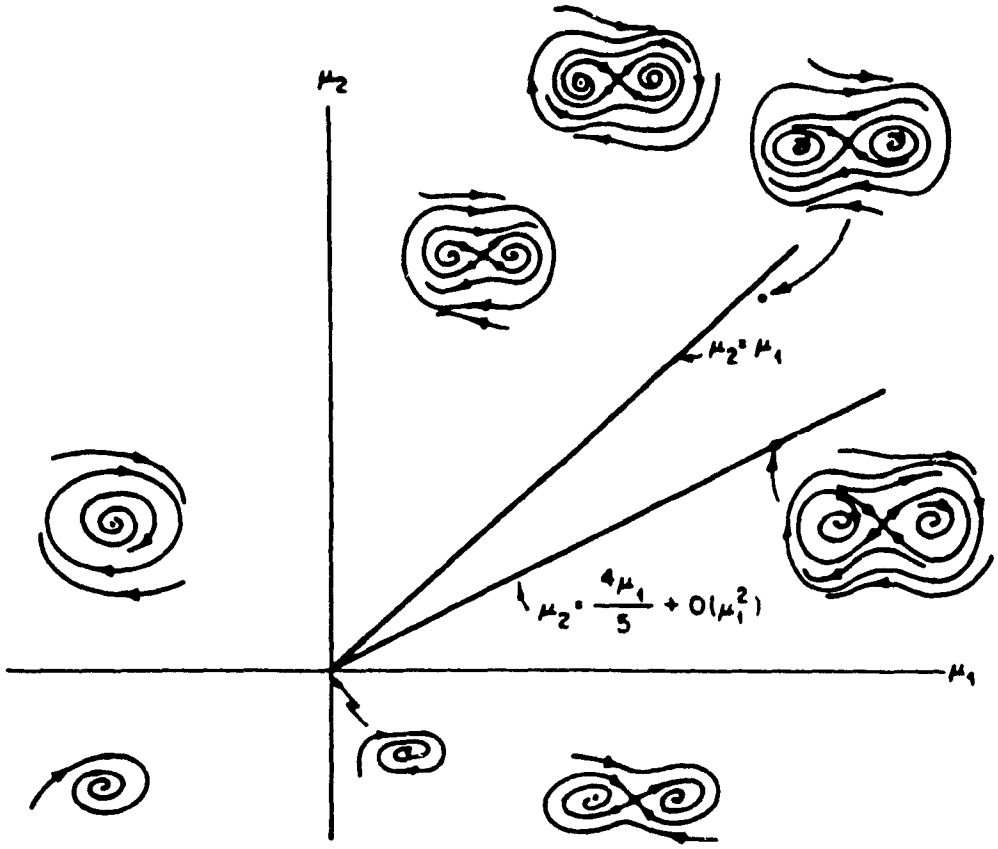

Fig.5.4(a) Codimension 2 bifurcation diagram for the double-zero eigenvalue (taken from Guckenheimer and Holmes 1983).

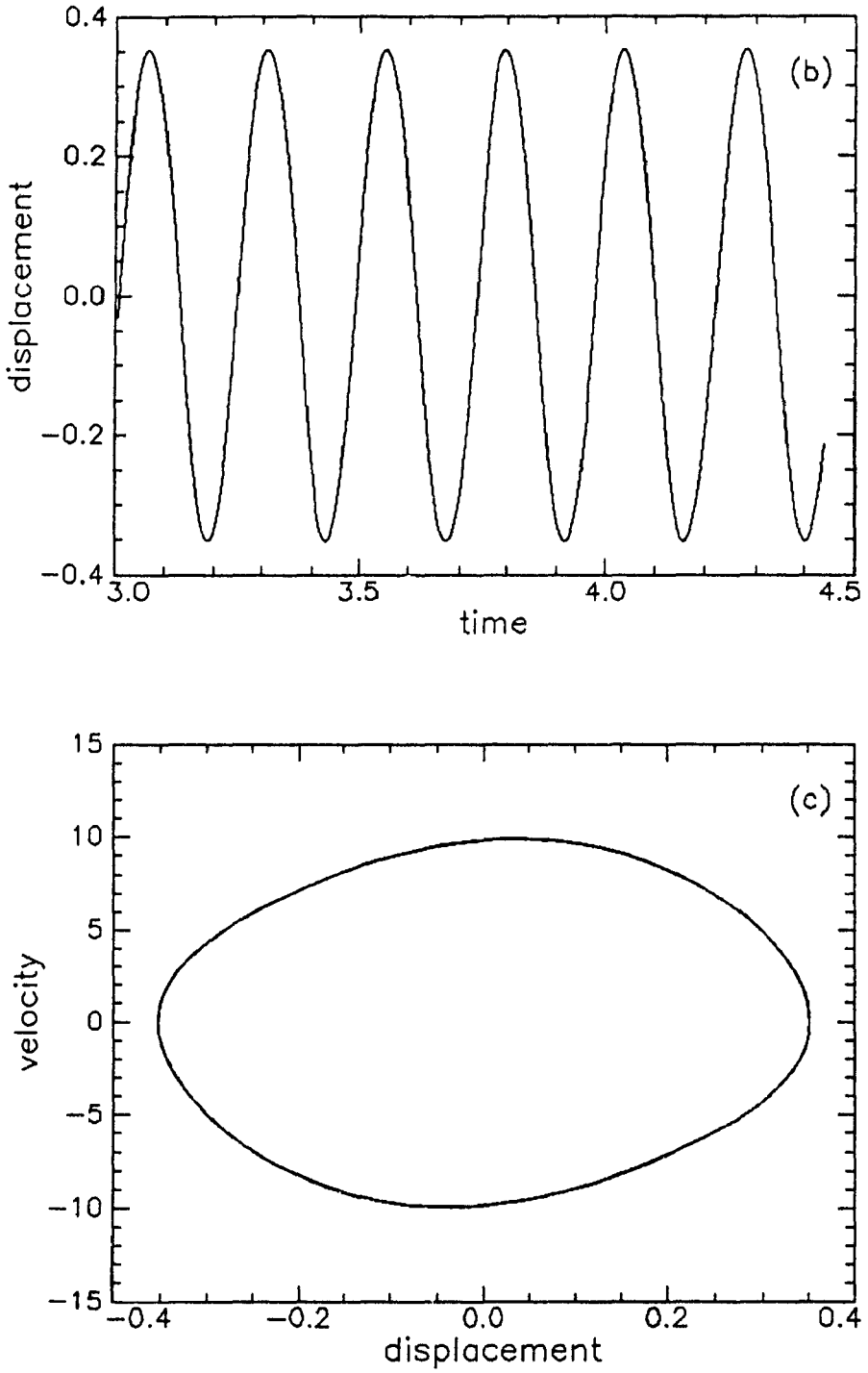

Fig.5.4 (b) Time trace, (c) phase plot illustrating the onset of flutter. U = 14.61, γ = 4.96, K = 100, ξ_s = 0.8, β = 0.18, α = 0.005.

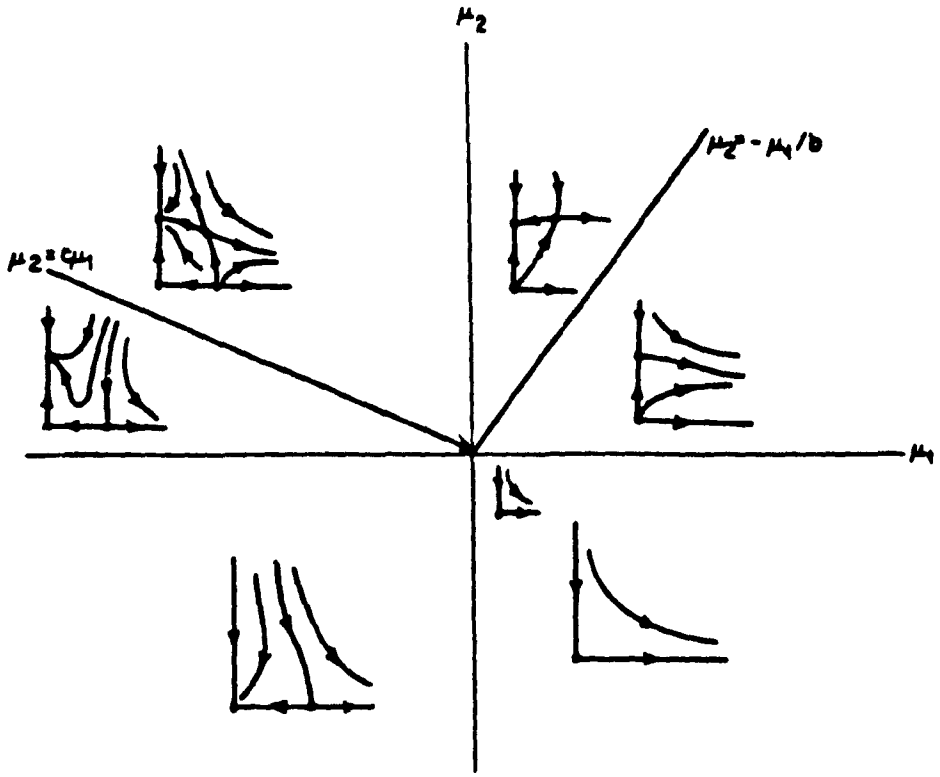

Fig.5.5(a) Codimension 2 bifurcation diagram for the doubly-degenerate fixed point, Case 2.

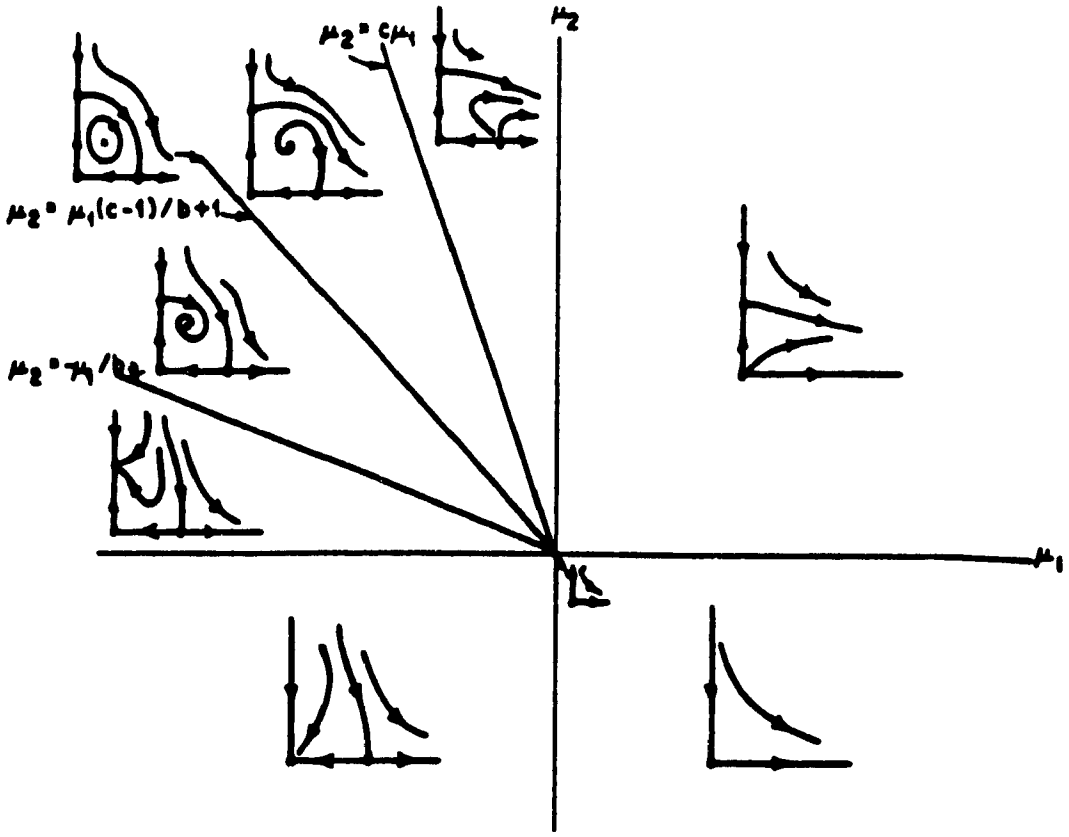

Fig.5.5(b) Codimension 2 bifurcation diagram for the doubly-degenerate fixed point, Cases 1 and 3 (taken from Guckenheimer and Holmes 1983).

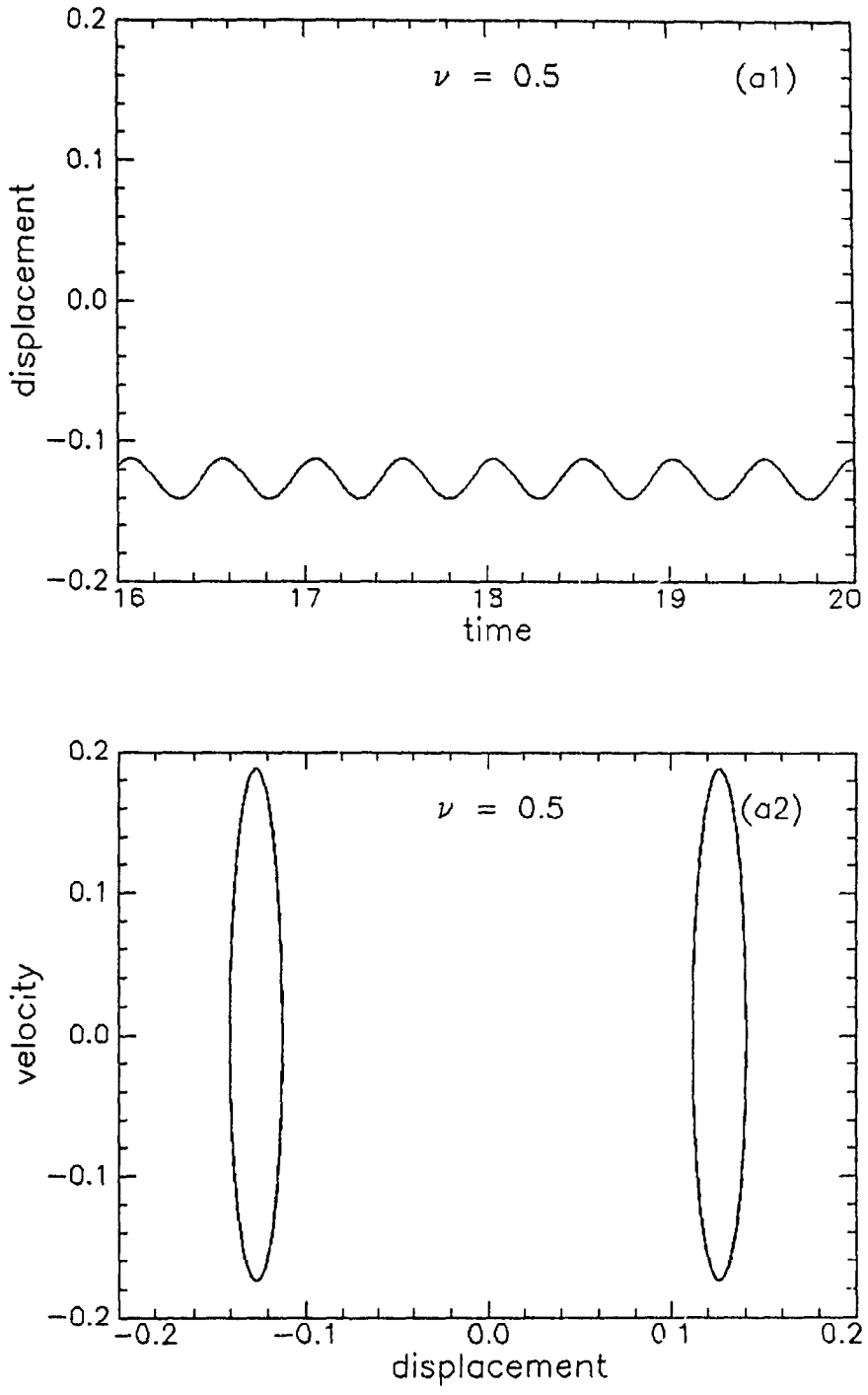

Fig.5.6(a) 1. Time trace, 2. phase plot for ν = 0.5, case 3 (only one time trace is represented).

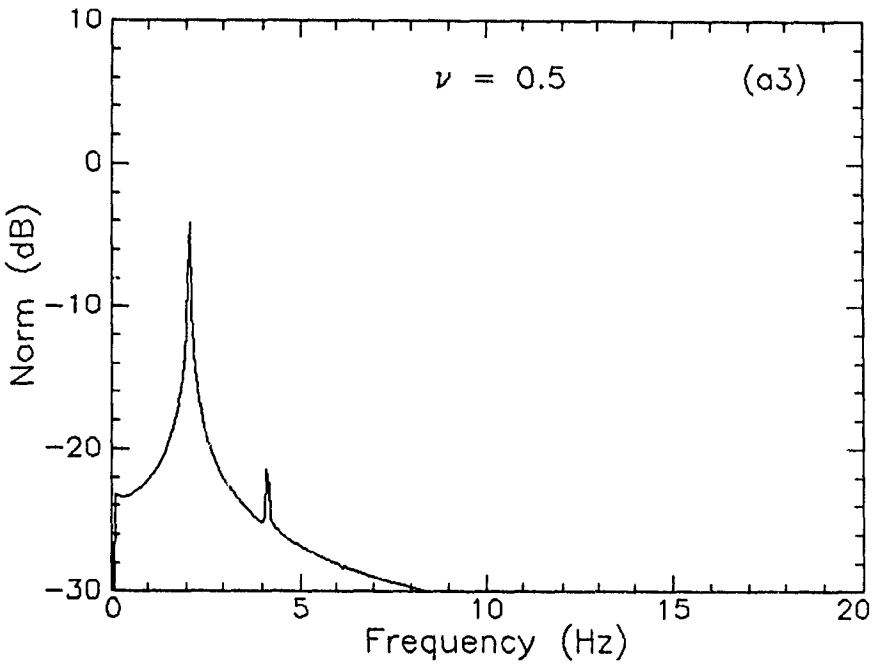

Fig.5.6(a) 3. Power spectrum for ν = 0.5, case 3.

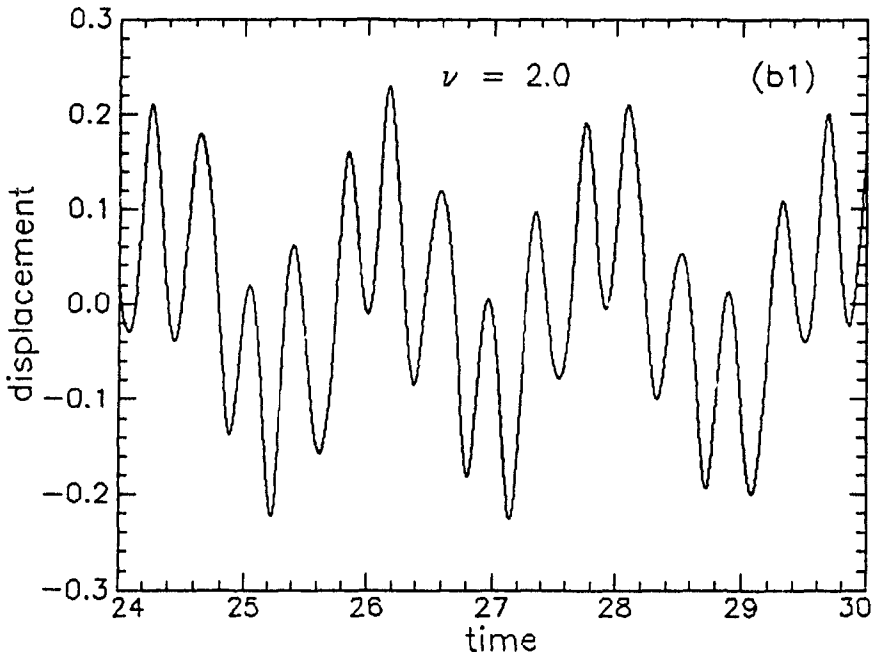

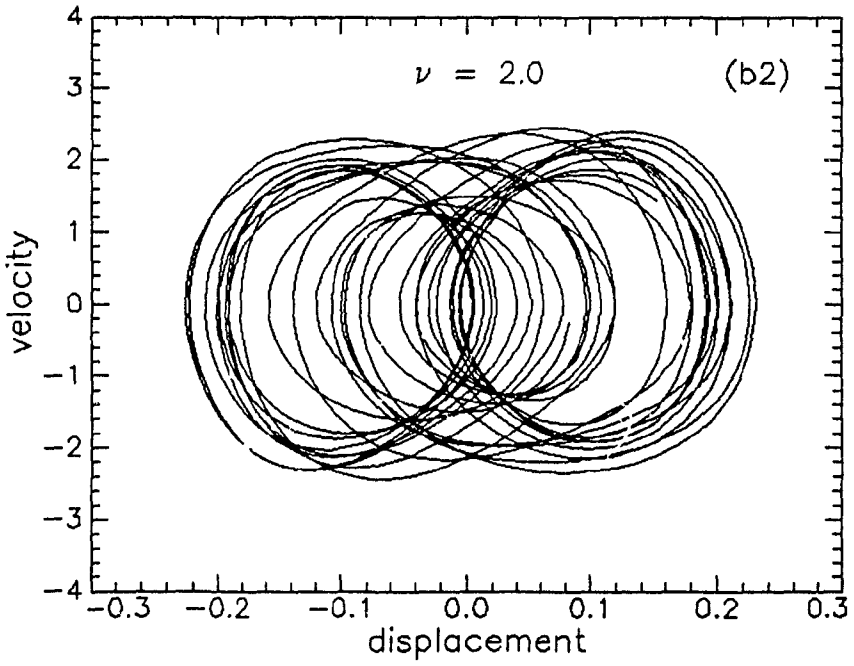

Fig.5.6(b) 1. Time trace, 2. phase plot for ν = 2, case 3.

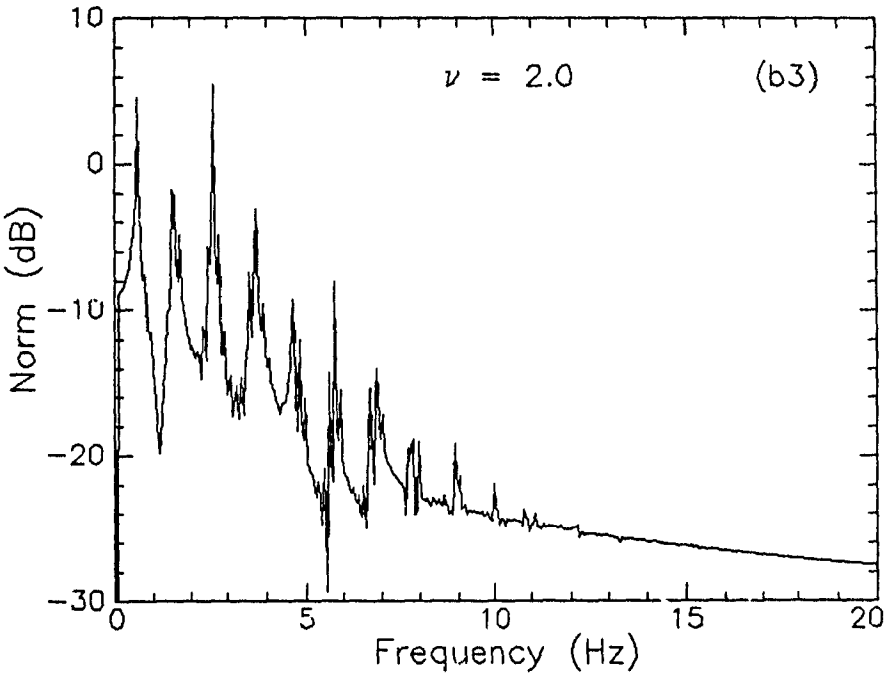

Fig.5.6(b) 3. Power spectrum for ν = 2, case 3.

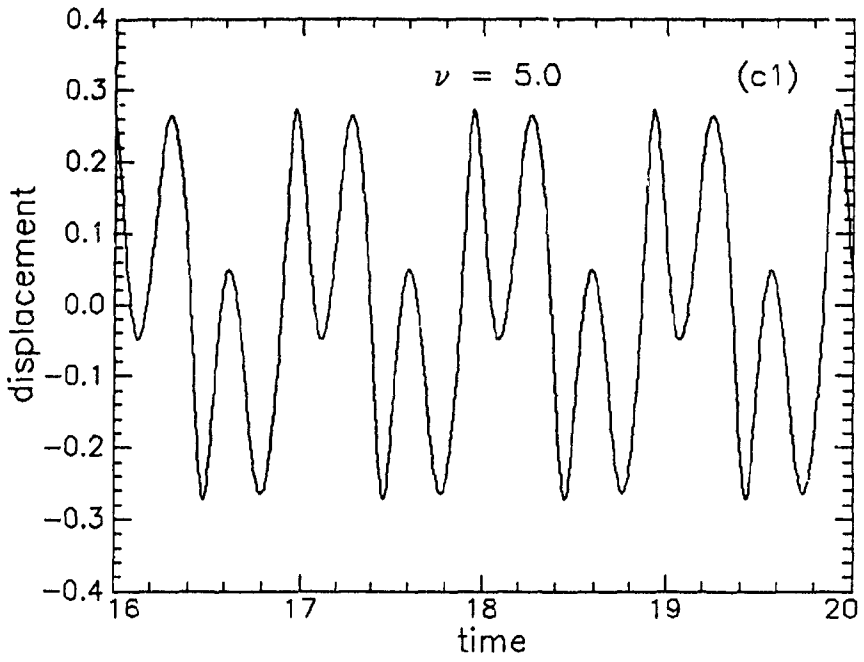

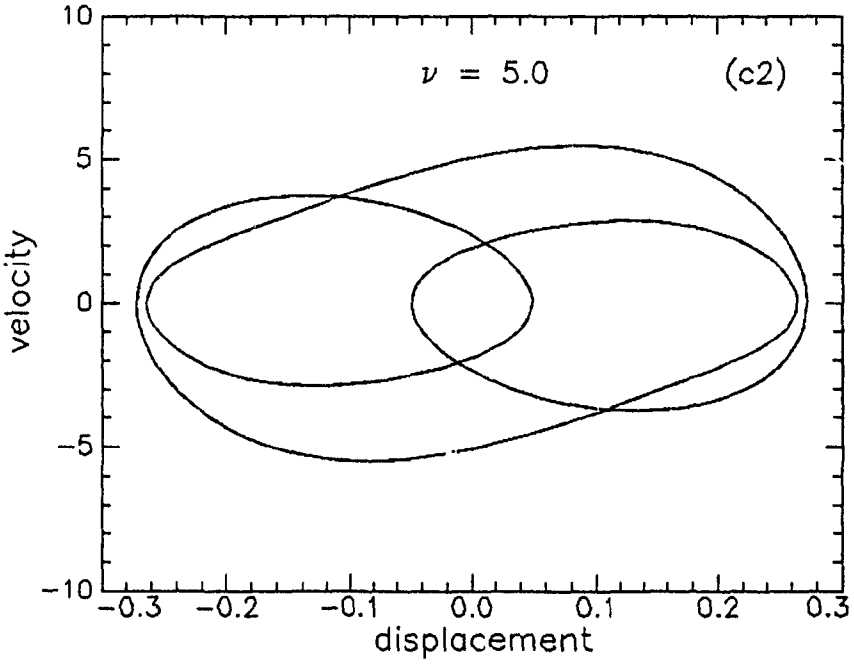

Fig.5.6(c) **1. Time trace, 2. phase plot for ν = 5, case 3.**

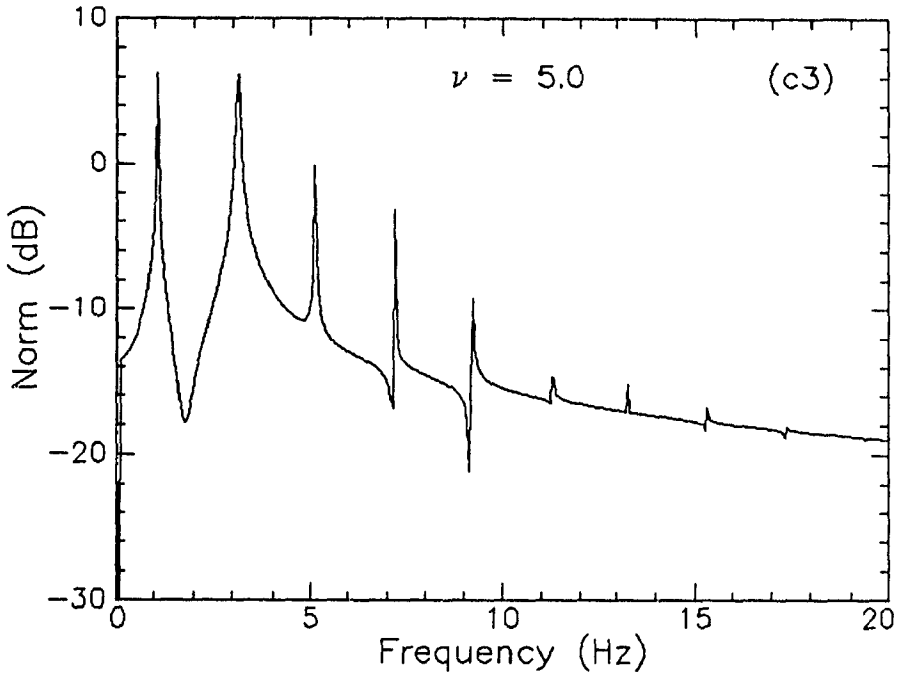

Fig.5.6(c) 3. Power spectrum for ν = 5, case 3.

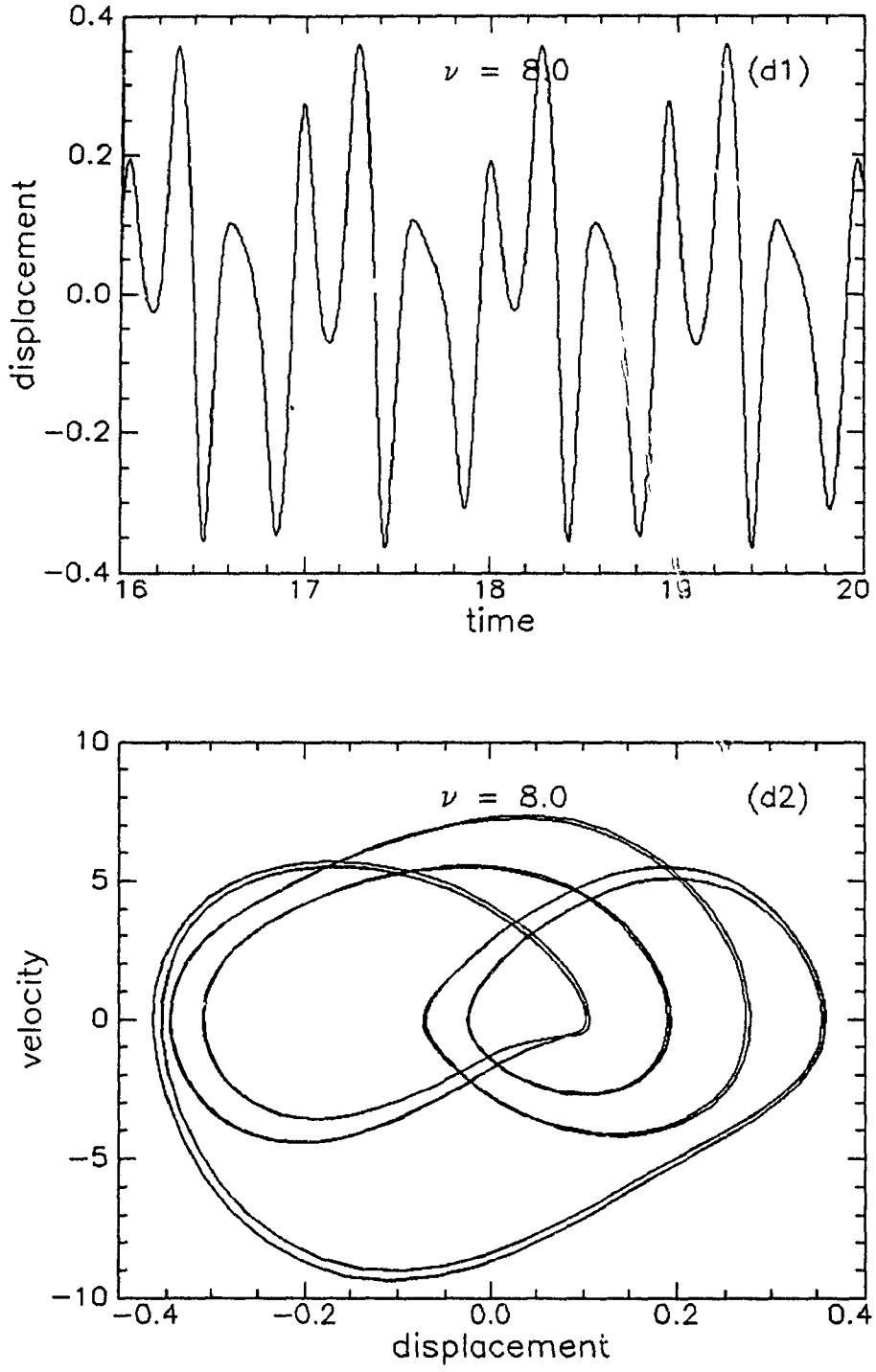

Fig.5.6(d) 1. Time trace, 2. phase plot for ν = 8, case 3.

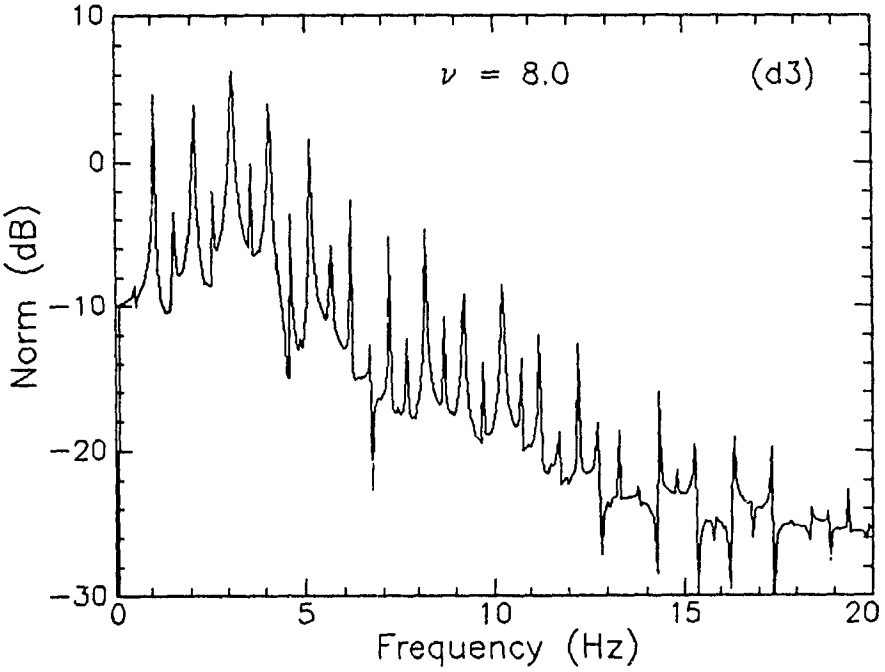

Fig.5.6(d) 3. Power spectrum for ν = 8, case 3.

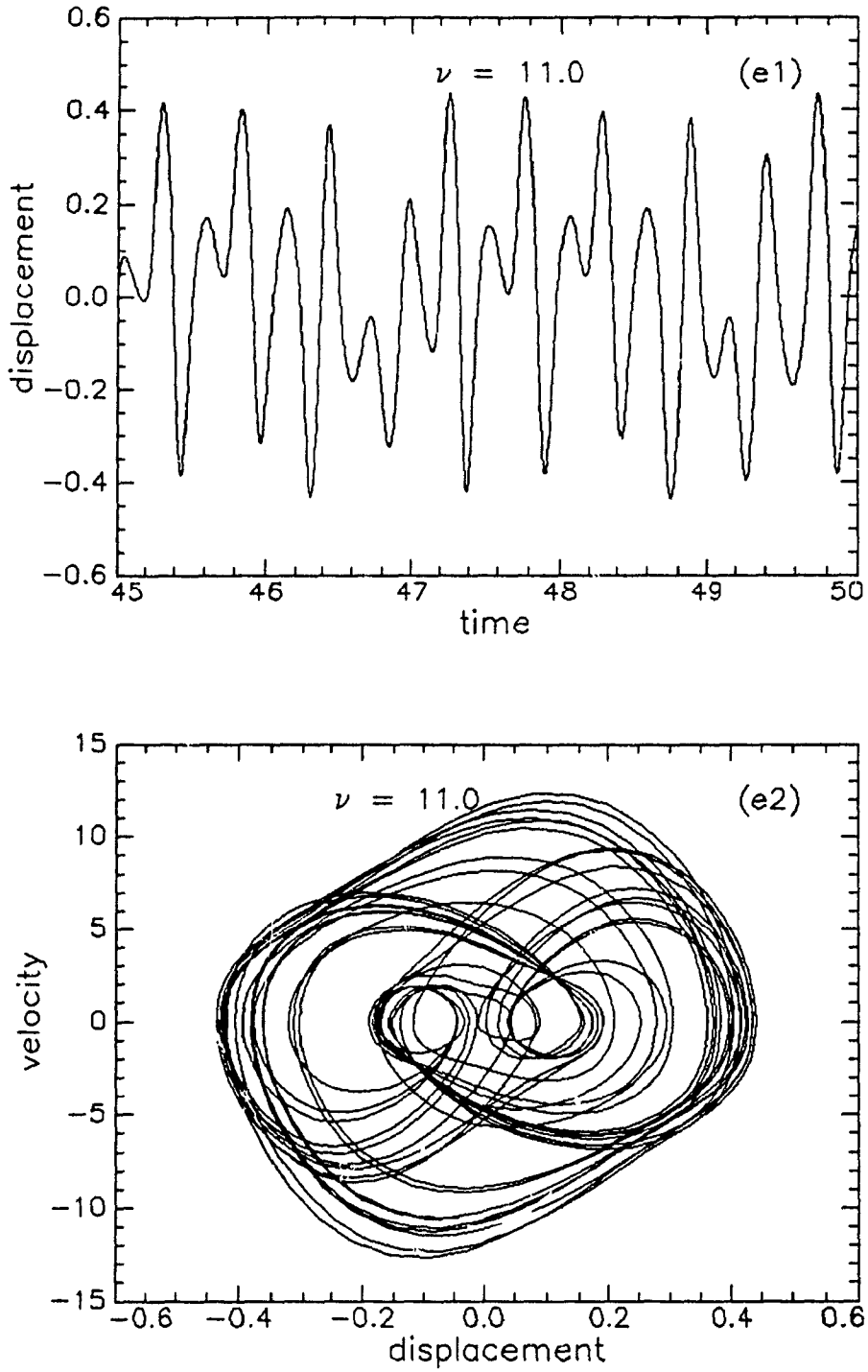

Fig.5.6(e) 1. Time trace, 2. phase plot for ν = 11, case 3.

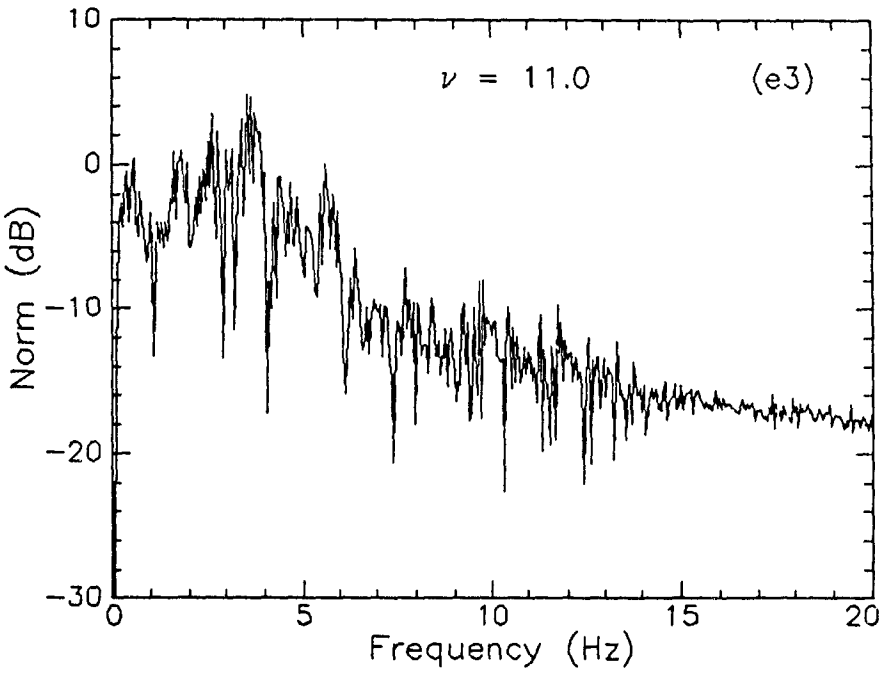

Fig.5.6(e) 3. Power spectrum for ν = 11, case 3.

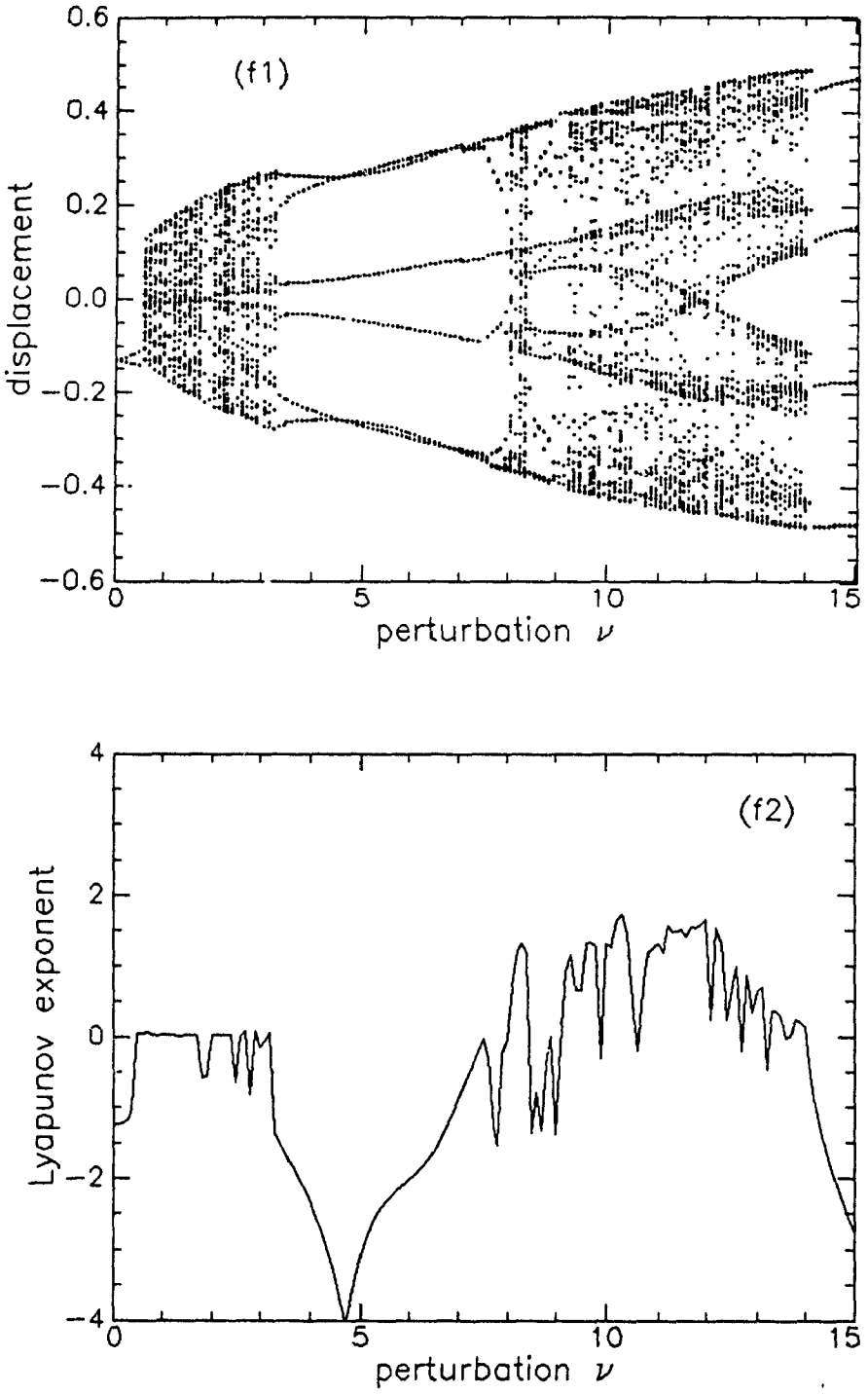

Fig.5.6(f) Bifurcation diagrams, 1. Tip maximum displacements, 2. Lyapunov exponents, function of the flow perturbation.

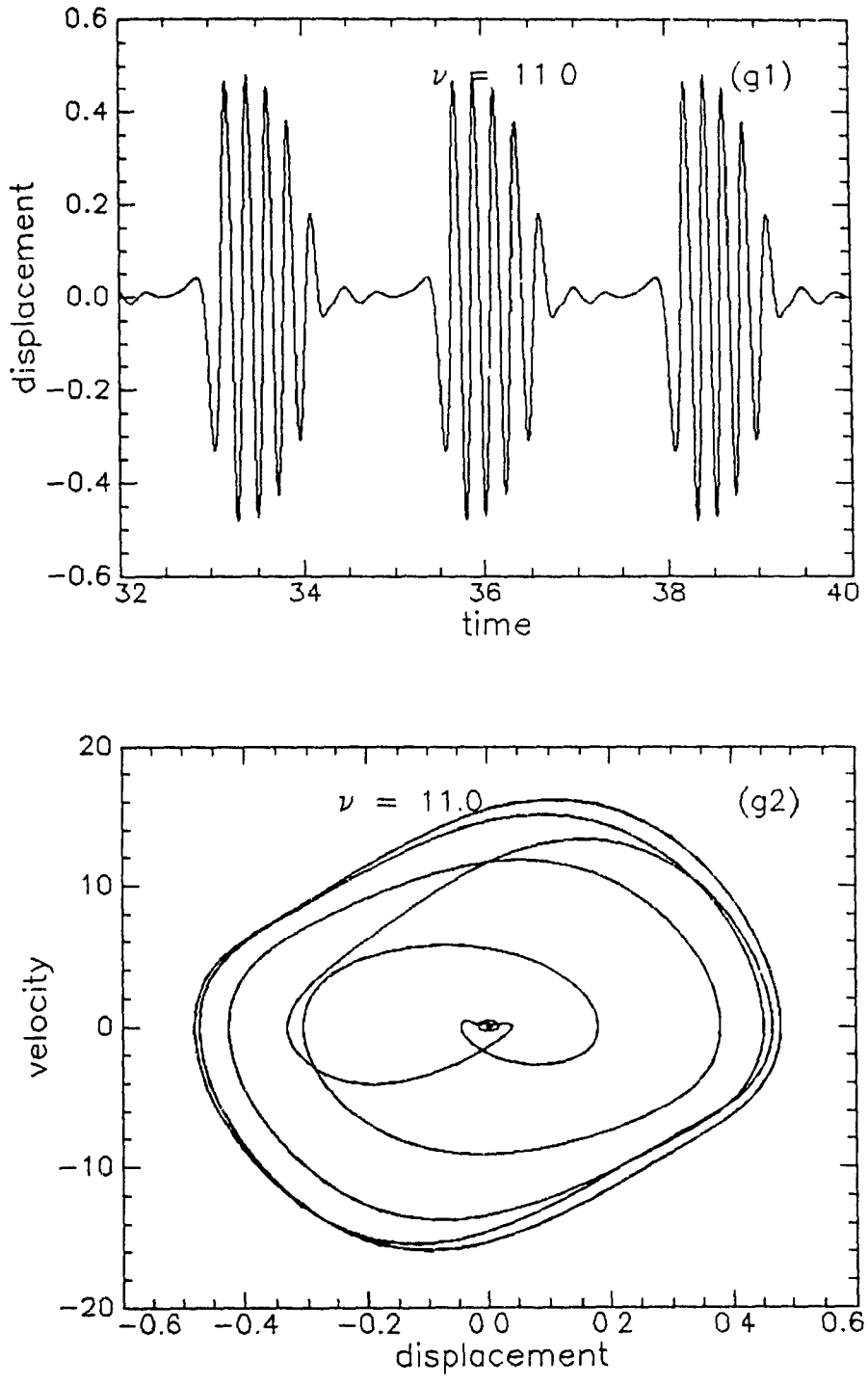

Fig.5.6(g) Effect of the forcing frequency. 1. Time trace, 2. phase plot, for $\nu = 11$, $\omega = 2.5$.

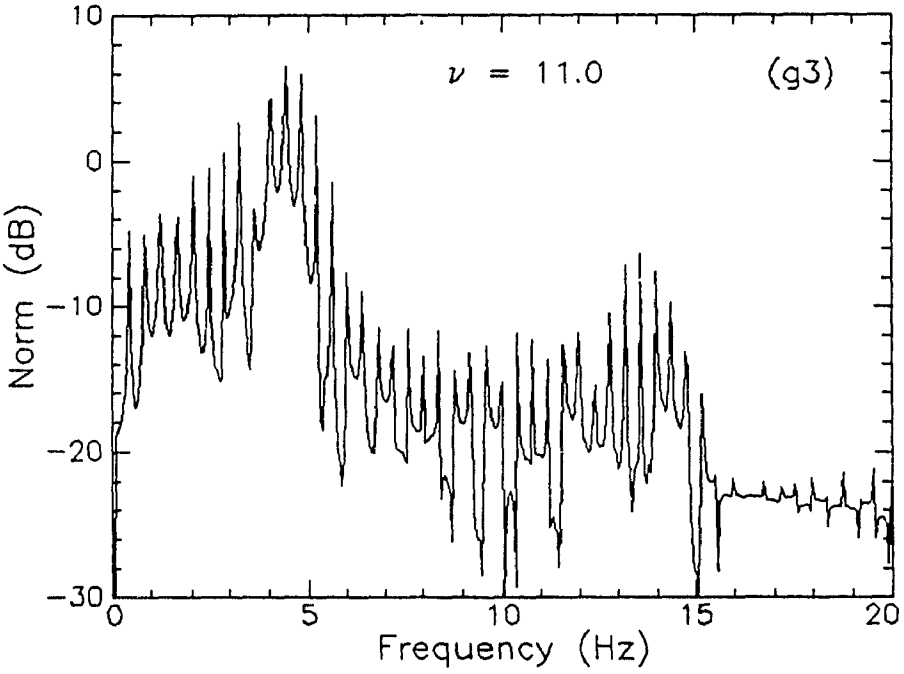

Fig.5.6(g) 3. Power spectrum for $\nu = 11$, $\omega = 2.5$.

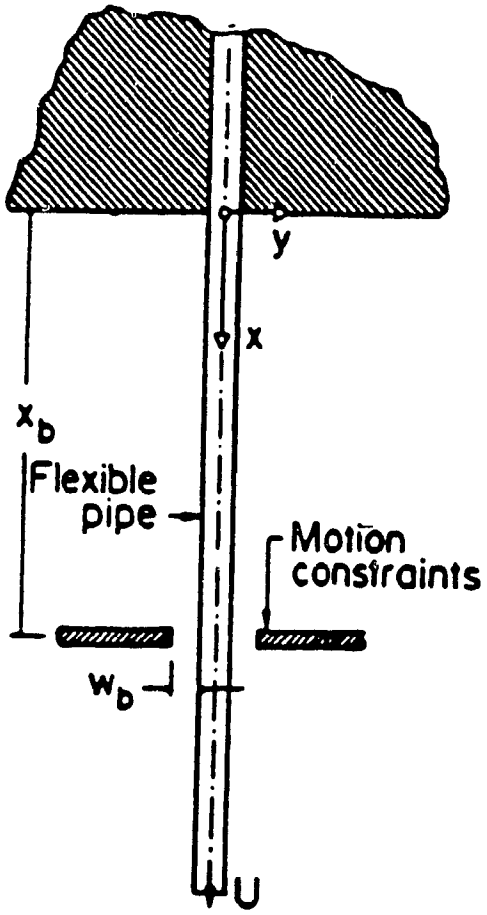

Fig.5.7 (a) Schematic of the constrained pipe.

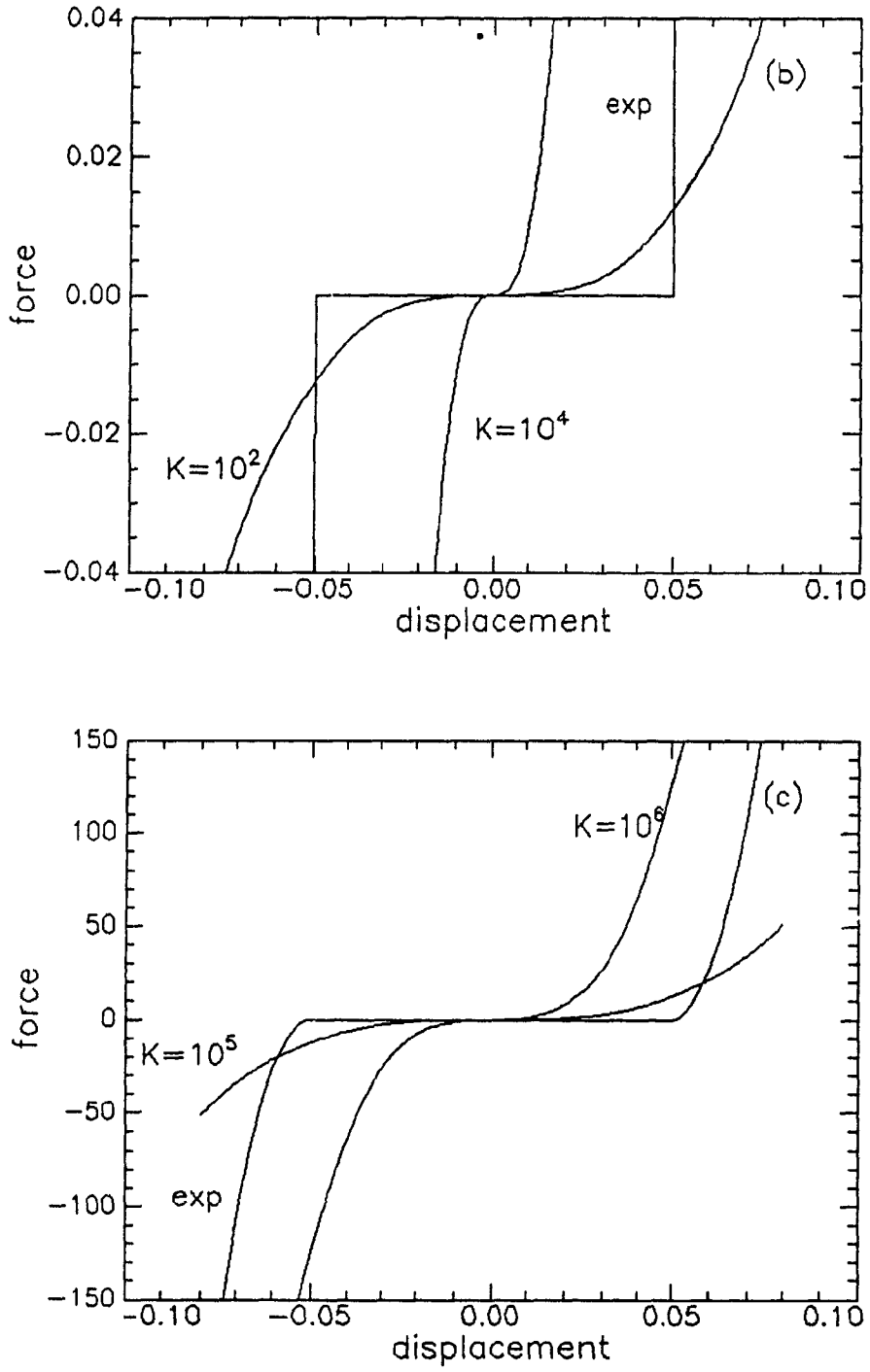

Fig.5.7 Force-displacement curves for different spring stiffness K; exp represents the experimental curve.

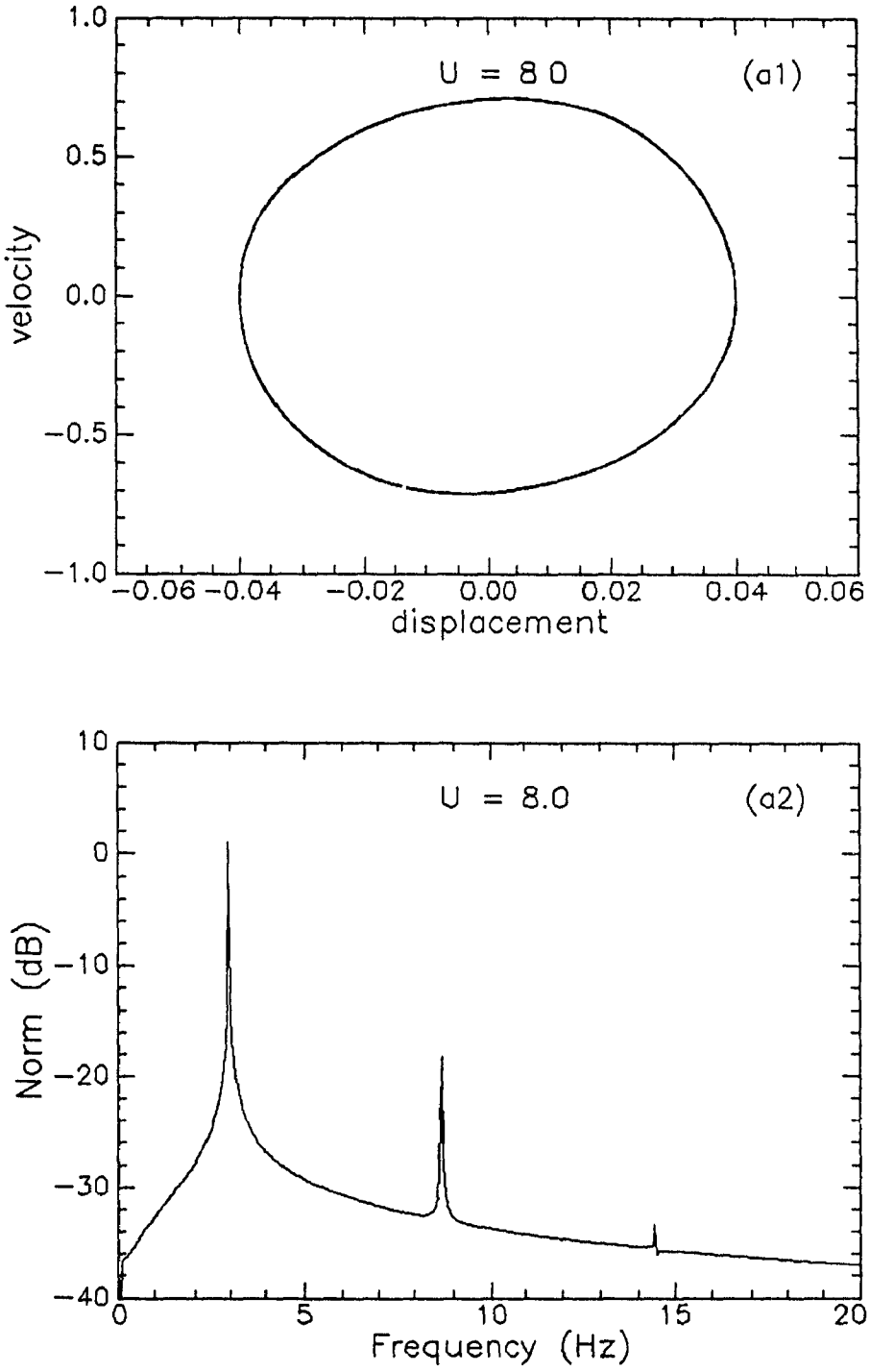

Fig.5.8(a) Phase portrait and power spectrum, U = 8, $K = 10^5$, $\xi_b = 0.75$, $\gamma = 26.75$, $\beta = 0.213$, $\alpha = 0.005$.

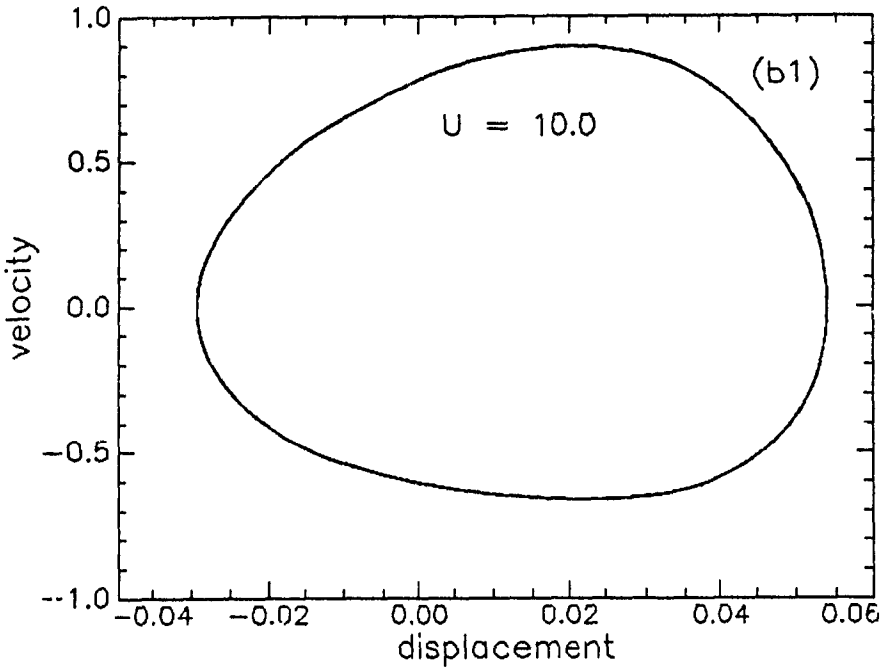

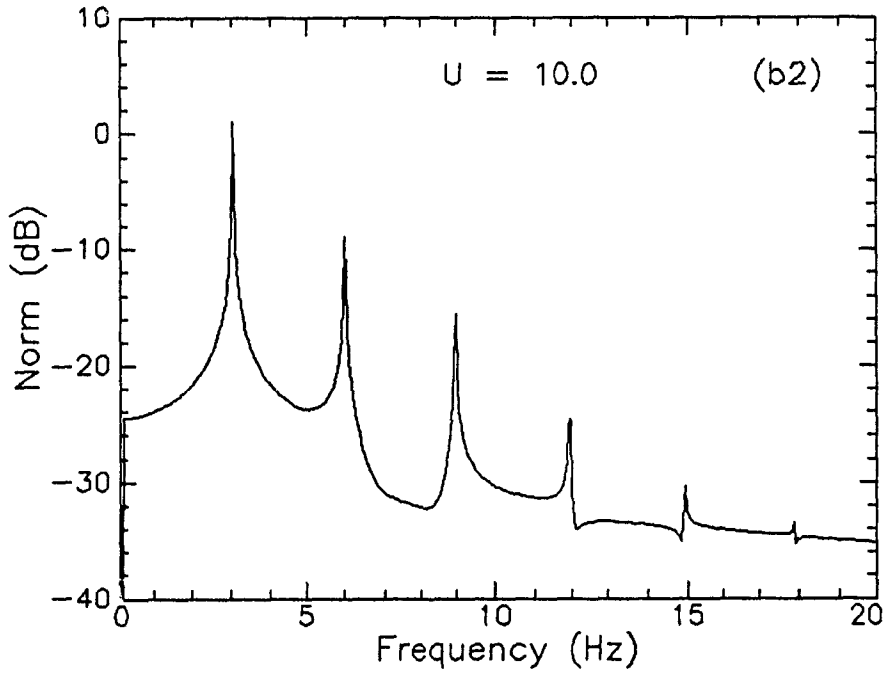

Fig.5.8(b) Phase portrait and power spectrum illustrating the pitchfork bifurcation, $U = 10$, $K = 10^5$, $\xi_b = 0.75$, $\gamma = 26.75$, $\beta = 0.213$, $\alpha = 0.005$.

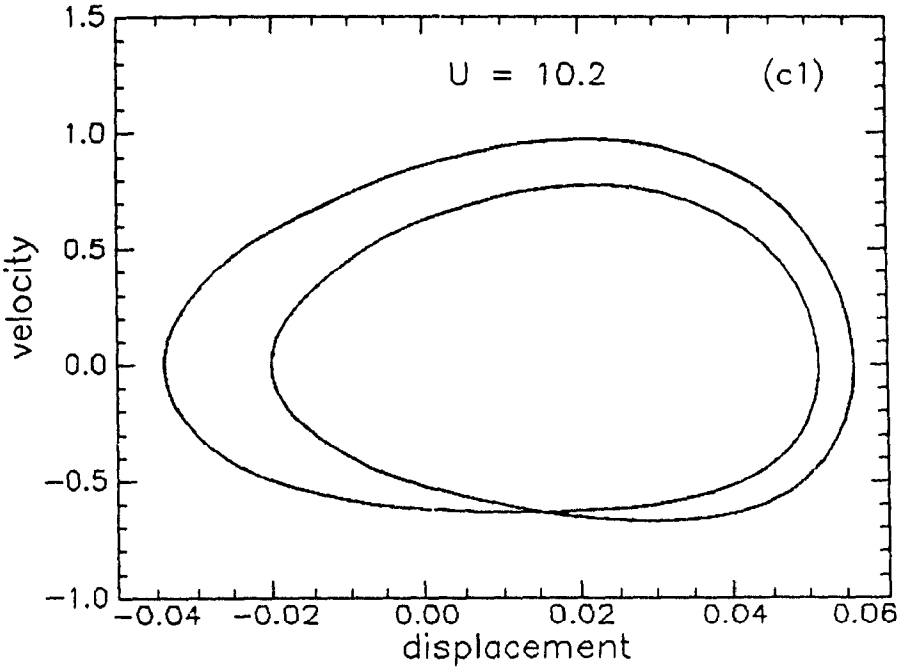

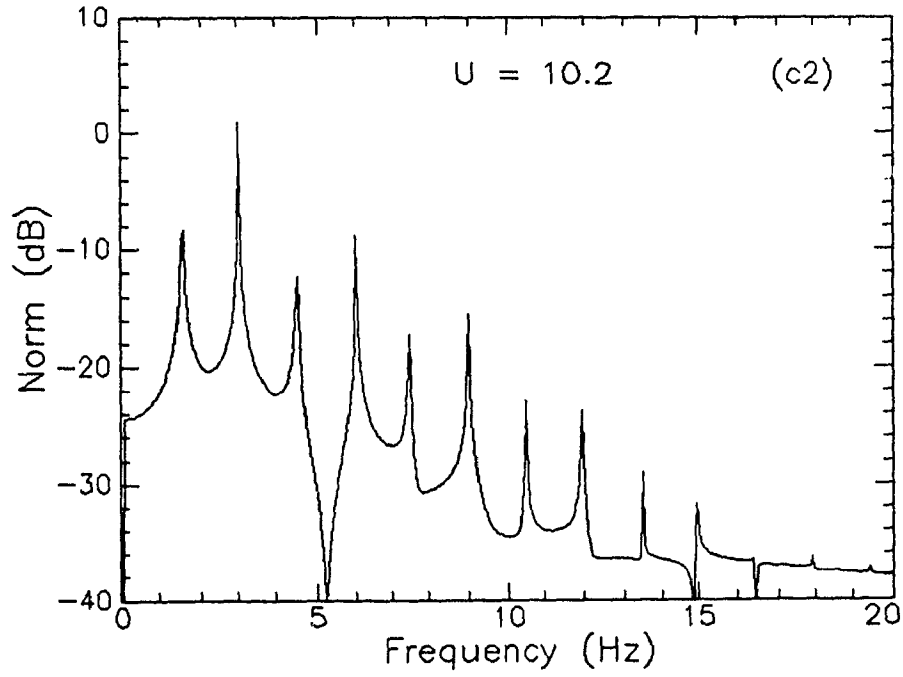

Fig.5.8(c) **Phase portrait and power spectrum, period-doubling; U = 10.2, K = 10^5, ξ_b = 0.75, γ = 26.75, β = 0.213, α = 0.005.**

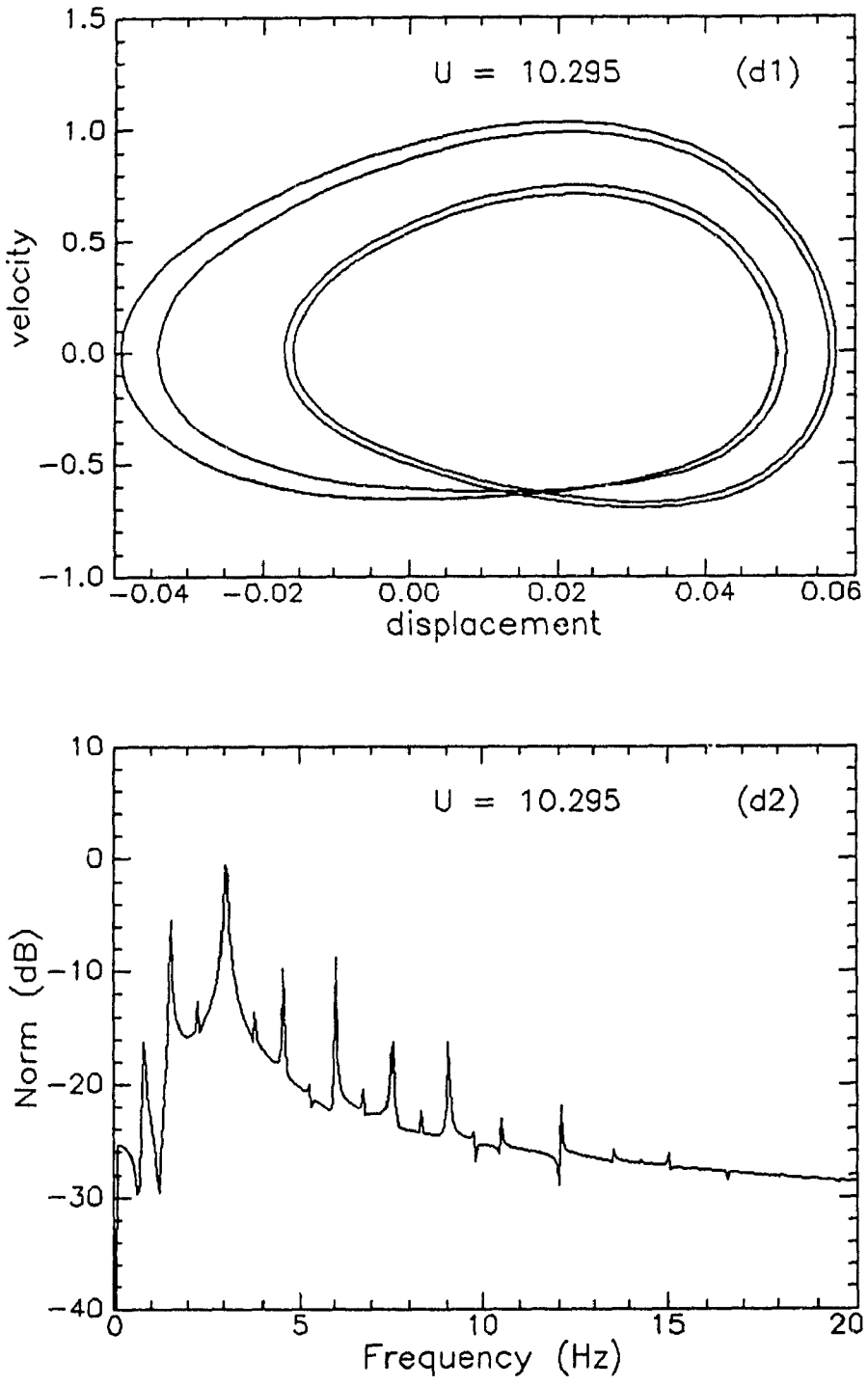

Fig.5.8(d) Phase portrait and power spectrum, second period-doubling; U = 10.295, K = 10^5, ξ_b = 0.75, γ = 26.75, β = 0.213, α = 0.005.

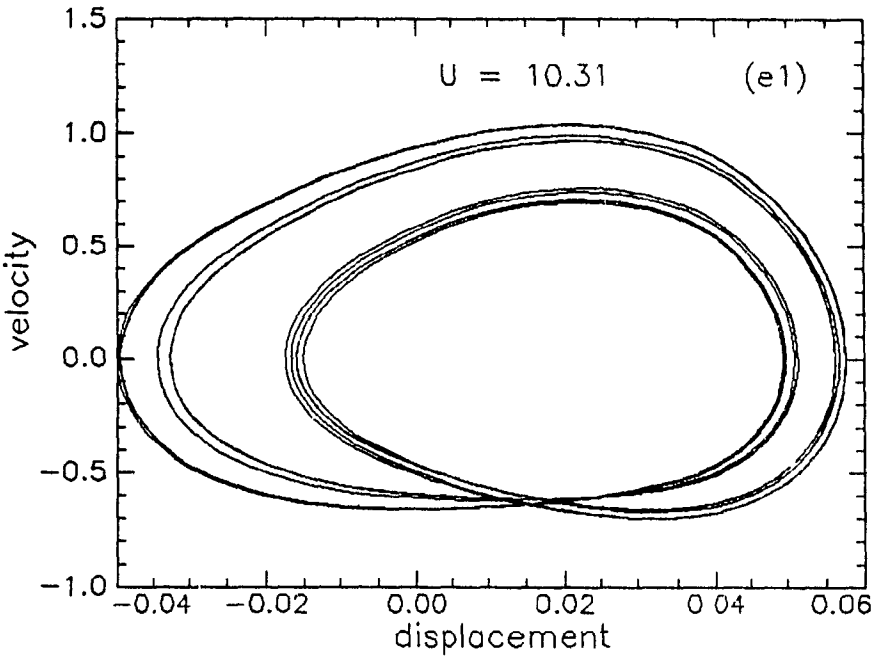

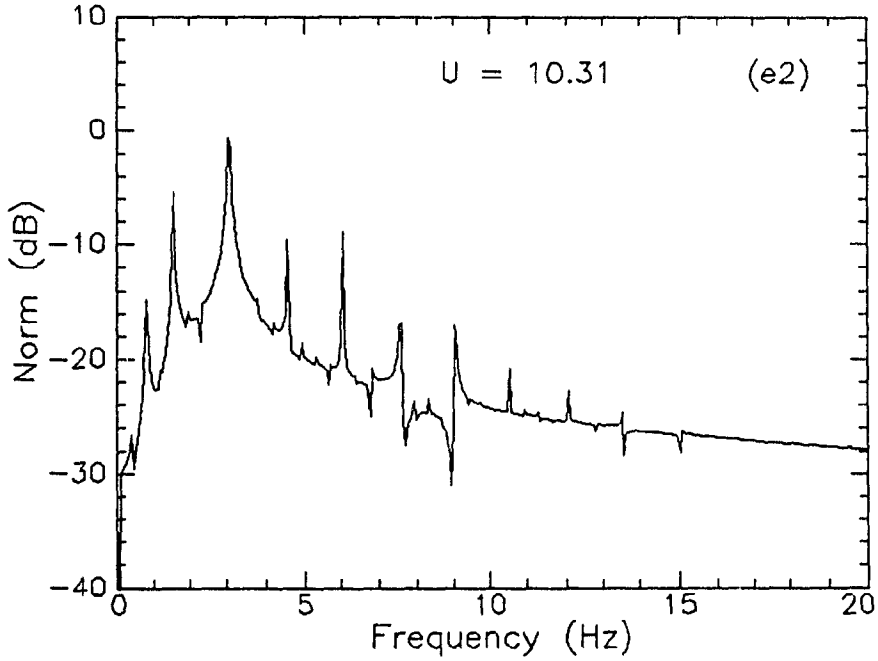

Fig.5.8(e) Phase portrait and power spectrum, U = 10.31, $K = 10^5$, $\xi_b = 0.75$, $\gamma = 26.75$, $\beta = 0.213$, $\alpha = 0.005$.

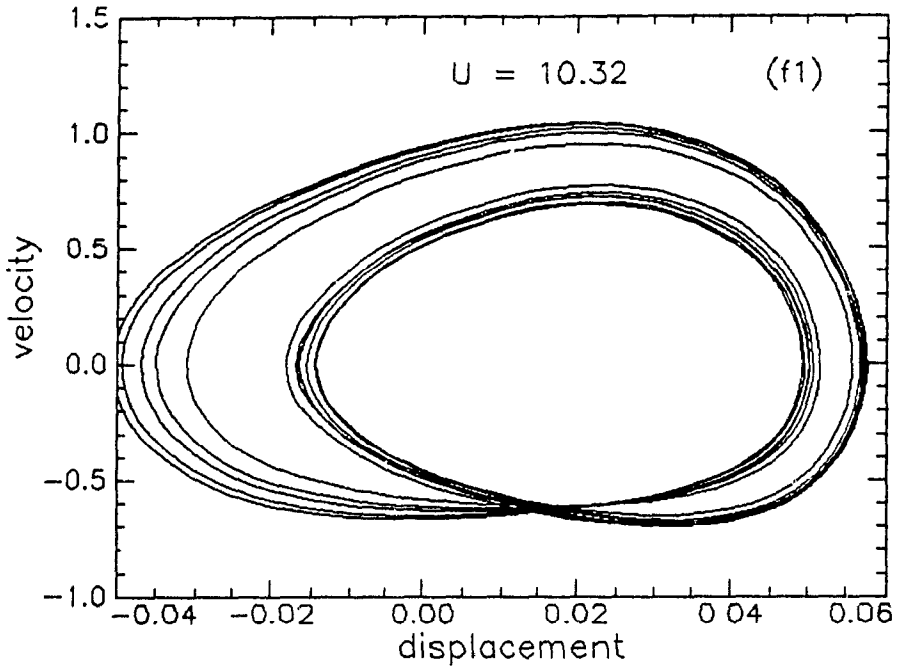

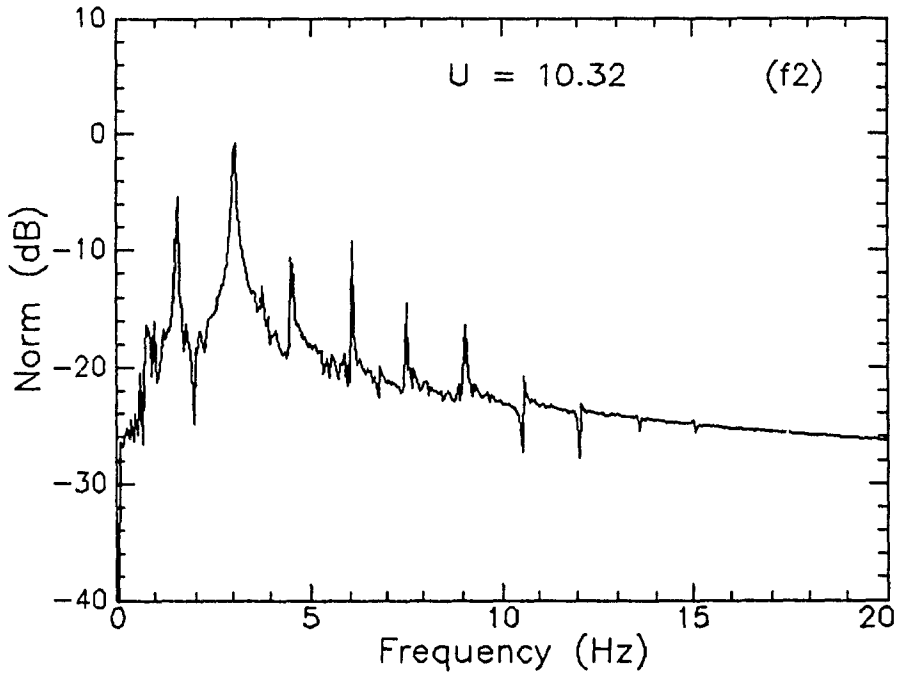

Fig.5.8(f) Phase portrait and power spectrum, U = 10.32, $K = 10^5$, $\xi_b = 0.75$, $\gamma = 26.75$, $\beta = 0.213$, $\alpha = 0.005$.

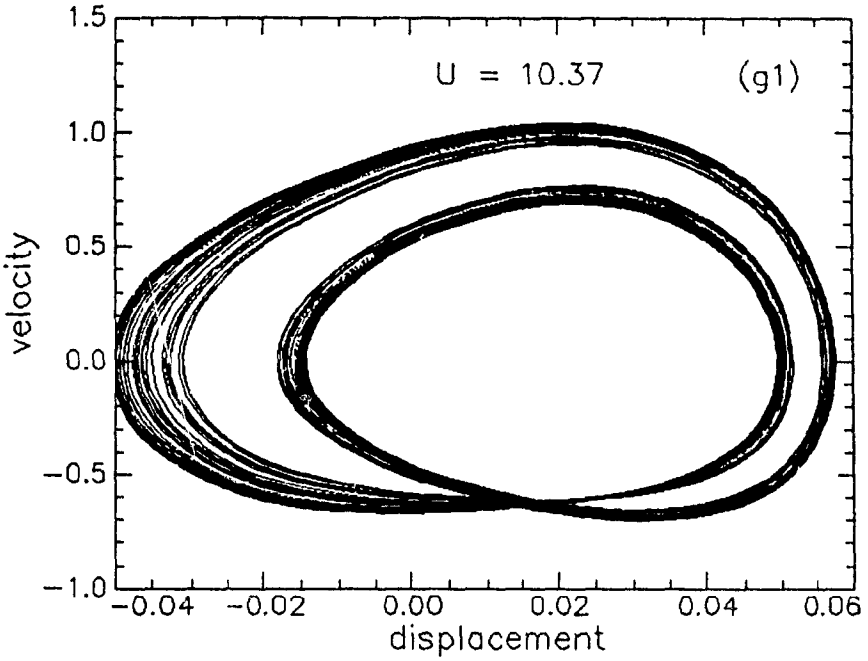

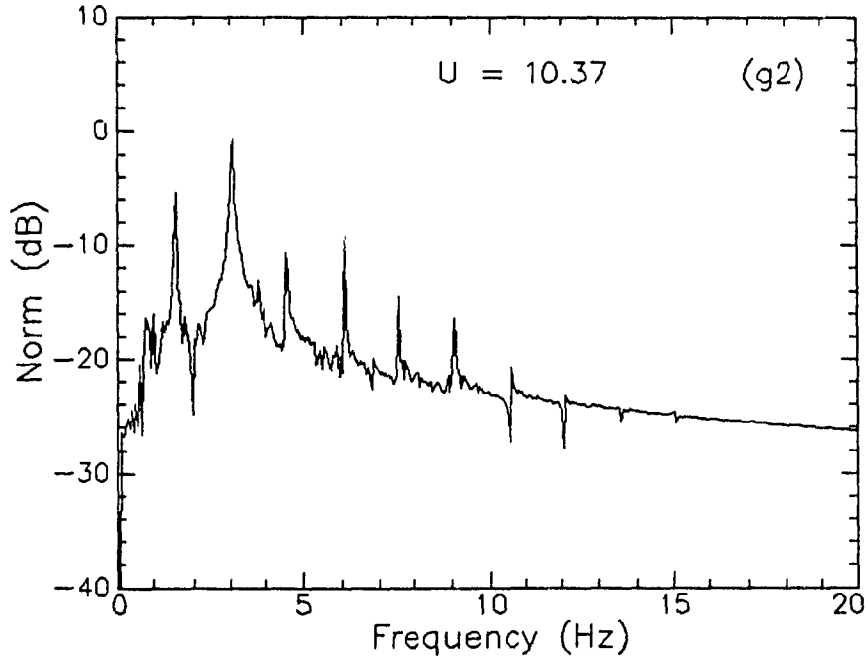

Fig.5.8(g) Phase portrait and power spectrum, U = 10.37, $K = 10^5$, $\xi_b = 0.75$, $\gamma = 26.75$, $\beta = 0.213$, $\alpha = 0.005$.

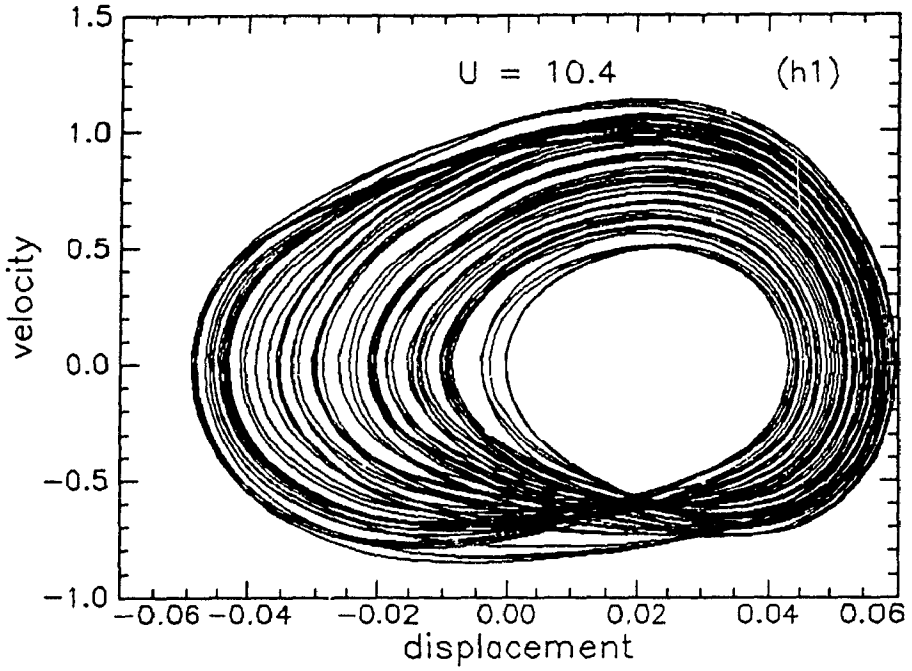

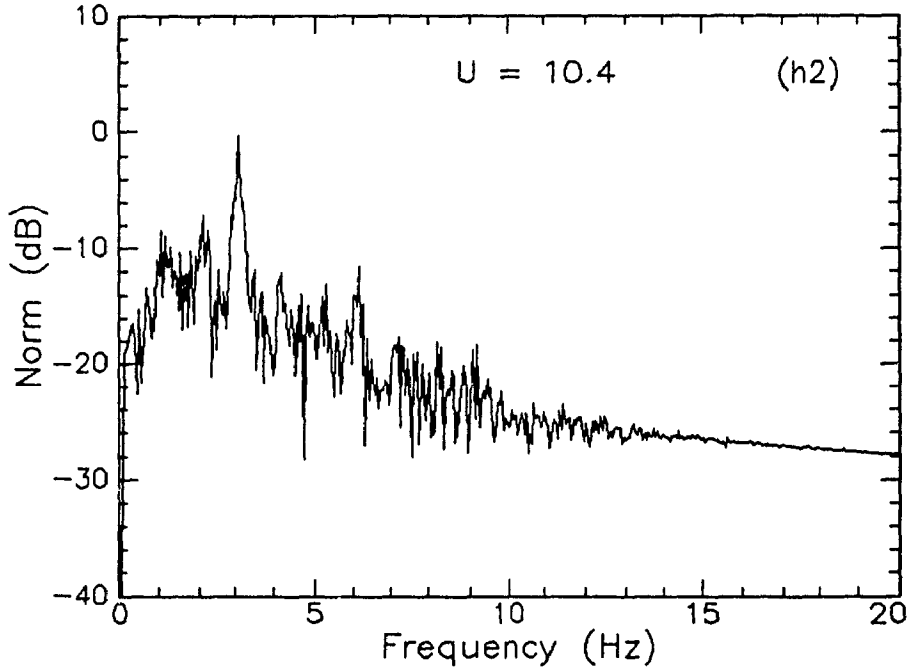

Fig.5.8(h) Phase portrait and power spectrum, U = 10.4, $K = 10^5$, $\xi_b = 0.75$, $\gamma = 26.75$, $\beta = 0.213$, $\alpha = 0.005$.

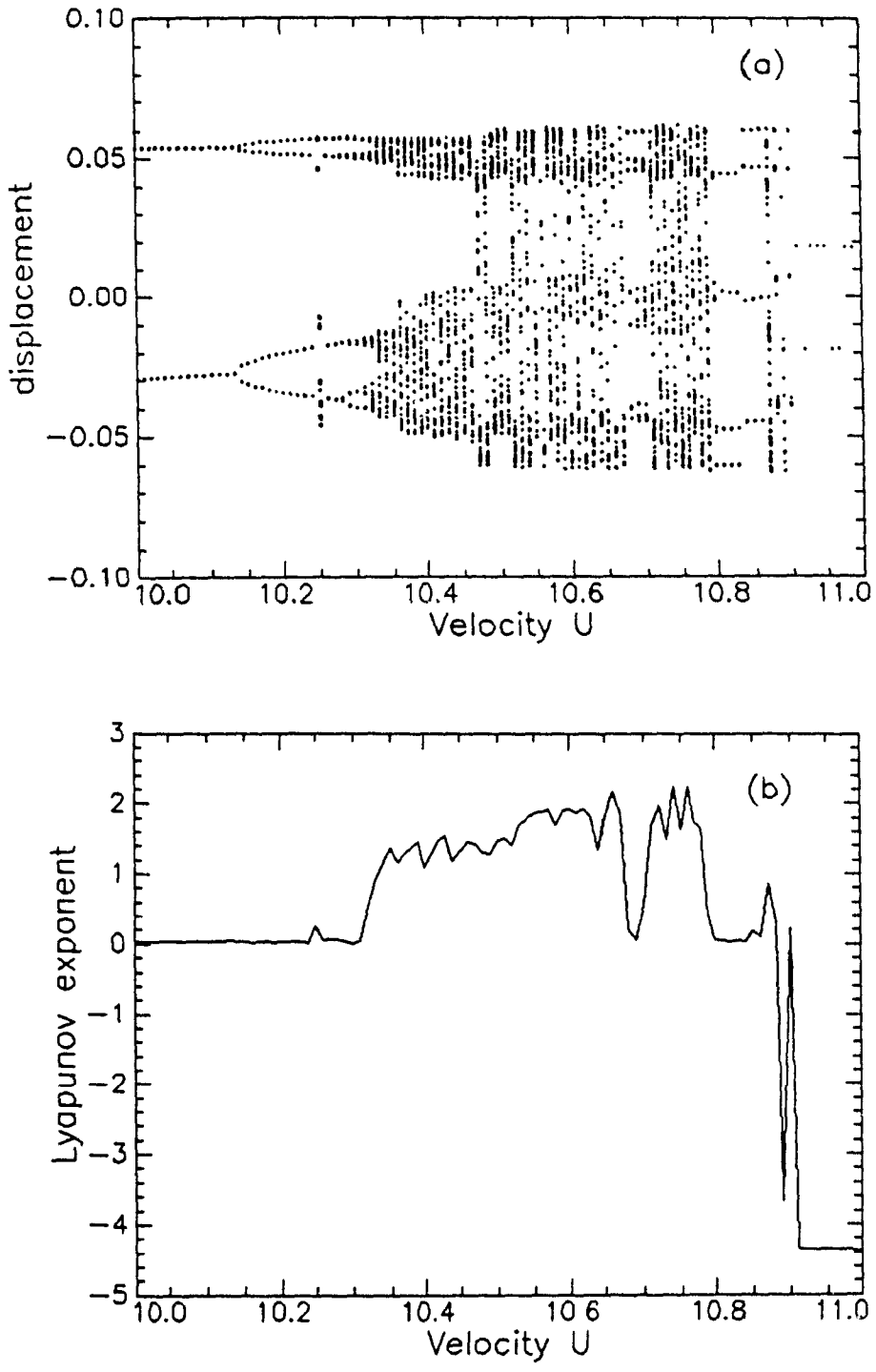

Fig.5.9 Bifurcation diagrams (a) Tip end displacements, (b) Lyapunov exponents, function of the flow velocity. $K = 10^5$, $\xi_b = 0.8$, $\gamma = 26.75$, $\beta = 0.213$, $\alpha = 0.005$.

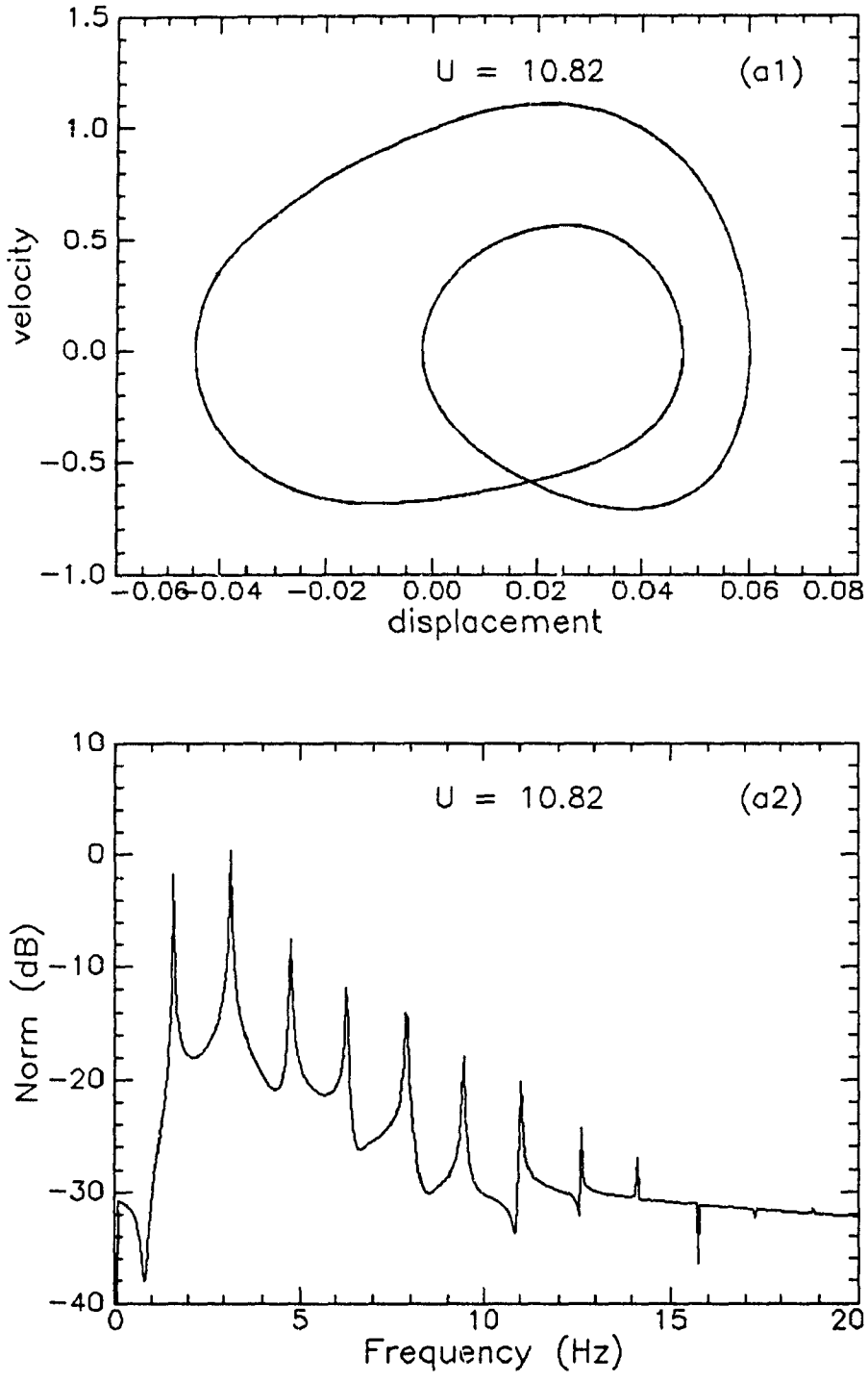

Fig.5.10(a) Phase portrait and power spectrum beyond the chaotic region; periodic motion at U = 10.82.

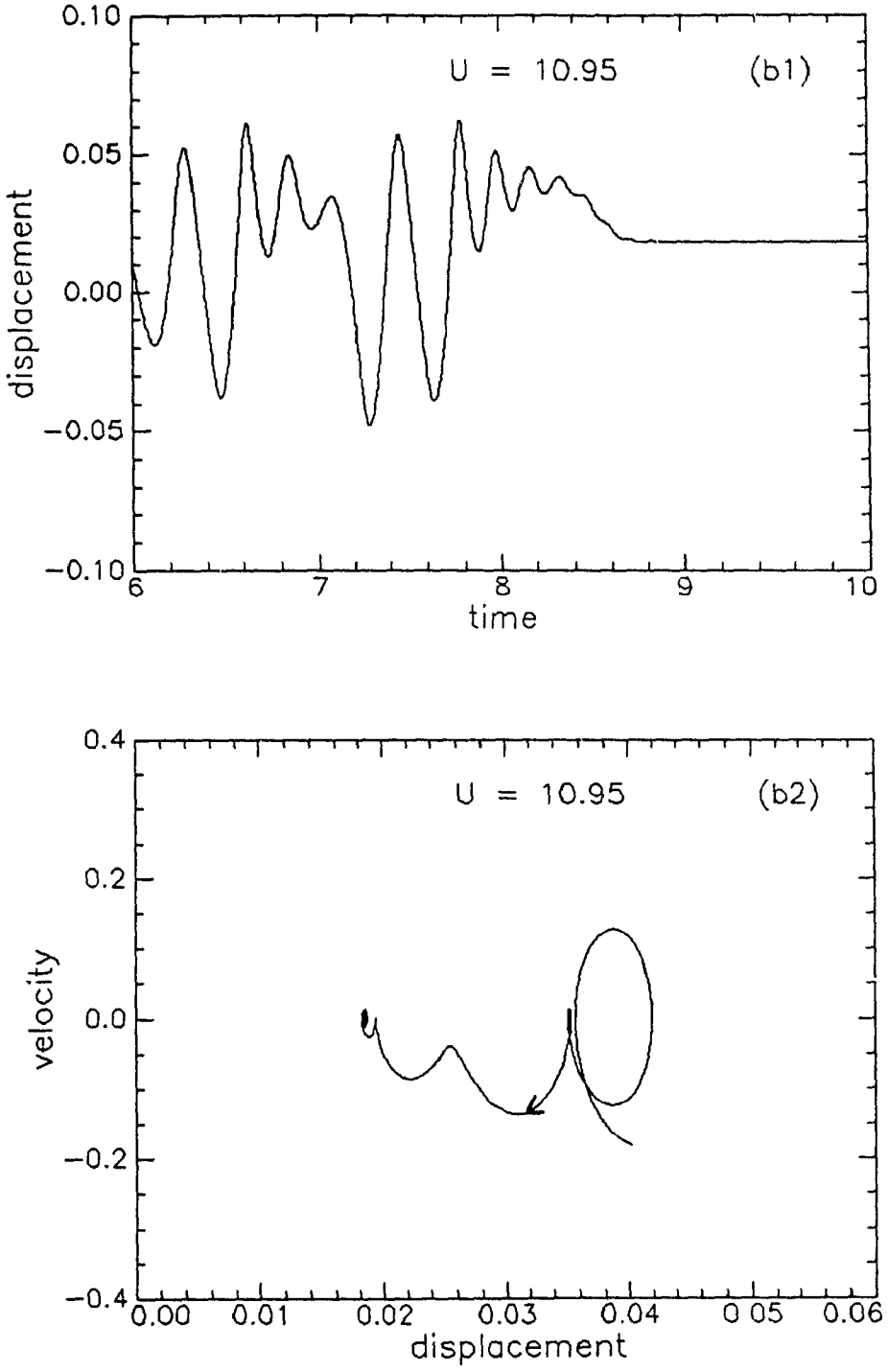

Fig.5.10(b) Time trace and phase portrait beyond the chaotic and periodic regions; static instability at U = 10.95.

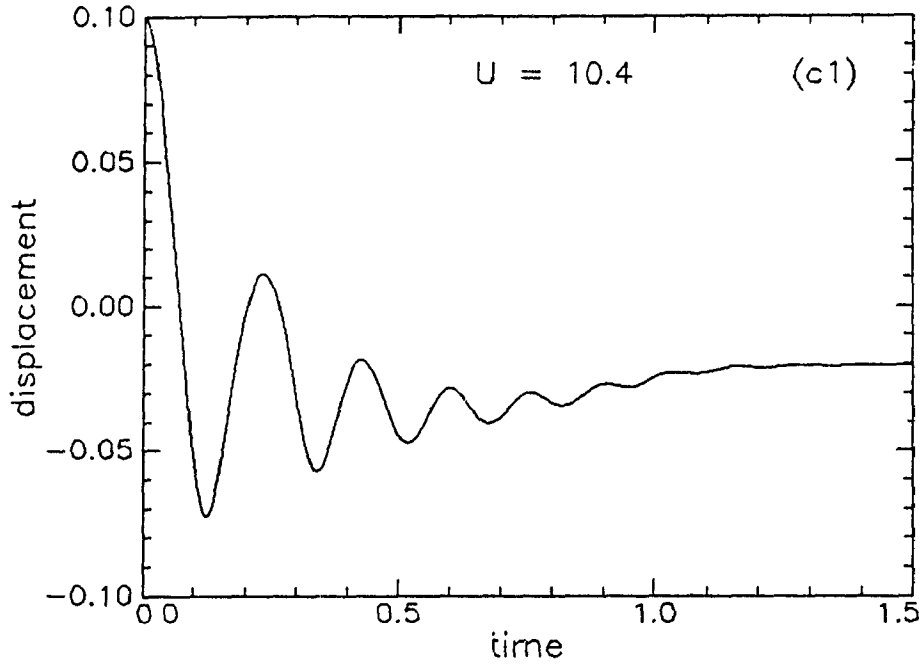

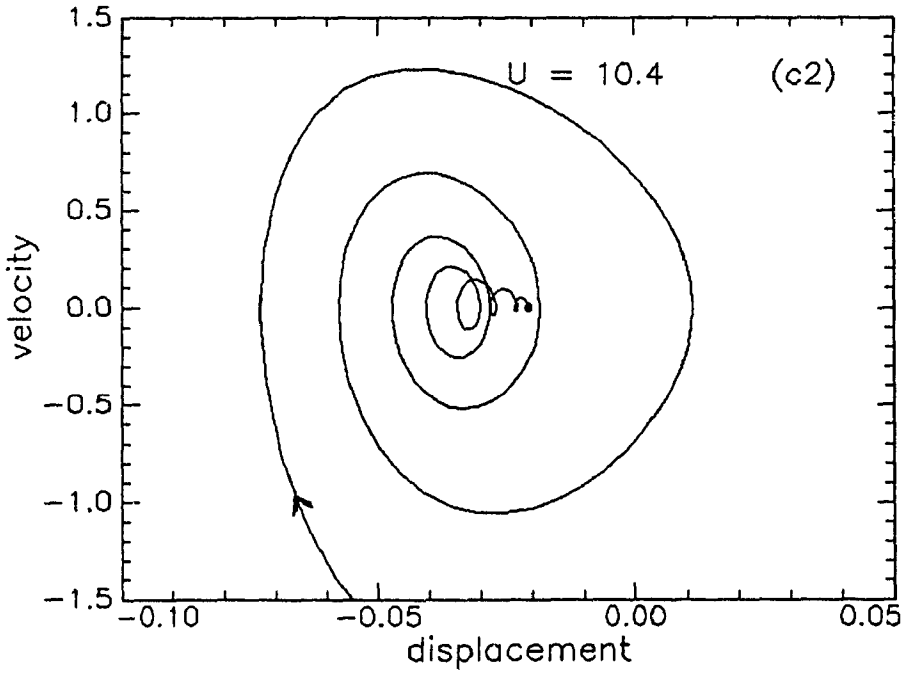

Fig.5.10(c) Time trace and phase portrait proving the existence of a stable fixed point in the chaotic region at U = 10.4.